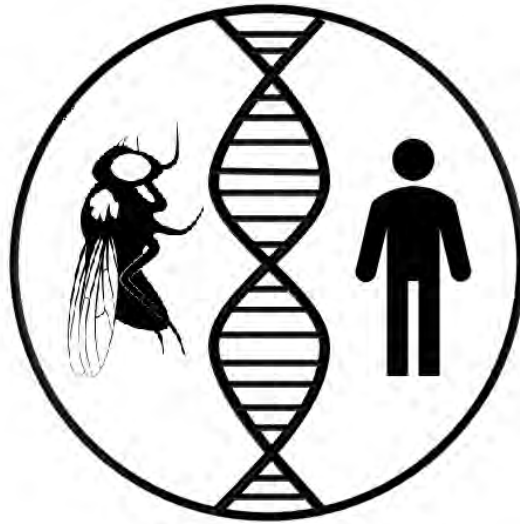


Characterisation of Host Gut-Microbiota Interaction in the *Drosophila* Model of Dextran Sulfate Sodium (DSS)-induced Colitis



DISSERTATION

zur Erlangung des Doktorgrades
der Mathematisch-Naturwissenschaftlichen Fakultät
der Christian-Albrechts-Universität zu Kiel

vorgelegt von

Mohsen Mahmoud Mohammed Hegab

Kiel, 2022

Erster Gutachter: Prof. Dr. Thomas Roeder

Zweiter Gutachter: Prof. Dr. Holger Heine

Tag der mündlichen Prüfung: 27.10.2022

Zum Druck genehmigt:

gez. Dekan: Prof. Dr. Frank Kempken

Declaration

I, Mohsen Mahmoud Mohammed Hegab, hereby declare that my doctoral dissertation titled “Characterisation of Host Gut- Microbiota Interaction in the *Drosophila* Model of Dextran Sodium Sulphate (DSS)-induced Colitis” was prepared according to the Rules of Good Scientific Practice of the German Research Foundation and represents my original research results. The entire work has been written by myself using the references and resources indicated herein. Any work of others has been appropriately marked. This dissertation is being submitted for the degree of Doctor of Natural Sciences at Christian-Albrecht University of Kiel, Germany, and has not been presented to any other university as part of an examination or degree.

Kiel,

Place, Date

Signature

Table of contents

	Page
List of abbreviations	I
Summary	V
Zusammenfassung	VII
Acknowledgements	IX
List of figures	X
List of tables	XVI
1 Introduction	1
1.1 Inflammatory bowel diseases (IBD)	1
1.1.1 IBD Phenotypes, clinical manifestations and global burden	1
1.1.2 Etiology and pathophysiology of IBD	3
1.1.2.1 Risk factors of IBD	3
1.1.2.1.1 Genetics of IBD	3
1.1.2.1.2 Microbiota in IBD	4
1.1.2.1.3 Environmental risk factors	5
1.1.3 Experimental models of intestinal inflammation and IBD	6
1.1.3.1 DSS-induced colitis	7
1.2 <i>Drosophila</i> as a model of human gastrointestinal disease(s)	8
1.2.1 Translational impact of <i>Drosophila</i> in human biology and medicine	8
1.2.2 Impact of <i>Drosophila</i> genetics on translating human GWAS-reported genes and drug discovery	9
1.2.3 The <i>Drosophila</i> is an effective model in interrogating host-microbiota interactions	9
1.2.4 Feasibility of ectopic gene expression using the <i>Drosophila</i> bipartite GAL4–UAS system	10

1.2.5 The <i>Drosophila</i> is an effective model of human intestinal pathology	11
1.2.6 Anatomy and Physiology of the <i>Drosophila</i> gut	11
1.2.7 Evolutionary conservation of cellular junctions between the <i>Drosophila</i> and vertebrates	12
1.2.8 Evolutionary conservation of core components of the JAK/STAT pathway between <i>Drosophila</i> and vertebrates	13
1.2.9 <i>Drosophila</i> Plasmatocytes are functional homolog of vertebrate macrophages	14
1.3 Aim of the study	16
2. Materials and Methods	17
2.1 Materials	17
2.1.1 Laboratory equipments	17
2.1.2 Chemicals	19
2.1.3 Antibodies	21
2.1.4 Enzymes	21
2.1.5 Bacterial strains	22
2.1.6 Oligonucleotides	22
2.1.7 Solutions and media	24
2.1.8. <i>Drosophila</i> stocks	26
2.2 Methods	26
2.2.1 <i>Drosophila</i> standard and experimental media	26
2.2.2 <i>Drosophila</i> husbandry and experimental condition	27
2.2.3 <i>Drosophila</i> GAL4/UAS crossing	27
2.2.4 Induction of gut inflammation by Dextran sulfate sodium	27
2.2.5 Characterization of DSS-induced colitis-like phenotype	27
2.2.5.1 Survival analysis	27
2.2.5.2 Determination of total activity	28

2.2.6 Determination of Cumulative Food Consumption and Excretion	28
2.2.6.1 Determination of food consumption	28
2.2.6.2 Egestion rate	29
2.2.6.3 Quantification of fecal consistency and luminal content	29
2.2.7 Measurement of body weight	30
2.2.8 Body fat quantification	30
2.2.9 Characterization of barrier dysfunction”leaky gut” phenotype	31
2.2.10 Immunohistochemistry and microscopy	31
2.2.11 Relative Quantification of Immunofluorescence image	31
2.2.12 β -galactosidase staining	32
2.2.13 Establishment of axenic (Germ-free) fly culture	32
2.2.14 Preparation, storage and re-colonization of total microbial community	33
2.2.15 Isolation of DNA-free RNA from fly gut tissues	34
2.2.16 Nucleic acid Quantification and purity measurement	35
2.2.17 Agarose gel electrophoresis	35
2.2.18 Establishment of RT-qPCR assay, QC, and data analysis.	35
2.2.19 Bacterial DNA isolation from tissue and fecal samples	37
2.2.20 Targeted high-throughput 16S rRNA amplicon sequencing	38
2.2.21 Integrated analysis of 16S rRNA gene amplicon	39
2.2.22 Preparation, storage and transplantation of fecal microbiota	40
2.2.23 Statistical analysis	41
3 Results	43
3.1 Establishment of the <i>Drosophila</i> DSS-induced colitis model	43
3.1.1 DSS treatment induces mortality in <i>Drosophila</i> with male-bias survival advantage	43
3.1.2 Post-induction phases of DSS treatment is an informative	44

survival-based proxy for disease progression	
3.1.3 Longitudinal analysis of the DSS effect on <i>Drosophila</i> reveals a significant reduction in mortality after 6-day recovery period	45
3.1.4 DSS treatment triggers rapid decline in the <i>Drosophila</i> total activity	46
3.1.5 DSS treatment for 6 days reduces the <i>Drosophila</i> excreta egestion	47
3.1.6 DSS treatment for 6 days reduces the <i>Drosophila</i> food consumption	47
3.1.7 DSS treatment triggers <i>Drosophila</i> weight loss	47
3.1.8 DSS treatment triggers plasmatocytes recruitment to the injured gut	49
3.1.9 DSS treatment compromises the integrity of the <i>Drosophila</i> intestinal barrier (the “leaky gut” phenotype)	50
3.1.10. Structural characterization of the DSS-induced leakiness	52
3.1.11. DSS treatment triggers hyperproliferation in the <i>Drosophila</i> midgut	54
3.1.12 DSS treatment triggers midgut hyperproliferation in axenic female <i>Drosophila</i>	57
3.1.13 Re-colonization of treatment-naive germ-free <i>esg-Gal4>GFP</i> recipient <i>Drosophila</i> adults with total microbial community from day-12 DSS-treated donors induces inducing midgut dysplasia.	57
3.1.14 DSS treatment induces over-expression of <i>Upd3</i> in the <i>Drosophila</i> midgut.	59
3.2 Spatiotemporal gut-wide multiple gene expression analysis in DSS-induced <i>Drosophila</i> colitis-like model.	62
3.2.1 DSS induces transcriptional dysregulation in the <i>Drosophila</i> anterior midgut (AMG) after 6-day treatment.	62
3.2.2 DSS induces transcriptional dysregulation in the <i>Drosophila</i> posterior midgut (PMG) after 6-day treatment	63
3.2.3 DSS induces transcriptional dysregulation in the <i>Drosophila</i> hindgut (HG) after 6-day treatment	64
3.2.4 DSS induces transcriptional dysregulation in the <i>Drosophila</i>	65

anterior midgut (AMG) after 12-day treatment	
3.2.5 DSS induces transcriptional dysregulation in the <i>Drosophila</i> posterior midgut (PMG) after 12-day treatment	66
3.2.6 DSS induces transcriptional dysregulation in the <i>Drosophila</i> hindgut (HG) after 12-day treatment	67
3.2.7 Spatiotemporal gut-wide transcriptional dysregulation in the <i>Drosophila</i> DSS-induced colitis model	68
3.2.8 Gene-gene interactions in the <i>Drosophila</i> gut at day-6 post DSS treatment.	69
3.2.9 Gene-gene interactions in the <i>Drosophila</i> gut at day-12 post DSS treatment.	70
3.2.10 Six-day recovery period impacts the restoration of transcriptional dysregulation in the <i>Drosophila</i> anterior midgut	71
3.2.11 Six-day recovery period impacts the restoration of transcriptional dysregulation transcriptional dysregulation in the <i>Drosophila</i> posterior midgut	72
3.2.12 Six-day recovery period impacts the restoration of transcriptional dysregulation in the <i>Drosophila</i> hindgut	73
3.2.13 Gene-gene interactions in the <i>Drosophila</i> gut after 6-day recovery period	74
3.3 Spatiotemporal gut-wide microbiota profiling in DSS-induced <i>Drosophila</i> colitis-like model	75
3.3.1 Effect of 6-day DSS treatment on the <i>Drosophila</i> fecal microbiota community structure	75
3.3.2 Effect of 6-day DSS treatment for on the <i>Drosophila</i> fecal microbiota abundance at higher taxonomic ranks	76
3.3.3 Effect of 6-day DSS treatment on the <i>Drosophila</i> fecal microbiota abundance at lower taxonomic ranks	77
3.3.4 Effect of DSS treatment for 6 days on the interaction of different parameters of fecal microbiota community and physiologic correlates	78
3.3.5 Effect of 6-day DSS treatment on the <i>Drosophila</i> midgut microbiota community structure	79
3.3.6 Effect of 6-day DSS treatment for on the <i>Drosophila</i> midgut	80

microbiota abundance at higher taxonomic ranks	
3.3.7 Effect of 6-day DSS treatment on the <i>Drosophila</i> midgut microbiota abundance at lower taxonomic ranks	81
3.3.8 Effect of 6-day DSS treatment on the <i>Drosophila</i> hindgut microbiota community structure	82
3.3.9 Effect of 6-day DSS treatment for on the <i>Drosophila</i> hindgut microbiota abundance at higher taxonomic ranks	83
3.3.10 Effect of 6-day DSS treatment on the <i>Drosophila</i> hindgut microbiota abundance at lower taxonomic ranks	84
3.3.11 Effect of 12-day DSS treatment on the <i>Drosophila</i> fecal microbiota community structure	85
3.3.12 Effect of 12-day DSS treatment for on the <i>Drosophila</i> fecal microbiota abundance at higher taxonomic ranks	86
3.3.13 Effect of 12-day DSS treatment on the <i>Drosophila</i> fecal microbiota abundance at lower taxonomic ranks	87
3.3.14 Effect of 12-day DSS treatment on the <i>Drosophila</i> midgut microbiota community structure	88
3.3.15 Effect of 12-day DSS treatment for on the <i>Drosophila</i> midgut microbiota abundance at higher taxonomic ranks	89
3.3.16 Effect of 12-day DSS treatment on the <i>Drosophila</i> midgut microbiota abundance at lower taxonomic ranks	90
3.3.17 Effect of 12-day DSS treatment on the <i>Drosophila</i> hindgut microbiota community structure	91
3.3.18 Effect of 12-day DSS treatment for on the <i>Drosophila</i> hindgut microbiota abundance at higher taxonomic ranks	92
3.3.19 Effect of 12-day DSS treatment on the <i>Drosophila</i> hindgut microbiota abundance at lower taxonomic ranks	93
3.3.20 Effect of 6-day recovery period on the <i>Drosophila</i> fecal microbiota community structure	94
3.3.21 Effect of 6-day recovery period on the <i>Drosophila</i> fecal microbiota abundance at higher taxonomic ranks	95
3.3.22 Effect of 6-day recovery period on the <i>Drosophila</i> fecal microbiota abundance at lower taxonomic ranks	96

3.3.23 Effect of 6-day recovery period on the <i>Drosophila</i> midgut microbiota community structure	97
3.3.24 Effect of 6-day recovery period on the <i>Drosophila</i> midgut microbiota abundance at higher taxonomic ranks	98
3.3.25 Effect of 6-day recovery period on the <i>Drosophila</i> midgut microbiota abundance at lower taxonomic ranks	99
3.3.26 Effect of 6-day recovery period on the <i>Drosophila</i> hindgut microbiota community structure	100
3.3.27 Effect of 6-day recovery period on the <i>Drosophila</i> hindgut microbiota abundance at higher taxonomic ranks	101
3.3.28 Effect of 6-day recovery period on the <i>Drosophila</i> hindgut microbiota abundance at lower taxonomic ranks	102
3.3.29 Effect of 6-day DSS treatment on the male <i>Drosophila</i> fecal microbiota community structure	103
3.3.30 Effect of 6-day DSS treatment for on the male <i>Drosophila</i> fecal microbiota abundance at higher taxonomic ranks	104
3.3.30 Effect of 6-day DSS treatment on the male <i>Drosophila</i> fecal microbiota abundance at lower taxonomic ranks	105
4. Discussion	106
4.1. DSS-induced <i>Drosophila</i> colitis-like model has a theoretical rationale	106
4.2. Developing reproducible and quantitative disease endpoints (DEs) of DSS-induced colitis-like phenotype in the <i>Drosophila</i> .	107
4.2.1. Disease endpoint 1: Reduced survival and activity in DSS-induced colitis that mimics the rodent model, but with reversed sexual dimorphism	107
4.2.2. Disease endpoint 2: Appetite loss is a surrogate marker of DSS-induced colitis	108
4.2.3. Disease endpoint 3: Weight loss is an informative extra-intestinal marker of DSS-induced colitis	109
4.2.4. Disease endpoint 4: Migration of <i>Drosophila</i> plasmatocytes (macrophage-like) to the injured gut is a quantitative surrogate marker of DSS-induced colitis.	109
4.2.5. Disease endpoint 5: Smurfness combined with disrupted visceral	111

muscle and tight junction is more frequent in the <i>Drosophila</i> DSS-induced colitis.	
4.2.6. Disease endpoint 6: Epithelial dysplasia of the <i>Drosophila</i> midgut progenitor cells is reliable marker of <i>Drosophila</i> DSS-induced colitis.	115
4.3. <i>Drosophila</i> DSS-induced colitis is an informative model of host-microbiota interaction in the human IBD	116
4.3.1. Characteristics of fecal-associated and tissue-associated microbiotas in-house reared <i>w¹¹¹⁸</i> <i>Drosophila</i>	117
4.3.2. Community structure of the <i>Drosophila</i> DSS-induced colitis model	119
4.3.3. Microbial imbalance of the <i>Drosophila</i> DSS-induced colitis at different taxonomic levels	120
5. Conclusion& outlook	121
6. References	123
7. Appendix	139

List of abbreviations & units

Abbreviations	
α	Anti OR alpha
Ab	Antibody
AMG	Anterior midgut
AMP	Antimicrobial peptide
ANOVA	Analysis of variance
AU	Arbitrary unit
BSA	Bovine serum albumin
BR	Biological replicate
CAFE	Capillary Feeder
CD	Crohn's disease.
cDNA	Complimentary DNA
Ct	Cycle threshold
CTRL/Ctrl	Control (un-treated)
DAM	<i>Drosophila</i> Activity Monitoring System
DAPI	4',6-diamidino-2-phenylindole
DE	Disease endpoint
DEcad	<i>Drosophila</i> Cadherin
DIS	DSS-induced smurfness
Dlg	Disks large (<i>Drosophila</i> gene/protein)
DNA	deoxyribonucleic acid
dNTP	Deoxyribonucleotide triphosphates
DSS	Dextran sulfate sodium OR dextran sodium sulfate
E	Effeciency
EB	Enteroblasts
EC	Enterocyte
<i>E. coli</i>	<i>Escherichia coli</i>
EDTA	Ethylenediaminetetraacetic acid

eGFP	Enhanced green fluorescent protein
EIMs	Extra-intestinal manifestations
<i>et al.</i>	<i>et alumni</i>
EtOH	Ethanol
F	Forward
Fig.	Figure
<i>Gapdh</i>	Glyceraldehyde 3-phosphate dehydrogenase
GFP	Green fluorescent protein
HG	Hindgut
HPLC	High pressure liquid chromatography
HL3	Hemolymph-like buffer
IBDs	Inflammatory bowel diseases
IL	Interleukin
IMNGS	Integrated Microbial Next Generation Sequencing
ISCs	Intestinal stem cells
JAK-STAT	Janus kinase signal transducers and activators of transcription
K	= 1000
kune	Kune-kune (<i>Drosophila</i> gene/protein)
LD	Light/Dark
LG	Leaky gut
MDS	Multidimensional scaling
metaNMDS	Non-metric Multidimensional scaling
mRNA	Messenger RNA
MG	Midgut
NM/nm	Normal media (i.e. control, untreated group)
NGS	Normal goat serum
OD	Optical density
OTU	Operational Taxonomic Unit
PFA	Paraformaldehyde

PBS	Phosphate buffered saline
PBT	PBS-triton-X 100
Pck	Pickel (<i>Drosophila</i> gene/protein)
PCR	Polymerase chain reaction
pH	<i>potentia Hydrogenii</i>
PMG	Posterior midgut
PMM	Plasmatocyte migration marker
Pyd	Polychaetoid (<i>Drosophila</i> gene/protein)
R	Replica (in experimental groups) OR reverse (in PCR primer) OR R in programming language)
RFP	Red fluorescent protein
RpL	60S ribosomal protein L32
RNA	Ribonucleic acid
16S rRNA	16 S ribosomal RNA gene
Sinu	Sinous (<i>Drosophila</i> gene/protein)
Socs	Suppressor of Cytokine Signaling
RT-qPCR	Reverse transcription-quantitative polymerase chain reaction
TEM	Transmission electron microscopy
sm	Smurf
Tris	Tris-(hydroxymethyl)-aminomethane
UAS	Upstream activating sequence
UC	Ulcerative colitis.
Upd	Unpaired (<i>Drosophila</i> gene/protein)
ZOTU	zero-radius OTU Operational Taxonomic Unit
Units	
bp	Base pair
Da	Dalton
g)	Gram (weight) OR respective gravity (centrifugation)

h	hour
mg	Milligram
μ l	Microliter
μ m	Micrometer
Min	minutes
ml	Milliliter
Sec	Second

Summary

Inflammatory bowel diseases appear as highly heterogeneous, less-manageable chronic diseases. There is a remarkable progress in developing experimental colitis models which is a prerequisite to enrich the pharmacological armamentarium with new drugs. Yet, dextran sulfate sodium (DSS)-induced colitis is widely implemented in different vertebrate model organisms. Although DSS was used to study multiple evolutionary-conserved pathways of cell injury in the *Drosophila* gut, a deep and integrative phenotyping of the DSS-induced injury is lacking. Here, a translational *Drosophila* model of DSS-induced colitis was established followed by a systematic characterization of disease endpoints and interrogation of host-microbiota interactions. Disease endpoints represent intestinal and extra-intestinal manifestations of the DSS-induced colitis. Significant reduction in the total activity, the food consumption, the excreta egestion and the body weight as well as marked gut leakiness and epithelial dysplasia were the main characteristic core phenotyping parameters (CPPs). Additionally, a significant increase of plasmacytes (functional homolog of macrophages) recruitment to the injured gut was observed in response to DSS treatment. Inspired by the fact that the *Drosophila* gut is highly compartmentalized, gene expression and co-expression analyses were independently conducted on anterior and posterior midgut regions as well as the hindgut. Gene expression analysis revealed that *Drosophila* Disks large1 (*Dlg1*), E-cadherin (*DEcad*), *Kune-kune*, Unpaired (*Upd3*), *Drosomyacin* and *Attacin*, were differentially expressed along the *Drosophila* gut axis and share common and distinct transcriptional signatures in DSS-treatment group compared to controls. Furthermore, integrating the phenotypic and regionalized gene expression data suggested that the *Drosophila* hindgut was more resistant to DSS-induced injury. On the other hand, anterior and posterior midgut regions were severely affected by DSS treatment in terms of leakiness and dysplasia, respectively. Given that microbiota plays a cardinal role in modulating gut physiology, targeted metagenomics was conducted on the established *Drosophila* DSS-colitis model. Results underscored that 16S rRNA profiling of tissue-associated microbiota was superior to that of the fecal microbiota community. Moreover, profiling midgut microbiome after DSS treatment identified a regionalized microbiota signature that was characterized by a significant reduction of *alpha*-diversity and blooming of Proteobacteria. This dysbiotic signature was widely reported as a hallmark of both IBD and DSS colitis murine model. Altogether, integrating the differential gene expression and 16S rRNA

profiling data added another layer of understanding the host-microbiota cross-talk in DSS-induced colitis. However, the suggestive selective dominance of Proteobacteria warrants investigation in future studies. Above all, the established *Drosophila* DSS-induced colitis model is not only successful in recapitulating multiple aspects of experimental colitis, but it also provides a general framework in the context of *Drosophila* model of human diseases.

Zusammenfassung

Entzündliche Darmerkrankungen treten als sehr heterogene, schwer beherrschbare chronische Erkrankungen auf. Es gibt bemerkenswerte Fortschritte bei der Entwicklung experimenteller Colitis-Modelle, die eine Voraussetzung dafür sind, dass neue Medikamente entwickelt werden. Eine durch Natrium-Dextransulfat (DSS) ausgelöste Kolitis wird in verschiedenen Wirbeltiermodellen weithin eingesetzt. Obwohl DSS verwendet wurde, um evolutionär konservierte Wege der Zellschädigung im *Drosophila*-Darm zu untersuchen, fehlt eine tiefgehende und integrative Phänotypisierung der DSS-induzierten Schädigung. Im Rahmen dieser Arbeit wurde ein translationales *Drosophila*-Modell der DSS-induzierten Kolitis etabliert, das anschließend einer systematischen Charakterisierung der Krankheitsendpunkte und der Untersuchung der Wirt-Mikrobiota-Interaktionen unterzogen wurde. Die Krankheitsendpunkte repräsentieren intestinale und extra-intestinale Manifestationen der DSS-induzierten Kolitis. Eine signifikante Verringerung der Gesamtaktivität, der Nahrungsaufnahme, der Ausscheidungen und des Körpergewichts sowie eine ausgeprägte Durchlässigkeit des Darms und eine Epitheldysplasie waren die wichtigsten charakteristischen Phänotypisierungsparameter (CPPs). Darüber hinaus wurde als Reaktion auf die DSS-Behandlung eine signifikante Zunahme der Rekrutierung von Plasmatozyten (funktionelle Homologe der Makrophagen) in den geschädigten Darm beobachtet. Da der Darm von *Drosophila* stark kompartimentiert ist, wurden Genexpressionsanalysen unabhängig voneinander in den vorderen und hinteren Mitteldarmregionen sowie im Hinterdarm durchgeführt. Die Genexpressionsanalyse ergab, dass *Drosophila* Disks *large1* (*Dlg1*), *E-Cadherin* (*DEcad*), *Kune-kune*, *Unpaired* (*Upd3*), *Drosomyacin* und *Attacin* entlang der *Drosophila*-Darmachse unterschiedlich exprimiert wurden und in der DSS-Behandlungsgruppe im Vergleich zu den Kontrollen gemeinsame und unterschiedliche Transkriptionssignaturen aufweisen. Die Integration der phänotypischen und regionalisierten Genexpressionsdaten deutet außerdem darauf hin, dass der *Drosophila*-Hinterdarm resistenter gegen DSS-induzierte Verletzungen ist. Andererseits waren die vorderen und hinteren Mitteldarmregionen durch die DSS-Behandlung in Bezug auf Durchlässigkeiten bzw. Dysplasien stark beeinträchtigt. In Anbetracht der Tatsache, dass die Mikrobiota eine zentrale Rolle bei der Modulation der Darmphysiologie spielt, wurde eine metagenomische Analyse an dem etablierten *Drosophila* DSS-Kolitis-Modell durchgeführt. Die Ergebnisse unterstrichen, dass die 16S rRNA-

Profilierung der gewebeassoziierten Mikrobiota derjenigen überlegen war, die sich allein auf Nutzung der Fäzes bezog. Darüber hinaus wurde bei der Profilierung des Mikrobioms des Mitteldarms nach der DSS-Behandlung eine regionalisierte Mikrobiota-Signatur identifiziert, die durch eine signifikante Verringerung der Alpha-Diversität und ein Aufkommen von Proteobakterien gekennzeichnet war. Diese dysbiotische Signatur wurde weithin als Kennzeichen sowohl für IBD als auch für DSS-Kolitis im Mausmodell beschrieben. Insgesamt hat die Integration der unterschiedlichen Genexpressions- und 16S rRNA-Profilierungsdaten eine weitere das Verständnis des Wirts-Mikrobiota-Zusammenspiels bei DSS-induzierter Kolitis erweitert. Die selektive Dominanz von Proteobakterien sollte jedoch in zukünftigen Studien untersucht werden. Vor allem aber ist das etablierte *Drosophila*-Modell für DSS-induzierte Kolitis nicht nur in der Lage verschiedene Aspekte der experimentellen Kolitis zu rekapitulieren, sondern es reiht sich in den Kanon der *Drosophila*-Modelle für menschliche Krankheiten ein.

Acknowledgements

I wish to express my sincere gratitude to Prof. Thomas Roeder for his support, guidance and ample freedom to cultivate my interest in gut physiology and microbiomics. I would like to thank my thesis advisory committee (TAC) at the International Max Planck Research School (IMPRS) for Evolutionary Biology, Prof John Baines and Prof. Dietrich Ober for their valuable comments and encouragement.

I would also like to thank my colleagues in the AG Roeder. In particular, I want to thank Reshmi Raveendran and Dr. Kerstin Mehnert for their support during the application to Max Planck Institute. I want also to deeply thank Mrs. Britta Laubenstein for the technical support in RTqPCR experiment and providing other lab protocols. I would also like to thank Prof. Christian Kost for providing the pJBA24-egfp24 and pJ

BA24-mCherry plasmids.

During the doctoral training, I have received multiple training seminars/ workshops/ courses in evolutionary biology, symbiosis, microbial bioinformatics, as well as transferable skills. As such, I want to express heartfelt thanks to the managing staff of the IMPRS evolutionary Biology in plön, The CRC 1182 “Origin and function of Metaorganisms” in Kiel, the German Network for Bioinformatics Infrastructure (de.NBI) in Bielefeld and the graduate center of the Christian-Albrechts University of Kiel.

During my study endeavor, I got funding from the different organizations. Therefore, I would like to thank the managing bodies of the DAAD for funding half of my stay in Germany, of the IMPRS for funding the attendance of the European Drosophila Research Conferences (EDRC) in Heidelberg and in London, and of the graduate center of the Christian-Albrechts University of Kiel for funding the course “interactive and authentic microbiology education”.

Last but not least, I want to thank my parents, my wife, my brothers and sisters and my friends (Dr. Ibrahim Ewess, Hazem Ewess, Mostafa Trad, Motagaly, Mohamed Ahmed) for the unwavering love and support.

I also appreciate all the challenges I faced during my study, it contributed significantly to my experience and added an extra layer of resilience to my personality.

List of figures

	Description	Page
Fig. 1.1	Epidemiological stages of IBD	2
Fig. 1.2	Schematized correlation of main factors involved in the IBD pathogenesis.	3
Fig. 1.3	Composition of dominant microbial community in the human GI tract IBD.	5
Fig. 1.4	Schematic representation of the toxic effect of DSS on the intestinal epithelium.	8
Fig. 1.5	Schematic representation of GAL4/UAS system.	10
Fig. 1.6	Anatomical description of homology between human and fly digestive tract.	11
Fig. 1.7 (A&B)	Diagrammatic representation of the adult <i>Drosophila</i> gut regions and Midgut cell-types.	12
Fig. 1.8	Diagrammatic representation of the organization of epithelial junctions in vertebrates and <i>Drosophila</i> .	13
Fig. 1.9 (A&B)	Diagrammatic representation of interaction network in the damaged gut epithelia and induced signalling cascade.	15
Fig. 1.10 (A&B)	A scheme depicts F1 generation of crossing a hemocyte-specific expression (<i>hemolymphin</i> gene, <i>Hml</i>) with GFP-UAS-2xGFP.	15
Fig. 2.1	Schematic diagram illustrating the set up of CAFE assay.	29
Fig.2.2	Schematic illustration of the E. coli LacZ reporter gene encoding for the β -galactosidase staining.	33
Fig.3.1	Effect of DSS treatment on in conventional w^{1118} male and female flies.	43
Fig.3.2	Phases of DSS- post induction in conventional w^{1118} flies.	44
Fig.3.3	Effect of 6- day recovery on the DSS-driven mortality.	45
Fig.3.4	Locomotor activity and sleeping behavior of female flies after DSS treatment.	46
Fig.3.5	Quantification of fecal spots and consistency after 6-day DSS treatment of female <i>Drosophila</i> .	48
Fig.3.6	Quantification of food consumption after 6-day DSS treatment of female <i>Drosophila</i> .	48
Fig.3.7	Characterization of weight-loss phenotype after 6-Day DSS treatment in female <i>Drosophila</i> .	48

Fig.3.8	Characterization of plasmatocytes migration phenotype in female <i>Drosophila</i> with GFP-labeled plasmatocytes 6-Day DSS treatment	49
Fig.3.9	Representative images of different grades of the gut leakiness in the DSS-treated group.	50
Fig.3.10	Representative images of DSS-induced Leaky gut.	51
Fig.3.11	Representative images show transmigration of luminal cargo labeled with different tracer in w^{1118} flies.	51
Fig.3.12	Representative Z-stacked images of dissected posterior midgut of w^{1118} flies in DSS and control groups after staining actin with Phalloidin-TRITC.	52
Fig.3.13	Representative images dissected posterior midgut of the How-Gla4>UAS-20xGFP flies in the DSS and control groups after immunostaining with GFP antibody.	52
Fig.3.14	Representative images of dissected posterior midgut of w^{1118} flies after immunostaining with anti-coracle antibody.	53
Fig.3.15	Representative Z-stack images of dissected posterior midgut of w^{1118} flies after immunostaining with anti-Discs large (Dlg) protein antibody.	53
Fig.3.16	Representative images of dissected midgut of esg-Gal4>GFP female <i>Drosophila</i> after immunostaining with anti-GFP antibody.	55
Fig.3.17	Representative images of dissected midgut of esg-Gal4>GFP male <i>Drosophila</i> after immunostaining with anti-GFP antibody.	55
Fig.3.18	Representative Z-stack images of dissected midgut of Su(H)GBE-Gal4>GFP female <i>Drosophila</i> .	56
Fig.3.19	Representative Z-stack images of dissected midgut of <i>DI</i> -Gal4>GFP female <i>Drosophila</i> .	56
Fig.3.20	Representative images of dissected gut of axenic esg-Gal4>GFP female <i>Drosophila</i> .	58
Fig.3.21	Representative images of re-colonizing total microbial community from conventionalized DSS-treated and untreated w^{1118} <i>Drosophila</i> donors to the germ-free esg-Gal4>GFP <i>Drosophila</i> recipients.	58
Fig.3.22	Representative images of dissected gut from Upd3-Gal4>LacZ <i>Drosophila</i> reporter line after x-Gal staining in DSS- treated and control groups.	60

Fig.3.23	Representative images of dissected gut from Upd3-Gal4 >GFP <i>Drosophila</i> reporter line after immunostaining with α -GFP Ab in DSS- treated and control groups.	60
Fig.3.24	Densitometric semi- quantification of the Upd3-GFP signals in the <i>Drosophila</i> Upd3 >GFP reporter line after immunostaining with α -GFP Ab in DSS- treated and control groups.	61
Fig.3.25	Effect of DSS treatment for 6 days on the transcriptional profile of candidate genes in the <i>Drosophila</i> anterior midgut.	62
Fig.3.26	Effect of DSS treatment for 6 days on the transcriptional profile of candidate genes in the <i>Drosophila</i> posterior midgut.	63
Fig.3.27	Effect of DSS treatment for 6 days on the transcriptional profile of candidate genes in the <i>Drosophila</i> hindgut.	64
Fig.3.28	Effect of DSS treatment for 12 days on the transcriptional profile of candidate genes in the <i>Drosophila</i> anterior midgut.	65
Fig.3.29	Effect of DSS treatment for 12 days on the transcriptional profile of candidate genes in the <i>Drosophila</i> posterior midgut.	66
Fig.3.30	Effect of DSS treatment for 12 days on the transcriptional profile of candidate genes in the <i>Drosophila</i> hindgut.	67
Fig.3.31	Volcano plot depicts the top 15 up-regulated genes in the <i>Drosophila</i> gut at day 6 and 12 post DSS treatment	68
Fig.3.32	Corrplot depicts the pairwise correlation between fold change of candidate transcript expression in different gut regions at day-6 post DSS treatment	69
Fig.3.33	Corrplot depicts the pairwise correlation between fold change of candidate transcript expression in different gut regions at day-12 post DSS treatment	70
Fig.3.34	Effect of 6-day recovery period after 6-day DSS treatment on the transcriptional profile of candidate genes in the <i>Drosophila</i> anterior midgut	71
Fig.3.35	Effect of 6-day recovery period after 6-day DSS treatment on the transcriptional profile of candidate genes in the <i>Drosophila</i> posterior midgut	72
Fig.3.36	Effect of 6-day recovery period after 6-day DSS treatment on the transcriptional profile of candidate genes in the	73

	<i>Drosophila</i> hindgut.	
Fig.3.37	Corrplot depicts the pairwise correlation between fold change of candidate transcript expression in different gut regions after 6-day recovery period.	74
Fig.3.38	Graphs depict multiple aspects of fecal microbiota community structure after 6-day post DSS treatment.	75
Fig.3.39	Graphs depict differentially abundant and discriminating taxa of fecal microbiota after 6-day post DSS treatment.	76
Fig.3.40	Graphs depict selected differentially abundant families, classes and microbial biomarker(s) of fecal microbiota after 6-day post DSS treatment.	77
Fig.3.41	A graphical display of correlations arrays across differentially-abundant taxonomic ranks of fecal microbiota and physiologic parameters after 6-day post DSS treatment.	78
Fig.3.42	Graphs depict multiple aspects of midgut microbiota community structure after 6-day post DSS treatment.	79
Fig.3.43	Graphs depict differentially abundant and discriminating taxa in the midgut microbiota after 6-day post DSS treatment.	80
Fig.3.44	Graphs depict selected differentially abundant families, classes and microbial biomarker(s) midgut microbiota after 6-day post DSS treatment.	81
Fig.3.45	Graphs depict multiple aspects of hindgut microbiota community structure after 6-day post DSS treatment	82
Fig.3.46	Graphs depict differentially abundant and discriminating taxa in the hindgut microbiota after 6-day post DSS treatment.	83
Fig.3.47	Graphs depict selected differentially abundant families, classes and microbial biomarker(s) of hindgut microbiota after 6-day post DSS treatment.	84
Fig.3.48	Graphs depict multiple aspects of fecal microbiota community structure after 12-day post DSS treatment.	85
Fig.3.49	Graphs depict differentially abundant and discriminating taxa of fecal microbiota after 12-day post DSS treatment.	86
Fig.3.50	Graphs depict differentially abundant and discriminating taxa of fecal microbiota after 12-day post DSS treatment.	87
Fig.3.51	Graphs depict multiple aspects of midgut microbiota community structure after 12-day post DSS treatment.	88

Fig.3.52	Graphs depict differentially abundant and discriminating taxa in the midgut microbiota after 12-day post DSS treatment.	89
Fig.3.53	Graphs depict selected differentially abundant families, classes and microbial biomarker(s) midgut microbiota after 12-day post DSS treatment	90
Fig.3.54	Graphs depict multiple aspects of hindgut microbiota community structure after 12-day post DSS treatment.	91
Fig.3.55	Graphs depict differentially abundant and discriminating taxa in the hindgut microbiota after 12-day post DSS treatment.	92
Fig.3.56	Graphs depict selected differentially abundant families, classes and microbial biomarker(s) of hindgut microbiota after 12-day post DSS treatment.	93
Fig.3.57	Graphs depict multiple aspects of fecal microbiota community structure after 6-day recovery period post 6-days DSS treatment.	94
Fig.3.58	Graphs depict selected differentially abundant families, classes and microbial biomarker(s) of fecal microbiota after 6-day recovery period post 6-days DSS treatment.	95
Fig.3.59	Graphs depict selected differentially abundant families, classes and microbial biomarker(s) of midgut microbiota after 6-day recovery period post DSS treatment.	96
Fig.3.60	Graphs depict multiple aspects of midgut microbiota community structure after 6-day recovery period post 6-days DSS treatment.	97
Fig.3.61	Graphs depict differentially abundant and discriminating taxa in the midgut microbiota after 6-day recovery period post 6-days DSS treatment.	98
Fig.3.62	Graphs depict selected differentially abundant families, classes and microbial biomarker(s) of midgut microbiota after 6-day recovery period post 6-days DSS treatment.	99
Fig.3.63	Graphs depict multiple aspects of hindgut microbiota community structure after 6-day recovery period post 6-days DSS treatment.	100
Fig.3.64	Graphs depict differentially abundant and discriminating taxa in the hindgut microbiota after 6-day recovery period post 6-days DSS treatment.	101
Fig.3.65	Graphs depict selected differentially abundant families, classes and microbial biomarker(s) of hindgut microbiota	102

	after 6-day recovery post 6-days DSS treatment.	
Fig.3.66	Graphs depict multiple aspects of male fecal microbiota community structure after 6-day DSS treatment.	103
Fig.3.67	Graphs depict differentially abundant and discriminating taxa in the male fecal microbiota after 6-day DSS treatment.	104
Fig.3.68	Graphs depict selected differentially abundant families, classes and microbial biomarker(s) of male fecal microbiota after 6-day DSS treatment.	105
Fig.7.1	Representative images of dissected gut of <i>w¹¹¹⁸</i> female <i>Drosophila</i> .	140
Fig.7.2	Representative images of dissected gut of DSS-treated <i>esg-Gal4>GFP Drosophila</i> .	140
Fig.7.3	Representative image of 2% agarose gel electrophoresis of 16s rRNA diagnostic PCR using 16SA1 and 16SB1 primers targeting 16s rRNA gene.	141
Fig.7.4	Representative MRS agar plate showing a growth of <i>Lactobacillus</i> sp as a viability indicator of microbial community preparations.	141
Fig.7.5	Prioritization of candidate septate junction genes, differentially expressed in the <i>Drosophila</i> gut.	142
Fig.7.6	Ecological distribution of major phyla in the <i>Drosophila</i> fecal, midgut tissue and hindgut tissue samples based on Illumina Miseq sequencing of the V1-V2 region the bacterial 16S rRNA gene.	146
Fig.7.7	Graphs depict a significant difference in community structure between fecal, midgut and hindgut tissue samples.	147
Fig.7.8	Image denotes AREsite2 graphical output of testing potential AU-rich elements in <i>Dlg1</i> gene	152

List of tables

	Description	Page
--	-------------	------

Table 1-1	Clinical and pathological features of UC and CD.	2
Table 2-1	List of laboratory equipments.	17
Table 2-2	List of chemicals and reagents.	19
Table 2-3	List of primary antibodies.	21
Table 2-4	List of secondary antibodies.	21
Table 2-5	List of molecular biology enzymes.	21
Table 2-6	List of oligonucleotides.	23
Table 2-7	Solutions and media.	24
Table 2-8	Fly lines used in the current study.	26
Table 2-9	Thermal cycling program for RT-qPCR.	37
Table 7-1	Cumulative death events induced by LG.	139
Table 7-2	A Summary of average fold change in transcript levels and corresponding significance.	142
Table 7-3	A Summary of average fold change in transcript levels in DSS- treated and recovery groups	144
Table 7-4	A Summary of % relative abundance of the major phyla in <i>Drosophila</i> fecal droppings, midgut tissue and hindgut tissue.	145
Table 7-5	Correlation coefficient r and significance of the fecal microbiota correlation matrix (Corrplot).	148
Table 7-6	A Summary of relative change in the <i>Drosophila</i> fecal microbiota abundance after 6-day and 12-day DSS treatment.	149
Table 7-7	A Summary of relative change in the <i>Drosophila</i> midgut microbiota abundance after 6-day and 12-day DSS treatment.	150
Table 7-8	A Summary of relative change in the <i>Drosophila</i> hindgut microbiota abundance after 6-day and 12-day DSS treatment.	151

1. Introduction

1.1 Inflammatory bowel diseases (IBDs)

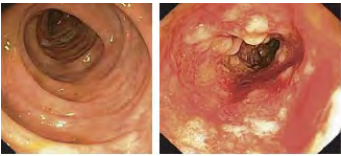
1.1.1 IBD Phenotypes, clinical manifestations and global burden

Crohn's disease (CD), ulcerative colitis (UC), and indeterminate colitis (IC) are summarized as inflammatory bowel diseases (IBD, OMIM 266600), which are characterized by inflammation and ulceration of either the mucosal layer only or with involvement of submucosal layers of the entire gastrointestinal tract or parts of it (Table 1-1). Classically, IBDs are defined as chronic, relapsing, complex immunologically mediated diseases [1], [2], [3].

Clinical symptoms of CD and UC comprise intestinal as well as extra-intestinal manifestations (EIMs). Intestinal manifestations include abdominal pain, chronic diarrhea with or without rectal blood and mucus in feces. Classically, the inflammatory response in CD attacks the entire intestinal wall of all parts of the digestive tract with subsequent perianal abscess and fistula formation and increased risk for intestinal carcinoma. In contrast, UC is a cyclical occurring disease that affects the lining of the rectum and colon with a variable degree of intensity presented as phases of exacerbation and remission [2], [4], [5], [6]. In principle, IBDs are systemic diseases, and their EIMs show that inflammation evoked in the gut may also affect multiple organs beyond the intestine, including mouth, eyes, skin, and the musculoskeletal, hepatobiliary and renal systems [7].

The incidence for IBD was traditionally highest in North America and Western Europe with a global increase over the second half of the twentieth century (Fig.1.1). The annual incidence of UC and CD in North America is reported to be 19.2 per 100,000 and 20.2 per 100,000, respectively. In Europe, the incidence is 0.6–24.3 per 100,000 and 0.3–12.7 per 100,000, respectively. In non-westernized nations (Asia and Middle East), the incidence of UC and CD is reported to be 6.3 per 100,000 and 5.0 per 100,000, respectively [3], [8], [9], [10].

Table 1-1: Clinical and pathological features of UC and CD.

	Ulcerative colitis (UC)	Crohn's disease (CD)
Transmural mucosal inflammation	No	Yes
Distorted crypt architecture	Yes	Uncommon
Cryptitis and crypt abscess	Yes	Yes
Granulomas	No	Yes, but rarely in mucosal biopsies
Fissures	Rarely	Common
Endoscopic characteristics (Adapted from Baumgart & Sandborn, 2007)[11]	 <p>(Left): Typical post-inflammatory changes (i.e. loss of fine vascular pattern). (Right): Pancolitis with irregular ulcers due to extensive ulcerations and haemorrhage.</p>	 <p>(Left): Friability of mucosa with erythema, loss of ramifying vascular pattern. (Right): Linear and serpiginous ulcers and patchy inflammation.</p>

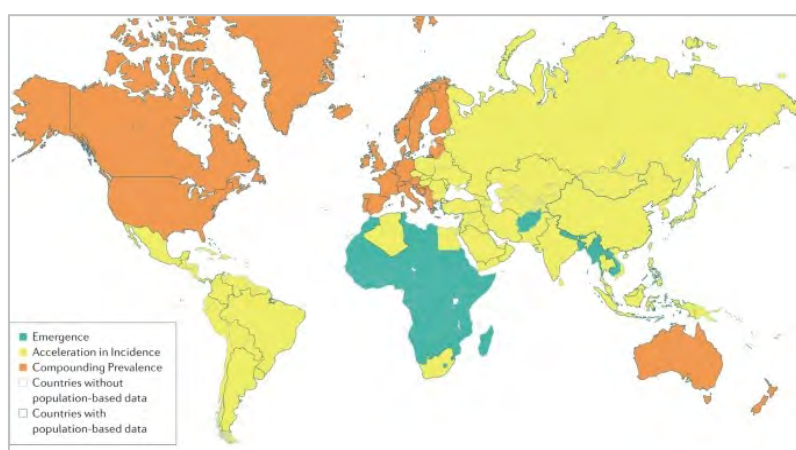


Fig. 1.1: Epidemiological stages of IBD (Adapted from Kaplan & Windsor, 2021) [9]

1.1.2 Etiology and pathophysiology of IBD

1.1.2.1 Risk factors of IBD

Inflammatory bowel diseases are reported to have unequivocal genetic contribution mediated through a set of risk genes/alleles that contribute to the aggressive altered immune response, which is also triggered by heterogeneous environmental factors under influence of the intestinal microbiome (Fig.1.2). Since these factors explain only a small fraction of the disease risk, prediction of response/relapse to treatment remains mostly elusive. It is evident that external factors play a crucial role in modifying the risk of IBD and in precipitating relapses in patients with established disease [12], [13].

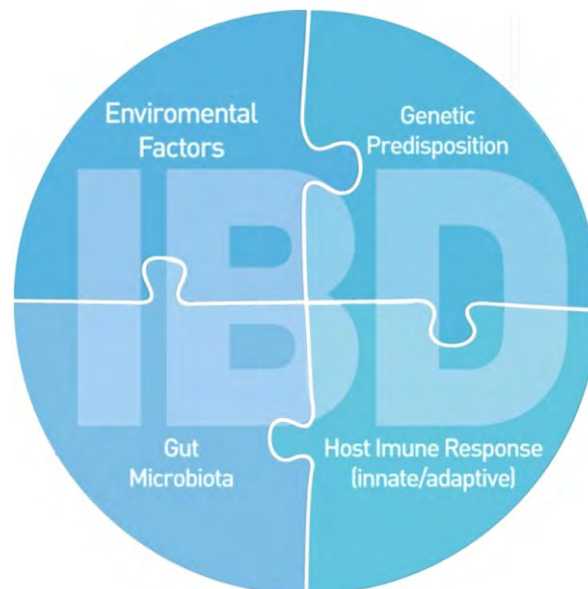


Fig. 1.2: Schematized correlation of main factors involved in the IBD pathogenesis. Each of the mentioned factors fit together as separate pieces of puzzle, together creating a complex clinical and pathological image of the IBD. (Adapted from Brajdić & Mijandrušić-Sinčić, 2012 [13]).

1.1.2.1.1 Genetics of IBD

Population-based genetic studies on IBDs demonstrated a marked concordance between twins, which is stronger for CD than UC. An increased risk (8- to 10 fold) of disease susceptibility was also reported among relatives of diagnosed patients [14],[15], [16]. Several multi-ethnic genome-wide association studies (GWAS)

reported a catalogue of IBD-associated single nucleotide polymorphisms (SNPs) of which the *NOD2*, *FUT2*, multiple autophagy-related genes (*IRGM*, *ATG16L1*, *ATG7*, *LRRK2*, *p62*, *optineurin* and *TFEB*) and autoimmune diseases-related genes (*IL23R* and *PTPN2*) are widely studied in the context of intestinal homeostasis and subsets of IBDs [17], [18], [19].

1.1.2.1.2 Microbiota in IBD

Microbial communities of the human gut are composed of 500-1000 resident species. The number of dominant species increases from the stomach to the colon due to gradient of mucus and pH (Fig.1.3). The highly dominating microbial phyla are Firmicutes, Bacteroidetes, Proteobacteria, and Actinobacteria [20]. Several studies reported the association of microbiota composition, diversity and colonization with multiple aspects of human health; such as physiological and metabolic homeostasis, and proper immune response [21], [22].

Association of substantial alteration of gut microbial communities (referred as 'dysbiosis') with both CD and UC has been reported either as a cause or consequence of host inflammatory responses. Bacterial dysbiosis has been reported for fecal and endoscopic brush (mucosa-associated) samples. Dysbiosis in IBD is more pronounced for CD than for UC and for inflamed versus non-inflamed tissues. It is characterized by a reduction in diversity of luminal microbial communities showing reduced abundance of Firmicutes and Bacteroidetes, whereas Proteobacteria are expanded. Furthermore, disordered interaction between the mucosa and microbiota also contributes to disrupted homeostasis in IBD [3], [23], [24], [25], [26], [27].

Metagenomic and metaproteomic studies provided compelling evidence of host-microbe interactions in IBD. Published data reported that 12% of all metabolic pathways were significantly altered in IBD, with a marked decrease in biosynthetic capacity for short chain fatty acids (SCFAs) biosynthesis, however showing increased propensity for managing oxidative stress [28], [29].

Functional studies on microbiome in IBD has informed further fecal bacterio-therapeutic strategies to restore microbial diversity using fecal material transferred from a healthy donor to IBD patient. Indeed, restoring functionality of dysbiotic microbial communities has shown to be highly efficacious in treating IBD [30], [31].

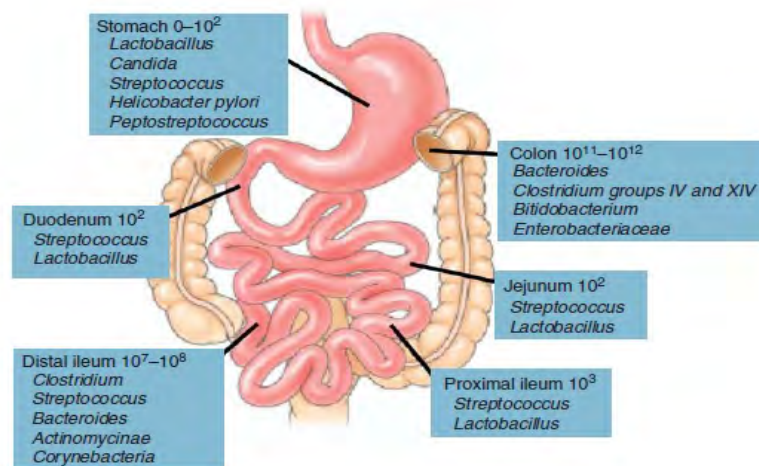


Fig. 1.3: Composition of dominant microbial community in the human GI tract IBD. (Adapted from Sartor & Mazmanian, 2012 [20]).

1.1.2.1.3 Environmental risk factors

Epidemiological studies showed that the prevalence of IBD dramatically increased in northern Europe, the United Kingdom and North America in the second half of the twentieth century and is also increasing in the rest of the world, proportionally to the adoption of a western lifestyle.

Many intervention studies reported improvement of disease severity after modifying environmental factors [3], [32]. Several studies have reported inverse association between smoking and UC but not with CD [34], [35], [36]. Recent metagenomic study on experimental colitis revealed that positive effect of smoking on gut microbial ecology and resolution of inflammation [37].

Most epidemiological studies of diet and IBD reported an inverse association between long-term fiber intake and the risk of Crohn's disease with emphasis on soluble fiber (from fruits and vegetables). Soluble fiber is metabolized by the intestinal bacteria to SCFAs that confer protective effect by maintaining the integrity and permeability of the epithelial barrier [38], [39], [40], [41]. Moreover, dietary fat

particularly the milk-derived saturated fats reported to be associated with the severity of IBD. High consumption of omega-6 PUFA and low consumption of n-3 PUFA has been associated with an increased risk of both CD and UC, which is attributed to the blooming of a pathogenic, sulfite-reducing member of the Deltaproteobacteria [42], [43].

1.1.3 Experimental models of intestinal inflammation and IBD

Rodents have given a supreme position as a classical model system for human disease owing to multiple similarities at the behavioral, anatomical, physiological and histological levels. More recently, other vertebrates and invertebrates model organisms (such as *Danio rerio*, *Drosophila melanogaster*, and *Caenorhabditis elegans*) have been introduced as a human disease models due to their advantages in terms of small body size, reduced breeding costs, affordable transgenesis, accessibility for live imaging, chemical library drug screens as well as production of germ-free animals for studying host-microbiota interaction [44], [45], [46].

Successful development of a number of in vivo models of experimental colitis has dramatically increased in recent years including signaling molecule-deficient animals. Although none of these models exactly mimics all pathologic aspects of the disease, they have proven to recapitulate IBD-like symptoms at the immunologic and molecular levels [46], [47], [48], [49].

Most of the models of experimental colitis were developed to study the etiology of IBD by recapitulating the acute phase of intestinal injury; however, other models focused on the chronic phase to evaluate disease [50], [51].

Chemically-induced colitis models include treatment with haptening substances in ethanol such as trinitrobenzene sulfonic acid (TNBS) and oxazolone, whereas dextran sulfate sodium (DSS) is applied to induce both acute and chronic colitis. Moreover, models of inflammation-associated colorectal carcinoma is established by combined effect of a single dose of the colon carcinogen azoxymethane (AOM) followed by induction of chronic colitis by DSS. Models of TNBS and oxazolone colitis have been proved useful in studying the role of T helper cell-dependent mucosal immune responses in the development of colitis; however, they have limitations such as strain-dependent optimization and inapplicability in other invertebrate model organisms [52], [53].

1.1.3.1 DSS-induced colitis

Oral administration of DSS of molecular weight (36,000-50,000 Da) in drinking water is proven to reproducibly induce experimental colitis after several days. Animal model of DSS colitis has multiple advantages including *ad libitum* delivery via drinking water, induction of consistent colitis with a defined disease onset and quantifiable phenotypic readouts. Furthermore, lack of involvement of adaptive immune response in the acute phase of DSS colitis broadens the application of DSS to study the role of innate immune mechanisms of colitis [51], [54], [55], [56]. By contrast, the main drawback of DSS colitis model is the heterogeneous response to DSS in terms of susceptibility, onset, and severity [57].

Increased intestinal permeability is the hallmark acute DSS colitis. Bloody diarrhea, ulcerations and infiltrations with granulocytes followed by increased mortality have been widely reported as severe symptoms of colitis [47]. It is extensively reported that DSS has a direct toxic effect on the intestinal epithelial cells of the basal crypts, hence compromises the integrity of the mucosal barrier [49] as depicted in (Fig. 1.4).

The toxic effect of DSS on colonic epithelia and barrier integrity is attributed to its high content of negatively- charged sulfate groups. Recent report suggested that DSS forming nanolipocomplexes with medium-chain-length fatty acids in the colon; however the underlying mechanism of transcellular permeability induction remains elusive [49], [58]. Interestingly, development of DSS colitis is associated with dysbiosis. Taxonomic and functional metagenomic analyses revealed reduced microbial diversity with metabolic shift towards high metabolic activity for fatty acid biosynthesis, pyruvate metabolism, and lysine degradation [59], [60].

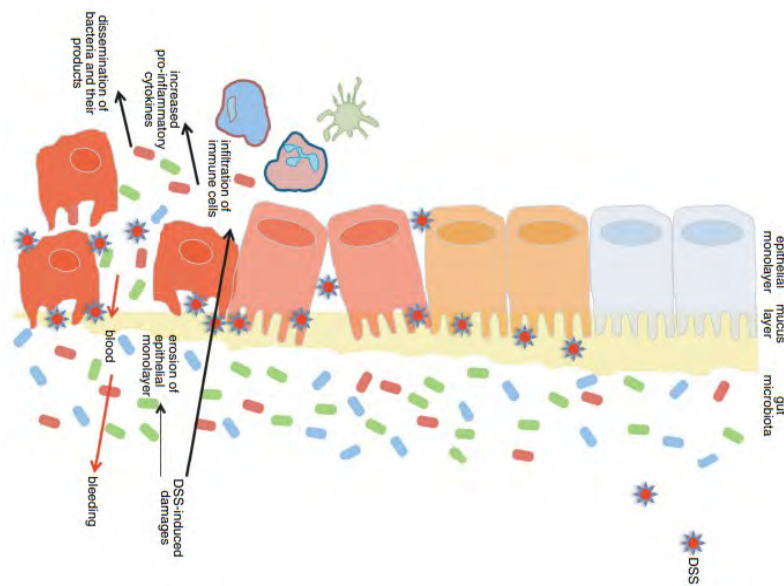


Fig. 1.4: Schematic representation of the toxic effect of DSS on the intestinal epithelium. (Adapted from Chassaing et al., 2014 [49])

1.2 *Drosophila* as a model of human gastrointestinal disease(s)

1.2.1 Translational impact of *Drosophila* in human biology and medicine

The fruit fly *Drosophila melanogaster* (henceforth *Drosophila*) has been widely-recognized as one of the most-prominent model organisms and used successfully to study multiple aspects of human developmental and evolutionary biology at both the basic and translational levels. Such agreeable appreciation is attributed to several reasons: as two-thirds of all human disease-causing genes have *Drosophila* orthologs; as striking multiple homology between flies and vertebrates (including humans) is obvious at the level of organismal behavior and (patho) physiology, structure and function of internal organs/ tissues, signal transduction and metabolic pathways; as forward and reverse genetics are generally easier to perform, *Drosophila* system have powerful functional readouts; as cost-effective, feasible experimental tractability and simple gnotobiology are advantageous in flies; as the fast expanding and dynamic inter- and multi-disciplinarily fly community is accumulating various genetic tools and assays that opens the doors for development of in vivo chemical screening platforms [61 — 70]. Furthermore, the availability of annotated genomes, transcriptomes and microbiomes as well as the presence of various databases and query tools has placed the *Drosophila* research at the forefront [71].

1.2.2 Impact of *Drosophila* genetics on translating human GWAS-reported genes and drug discovery

Human GWAS have been successful in identifying risk loci associated with disease condition, but do not typically identify specific causative genetic elements. Some of the discovered genes are evolutionary conserved throughout evolution [72], [73]. *Drosophila* transgenesis proves an exciting tool in testing whether a candidate gene is likely to be functionally linked to the corresponding human disease. This valuable framework aids in filtering/prioritizing the enormous data generated by genomics [74]. Interestingly, feasibility of manipulating diet in *Drosophila* provided an effective whole animal pre-clinical model for identifying therapeutically useful compounds [73], [75].

1.2.3 The *Drosophila* is an effective model in interrogating host-microbiota interactions

Recently, the holobiont concept has adopted to study the interactions between host's ecosystems and the associated microbial communities in the context of health and in disease [76]. Interestingly, research on host-microbiota interactions (HMIs) has emerged as a cross-disciplinary field. Experimental studies on model and non-model organisms are indispensable to understand the crosstalk between the host and the microbiota, and may provide opportunities to modulate the complex microbiome in different experimental settings [77], [78], [79], [80]. In the *Drosophila* gut, the most prevalent microbiotas are reported to be affiliated with the phyla Firmicutes and Proteobacteria and the related families Acetobacteraceae, Lactobacillales, and Enterobacteriaceae [77], [81]. Application of gnotobiotics in *Drosophila* experimental research (such as germ-free, conventional or mono- or bi-association with defined microbial communities) paved the way for establishing high-throughput *in vivo* platform for functional profiling of microbiota communities as well as investigating prebiotics and probiotics [81], [83], [84].

1.2.4 Feasibility of ectopic gene expression using the *Drosophila bipartite* GAL4–UAS system

One of the exciting advantages for using *Drosophila* as research model is the availability of powerful binary GAL4/UAS system. It is designed to allow ectopic over-expression or silencing a (cloned) gene of interest in different spatial and temporal patterns (Fig. 1.5). In brief, the two essential components, GAL4 and UAS are separately inserted into two transgenic fly lines. On one hand, the GAL4 gene is under the control of an endogenous gene promoter creating a driver line. On the other hand, a gene of interest is introduced under the control of upstream activating sequence (UAS) to create a responder line. Importantly, both units have no effect on the host organism. Upon crossing the driver GAL4 line with the responder UAS line, the progeny has the gene of interest expressed in a cell-specific or tissue-specific manner [85], [86], [87].

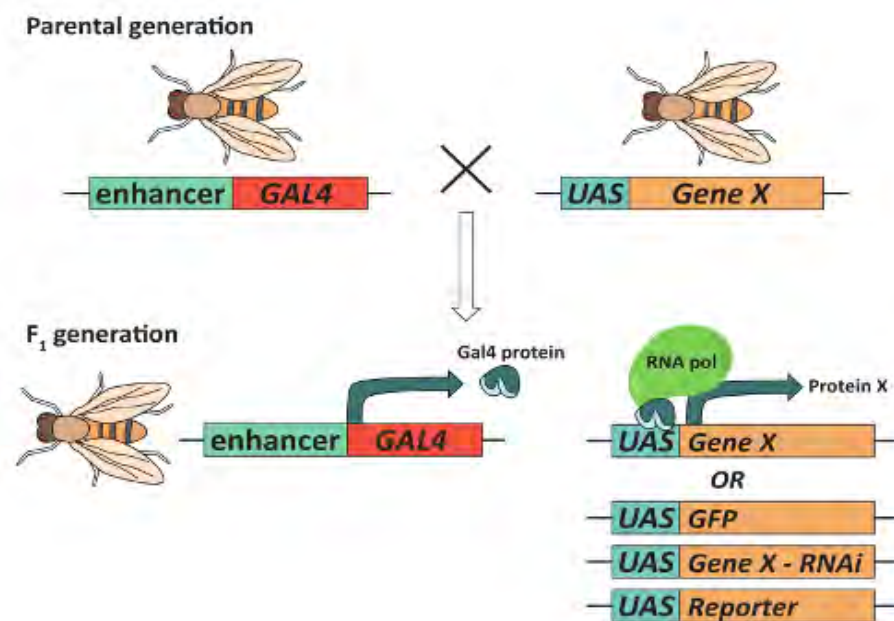


Fig. 1.5: Schematic representation of GAL4/UAS system (Adapted from Kelly et al., 2017 [81]).

1.2.5 The *Drosophila* is an effective model of human intestinal pathology

The fruit-fly *Drosophila melanogaster* has been proven as a powerful model for studying intestinal pathology. In contrast to the *in vitro/ ex vivo* systems, *Drosophila* suited for the manipulating multiple signaling components in the gut milieu. The striking anatomical and histologic similarities between the human GI tract and fly gut helps several research on intestinal stem cell physiology during stress, infection and aging (Fig. 1.6) [88],[89], [90], [91].

1.2.6 Anatomy and Physiology of the *Drosophila* gut

Formerly, it was believed that *Drosophila* adult gut is composed of three main regions: the foregut, the midgut and the hindgut. It is evident that the fore- and hindgut have an ectodermal origin, whereas the midgut has an endodermal origin. Unlike the mammalian system, the Malpighian tubules in flies connect the gut at the midgut-hindgut junction to release urine into the hindgut gut [92]. It was recently reported that the *Drosophila* midgut consists of five morphologically and functionally distinct regions (Fig.1.7), named R1-R5. Those sub-regions are separated by anatomical boundaries to form physiologically and transcriptionally-defined compartments [89],[93],[94],[95], [96].

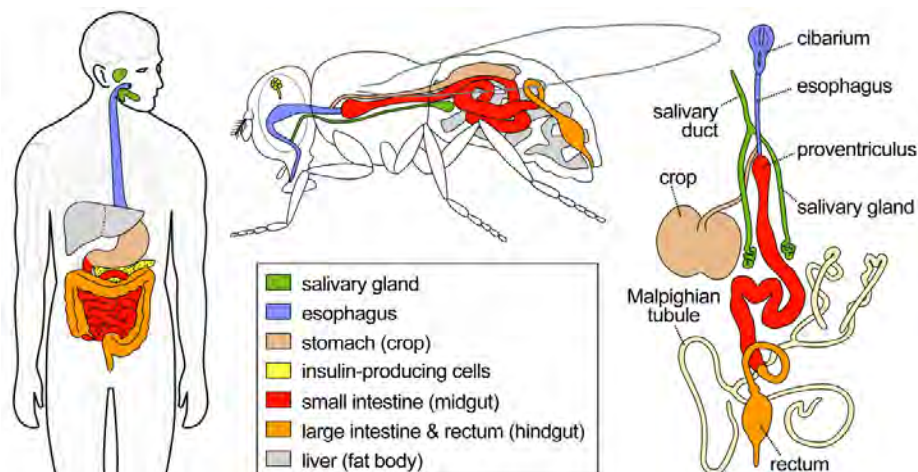


Fig. 1.6: Anatomical description of homology between human (left) and fly (right) digestive tract. Colors indicate functionally related structures of the Gut (Adapted from Andreas Prokop <https://droso4schools.wordpress.com/organs/>)

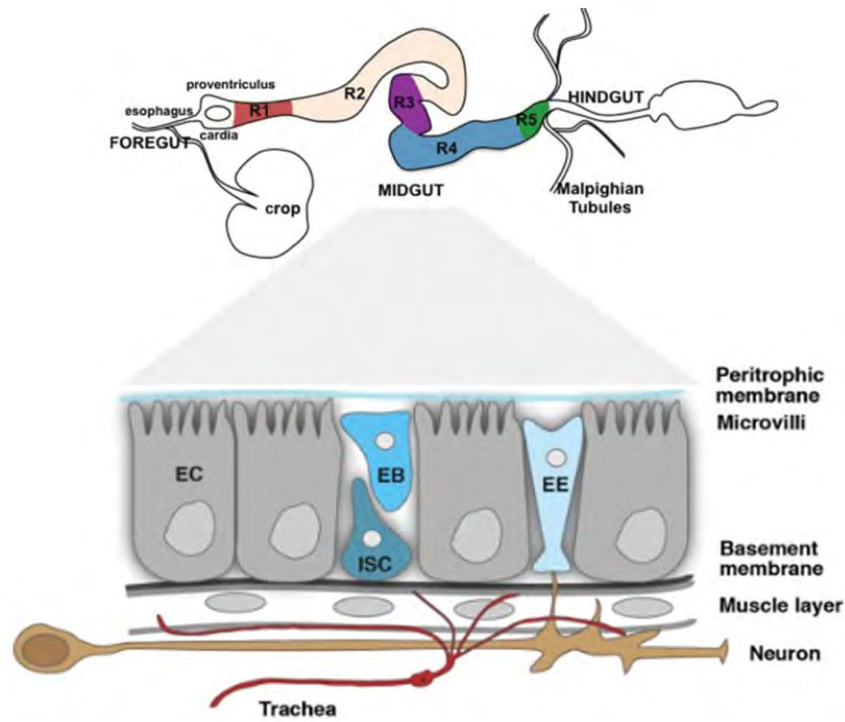


Fig. 1.7: (A) Diagrammatic representation of the adult *Drosophila* gut regions, R1–R5: regions of the FG: foregut, MG: midgut, HG: hindgut (Adapted from Dutta et al., 2015) [94]. (B) Midgut cell-types, EC: enterocyte; EB: enteroblast; ISC: intestinal stem cell; EE: enteroendocrine (Adapted from Miguel-Aliaga et al., 2018 [96]).

1.2.7 Evolutionary conservation of cellular junctions between the *Drosophila* and vertebrates

In principle, an intestinal epithelium requires neighbouring cells to interact via intercellular junctions to ultimately form a physical barrier. This requires tight junctions to form the border between the apical and basolateral plasma-membrane domain. The intact semipermeable paracellular diffusion barrier is instrumental in protection of the bodies' internal milieu from luminal microbes and their related antigenic products; transport of macromolecules across the epithelial cell layer; and formation of signalling hubs that control cell behaviour and differentiation [97], [98],[99]. Adherens junctions of vertebrates and *Drosophila* share evolutionary conservation in composition and function. Other elements of epithelial junctions have some differences in organization (Fig. 1.8). The *Drosophila* junctions (Adherens and septate) are controlled by protein complexes that assemble around transmembrane proteins or associate with the plasma membrane such as *Drosophila* (DECad); kune-kune (kune), sinuous (sinu); polychaetoid (pyd), discs

large 1 (dlg1), Crumbs, and Neurexin IV [100], [101], [102]. Interestingly, increased barrier permeability and barrier dysfunction in the *Drosophila* are routinely assessed by administration of non-absorbable dye with monitoring of gut leakiness, referred to as “Smurfs” phenotype [103], [104]

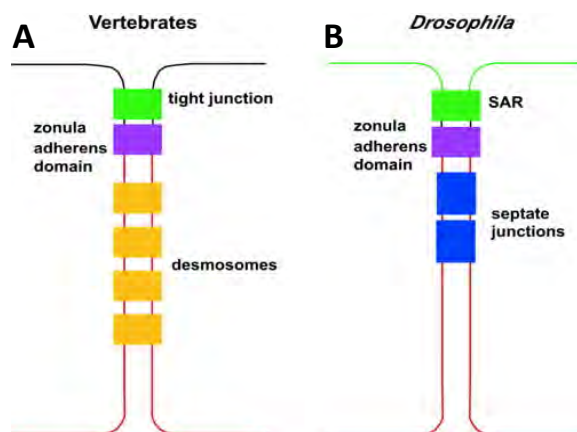


Fig. 1.8: Diagrammatic representation of the organization of epithelial junctions in vertebrates **(A)** and *Drosophila* **(B)** shows localization of molecular domains of different junctions at the apical–basal axis: sub-apical (SAR) regions, adherens domain, septate junction (SJ). (Adapted from Lynch AM& Hardin, 2009 [100]).

1.2.8 Evolutionary conservation of core components of the JAK/STAT pathway between *Drosophila* and vertebrates

Regenerative inflammation of the damaged gut epithelium is reported to be driven by a multiple signaling of homeostatic turnover and injury repair across the intestinal microenvironment. It requires multiple interactions between different *Drosophila* gut cells, mainly the intestinal stem cells (ISC) as a driver of repairing cascade. A harmonic involvement of other cells such as enterocytes (EE), enteroendocrine (EE) visceral muscle (VM) and basement membrane (BM) is reported as well [105], [106].

There is an obvious conservation between the *Drosophila* and the mammalian JAK/STAT pathway and their functioning in inducing localized and systemic immune immunity as well as tissue growth and maintenance. In humans, the four JAKs (JAK1, JAK2, JAK3 and TYK2) and seven STATs (STAT1, STAT2, STAT3, STAT4, STAT5A, STAT5B and STAT6) mediate responses to a number of ligands such as cytokines and interferons. Interestingly, the *Drosophila* JAK/STAT pathway has

similar essential signalling components with less redundancy (Fig. 1.9). The *Drosophila* JAK/STAT ligands consist of only three cytokine-like proteins called unpaired (upd), upd2, and upd3 cytokines [107], [108], [109].

1.2.9 *Drosophila* Plasmatocytes are functional homolog of vertebrate macrophages

The *Drosophila* hemocyte lineages give rise to plasmatocytes (>90%), which function as primary phagocytic cells; crystal cells, which function in melanization-mediated wound healing and clotting and; and lamellocytes, which function in encapsulation. Interestingly, plasmatocytes are functionally analogous to vertebrate leukocyte/ macrophages, whereas immune challenge-induced lamellocytes are analogous to granuloma formation in vertebrates [110], [111], [112], [113]. The intestinal macrophages are instrumental in maintaining the *Drosophila* gut homeostasis both under physiologic and stress conditions. They play a central role in innate immunity, producing antimicrobial peptides and pro-inflammatory mediators, phagocytosis of pathogens and apoptotic cells. They function also to control tissue regeneration by regulating stem cell proliferation and differentiation. Under conditions of tissue damage, they migrate to reside and deposit extracellular matrix (ECM) components such as Collagen IV within the injured tissue [114], [115], [116], [117], [118].

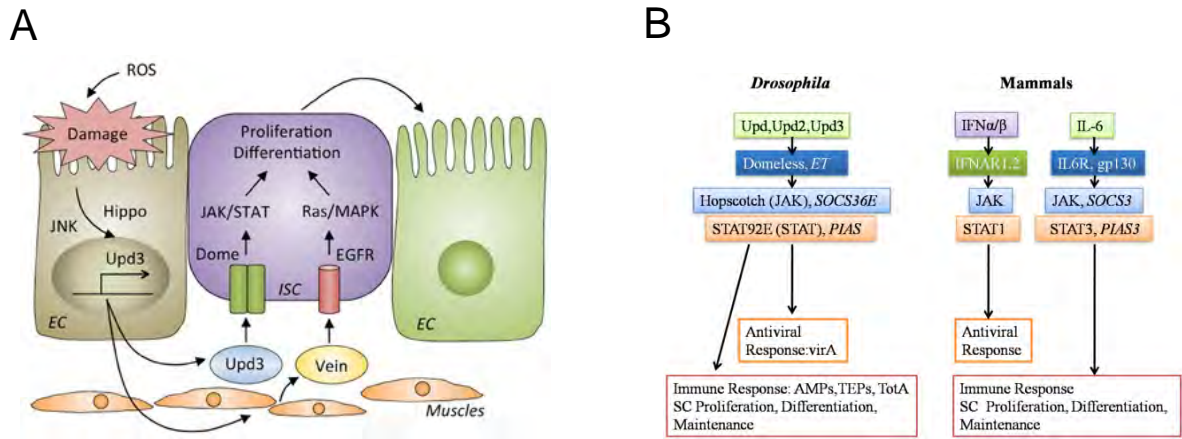


Fig. 1.9: (A) Diagrammatic representation of interaction network in the damaged gut epithelia and induced signalling cascade. (B) Conservation and commonalities between the *Drosophila* and the mammalian JAK/STAT (Adapted from Kuraishi et al., 2013 [108]; Panayidou & Apidianakis, 2013 [109]).

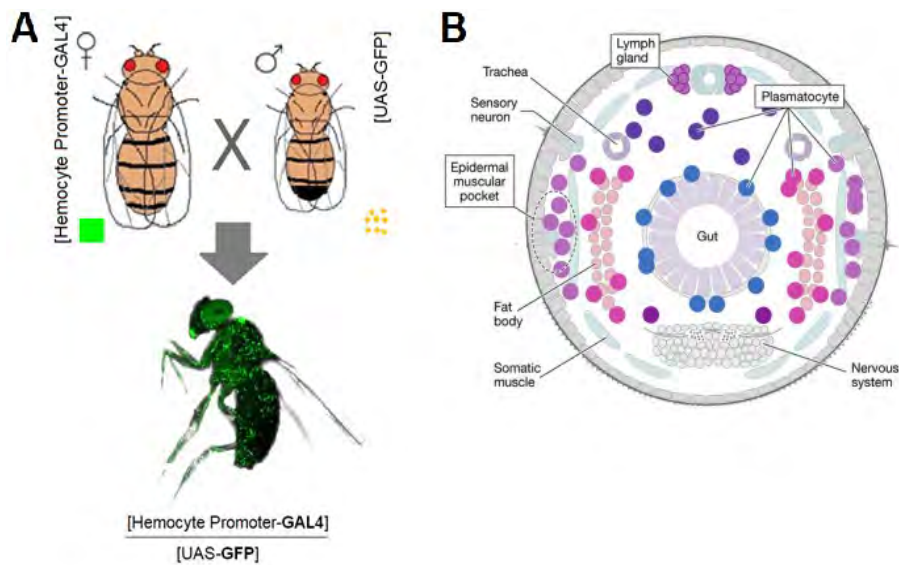


Fig. 1.10: (A) A scheme depicts F1 generation of crossing a hemocyte-specific expression (*hemolymphin* gene, *Hml*) with GFP-UAS-2xGFP (Adapted from Leitão, 2009 [116]; Woodcock et al., 2015 [117]). (B) Cross-section of the *Drosophila* larva represents different localizations of plasmatocytes subsets: associated with the gut and other organs or circulating in the hemolymph (Adapted from 2020 [118]).

1.3 Aim of the study

The aim of the current study was threefold:

- To establish the *Drosophila* model of DSS-induced colitis with subsequent systematic phenotyping.
- To study spatiotemporal effects of DSS on expression of the candidate genes in the gut
- To study spatiotemporal effects of DSS on the microbial ecology of fecal and tissue-associated microbiota in terms of community structure and composition.

2. Materials and Methods

2.1 Materials

All fly disposables were supplied by Greiner Bio-One GmbH, Frickenhausen, Germany. Components of nutrient media, materials were obtained from local suppliers. Plastic ware in forms of Petri dishes, Falcon tubes, Pipette tips were supplied by Nerbe Plus, Winsen/Luhe. Sterile cotton swabs were purchased from Greiner Bio One, Germany. Blotting paper 330g/m² was purchased from A. Hartenstein GmbH for Laboratory Equipment Supplier, Würzburg, Germany.

2.1.1 Laboratory equipments

Low- and Medium-throughput instruments were supplied by in the departmental and institutional facility. MiSeq Sequencing platform was operated at the core facility lab at center of molecular biology (ZMB) Kiel. All equipments used for this study are listed in Table 2-1.

Table 2-1: List of laboratory equipments

Item	Manufacturer (location)
Agarose gel electrophoresis unit	Biometra GmbH, Göttingen, Germany
Analytical balance ABS	Kern & Sohn GmbH, Balingen-Frommern
Autoclave Steam Sterilizer Varioklav [®]	H+P Medizintechnik GmbH, Oberschleisheim, German
Balance MXX-412	Denver Instruments, New York, USA
Bead Ruptor 24	Omni International, Kennesaw, GA, USA
Binocular	Nikon, Düsseldorf, Germany
Capillaries 0,5 µl	Paul Marienfeld GmbH, Lauda-Königshofen, Germany
Casting system compact	Biometra, Göttingen, Germany
Centrifuge, 5415 D; rotor: F45-24-11	Eppendorf, Hamburg, Germany
Centrifuge 5417 R, rotor FA-45-30-11	Eppendorf, Hamburg, Germany
Centrifuge: Heraeus Fresco 17	Thermo Electron LED GmbH, Osterode am Harz, Gern
Centrifuge: Sproud	Heathrow Scientific [®] , Illinois, USA.

DeNovix Ds-11 Spectrophotometer	DeNovix Inc. Wilmington, USA
DNA ladder (GeneRuler 1Kb)	Fisher Scientific, Darmstadt, Germany.
Dry block & heat bath HB-130	UniTek Industrie Elektronik GmbH, Leutenbach, Germany
<i>Drosophila</i> Activity Monitor (DAM) with Data Acquisition Software	Trikenetics, Waltham, USA
Electrophoresis power supply, EV245	Consort, Parklaan, Belgium
Electrophoresis power supply, EV202	Consort Parklaan, Belgium
Flourescence microscope Axio Imager.Z1 with Axiocam MRM, ApoTome	Zeiss, Oberkochen, Germany
Imager FLA-5000	Fujifilm, Tokyo, Japan.
Incubation shaker, Heidolph Unimax 1010	Heidolph Instruments GmbH, Schwabach, Germany.
Lab guard ES Class II Safety Cabinet	IBS Integra Biosciences, Biebertal, Germany.
Leica TCS SP3 confocal Microsystems	Leica, Heidelberg, Germany
Microscope SZX12 + camera DP 71, Olympus	Olympus GmbH, Hamburg, Germany.
Molecular Imager Gel Doc system	Bio-Rad, Munich, Germany
Nanodrop ND-1000 spectrophotometer	Peqlab, Erlangen, Germany
Omni Bead Ruptor 24	Omni International Inc, Kennesaw, USA
pH meter, model 330	Wissenschaftlich-Technische Werkstätten GmbH Weill Germany
Platform Shaker MR Hei-Standard MR 3001	Heidolph, Schwabach, Germany
Savant DNA Speed Vac [®] DNA 120	Fisher Scientific, Darmstadt, Germany
StepOne Real-Time-PCR System	Applied Biosystems, Darmstadt, Germany
Syringe filters, Minisart [®] sterile	Sartorius AG, Göttingen, Germany.
Table autoclave Omni Perfect	Beem [®] , Rosbach, Germany
Thermal cycler	Sensoquest, Göttingen, Germany
Ultraviolet Sterilizing PCR workstation	Peqlab Biotechnologie GmbH, Erlangen, Germany.
Water bath, thermostat 2761	Eppendorf, Hamburg, Germany

2.1.2 Chemicals

All chemicals used for this study are listed in Table 2-2. All fine chemicals were purchased with high quality or HPLC- / molecular biology grade (for molecular biology experiments), unless stated otherwise.

Table 2-2: List of chemicals and reagents

Chemicals	Manufacturer (Location)
1 kbp-GeneRuler™	Fermentas, St. Leon-Roth, Germany.
50 bp-GeneRuler™	Fermentas, St. Leon-Roth, Germany.
Acetic acid	Carl Roth, Karlsruhe, Germany.
Agarose	Biozym Scientific GmbH, Hessisch Oldendorf, Germany.
Bacto™ Yeast Extract	BD Diag, Maryland, USA.
Blue and red food dye	Ruth, Bochum, Germany.
Chloroform	Carl Roth, Karlsruhe, Germany.
DAPI	Invitrogen, Darmstadt, Germany.
Dextran sulfate sodium salt (36,000-50,000 M.Wt.) Colitis Grade, Lot No. Q5930.	MP Biomedicals, Santa Ana, CA, USA
Dideoxynucleotide set	Promega, Mannheim, Germany.
Ethanol	Carl Roth, Karlsruhe, Germany.
Ethidium bromide	AppliChem, Darmstadt, Germany.
Ethylene diamine tetraacetic acid	Carl Roth, Karlsruhe, Germany
Fluorescein sodium salt (fluorescent tracer)	Sigma-Aldrich, Steinheim, Germany
Glucose monohydrate	Carl Roth, Karlsruhe, Germany
Glycerol	Carl Roth, Karlsruhe, Germany
Glycogen	Sigma-Aldrich, Steinheim, Germany
Goat serum	Sigma-Aldrich, Steinheim, Germany
Isopropyl alcohol	Carl Roth, Karlsruhe, Germany
LB agar	Carl Roth, Karlsruhe, Germany

LB medium	Carl Roth, Karlsruhe, Germany
Materpure DNA extraction Kit	Epicentre, Madison, USA
Methanol	Carl Roth, Karlsruhe, Germany
MRS Broth Difco™	BD Diagnostic Systems, USA
Nipagin	Carl Roth, Karlsruhe, Germany
Paraformaldehyde	Sigma-Aldrich, Steinheim, Germany
phalloidin –TRITC	Sigma-Aldrich, Steinheim, Germany
Phenol red	Sigma-Aldrich, Steinheim, Germany
Phenol Red Mannitol Broth	BD Diagnostic Systems, USA
Potassium chloride	Merck group, Darmstadt, Germany.
potassium dihydrogen phosphate	Carl Roth, Karlsruhe, Germany
potassium dihydrogen orthophosphate	Carl Roth, Karlsruhe, Germany
Probionic acid	Carl Roth, Karlsruhe, Germany
RNAmagic	Bio-Budget, Kredeld, Germany
RNAsecure™ RNase Inactivation	Thermo Fisher Scientific, Langenselbold, Germa
Schneider's <i>Drosophila</i> Media	Thermo Fisher Scientific, Langenselbold, Germa
SuperScript IV First-Strand Synthesis	Thermo Fisher Scientific, Langenselbold, Germa
Sodium chloride	Carl Roth, Karlsruhe, Germany
Sodium hydroxide	Carl Roth, Karlsruhe, Germany
sodium hypochlorite	Carl Roth, Karlsruhe, Germany
SYBR® Green	Invitrogen, Darmstadt, Germany
Tween 20	Sigma-Aldrich, Steinheim, Germany
Triolein	Sigma-Aldrich, Steinheim, Germany
Tris-(hydroxymethyl)-aminomethane (Tris)	Carl Roth, Karlsruhe, Germany
Triton X-100	Sigma-Aldrich, Steinheim, Germany
Triglyceride assay kit	Thermo Fisher Scientific, Langenselbold, Germa
Washing Buffer for IHC	Aptum Biologics Ltd., Southampton, UK
Yeast extracts	Carl Roth, Karlsruhe, Germany

Water ROTISOLV® HPLC Gradient Grade	Carl Roth, Karlsruhe, Germany
-------------------------------------	-------------------------------

2.1.3 Antibodies

Antibodies used for immunostaining are listed in Table 2-3 for primary antibodies and Table 2-4 for secondary antibodies. Antibodies were stored at -80°C freezer as glycerol stocks (1:1).

Table 2-3: List of primary antibodies

Antibodies	Source	Working dilution
Mouse α -coracle	Developmental studies Hybridoma Bank, Iowa, IA	1:200
Mouse α -dlg	Developmental studies Hybridoma Bank, Iowa, IA	1:500
Rabbit α -GFP	Developmental studies Hybridoma Bank, Iowa, IA	1:500

Table 2-4: List of secondary antibodies

Antibodies	Source	Working dilution
Goat α -mouse Dylight 549	Jackson ImmunoResearch Lab	1:500
α -mouse Alexa Flour 555	Life Technologies, Darmstadt	1:500
Goat α -rabbit Dylight 488	Jackson ImmunoResearch Lab	1:1000

2.1.4 Enzymes

Antibodies used for metabolic assays and molecular biology experiments are listed in Table 2-5.

Table 2-5: List of molecular biology enzymes

Item	Supplier
Taq DNA Polymerase (5 U/ μ l)	Invitrogen, Darmstadt, Germany
DNAse	Thermo fisher scientific, Waltham, MA, USA
Lysozyme from chicken egg white	Sigma-Aldrich, Steinheim, Germany
Proteinase K	Thermo fisher scientific, Waltham, MA, USA

RNase inhibitor (40U/μl)	Invitrogen, Darmstadt, Germany
SuperScript™IV Reverse transcriptase	Invitrogen, Darmstadt, Germany

2.1.5 Bacterial strains

Wild-Type *E. coli* BW25113 transformed with either two plasmids that constitutively express the ampicillin resistance gene *bla*, together with either pJBA24-eglp24 or pJBA24-mCherry was gifted by Dr. Christian Kost, at the Department of Ecology, School of Biology/ Chemistry, University of Osnabrück, Germany.

2.1.6 Oligonucleotides

Oligonucleotides used in qRT PCR assays were either designed using Primer3 freeware (v. 0.4.0) or obtained from published reports (Clark RI et al., 2015 for qRT-PCR assays) with further check using corresponding gene sequences retrieved from flybase and mapping with SerialCloner freeware (v. 2.6.1). Primers listed in Table 2-6 and were obtained from Eurofins MWG Operon ILC and life Technologies GmbH, Darmstadt Germany.

2.1.7 Solutions and media

All buffers were prepared using deionized water, filtered through an ion-exchange unit (Membra Pure) followed by sterilization by steam autoclave run at 120° C for 15 minutes (Table 2-7). Heat-sensitive media was sterilized by 0,2 micron filter.

Table 2-6: List of oligonucleotides

Gene annotation	Primer ID	Sequence (3'→5')	coordinates
Dmel_ CG12051	<i>Actin42A_F</i>	CTCATCGAACACACCCATTG	1449
	<i>Actin42A_R</i>	TTCTGAAGGAGCGGAAGTGT	1533
Dmel_ CG12055	<i>Gapdh-1_F</i>	CAGTGCTGGAGCCGAGTATGTGG	517
	<i>Gapdh-1_R</i>	TGCACGAGGCGTTGGAGACC	691
Dmel_ CG4651	<i>RpL13_F</i>	CAGGCATGCGAACCGCGTCAA	421
	<i>RpL13_R</i>	GCAATGCCGATGGTCTTGGCGA	649
Dmel_ CG7939	<i>RpL32_F</i>	CCGCTTCAAGGGACAGTATC	582
	<i>RpL32_R</i>	GACAATCTCCTTGCGCTTCT	758
Dmel_ CG33542	<i>Upd3_F</i>	GAGAACACCTGCAATCTGAA	2574
	<i>Upd3_R</i>	AGAGTCTTGGTGCTCACTGT	2850
Dmel_ CG15154	<i>Socs36E_F</i>	GAGATCCTCACAGAGGCCACT	10029
	<i>Socs36E_R</i>	GCGAAACTTCCACCTGACC	10140
Dmel_ CG3722	<i>DEcad_F</i>	GACGAATCCATGTGCGAAAA	1325
	<i>DEcad_R</i>	TCACTGGCGCTGATAGTCAT	2511
Dmel_ CG14779	<i>Pck_F</i>	GCTCTCGCTTACCATCATCC	844
	<i>Pck_R</i>	TACGGCCAAAAACATGAACA	996
Dmel_ CG1298	<i>Kune_F</i>	AGGTTGTGGGCTCTGTTTTTC	498
	<i>Kune_R</i>	ATCCCGAGAATCTCCTTTGG	546
Dmel_ CG10624	<i>Sinu_F</i>	CATTGAATTGCATAAACTTCAGCTA	1780
	<i>Sinu_R</i>	GCGGAGTTTCGCTTACCTT	1854
Dmel_ CG43140	<i>Pyd_F*</i>	TGAATCGAGAGGCAACTTCTT	92813
	<i>Pyd_R*</i>	TTCTCGCGGGACAGACTC	92946
Dmel_ CG1725	<i>DLg1_F</i>	AGAGTCGCGATGAGAAGAATG	29117
	<i>DLg1_R</i>	GCTGGTGCTGCTCACAACCT	30104
Dmel_ CG10810	<i>Dro_F</i>	ACCAAGCTCCGTGAGAACCTT	36
	<i>Dro_R</i>	TTGTATCTTCCGGACAGGCAG	144
Dmel_ CG10146	<i>Attacin_F</i>	AGGAGGCCCATGCCAATTTA	419

	<i>Attacin_R</i>	ATTCCTGGGAAGTTGCTGTG	574
16S rRNA gene (diagnostic PCR)	16SA1	AGAGTTTGATCMTGGCTCAG	Ref. [120]
	16SB1	TACGGYTACCTTGTTACGACTT	
16S rRNA gene (ROI: V1-V2 region Illumina MiSeq)	27F	AGAGTTTGATCCTGGCTCAG	Ref. [121]
	338R	GCTGCCTCCCGTAGGAGT	

Table 2-7: Solutions and media

Medium	Composition
<u>A) Buffers for routine use</u>	
10 x PBS (pH 7.4)	1,37 M NaCl 2,7 M KCl 65 mM Na ₂ HPO ₄ 15 mM KH ₂ PO ₄
HL3 (pH 7.2)	70 mM NaCl 5 mM KCl 1,5 mM CaCl ₂ 20 mM MgCl ₂ 20 mM Glucose 10 mM NaHCO ₃ 5 mM Trehalose 115 mM Saccharose 5 mM HEPES
10 x TBE	0,89 M TRIS 0,89 M bor acid 2 mM (Na ₂)-EDTA
6x DNA loading dye (pH 8.0)	50% (v/v) glycerol 60 mM EDTA 6% SDS 0.9% bromophenol blue

<u>B) Standard I(rearing) fly medium</u>	
Nutrients	1 % agar-agar 6.25 % cornmeal 6.25 % yeast 2 % glucose 3 % molasses 3 % sugar beet syrup 3 % nipagin (10 % v/v) 1 % propionic acid (10 % v/v)
Nipagin stock solution in 70% ethanol	10% (w/v)
Propionic acid in H ₂ O	10% (v/v)
<u>C) Experimental liquid fly medium</u>	
	5% Yeast extract 10% Glucose monohydrate
	Gut flushing solution (10% Glucose in H ₂ O)
<u>D) Solutions for Immunohistochemistry</u>	
PFA	4% (w/v) dissolved in 1 x PBS, heated at 60- under stirring overnight then cooled down to then 0,3% Triton X-100 was added.
PBT	0,1 % (v/v) Tween-20 in 1 x PBS
Normal goat serum (NGS)	10 % (v/v) in PBT
<u>E) Media for bacterial cultivation</u>	
Lysogeny broth (LB) medium (pH 7.4)	1 % (w/v) tryptone 0.5 % (w/v) yeast extract 1 % (w/v) NaCl
MRS medium	5.5% (w/v) in H ₂ O 1.5% agar
Phenol red Mannitol medium	2% (w/v) in H ₂ O 1.5% agar
<u>F) Solution for bacterial DNA extraction</u>	
STET buffer (1X), pH 8.0	100mM NaCl 10mM Tris-HCl 1mM EDTA 5% Triton X-100 (v/v)

2.1.8. *Drosophila* stocks

Fly lines were usually obtained from the Bloomington stock centre listed in Table 2-8. Stocked flies were raised on standard medium kept at 25°C with 50%-60% relative humidity under a 12 h light/dark cycle.

Table 2-8: Fly lines used in the current study

Stock ID/ genotype	References
<i>w</i> ^[1118]	BDSC_5905
Oregon-R-C	RRID:BDSC_5
Canton-S	BDSC_64349
<i>upd3-Gal4;UAS-GFP</i>	Ref. [122]
<i>YW; esg-Gal4, UAS-GFP/CyO</i>	Ref. [123]
<i>P{UAS-Cameleon.2.1}82</i>	BDSC_6901
<i>DI-Gal4, UAS-CD8-GFP</i>	Ref. [124]
<i>Su(H)GBE-Gal4</i>	Ref. [124]
<i>Amon-Gal4</i>	Ref. [125]
<i>how-Gal4</i>	Ref. [126]
<i>Hml-Gal4, UAS-2xEGFP</i>	BDSC_30140; Ref. [116], [127]
<i>UAS-lacZ P{w[+mC]=UAS-lacZ.Exel}21; 3</i>	Bloomington stock #3956
<i>Upd3-Gal4</i>	BestGene

2.2 Methods

2.2.1 *Drosophila* standard and experimental media

Standard fly media is composed of 15.6 % Brewer's Yeast, 15.6 % cornmeal, 1% agar powder 2% glucose, 3% molasses and 3% syrup. The media was allowed to dissolve in hot sterile water and boiled for 15 minutes. Once the media cooled down to reach 40 °C, 3% nipagin and 1% propionic acid were added as preservatives. Experimental diet is composed of 10% Bacto™ Yeast Extract and 5% sucrose.

2.2.2 *Drosophila* husbandry and experimental condition

Adult flies were raised on standard medium-containing vials kept in temperature-controlled climate chamber set at 25°C, 50%-60% relative humidity under a 12 h light/dark cycle. Newly hatched flies were reared at a standard density (up to 100) and allowed to mate for at least five days. Sex-Sorted flies were allowed to adapt on experimental diet for 2 days at density of 20-25 flies/ vial.

2.2.3 *Drosophila* GAL4/UAS crossing

For crossing, 5-15 virgin females of the UAS strains and corresponding GAL4 males in a ratio 1:2 - 1:3 were used. Using the temperature-sensitive Gal4-tubGal80ts/ UAS system, gene expression for the F1-generation was temporarily controlled by keeping larval-adult stages at 17°C until induction of expression at 30°C was performed two days before experiments. Furthermore, F1-generation of crossing with RNAi-UAS lines was kept at 30°C at least three days before experiments and experiments were maintained at such higher temperature.

2.2.4 Induction of gut inflammation by Dextran sulfate sodium

Dextran sulfate sodium salt (DSS) with M.wt. 36-50 KDa, was added to the media in a final concentration of 5% (w/v). Flies were fed 5% DSS in medium *ad libitum*.

2.2.5 Characterization of DSS-induced colitis-like phenotype

2.2.5.1 Survival analysis

One-hundred flies were split into 4 biological replicates; each was kept at a density of 25 flies per vial. After synchronization of test or control fly cohorts by two-hour starvation, flies were allowed to access to the DSS-supplemented media or normal media, respectively. Alive Flies were transferred to fresh media -containing vials every three days. Dead flies were, however, removed from the experiment. Data recorded as percentage of living flies counted every 24 hours. Survival analysis of Kaplan-Meier estimate was applied to DSS vs. mock-treated fly cohorts.

2.2.5.2 Determination of total activity

Activity of flies was monitored using the *Drosophila* Activity Monitoring System (DAM2 System). Fly cohorts were split 32 biological replicates for each treatment group. A single fly was transferred to each glass tubes (2.5 cm × 12.5 cm) containing diet to be housed in climate chamber for twelve-fifteen days at 25°C, 50 - 60% relative under a 12 h light/dark (LD) cycle condition. In principle, DAM file scan software records sum of movement for flies automatically every 2 min during the testing period. Fly activity is expressed as arbitrary units representing the number of events in which each fly was able to cross an infrared beam. Fly activity is expressed as arbitrary units (AU) representing the number of events in which each fly was able to cross an infrared beam. Activity results were presented as mean total activities per day. Results were presented as total activities per fly per day. Checking for outliers was performed by applying Grubbs' test.

2.2.6 Determination of Cumulative Food Consumption and Excretion

2.2.6.1 Determination of food consumption

The Capillary Feeder (CAFE) assay was performed with modification of the originally-published method [128]. Briefly, a hole was drilled in the cap of plastic tube (84×30 mm) to fit a 100 μ L-sized pipette tip. The tip was inserted to act as a gentle holder for the glass capillary. Plastic tubes were drilled to form five small holes (smaller than the fly body size), which aim at equilibrating the inside (tube) and outside (temperature/humidity) environment, in turn decreasing loss in the liquid food. Capillary tubes were filled with experimental liquid fly medium with the capillary action. The capillary tube filled with the colored liquid food is inserted vertically inside the tube through the plastic holder. One side of the capillary is facing flies, while the other side is outside the tube. Since experiment was carried out in 12/12 h (day/night) regime at 25°C with 60% relative humidity, a drop of a mineral oil was added to the outer side of the capillary to minimize potential evaporation (Fig. 2.1). For obtaining a reasonable effect size, number of biological replicates was not set below 10/ treatment groups with extra 2 blank tubes without flies that served as evaporation controls. In order to avoid type II error (false-negativity), all fly cohorts were allowed to pre-acclimatize in the CAFE tubes on normal media 1 day before the planned experiments and they were also synchronized by fasting for 2 hours before the planned experiments. All measurements and calculations were made according to the original protocol.

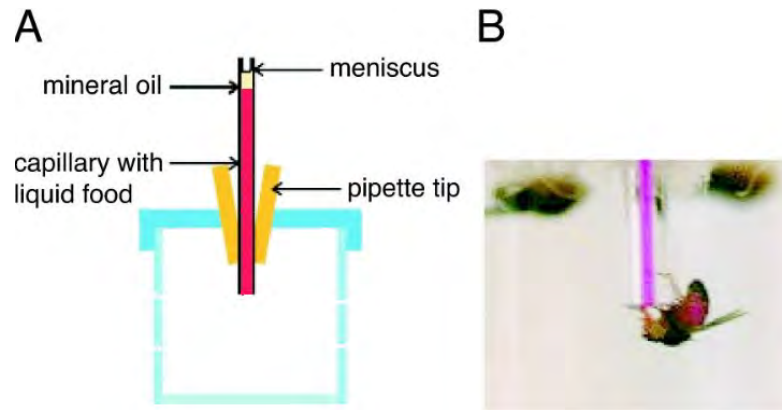


Fig. 2.1: Schematic diagram illustrating the set up of CAFE assay. **(A)** Liquid food, topped with an oil layer to minimize evaporation. **(B)** A Fly approaches the capillary to feed on a red-dyed liquid food. The dye has a dual role: to roughly ensure the food consumption by monitoring the fly proboscis / abdominal coloration and to accurately calculate the food consumption by measuring the volume consumed at the end of the experiment. (Modified from Ja et al., 2007 [128]).

2.2.6.2 Egestion rate

A small piece of normal media supplemented with 2.5% (w/v) (f.c. 0.5%) Brilliant Blue FCF food dye (E133, Ruth, Bochum, Germany) was transferred as a cube (0.6 mm²) to the bottom of a polystyrene Petri dish (35 mm diameter, 10 mm height). Five biological replicates with N=10 flies/replicate were incubated at 25 °C for 12 hours (day cycle) after pre-acclimatization and synchronized fasting (on 2% agar) in similar conditions for 2 hours. Total number of fecal spots was counted manually three times (to avoid observer bias) for each petri dish considering all spots on the bottom, side and lid. Normalization of fecal spot counts was done by dividing the average of spot counts by number of flies. Final results were expressed as 'egestion rate' - fly spots/ fly/ hr - and analyzed statistically by considering two-tailed test.

2.2.6.3 Quantification of fecal consistency and luminal content

Fecal deposits left on the petri dishes were solublized with 200 µl PBS pre-heated at 90 °C then diluted up to 300 µl, and further vortexed and heated at 90 °C for 5 min. Solution was homogenized with bead rupture S=3:25, T=1min, 3 pause. Undigested food debris was sedimented by centrifugation at 12K rpm for 5 min and volume was checked and equalized to 500 µl. A volume of 50 µl was applied on 96 well plate for absorbance measurement at 630nm. Standard curve was managed

by 1:1 dilution starting with Blue dye concentration of 1 mg/ml (1000 $\mu\text{g/ml}$). Giving that the molar mass of blue dye is 792.85 g/mol, results were expressed as concentration ($\mu\text{M L}^{-1}$)

2.2.7 Measurement of body weight

Flies were collected in groups of five (per vial) to be starved under non-dehydrating conditions for one hour. Each group was anaesthetized on ice and weighed to 0.1 mg accuracy with an analytical balance. Unless otherwise stated, each fly group was homogenized in 1X PBS using bead rupture for 2 minutes, centrifuged at 14K rpm for 1 minute with further heat-inactivation of endogenous enzymes at 70 °C for 5 min. Supernatant was transferred to fresh 1.5 eppendorf and stored at -20 for spectrometric determination of multiple total body metabolites.

2.2.8 Body fat quantification:

Total triacylglycerols (TAGs) was measured using the coupled colorimetric assay (CCA) as described previously [129]. Flies grouped into 8 biological replicates (per treatment group). Five flies from each replicate were homogenized in 1X PBS containing 0.05% Tween-20 using a bead Ruptor 3.25 m/s for 2 minutes followed by heat-inactivation of endogenous enzymes at 70 °C for 5 min. Supernatant was transferred to fresh 1.5 eppendorf and stored at -20 for spectrometric determination of targeted analytes. Triolein (40 μg) was diluted in a series of 2-fold dilution was used as TAG standard for setting up standard curve. 50 μl of samples/ blank was pipette in technical duplicates into a 96 well microtiter plate. 200 μl of pre-warmed triglyceride reagent was added into each well and incubated at 37°C for 30 min with mild shaking. Then the absorbance was read at 540 nm using spectrophotometer. Value of TAG was normalized to mg fly wet weight and expressed as μg TAG equivalents. Final results were expressed as total fat (Glyceride) in μg / female fly wet weight (in μg).

2.2.9 Characterization of barrier dysfunction”leaky gut” phenotype

Fly medium containing 0.5% f.c. blue food dye (FD& C Blue Dye no. 1) and fluorescent tracer, sodium fluorescein (NaFl), were used to prove translocation of dietary content from the fly lumen to the hemocele. For testing the hypothesis of potential translocation of gut-associated microbe, fly medium was supplemented with wild-Type *E. coli* BW25113 transformed with pJBA24-egfp24 and pJBA24-mCherry plasmids with bacterial density (OD600=1).

2.2.10 Immunohistochemistry and microscopy

Adult *Drosophila* was dissected in Sylgard dish containing Schneider medium. The entire gastrointestinal tract was dragged from the anal pad following the published protocol [130]. Dissected gut was fixed over night in 4% PFA at 4° C. After three rinses in PBT buffer the tissue was blocked in 10% NGS for 30 minutes at room temperature with mild shaking. Gut specimens was incubated with primary antibody overnight at 4° C. In the next day, gut specimens was rinsed three times in PBT followed by addition of secondary antibody with overnight incubation at 4 C. In all tissue samples, nuclei were stained with DAPI and mounted with 80 % glycerol in PBS. All antibodies and their dilutions used for immunohistochemistry purposes are listed in Tables 2-3 and 2-4. For staining with Phalloidin-TRITC, fixed gut tissues were washed and incubated with dye (1: 100) in 1X PBS for 15 min. with further washing 3 times with 1X PBS. Microscopic analysis was performed either with an Olympus SZX12 stereomicroscope, equipped with an epifluorescence support, or with the Zeiss Axio Imager Z1. For Z-projections the ApoTome was used and the intestines were stacked in 2 µm slices. Captured images were analysed using CellSens, and/or AxioVision Rel4,8.

2.2.11 Relative Quantification of Immunofluorescence image

Dissected gut specimens were processed according to standard immunostaining protocol (mentioned previously). Mounted gut specimens were examined by fluorescence microscopy with multiple filters for DIC, DAPI and GFP. All GFP images were captured using Axio Imager Z1 with identical exposure time and

analyzed with similar parameters using ImageJ2 [131]. Corrected integrated density of multiple ROI was calculated using the formula: corrected integrated density = Integrated Density - (Area of selected cell X Mean fluorescence of background readings).

2.2.12 β -galactosidase staining

Adult *Drosophila* gut tissues were dissected in PBS then fixed for at least 15 - 20 min in 0.125% gluteraldehyde fixation solution followed by successive rinsing for 3 times for 5 min with 1xPBS. The tissues were transferred in pre-warmed (37°C) staining solution where X-Gal was added [132]. Tissues were incubated at 37°C in the dark (with shaking, if possible) for 2 hours with periodic monitoring of color reaction till sufficient intensity of blue staining is observed with no/ less background (detailed reaction mechanism of lacZ staining is depicted in (Fig. 2.2 [133]). Color reaction was stopped when the desired signal is obtained by washing in 1x PBS twice for 10 min each at room temperature. All tissues were mounted in 80% glycerol for microscopic examination.

2.2.13 Establishment of axenic (Germ-free) fly culture

In principle, two cardinal steps for establishing long-term microorganism-free fly line should be considered: dechoriation and sterilization of embryo with diluted hypochlorite bleach followed by transfer to a sterile diet. In the current study, 100 females were allowed to lay eggs for overnight. Eggs collected by paintbrush into a cell strainer soaked in a petri-dish filled with 1X PBS. The procedure was shifted to UV-sterilized biosafety cabinet where sterile media is placed. Eggs were dechoriated in two rounds of in 6% hypochlorite solution (2.5 minutes each) followed by two consecutive rinsing steps in 1X PBS. Sterilized eggs (40-50 eggs per vial) were transferred to a sterile media using a sterile paintbrush. Importantly, parallel establishment of conventionalized was performed by transferring non-dechoriated eggs to vials containing sterile media. Testing for microbiota-free condition has to be confirmed by diagnostic 16S rRNA PCR (amplicon size is approximately 1.5 kb [120]. at 37 °C for 48 hours. An additional biological replicate was left for periodic checking for germ-free condition during the experimentation period. The rest of the fly cohort was reared on sterile media until the time of experimentation.

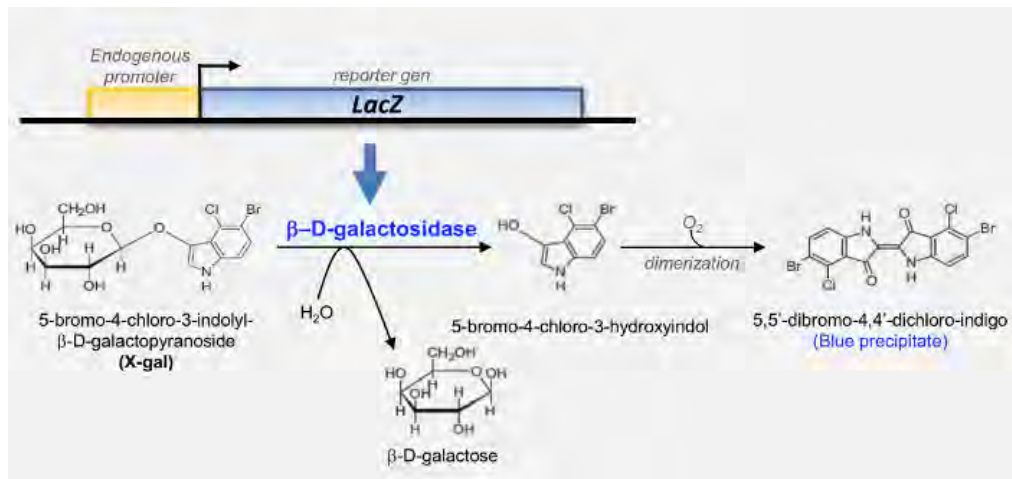


Fig.2.2: Schematic illustration of the E. coli LacZ reporter gene encoding for the β -galactosidase staining. In optimal staining condition, a substrate 5-bromo-4-chloro-3-indolyl- β -Dgalactopyranoside (X-gal) is hydrolyzed by β -galactosidase to form an intermediate (5-bromo-4-chloro-3-hydroxyindole) which dimerizes upon oxidation to form the final blue-colored product (5,5'-dibromo-4,4'-dichloro indigo). (Adapted from Blanco et al., 2018 [133]).

2.2.14 Preparation, storage and re-colonization of total microbial community

The experiment was designed to include 3 groups each include a cohort of 30 flies divided into 3 biological replicates. The groups were assigned to be the DSS-treated *Drosophila* at day 6 post treatment, the DSS-treated *Drosophila* at day 12 post treatment as well as one corresponding non-treated control at day 12. In a sterile vial, 30 adult female flies were collected randomly from each treatment groups, anesthetized on ice and exposed to body sterilization with 6% hypochlorite solution (2.5 minutes each) followed by two independent rinsing steps in 70% ethanol and autoclaved 1X PBS. Flies were collected in sterile screw-capped tubes containing pre-autoclaved ceramic beads and 0.7 mL autoclaved 1x PBS and undergone 1 cycle of gentle homogenization for 30 seconds at 3.25 m/s speed using Bead Ruptor 24 followed by low-speed centrifugation at 800 \times g for 3 minutes. Gut microbiota suspension (450 μ L) was mixed with equal volume of autoclaved 1x PBS, 0.15 ml autoclaved glycerol followed by gentle vortexing. Microbiota suspension was aliquoted in 3 cryo plastic tubes and stored at -80 $^{\circ}$ C. Each aliquot 350 μ l was thawed on ice immediately before use and mixed with equal volume filtere-sterilized 10% sucrose (2X) colored with 1% (f.c) brilliant Blue dye (dissolved in 1% PBS). Axenic flies were fed on autoclaved filter paper soaked with the blue-colored

microbiota-sucrose suspension. Frequent replenishment of microbiota suspension was performed by thawing another aliquot every other day in order to sustain microbial colonization. Viability of bacterial suspension (i.e. the presence of *Lactobacillus sp.* as indicators) after a single freezing-thawing event was checked by plating 100 μ L of the microbiota suspension on MRS agar plate at 37 °C for 48 hours.

2.2.15 Isolation of DNA-free RNA from fly gut tissues

Adult *Drosophila* was dissected in Sylgard dish containing Schneider medium. The entire gastrointestinal tract was dragged from the anal pad. For RT-qPCR, five independent biological replicates were prepared for each treatment groups. Each gut tissue was further dissected and collected in separate tubes (three tubes per biological replicate) as anterior midgut (AMG), posterior midgut (PMG), or hindgut (by removing anal pad and Malpighian tubules). Dissection was done in solution containing Schneider's medium supplemented with RNasecure™ (f.c.1X) pre-activated at 60 °C for 15 minutes. Fifteen dissected tissues from each gut region were collected in screw-capped tubes containing ceramic beads and 1 ml RNAmagic® solution. Two cycles of homogenization for 2 min at 3.25 m/s speed were performed using Bead Ruptor 24. An optimized protocol of extraction of a high yield, inhibitor-free and DNA-free RNA was conducted using RNAmagic® reagent with the PureLink® RNA Mini Kit combined with on-column DNase treatment protocol. Homogenized specimens in the form of tissue lysate were kept at room temperature for 5 minutes followed by addition of 0.2 mL chloroform with immediate vigorous shaking by hand for 15 seconds. Specimens were incubated at room temperature for 2–3 minutes followed by centrifugation at 12,000 \times g for 15 minutes at 4°C. A volume of 400 μ L of the upper phase was transferred to a fresh RNase-free tube containing an equal volume 70% followed by gentle inversion for 15-20 times. Less than 700 μ L of the RNA aggregate was transferred to a spin cartridge (with a Collection Tube). Routine mandatory steps of centrifugation at 12,000 \times g for 15 seconds at room temperature followed by discarding the flow-through and reinsertion of the collection tube were performed for Binding, Washing, and Elution (referred hereafter as “routine mandatory step”). A volume of 350 μ L of the wash buffer#1 was added to the spin cartridge containing the bound RNA followed by the

routine mandatory step. A volume of 80 μL of the PureLink® DNase mixture containing (8 μL of 10X DNase I buffer, 10 μL of DNase ($\sim 3\text{U}/\mu\text{L}$) and 62 μL of RNase-free water) was added to the spin cartridge containing the bound RNA. After incubation at room temperature for 15 minutes, another 350 μL of the wash buffer#1 was added followed by the routine mandatory step. A volume of 500 μL wash buffer#2 (diluted with ethanol) was added followed by the routine mandatory step. A volume of 25 μL of RNase-free water was pipetted onto the center of the spin cartridge reinserted into a fresh recovery tube followed by centrifugation at $12,000 \times g$ for 15 seconds at room temperature. RNA preparations were stored at -80°C .

2.2.16 Nucleic acid Quantification and purity measurement

Isolated DNA and RNA were assessed using Nanodrop for measuring concentration and different quality indices (A260/A280; A260/A230).

2.2.17 Agarose gel electrophoresis

Agarose gel electrophoresis was used for analytical and preparative purposes. For a casting gel, 1-2 % (w/v) agarose was dissolved by heating it in a microwave oven in 1 x TBE buffer and supplemented with 3 μL ethidium bromide. The DNA samples, mixed with 5x DNA loading buffer, were loaded into the wells. DNA size standards (100 bp or 1 kb ladder) were run in parallel. Electrophoresis was performed at a constant voltage of 100 V for 45–60 min, depending on the desired resolution. For the purposes of documentation, DNA bands were visualized under UV light (312 nm) and gels were photographed using the gel imaging system.

2.2.18 Establishment of RT-qPCR assay, QC, and data analysis.

The reverse transcriptase polymerase chain reaction (RT-PCR) was used to test the expression of different genes in the *Drosophila* gut. In brief, cDNA synthesis was performed using SuperScript IV First-Strand Synthesis System. PCR amplification was carried out using Taq DNA polymerase in a total volume of 25 μL and the gene specific primers were used for PCR. The RT-qPCR for relative quantitative PCR was performed using StepOnePlus™ Real-Time PCR System. The total volume of 10 μL each reaction was loaded into 48 wells plate which consists of 5 μL SYBR

Green MasterMix, 0.25 μ l ROX, 0.5 μ l forward primer (5 μ M), 0.5 μ l reverse primer (5 μ M), 1 μ l cDNA (50 ng). Reaction condition and thermal cycling program are depicted in (Table 2-9).

In a preliminary test, the primer efficiencies for both gene of interest and reference were analyzed basing on the standard curve and the slope, which was derived from five serial dilutions of cDNA from 50 ng to 3.12 ng. The primer efficiencies were calculated according to the formula $E=10^{-1/\text{slope}}$ [134]. Multiple internal control genes were checked for stability using the NormFinder formula [135]. In the current study, the *Gapdh-1* was served as a reference gene for all assays. Relative expression ratio (fold change) of a target gene was determined based on the Ct values in comparison to a reference gene. A list of candidate genes related to the studied phenotype was selected for gene expression analysis. It includes 3 categories; genes regulating the *Drosophila* septate junction (*DEcad*, *Dlg1* and *Kune-kune*); genes regulating regenerative inflammatory signaling and ISCs proliferation (*Upd3* and *Socs36E*), as well as genes regulating antimicrobial defense and gut-microbiota interactions (*Drosopmycin* and *Attacin*). Each dataset contains a normalized delta-Ct value (Ct “target gene” - Ct “*Gapdh-1*”) for DSS-treatment group at day 6, day 12 post DSS treatment as well as after 6-day recovery period on normal media. Also, datasets were grouped according to the analyzed gut regions (anterior midgut “AMG”, posterior midgut “PMG” and hindgut “HG”. Since the datasets are two-dimensional addressing spatio-temporal effect of DSS, comparison of relative abundance of the candidate genes was disentangled into 2 levels: the time of DSS treatment and the impact of DSS on gut regions. Relative fold change in transcript abundance was calculated after normalization using the equation $2^{-\Delta\Delta\text{Ct}}$ method (I.e. ΔCt of DSS treatment - ΔCt controls). Volcano plot was also used to identify meaningful changes within a large data set by plotting the \log_2 of the fold change in gene expression on the x-axis versus statistical significance ($-\log_{10}$ p-value) on the y-axis.

Table 2-9: Thermal cycling program for RT-qPCR.

Step	Temperature	Time	Cycle number
cDNA master mix	65°C	5 min	
cDNA synthesis	25°C	10 min	
	50°C	20 min	
RT inactivation	80°C	10 min	
Taq activation	95°C	10 min	
Denaturation	95°C	15 sec	40
Primer annealing	60°C	20 sec	
Elongation	72°C	35 sec	
Hold	4°C	∞	

2.2.19 Bacterial DNA isolation from tissue and fecal samples

For extraction of DNA from fecal material, fly cohorts were split into three biological replicates per treatment group. A hundred flies were transferred to clean UV-sterilized plastic vials and allowed to drop fecal material on the plastic surface of the vial for 24 hours at standard fly husbandry conditions. Fecal spots were wiped out using sterile cotton swabs pre-wetted with sterile STET buffer. Each fecal material-loaded swab was cut to allow the cotton part releasing the adsorbed contents in sterile screw-cap tubes containing 500µL STET buffer. After vortex-shaking using a horizontal module for 30 minutes, a volume of 500µL fecal wash was transferred to a fresh screw-capped tube containing ceramic beads.

For gut tissues, adult flies soaked in 2% hypochlorite then washed two times with dist. H₂O followed by two times 70% ethanol and finally allowed to dry briefly on autoclaved filter paper. Dissection was done on glass slide using sterilized forceps. Dissected fly guts (whole midguts and hindguts; 15-20 per replicate) were collected in a tube contains 300µL STET buffer. Disruption of cell walls of gram-positive bacteria was performed using bead rupture for 2 minutes at power 3.25 for either fecal samples or tissue specimens, followed by brief centrifugation for 1 minute at 14K rpm.

For adult flies, 10 flies were collected in a sterile screw-cap tube containing 500µL STET buffer. Flies were undergone the same protocol of frass-loaded swabs.

Once bacterial cell lysate was made ready for DNA extraction, 25µL of lysozyme was added with further incubation at 37°C for 30 minutes together with mild shaking to ensure complete disruption of bacterial cell wall.

DNA extraction protocol was conducted following the instruction of Materpure DNA extraction Kit (fluid protocol). A detailed modified procedure is outlined as follows:

1. A volume of 300µL of fecal washing/ gut tissue issue lysate was added to tubes contains 300µL of 2X T and C Lysis Solution supplemented with 3 µL Protinase K followed by incubation at 56 °C for 30 minute with further inactivation step at 65°C for 3 minutes and brief spin down.
2. After bacterial cell lysate was allowed to equilibrate at room temperature, 500µL of cell lysate was transferred to fresh eppendorf contains 291µL of MPC protein, followed by vigorous vortexing and incubation at 4°C. Protein precipitation was performed by centrifugation at 14K rpm for 10 minutes.
3. DNA recovery was achieved by overlaying 400µl of the supernatant over a DNase-free eppendorf tubes containing equal volume of ice-cold isopropanol followed by inversion for 20-30 times and overnight incubation at -80°C. DNA precipitation was achieved by centrifugation at 14k rpm for 10 minutes.
4. Clean DNA prep was obtained after three rinsing runs with 70% Ethanol with subsequent centrifugation at 14K rpm for 10 minutes (for each run), followed by a final careful drying using SpeedVac.
5. DNA pellet was resuspended carefully using 35µl of TE Buffer.
6. DNA concentration and purity were measured using Nanodrop.

2.2.20 Targeted high-throughput 16S rRNA amplicon sequencing

Bacterial DNA samples were prepared from three independent experiments. Both *Drosophila* gut tissues (Whole midgut and hindgut) and fecal droppings were used for DNA extraction and further assessed for integrity and amplifiability by running diagnostic 16S rRNA PCR.

For 16S rRNA gene amplicon sequencing, the hypervariable V1 and V2 region of bacterial 16S rRNA gene were amplified using a primer set 27F and 338R [121].

The forward primer (5'- AATGATACGGCGACCACCGAGATCTACAC XXXXXXXX TATGGTAATTGT AGAGTTTGATCCTGGCTCAG-3') and reverse (5'- CAAGCAGAAGACGGCATAACGAGAT XXXXXXXX AGTCAGTCAGCC TGCTGCCTCCCGTAGGAGT -3') primer contained the illumina Adaptor p5 (forward) and p7 (reverse) – denoted by italics and the underlined sequences represent the sequencing primer including the broadly conserved bacterial primers 27F and 338R. Both primers contain a unique 8 base index (index; designated as XXXXXXXX) to tag each PCR product. For the PCR, 100 ng of template DNA was added to 25 µl PCR reactions performed using Phusion® Hot Start II DNA Polymerase (Finnzymes, Espoo, Finland). All dilutions were carried out using certified DNA-free PCR water (JT Baker). PCR reactions were assembled within a PCR hood in which all surfaces and pipettes had been decontaminated with DNAZap™ (Ambion) and UV irradiated for 30 min. The cycling conditions were as follows: initial denaturation for 30 sec at 98°C; 30 cycles of 9 sec at 98°C, 30 sec at 55°C, and 30 sec at 72°C; final extension for 10 min at 72°C. All reactions were performed in duplicate and combined after PCR.

For library preparation, PCR products were extracted with the Qiagen MiniElute Gel Extraction Kit and quantified with the Quant-iT™ dsDNA BR Assay Kit on a nanodrop 3300 fluorometer. Equimolar amounts of purified PCR product were pooled and further purified using Ampure Beads (Agencourt). A sample of the library was run on an Agilent Bioanalyzer prior to calculate the final concentration for the sequencing. PhiX Control library (v3) (Illumina) was combined with the amplicon library (expected at 10%). Amplicon libraries were subsequently sequenced on a MiSeq using the MiSeq Reagent Kit v3 600 cycles sequencing chemistry. The library was clustered to a density of approximately 1000 K/mm².

2.2.21 Integrated analysis of 16S rRNA gene amplicon

All 16S rRNA paired-end fastq files reads were checked for quality and sorted in specific dataset with the corresponding metadata. The 16S rRNA amplicon reads were preprocessed using the UPARSE-based IMNGS platform [136], [137]. Chimeras were removed using UCHIME [138]. Ten nucleotides on both the 5' and 3' end were trimmed for each of the R1 and R2 reads, respectively. The quality trim score was 5 and expected number of errors across assembled reads was 1. Sequences were clustered into operational taxonomic units (OTUs) at 97%

sequence identity using UPARSE v8.1.1861_i86. OTUs occurring at a relative abundance less than 0.25% (i.e., 0.0025) across all samples were removed to prevent the analysis of spurious OTUs. Also, each OTU included in the final OTU table was represented in at least one sample in the analyzed dataset. In order to resolve errors in amplicon sequence data at the level of single nucleotide, OTUs were denoised based on the unoise3 pipeline of usearch. zOTUs (zero-radiance OTUs) with Neighbor-Joining approximation was used in reconstruction phylogeny. Taxonomies were assigned with minimum identity (> 95%) to a maximum of genus level using the updated SILVA database version 132 [139]. The OTU table was then normalized by total count per column to account for differences in library size. Taxonomic classification at the species levels for relevant zOTUs was assigned based on EzBioCloud microbiome taxonomic profile (version 20200513) [140].

Downstream differential statistical analysis of zOTUs tables was performed in R [141]. It includes normalization step and calculating alpha-diversity indices (OTUs richness, evenness, and Shannon-effective) and beta-diversity (generalized UniFrac for calculation of the phylogenetic distance matrix), taxonomic assignment, statistical comparisons (using one-way ANOVA/ Kruskal-Wallis Rank Sum Test and/or unpaired t-Test/ Mann-Whitney U test as well as pairwise correlations (Pearson's correlation) within meta-variables and/or taxonomic variables [141], [142]. For statistical comparison of taxonomic composition, 2 cut-off values were assigned (abundance cutoff= 0.5; prevalence cutoff= 0.3) to avoid inclusion of zero-inflated dataset in statistical testing.

In addition, linear discriminant analysis (LDA) Effect Size (LEfSe) was applied (LDA>2) on genus-level taxonomy to calculate the effect size of each differentially abundant taxa between experimental groups [144]. Those discriminative zOTUs could be potential microbiomarkers (i.e. probiotic strain/pathobionts). Results were visually presented using GraphPad Prism 5 software.

2.2.22 Preparation, storage and re-colonization of microbiota preparation

In parallel to sampling flies after 6-day and 12-day of DSS treatment for conducting bacterial DNA extraction, 4 separate vials were allocated for each treatment group and corresponding controls. In each vial, 30 adult female *W¹¹¹⁸* flies were collected for re-colonization experiments. Next, flies were anesthetized on ice before body sterilization with 6% hypochlorite solution (2.5 minutes each) followed by two independent rinsing steps in 70% ethanol and 1X PBS. Flies were collected in

screw-capped tubes containing ceramic beads and 0.7 mL 1x PBS and undergone 1 cycle of gentle homogenization for 30 seconds at 3.25 m/s speed using Bead Ruptor 24 followed by low-speed centrifugation at 800 ×g for 3 minutes. Microbiota preparation (450mL) was mixed with equal volume 1x PBS, 0.1 mL autoclaved glycerol followed by gentle vortexing and aliquoted in cryo plastic tubes and stored at -80 oC. Each aliquot 400 mL was thawed on ice immediately before use and mixed with equal volume filtere-sterilized 10% sucrose (2X) colored with 1% (f.c) brilliant Blue dye (dissolved in 1% PBS). Axenic flies were fed on autoclaved filter paper soaked with the blue-colored microbiota-sucrose suspension. Frequent replenishment of microbiota suspension was performed by thawing another aliquot every other day in order to sustain microbial colonization. Viability of bacterial suspension (*Lactobacillus* spp. as an indicator) after a single freezing-thawing event was checked by plating 100mL of the microbiota suspension on MRS and Mannitol agar plate at 37 oC for 24- 48 hours.

2.2.23 Statistical analysis

For survival analysis, statistical significance of the Log-rank test statistics was performed using Microsoft Excel and GraphPad Prism 5 software with institutional license. Primary diagnostics of the datasets were performing using Shapiro test (for normality) and Fligner-Killeen test (for homogeneity of variance). Grubbs' test was used to check for outliers, whenever necessary. For analysis of variance, parametric unpaired Student's t-Test or one-way ANOVA and their nonparametric equivalents Wilcoxon “Mann–Whitney U test” and Kruskal test, respectively. For post-hoc pairwise multiple comparison, Tukey’s or Wilcoxon test were performed after ANOVA or Kruskal test, respectively. Unless stated otherwise, data related to DSS-treated group and control group were presented in red and black color, respectively.

For relative gene expression analysis, distribution-free nonparametric tests were performed. Statistical analysis of significant difference were defined as * $p < 0.05$, ** $p < 0.01$, *** $p < 0.001$ and NS $p > 0.05$.

For correlation analysis between continuous meta-variables and taxonomic variables (in microbiota analysis) or within-variable categories (in gene co-expression analysis), Pearson’s correlation was performed. Correlation coefficients of log-transformed data were calculated (default cutoff is 0.9/-0.9, default minimum

number of observation is 4). Significant pairs are determined by p-value (default cutoff is 0.05). Graphical illustration of correlation matrix (with and without significance cutoff) was performed using the corrplot R package (<https://github.com/taiyun/corrplot>). The output reflects visually absolute value of corresponding correlation coefficients that is proportional to the area and color intensity of circles (blue for positive and red for negative R , respectively). Threshold of meaningful correlation was set at $R= 0.8/ -0.8$ and $p < 0.5$; however results of correlation were carefully interpreted considering that correlation is not a true indicative of causality. Statistical output was presented in panel using the Microsoft Powerpoint and open-source Inkscape 0.92 graphic editor.

3 Results

3.1 Establishment of the *Drosophila* DSS-induced colitis model

3.1.1 DSS treatment induces mortality in *Drosophila* with male-bias survival advantage

In several animal models including rats [145], mice [146] and zebra fish [147], the most reproducible colitis induction protocol is based on the feeding of DSS salt of M.Wt (36-50 KDa). A concentrations of 5% DSS has been tested to induce typical inflammation phenotype. Survival analysis of DSS treated and control flies by Kaplan-Meier estimate showed significant mortality rates in both female and male flies after 5% DSS treatment (Fig.3.1). Gender bias was observed as female flies have higher mortality rate than males (Fig.3.1.1.B& C).

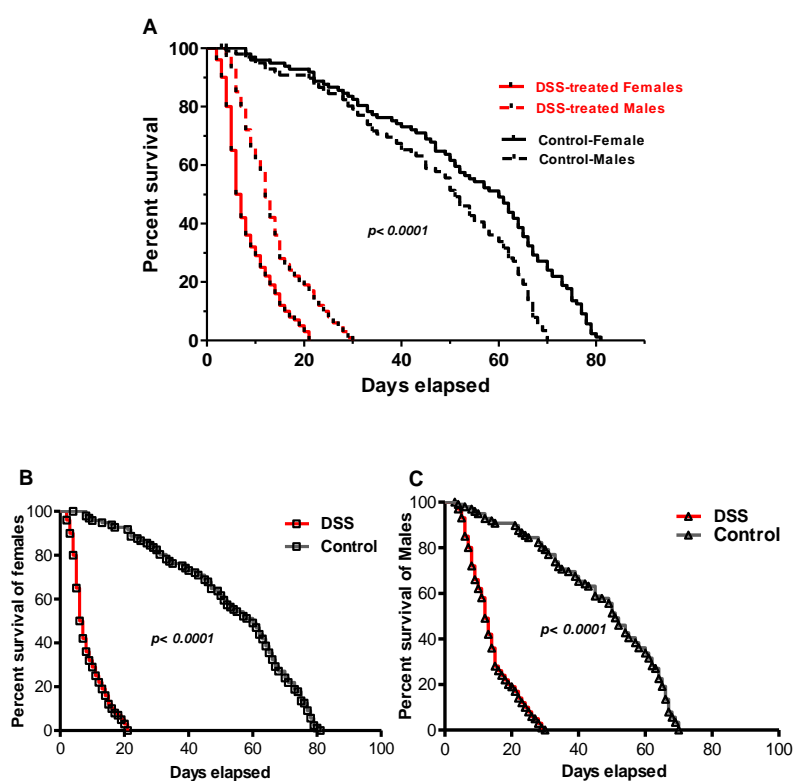


Fig.3.1: Effect of DSS treatment on in conventional w^{1118} male and female flies. (A) The effect of 5% DSS treatment on male and female flies showed a significant difference between DSS-treated and control groups with a Log-rank (Mantel–Cox) test of median survival $p < 0.0001$. **(B)** Female flies showed a higher mortality rate with median survival at day 6.5 with a Log-rank test for trend $p < 0.0001$. **(C)** DSS-treated male flies showed a reduced mortality rate compared with DSS-treated females with median survival at day 12 with a Log-rank test for trend $p < 0.0001$. Data represents counts of death event for 100 flies (5 replicates) in 3 independent experiments.

3.1.2 Post-induction phases of DSS treatment is an informative survival-based proxy for disease progression

In principle, survival analysis by Log-rank (Mantel–Cox) test was proven to be a gold standard in *Drosophila* research to address aspects of either life span or survival proportions after stress induction (i.e. infection). However, establishing a feasible and rapid alternative tool is still unmet need. Dividing survival curve into phases could help addressing different physiologic condition: low grade inflammation, active inflammation, followed by progression or recovery (aka remission).

In the present *Drosophila* DSS induction model, the proportion of flies-at-risk during specific period of treatment was retrieved from survival analysis output to be tested as a potential informative proxy for disease status. In the first phase of DSS-post induction (half median survival - to- median survival), number of flies-at-risk is significantly decreased ($p=0.03$), which could represents a significant transition from low-grade to active inflammation state (Fig.3.2.A). Second phase of DSS-post induction which characterized by high mortality rate could reflect advanced inflammation state (Fig.3.2.B).

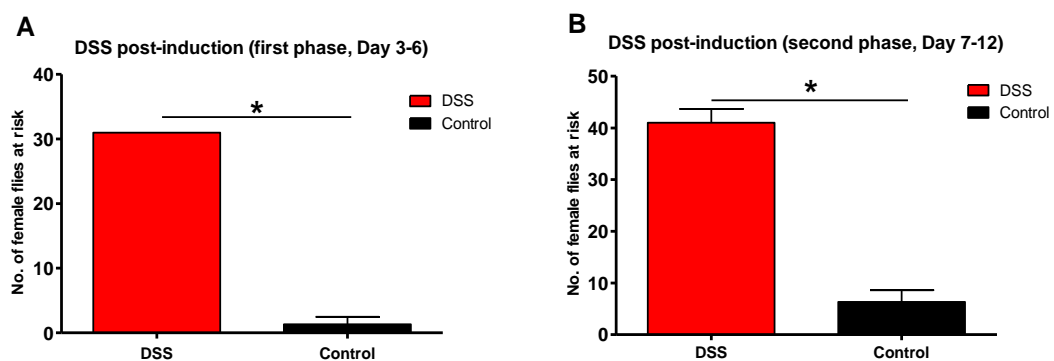


Fig.3.2: Phases of DSS- post induction in conventional w^{1118} flies are classified based on (A) pre-median survival windows and (B) post- median survival windows. Data represents counts of death event for 100 flies (5 replicates) in 3 independent experiments. Significance is calculated using the unpaired two-tailed Student's t-test. * $p \leq 0.05$.

3.1.3 Longitudinal analysis of the DSS effect on *Drosophila* reveals a significant reduction in mortality after 6-day recovery period

The reason behind testing the effect of DSS over time with intervention is to characterize longitudinally the phenotype. Study design represents 2 time points for sample/data collection. Experimental groups were classified in 5 groups: DSS-day6 vs. Control-day-6, DSS-day-12 vs. control-day-12, and 6-day-recovery (Fig.3.3). The latter was an extra DSS-day-6 group shifted on normal media for 6-days recovery period. This design is very informative when addressing dynamic interaction of host and gut microbiota. Furthermore, the including a new intervention group (recovery group) provides a possibility to recapitulate the state of clinical remission in IBD and opens up a new avenue for candidate drug testing.

It is obvious that there is a significant difference between DSS and control groups at both day3 and day 6 post-treatment, but not between the 2 DSS groups. At day 12, there is a highly significant difference between DSS group and both the corresponding controls and the recovery group ($p=0.0002$).

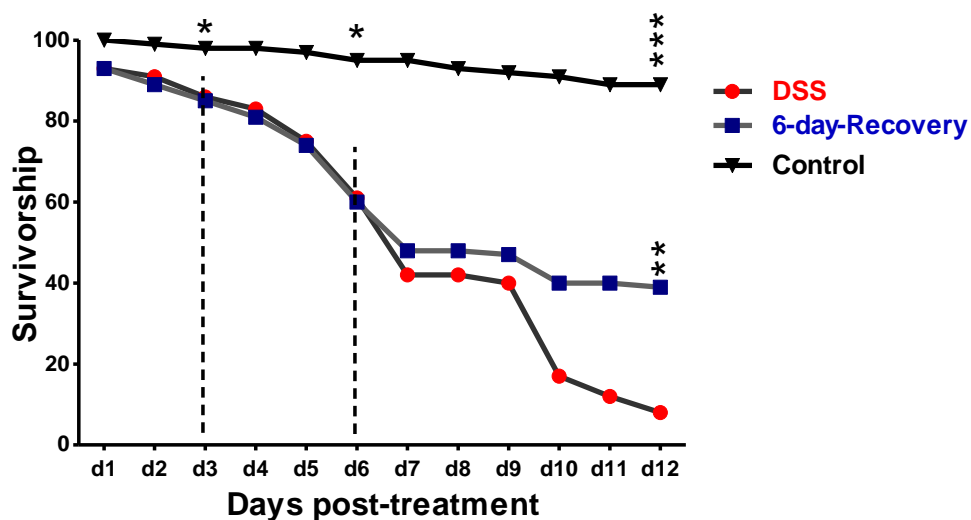


Fig.3.3: Effect of 6-day recovery on the DSS-driven mortality. zero represents the starting day for DSS treatment. Red color refers to DSS- treated group; black color refers to the control group, which fed on normal media; blue color refers to the recovery group which was shifted from DSS-treatment regime after 6 day6 to fed on normal media. Values are means of 3 independent replicates of 100 flies each. Significance is calculated using the one-way ANOVA with Tukey's multiple comparison test. Values represent %; * $p \leq 0.05$, *** $p \leq 0.001$.

3.1.4 DSS treatment triggers rapid decline in the *Drosophila* total activity

Analysis of locomotor activity of DSS vs. control female flies by using the Disease Activity Monitor (DAM) System showed a reduction in total activity starting from day 1 post treatment (Fig.3.4). Activity of DSS-fed flies was significantly reduced starting from the first day of treatment ($p < 0.0001$).

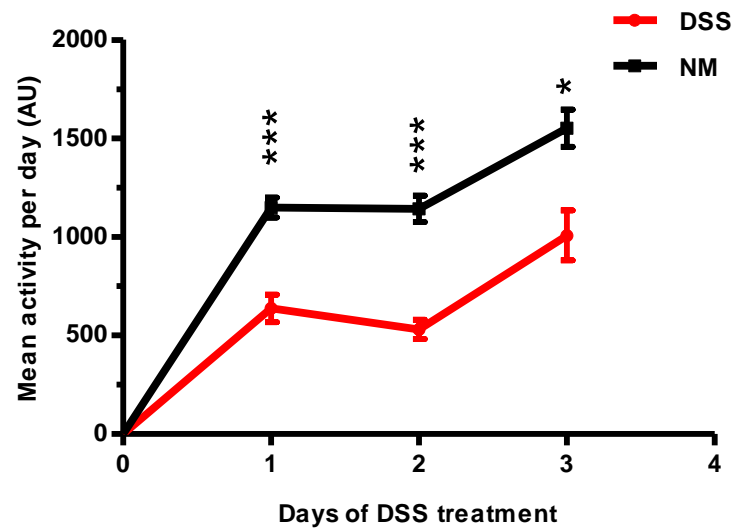


Fig.3.4: Locomotor activity and sleeping behavior of female flies after DSS treatment. Values represent means \pm SEM for 31 biological replicates per day. NM referred to the control group, which fed on normal media. Significance is calculated using the Kruskal-Wallis test with Dunn's multiple comparison. * $p \leq 0.05$, *** $p \leq 0.001$. Absence of data points after day 3 is attributed to the increased death events in treatment groups compared with the control groups.

3.1.5 DSS treatment for 6 days reduces the *Drosophila* excreta egestion

The intestinal physiology of *Drosophila* can be monitored in an invasive and a non-invasive manner by analysing the excreta produced by flies fed on a dye-supplemented diet. Several assays have been used to explore gut function and its regulation by longitudinally investigating the rate of excreta egestion [148], [149].

In the DSS-treated group, number of fecal spots is significantly reduced (-42,7%, $p=0.005$) compared to the corresponding controls (Fig.3.5).

3.1.6 DSS treatment for 6 days reduces the *Drosophila* food consumption

Physiology of food consumption and excretion in *Drosophila* is characterized by a complex neuroanatomical visceral control. The food consumption phenotype is measured using CAFE assay with dye-supplemented diet [128].

In the DSS-treated group, food consumption is significantly reduced (-63,5%, $p=0.001$) compared to the corresponding controls (Fig.3.6).

3.1.7 DSS treatment triggers *Drosophila* weight loss

Weight loss is one of the most robust physiological assays that reflect disturbance associated with the disease such as levels of storage macromolecules. It also could be regarded as a marker of disease activity in human IBD and murine DSS-induced colitis [150], [151], [152]. In The *Drosophila* model, weight loss was reported in different phenotypes as a proxy of nutritional abnormalities [129], [153], [154].

In the DSS-treated group, fly wet weight is significantly reduced (-7,3%, $p=0.02$) compared to the corresponding controls (Fig.3.7). However, the total body triglycerides shows a more pronounced and significant reduction in DSS-treated group (-34,4%, $p=0.002$)

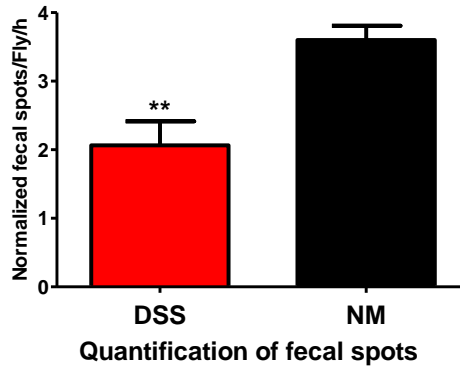


Fig.3.5: Quantification of fecal spots and consistency after 6-day DSS treatment of female *Drosophila*. Values represent means \pm SEM for 5 biological replicates. NM referred to the control group, which fed on normal media. Significance is calculated using the unpaired two-tailed Student's t-test, ** $p \leq 0.01$.

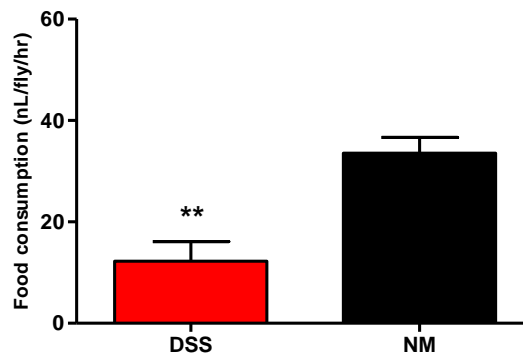


Fig.3.6: Quantification of food consumption after 6-day DSS treatment of female *Drosophila*. Values represent means \pm SEM for 12 biological replicates. NM referred to the control group, which fed on normal media. Significance is calculated using the unpaired two-tailed Mann-Whitney U test, ** $p \leq 0.01$.

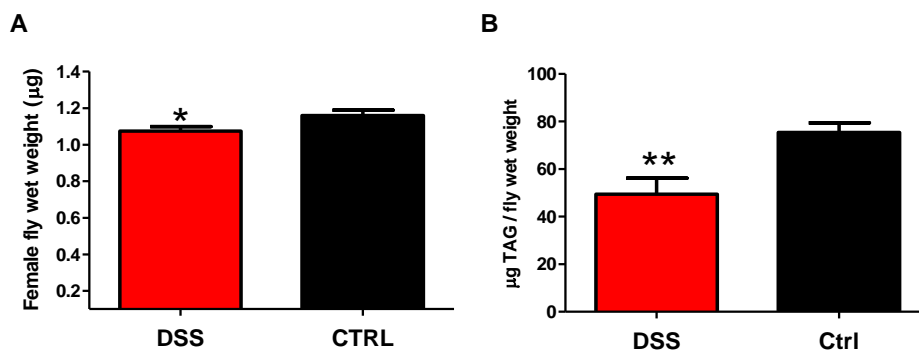


Fig.3.7: Characterization of weight-loss phenotype after 6-Day DSS treatment in female *Drosophila*. **(A)** Represents the reduction in the fly wet weight; **(B)** represents the normalized reduction of total body triglycerides (TAG). Values represent means \pm SEM for 8 biological replicates in both experiments. CTRL/ Ctrl referred to the control group, which fed on normal media. Significance is calculated using unpaired one-tailed Student's t-test, * $p \leq 0.05$ ** $p \leq 0.01$.

3.1.8 DSS treatment triggers plasmatocytes recruitment to the injured gut

Since it is widely reported that plasmatocytes are functional homolog of mammalian macrophages, hemocyte-reporter (*Hml-Gal4>UAS-2xEGFP*) is developed to label plasmatocytes with GFP for further in-depth analysis [110], [116], [127].

DSS treatment induces changes in plasmatocyte morphology and localization. The phenotype is characterized by marked plasmatocytic transmigration to the midgut. Counting the number of circulating GFP+ plasmatocytes revealed a significant reduction (-41,4%, $p=0,002$) in the abdominal area (Fig.3.8).

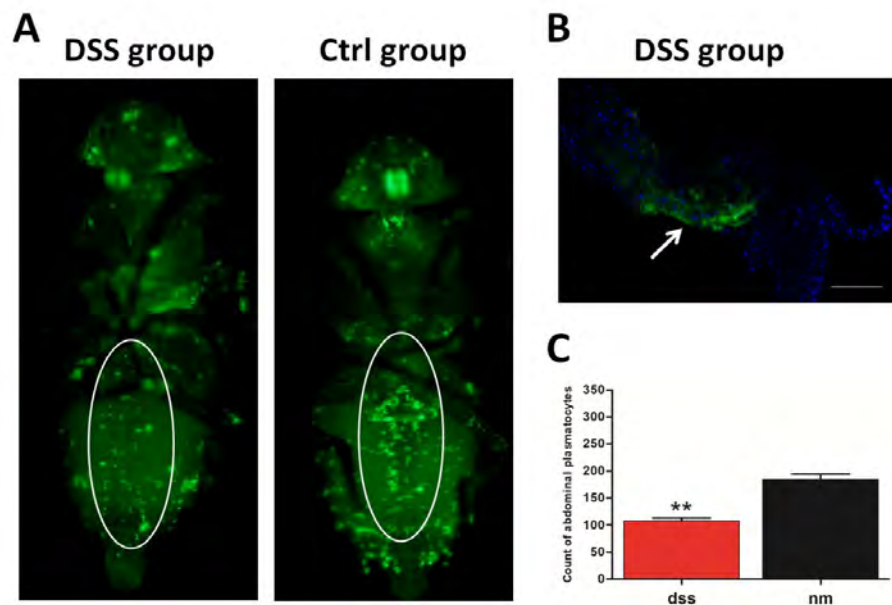


Fig.3.8: Characterization of plasmatocytes migration phenotype in female *Drosophila* with GFP+ plasmatocytes 6-Day post DSS treatment. Dorso-ventral imaging of *HmlΔ>GFP* female *Drosophila* with white ovals focusing on the plasmatocytes clumps in the abdominal region (A). Representative image of transmigration of the abdominal GFP+ plasmatocytes with white arrow denotes the posterior midgut (B). Quantification of the abdominal GFP+ plasmatocytes (C). Values represent means \pm SEM for 3 biological replicates. Ctrl/nm referred to the control group, which fed on normal media. Scale bar = 50 μ m. Significance is calculated using the unpaired two-tailed Student's t-test, ** $p\leq 0.01$.

3.1.9 DSS treatment compromises the integrity of the *Drosophila* intestinal barrier (the “leaky gut” phenotype)

Leaky gut (LG) is generally characterized by damage of epithelial tight junction of the gut with subsequent uncontrolled paracellular permeability. It is also reported that LG is implicated in the development of enteric infections in IBDs. [155]. Aging-induced gut-barrier leakiness in *Drosophila* was previously reported as ‘smurf’ phenotype [103].

Here, DSS-induced smurfness (referred to as DIS) was investigated at the organismal level. Cumulative death events due to LG at day 6 post treatment was markedly higher in DSS groups (25%) compared to non-treated controls (3%). Notably, 60,9% of the mortality at day 6 post DSS treatment is attributed to leaky gut (Appendix Table 7.1).

Gut leakiness is presented with gradient in the same animal cohort. Severity of LG is classified into smurfness grades based on the degree of luminal cargo transmigration (Fig.3.9). The highest smurfness grade is presented with massive distribution of blue dye in the body cavity (i.e. hemocele) compared to the lowest grade (Fig.3.10). Notably, severe phenotype showed a marked reduction of total physical activity.

The gut leakiness is evident to be independent of the molecular mass of the luminal tracer. Both non-microbial dietary cargo and bacterial cells can transmigrate across the compromised barrier (Fig.3.11).

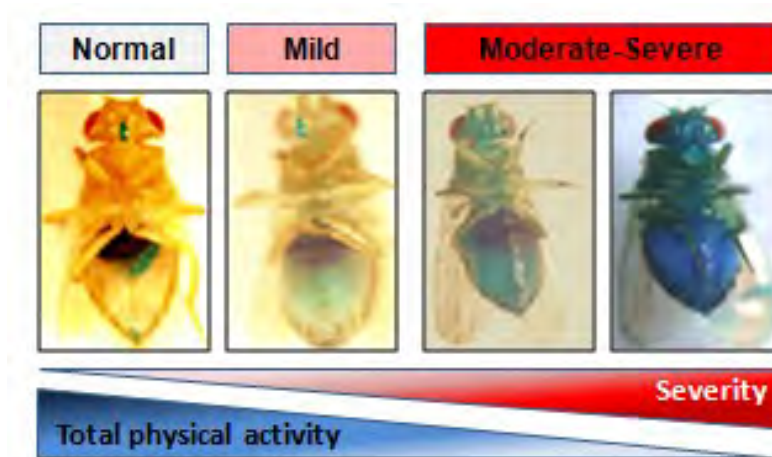


Fig.3.9: Representative images of different grades of the gut leakiness in the DSS-treated group

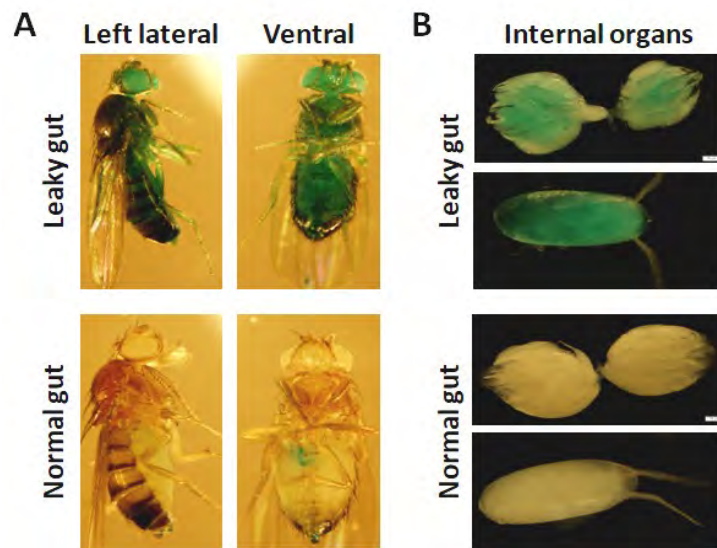


Fig.3.10: Representative images of DSS-induced Leaky gut. (A) Left panel shows DSS-induced transmigration of luminal cargo colored with a blue-dye (M.wt. 792.85 g/mol) to the entire body cavity. (B) Right panel shows blue coloration of the *Drosophila* ovary/ ovariole dissected from severely-affected animal with leaky gut.

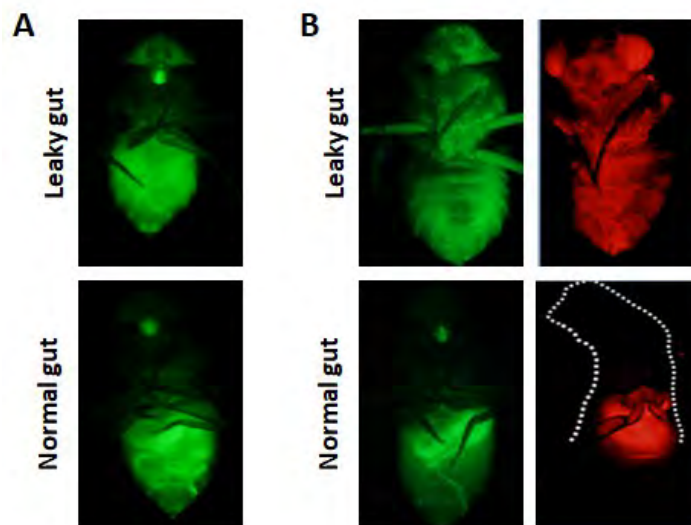


Fig.3.11: Representative images show transmigration of luminal cargo labeled with different tracer in A^{1118} flies. (A) Left panel shows DSS-treated animal shows transmigration of luminal cargo labeled with fluorescein sodium salt (fluorescent tracer, M.wt. 376.27 g/mol). (B) Right panel shows translocation *E. coli*-BW25113 labeled with the eGFP- and mCherry-containing plasmid pJBS24 which accounts for approximate size of 0.5 by 1.5 μm (ca. 1,8 μm^3) [119].

3.1.10. Structural characterization of the DSS-induced *Drosophila* leakiness

In DSS-treated group, loss of intestinal integrity is markedly observed in midgut region compared to the hindgut (Appendix Fig.7.1). Treatment with DSS for 6 days on shows a disruption of sarcometric integrity of visceral muscles (Fig.3.12; Fig.3.13). Similar disruptive effect on different elements of the gut septate junction (eg. Coracle and Discs large proteins) was also observed (Fig.3.14; Fig.3.15).

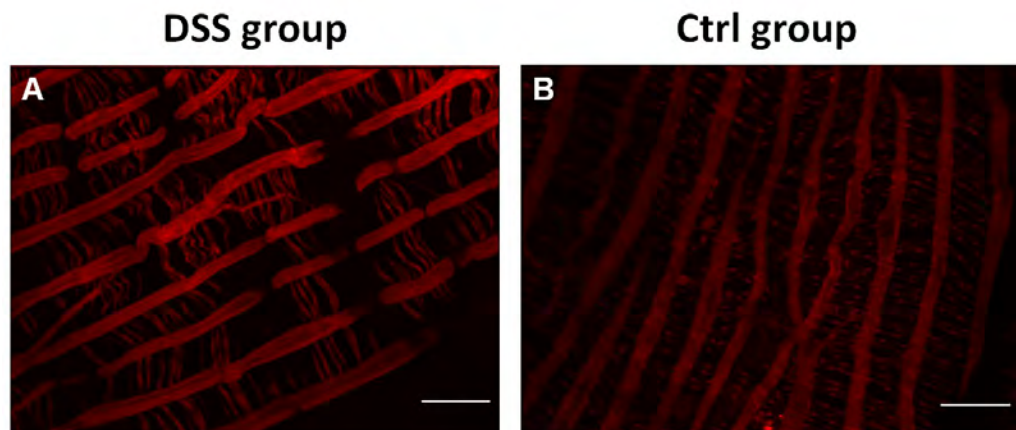


Fig.3.12: Representative Z-stacked images of dissected posterior midgut of *A¹¹¹⁸* flies in DSS and control groups after staining actin with Phalloidin-TRITC. Ctrl: controls. Scale bar = 20 μ m.

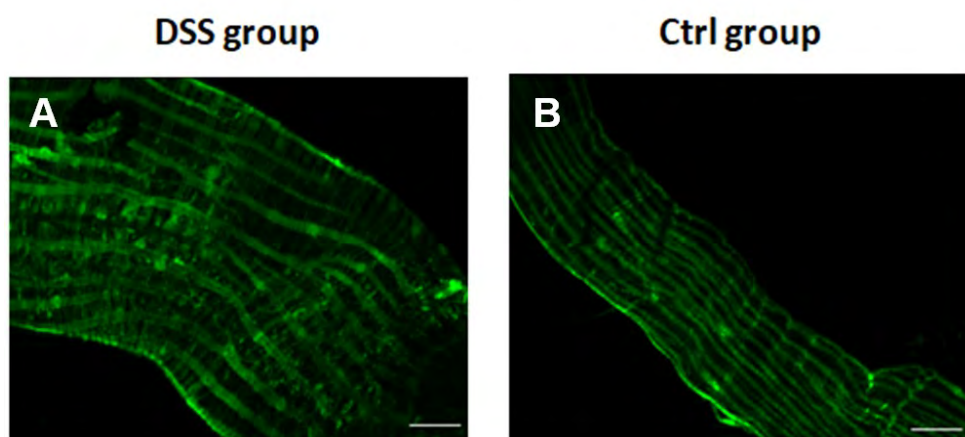


Fig.3.13: Representative images dissected posterior midgut of the *How-Gla4>UAS-20xGFP* flies in the DSS and control groups after immunostaining with GFP antibody. Ctrl: controls. Scale bar = 50 μ m.

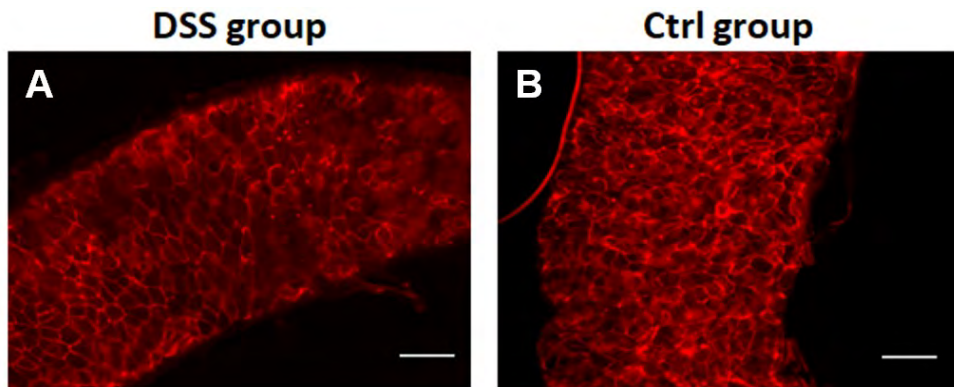


Fig.3.14: Representative images of dissected posterior midgut of A^{1118} flies after immunostaining with anti-coracle antibody. Ctrl: controls. Scale bar = 50 μm .

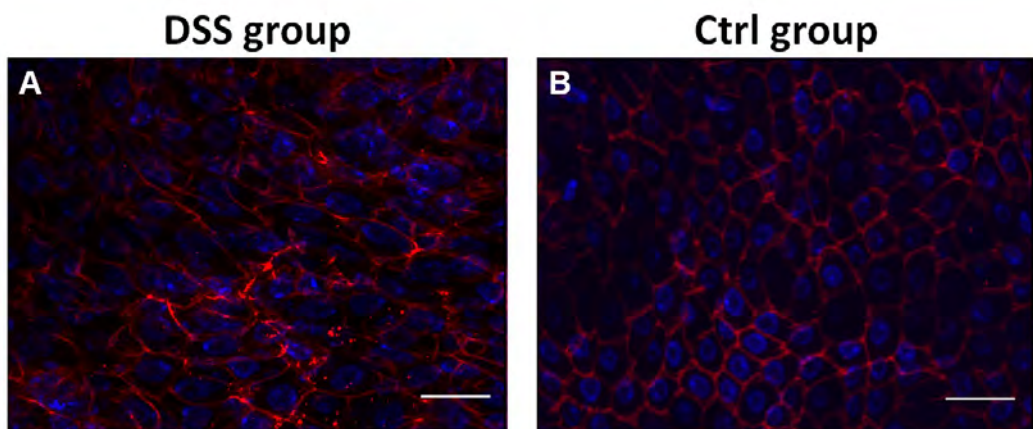


Fig.3.15: Representative Z-stack images of dissected posterior midgut of A^{1118} flies after immunostaining with anti-Discs large (Dlg) protein antibody. Ctrl: controls. Cell size and nuclei are visualized by DAPI - (blue) and anti-coracle staining (red), respectively. Scale bar = 20 μm .

3.1.11. DSS treatment triggers hyperproliferation in the *Drosophila* midgut

In principle, DSS is widely reported to induce multi-faceted toxicity to intestinal epithelium causing epithelial cell injury in different experimental animal models [156], [157], [158], [159], [160]. Consequent epithelial damage in The *Drosophila* midgut induces asymmetric division of underlying intestinal stem cells (ISCs) to give rise to enterocyte (EC) for ultimate tissue repair [161].

For investigating the impact of DSS on different cells in the gut milieu, *escargot*-reporter (*esg-Gal4>GFP*) was primarily used to mark progenitor cells (ISCs and enteroblasts “EB”). Treatment of female *Drosophila* with DSS for 6 days induces hyperproliferation of *esg+* cells with a consequent accumulation of mis-differentiated enteroblasts (i.e. with dysplasia). Notably, the dysplastic gut phenotype is presented in both anterior midgut (AMG) (Fig.3.16 A& B) and posterior midgut (PMG) (Fig.3.16 A´& B´) but not in the hindgut (Appendix Fig.7.2). After 6-day-recovery period on normal media, the effect of DSS is reversed to reach homeostatic state (Fig.3.16 C& C´). Also, similar effect of DSS on the midgut was observed in the male *Drosophila* (Fig.3.17).

A confirmatory experiments were conducted using *Su(H)GBE-Gal4>GFP* and *DI-Gal4>GFP* *Drosophila* lines, which specifically express GFP in the EB and ISCs, respectively. Treatment with DSS for 6 days exclusively triggers hyperproliferation of both EB (Fig.3.18) and ISCs (Fig.3.19) in both AMG and PMG.

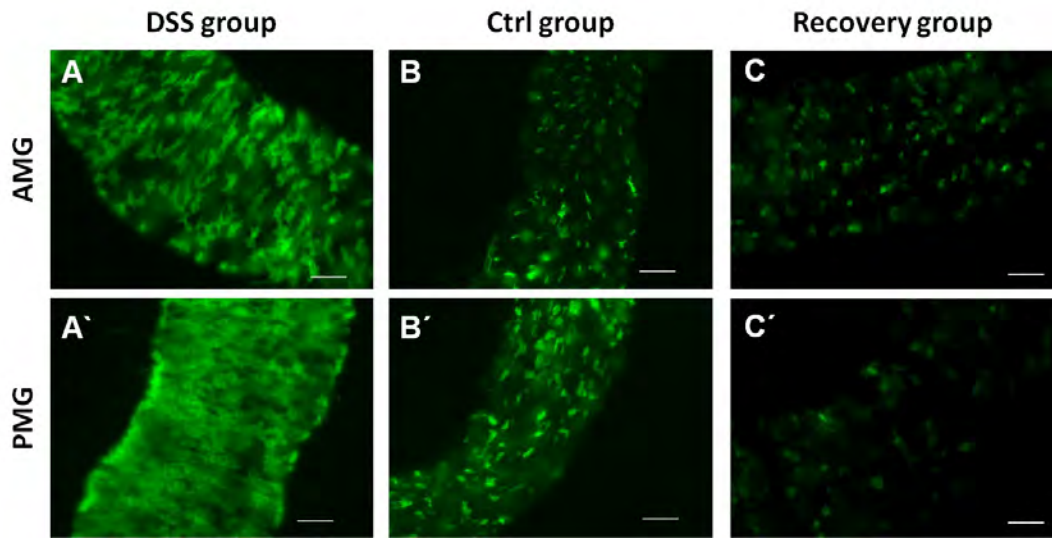


Fig.3.16: Representative images of dissected midgut of *esg-Gal4>GFP* female *Drosophila* after immunostaining with anti-GFP antibody. Ctrl: controls; GFP: green fluorescent protein, AMG: anterior midgut; PMG: posterior midgut. Scale bar = 50 μ m.

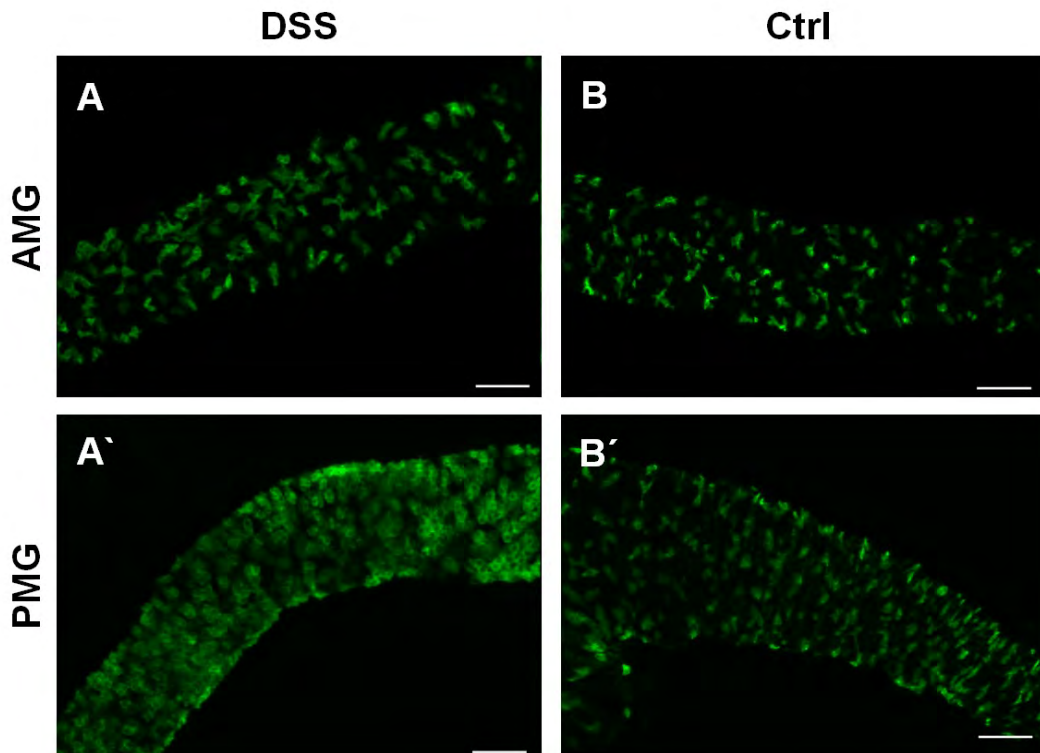


Fig.3.17: Representative images of dissected midgut of *esg-Gal4>GFP* male *Drosophila* after immunostaining with anti-GFP antibody.

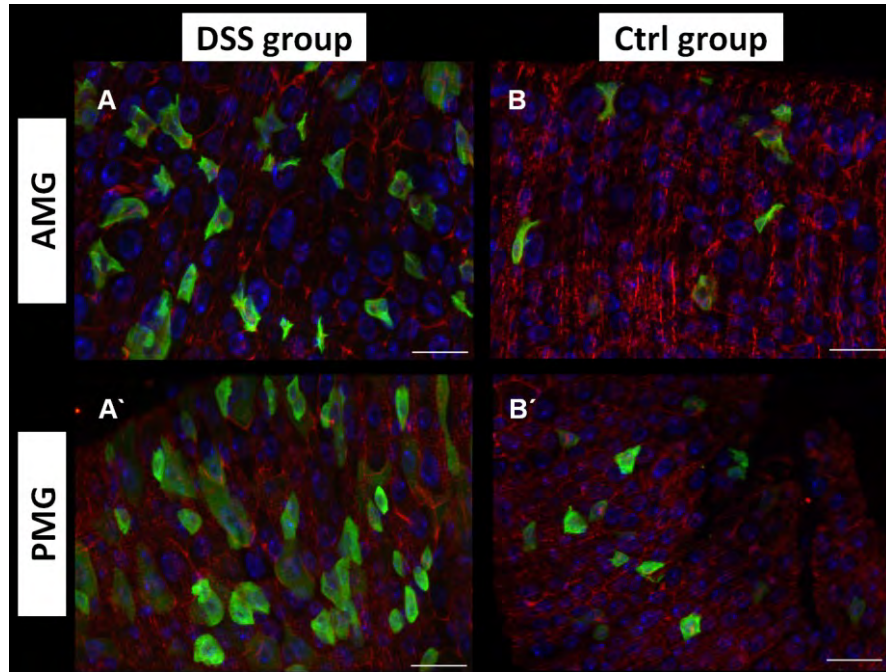


Fig.3.18: Representative Z-stack images of dissected midgut of Su(H)GBE-Gal4>GFP female *Drosophila*. Ctrl: controls; GFP: green fluorescent protein, AMG: anterior midgut; PMG: posterior midgut. Cell size and nuclei are visualized by DAPI - (blue) and anti-coracle staining (red), respectively. Scale bar = 20 μ m.

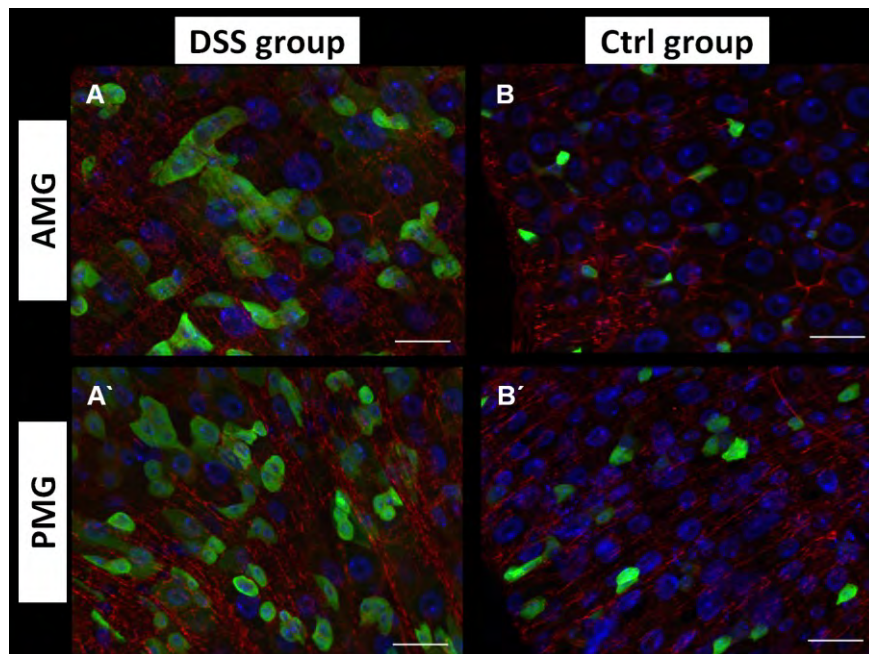


Fig.3.19: Representative Z-stack images of dissected midgut of *Dl*-Gal4>GFP female *Drosophila*. Ctrl: controls; GFP: green fluorescent protein, AMG: anterior midgut; PMG: posterior midgut. Cell size and nuclei are visualized by DAPI - (blue) and anti-coracle staining (red), respectively. Scale bar = 20 μ m.

3.1.12 DSS treatment triggers midgut hyperproliferation in axenic female *Drosophila*

To test whether the presence of specific gut bacterial community/ -ies before DSS treatment is essential in inducing dysbiosis, a cohort of germ-free (axenic) animals was prepared (as mentioned in section 2.2.13 pp. 33) and the successfulness of bacterial removal was validated (Appendix Fig.7.3).

Results indicate that sustained absence of gut microbiota prior to and during the course of DSS treatment has no protective effect from DSS-induced midgut dysplasia (Fig.3.20).

3.1.13 Re-colonization of germfree recipient *Drosophila* gut with total microbial community from day-12 DSS-treated donors induces midgut dysplasia.

Basically, previous studies on murine DSS-induced colitis have reported a significant disrupting effect of DSS on gut microbial ecology [162], [163], [164].

Here, the experiment was designed to test the functional implication of potentially dysbiotic microbial community on midgut cell proliferation. Firstly, recipient *esg-Gal4>GFP* female *Drosophila* was pre-made available as germ-free before feeding on the donor microbial community. Secondly, vials containing the total microbial community from adult *w¹¹¹⁸* female *Drosophila* donor were allowed to thaw on ice and undergone viability testing (Appendix Fig.7.4). Thirdly Microbial community preparations were transferred from DSS treated group at both day 6 and day 12 in parallel to the untreated controls from day 12. (as mentioned in section 2.2.14 pp. 34). The later was used to rule out any potential aging-related confounders

Notably, transfer of the microbial community derived from the day-12 post DSS treatment can recapitulate the typical midgut dysplasia driven by the DSS treatment. The failure of the microbial community derived from day-6 post DSS treatment can be only explained after community profiling via 16S rRNA amplicon sequencing (section 3.3).

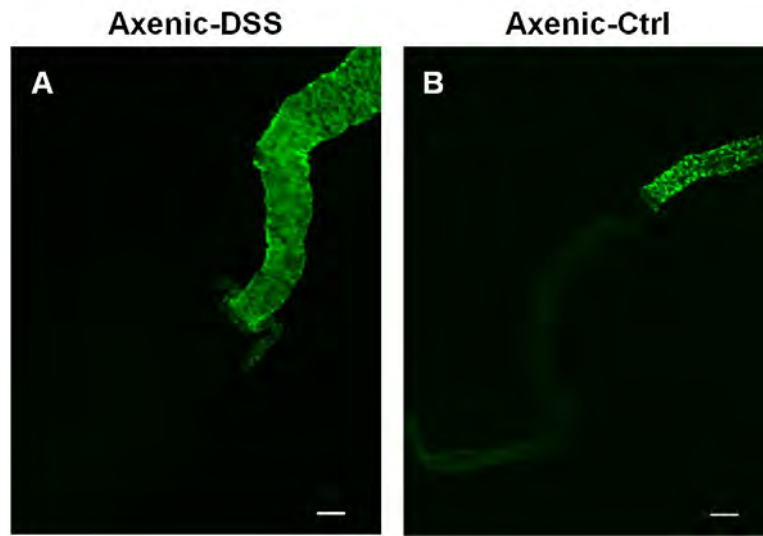


Fig.3.20: Representative images of dissected gut of axenic *esg-Gal4>GFP* female *Drosophila*. Ctrl: controls. Axenic refers to germ-free state. Scale bar = 100 μ m.

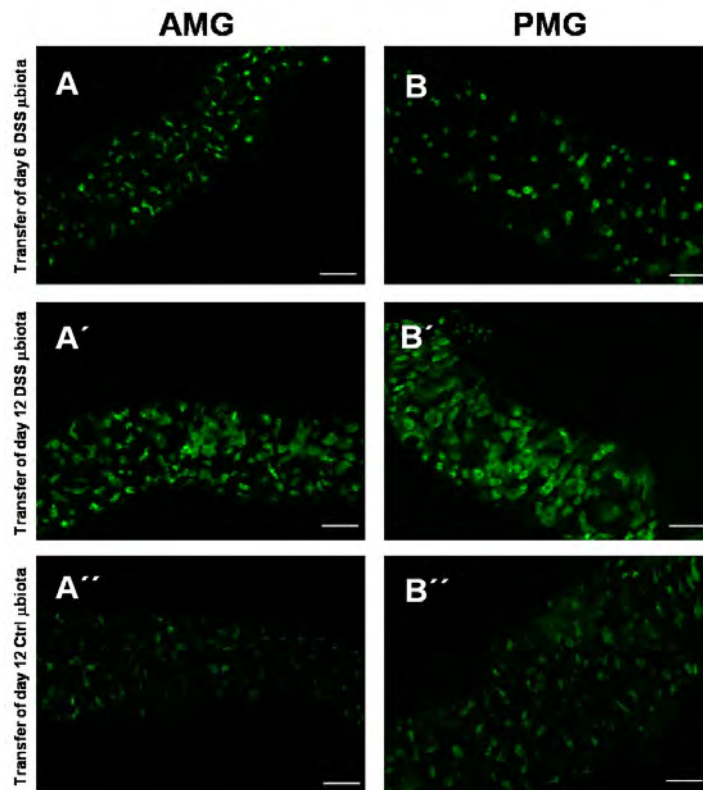


Fig.3.21: Representative images of dysbiosis after re-colonizing total microbial community from donor flies to the germfree *esg-Gal4>GFP* *Drosophila* recipients. AMG: anterior midgut; PMG: posterior midgut; μ biota: microbiota. Scale bar = 100 μ m.

3.1.14 DSS treatment induces over-expression of *Upd3* in the *Drosophila* midgut

In the *Drosophila* gut, multiple line of evidence highlighted that JAK/STAT signaling plays a major role in modulating gut homeostasis in response to environmental cues such as infection and high-fat diet. Damaged enterocytes secrete Upd3 (IL-6-like cytokine) to stimulates ISCs division mostly through JNK (basket)-dependent JAK/STAT signaling [165], [166]. Expression pattern of Upd3 was monitored *in vivo* using both *Upd3-Gal4> GFP* and *Upd3-Gal4 >LacZ* reporter *Drosophila* lines [167].

Here, the effect of 6-day period of DSS treatment on the expression of Upd3 was monitored visually by a qualitative measurement of the intensity of x-Gal staining as well as by semi-quantitative densitometric measurements of the Upd3-GFP signals (as mentioned in section 2.2.11 pp. 32). Further relative quantification of the expression of Upd3 gene and downstream effectors were examined later at the molecular level (section 3.2).

After DSS treatment, the *Drosophila* gut showed a strong Upd3 expression in the treated group compared to controls. These strong signals are obvious after staining with x-Gal (Fig.3.22) as well as with anti-GFP antibody (Fig.3.23). Notably, staining of Upd3 shows a strong expression in the anterior midgut (AMG) and posterior midgut (PMG) compared to the hindgut (HG). However, analysis of densitometric data shows a significant expression of Upd3 in the HG (Fig.3.24), which will be further tested with a higher sensitivity using RT-qPCR.

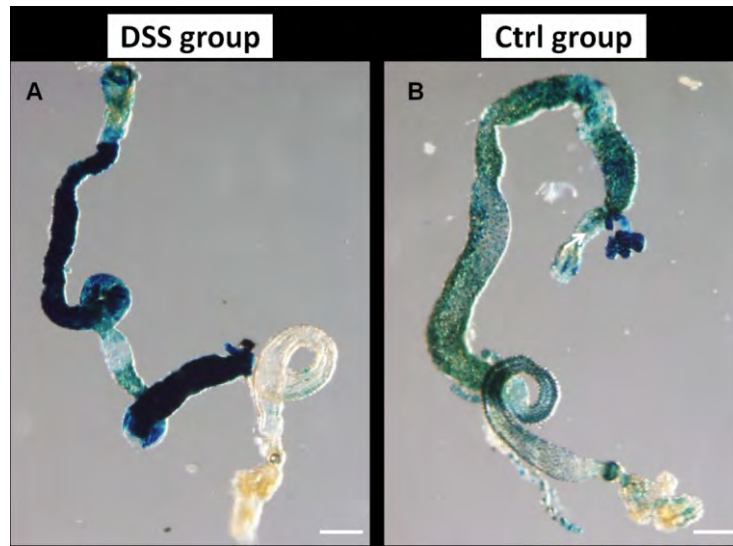


Fig.3.22: Representative images of dissected gut from Upd3-Gal4 >LacZ *Drosophila* reporter line after x-Gal staining in DSS- treated and control groups. Ctrl: controls. Scale bar = 100 μ m.

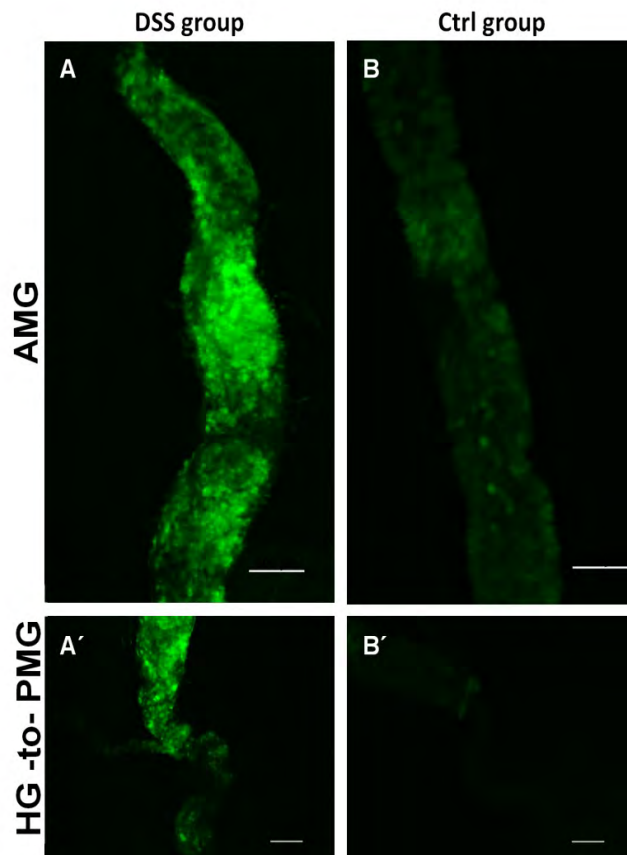


Fig.3.23: Representative images of dissected gut from Upd3-Gal4 >GFP *Drosophila* reporter line after immunostaining with α -GFP Ab in DSS- treated and control groups. Ctrl: controls.

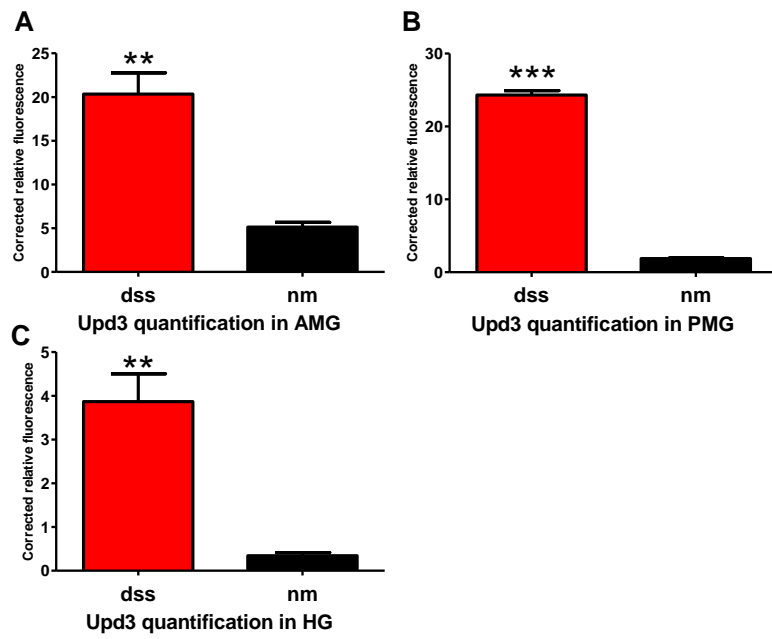


Fig.3.24: Densitometric semi- quantification of the Upd3-GFP signals in the *Drosophila* Upd3 >GFP reporter line after immunostaining with α -GFP Ab in DSS- treated and control groups. dss: DSS; nm refers to controls fed on normal media; AMG: anterior midgut; PMG: posterior midgut; HG: hindgutls.

3.2 Spatiotemporal gut-wide multiple gene expression analysis in DSS-induced *Drosophila* colitis-like model

3.2.1 DSS induces transcriptional dysregulation in the *Drosophila* anterior midgut (AMG) after 6-day treatment

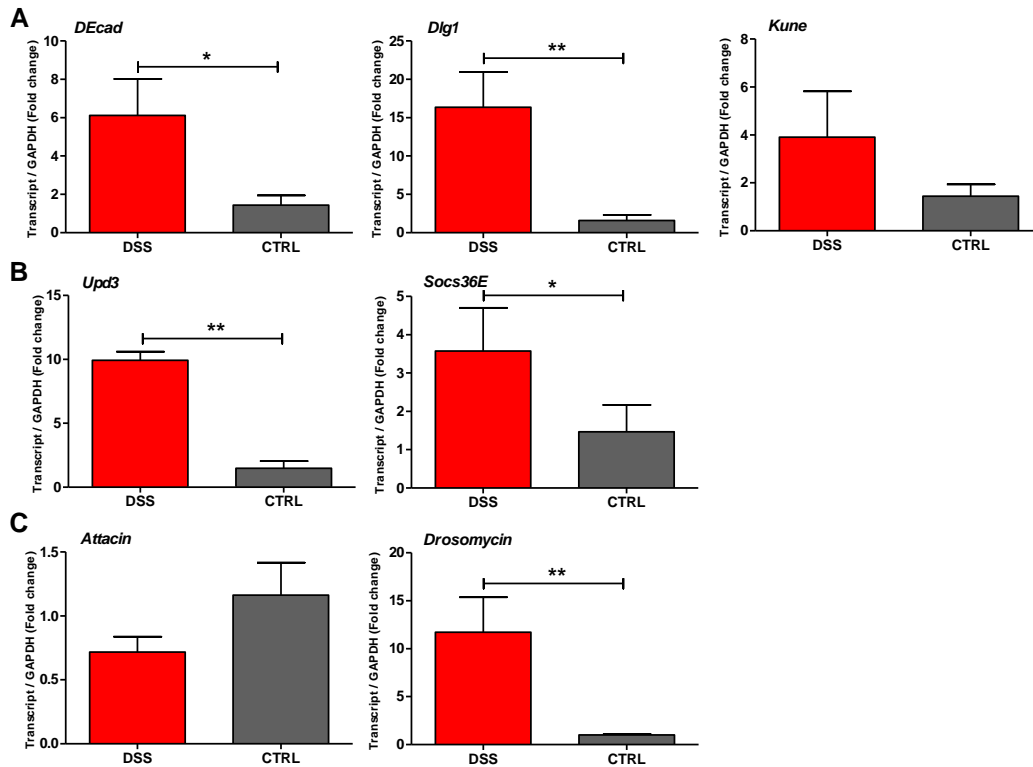


Fig.3.25: Effect of DSS treatment for 6 days on the transcriptional profile of candidate genes in the *Drosophila* anterior midgut. Each panel represents the mRNA levels of different gene categories: genes regulating the gut septate junction (Panel A); genes regulating the regenerative inflammatory signaling and ISCs proliferation (Panel B); and genes regulating antimicrobial defense and gut-microbiota interactions (Panel C). All transcripts are normalized by *Gapdh-1*. The differential expression is expressed as log fold change ($2^{-\Delta\Delta Ct}$) in transcript abundance in DSS-treated, and control groups. Values represent means \pm SEM for 5 biological replicates; * $p < 0.05$, ** $p < 0.01$.

3.2.2 DSS induces transcriptional dysregulation in the *Drosophila* posterior midgut (PMG) after 6-day treatment

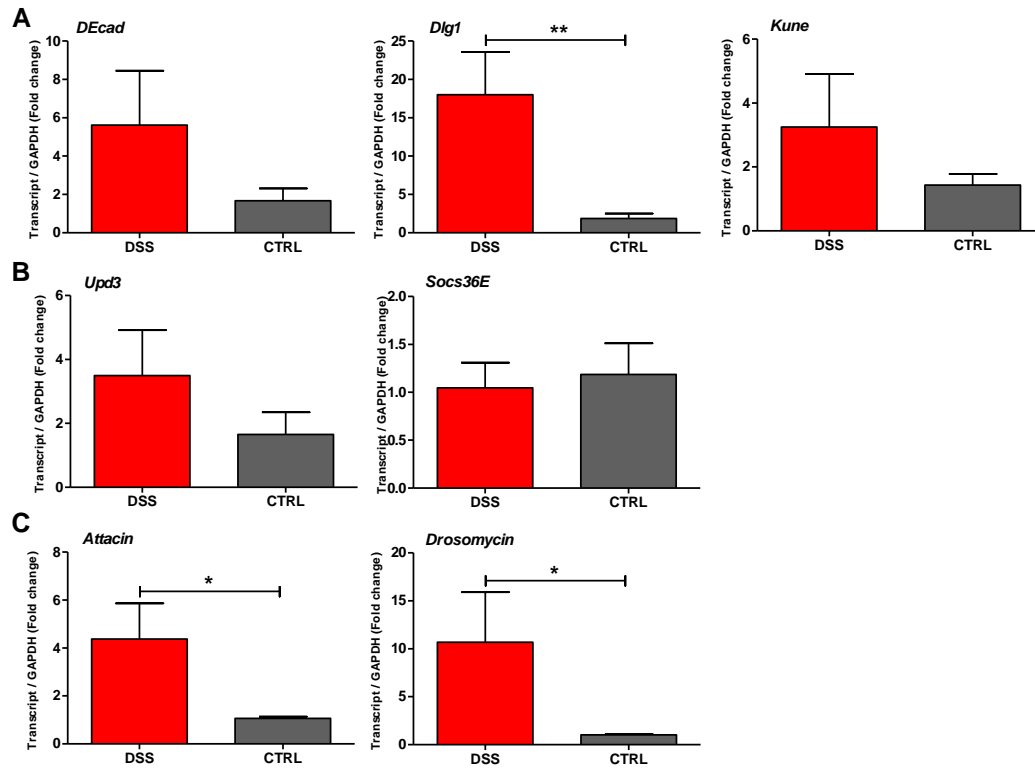


Fig.3.26: Effect of DSS treatment for 6 days on the transcriptional profile of candidate genes in the *Drosophila* posterior midgut. Each panel represents the mRNA levels of different gene categories: genes regulating the gut septate junction (Panel A); genes regulating the regenerative inflammatory signaling and ISCs proliferation (Panel B); and genes regulating antimicrobial defense and gut-microbiota interactions (Panel C). All transcripts are normalized by *Gapdh-1*. The differential expression is expressed as log fold change ($2^{-\Delta\Delta C_t}$) in transcript abundance in DSS-treated, and control groups. Values represent means \pm SEM for 5 biological replicates; * $p < 0.05$, ** $p < 0.01$.

3.2.3 DSS induces transcriptional dysregulation in the *Drosophila* hindgut (HG) after 6-day treatment

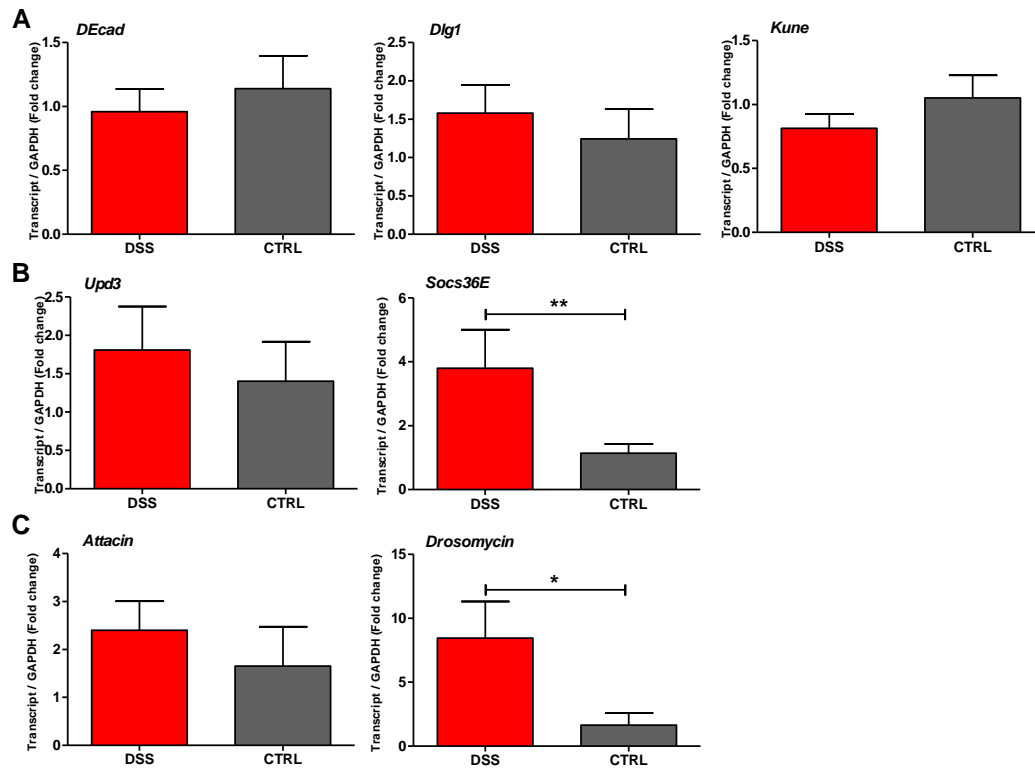


Fig.3.27: Effect of DSS treatment for 6 days on the transcriptional profile of candidate genes in the *Drosophila* hindgut. Each panel represents the mRNA levels of different gene categories: genes regulating the gut septate junction (Panel A); genes regulating the regenerative inflammatory signaling and ISCs proliferation (Panel B); and genes regulating antimicrobial defense and gut-microbiota interactions (Panel C). All transcripts are normalized by *Gapdh-1*. The differential expression is expressed as log fold change ($2^{-\Delta\Delta C_t}$) in transcript abundance in DSS-treated, and control groups. Values represent means \pm SEM for 5 biological replicates; *p<0.05, **p<0.01.

3.2.4 DSS induces transcriptional dysregulation in the *Drosophila* anterior midgut (AMG) after 12-day treatment

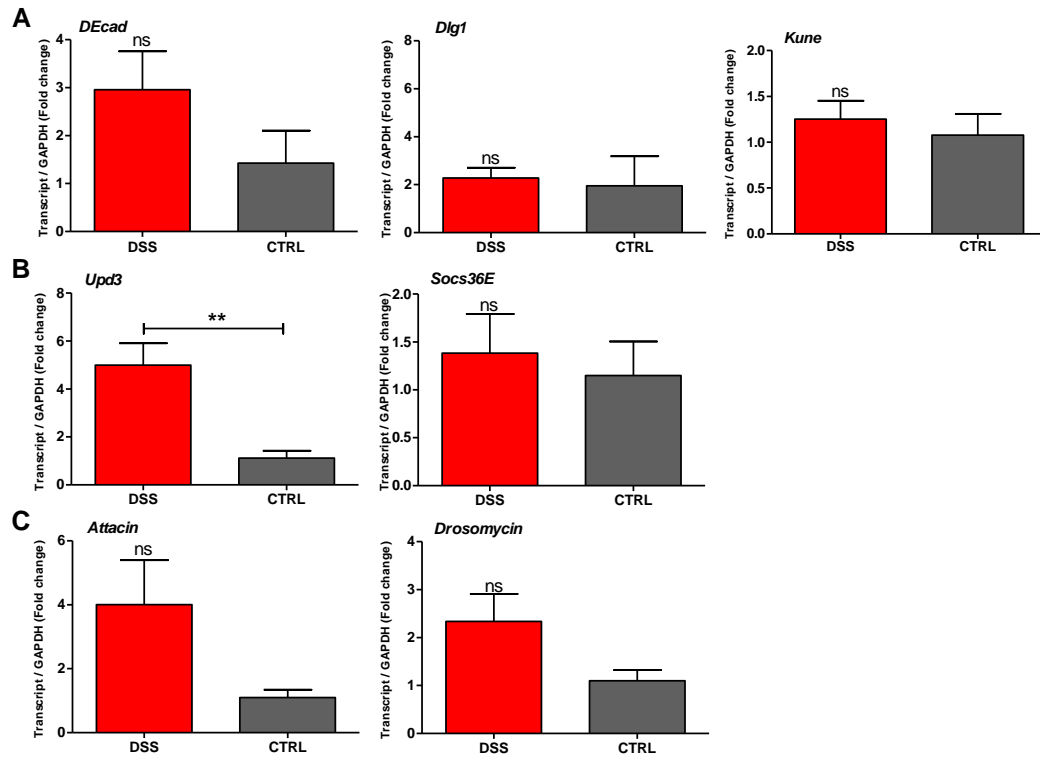


Fig.3.28: Effect of DSS treatment for 12 days on the transcriptional profile of candidate genes in the *Drosophila* anterior midgut. Each panel represents the mRNA levels of different gene categories: genes regulating the gut septate junction (Panel A); genes regulating the regenerative inflammatory signaling and ISCs proliferation (Panel B); and genes regulating antimicrobial defense and gut-microbiota interactions (Panel C). All transcripts are normalized by *Gapdh-1*. The differential expression is expressed as log fold change ($2^{-\Delta\Delta Ct}$) in transcript abundance in DSS-treated, and control groups. Values represent means \pm SEM for 5 biological replicates; * $p < 0.05$, ** $p < 0.01$, ns: non-significant.

3.2.5 DSS induces transcriptional dysregulation in the *Drosophila* posterior midgut (PMG) after 12-day treatment

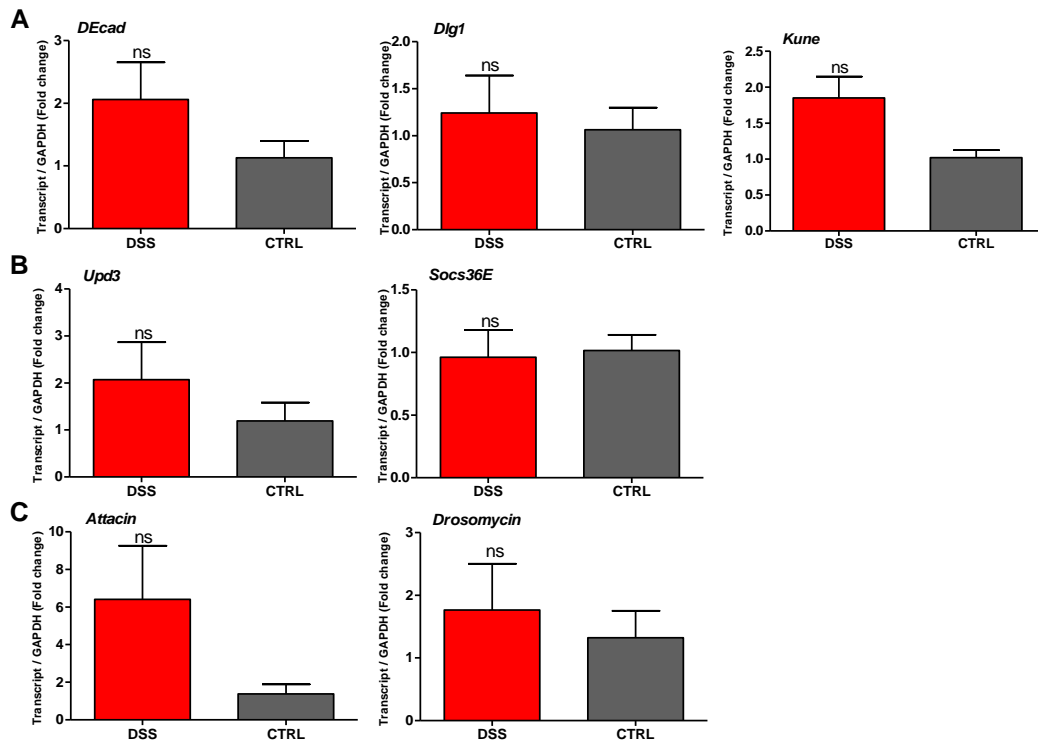


Fig.3.29: Effect of DSS treatment for 12 days on the transcriptional profile of candidate genes in the *Drosophila* posterior midgut. Each panel represents the mRNA levels of different gene categories: genes regulating the gut septate junction (Panel A); genes regulating the regenerative inflammatory signaling and ISCs proliferation (Panel B); and genes regulating antimicrobial defense and gut-microbiota interactions (Panel C). All transcripts are normalized by *Gapdh-1*. The differential expression is expressed as log fold change ($2^{-\Delta\Delta C_t}$) in transcript abundance in DSS-treated, and control groups. Values represent means \pm SEM for 5 biological replicates; * $p < 0.05$, ** $p < 0.01$, ns: non-significant.

3.2.6 DSS induces transcriptional dysregulation in the *Drosophila* hindgut (HG) after 12-day treatment

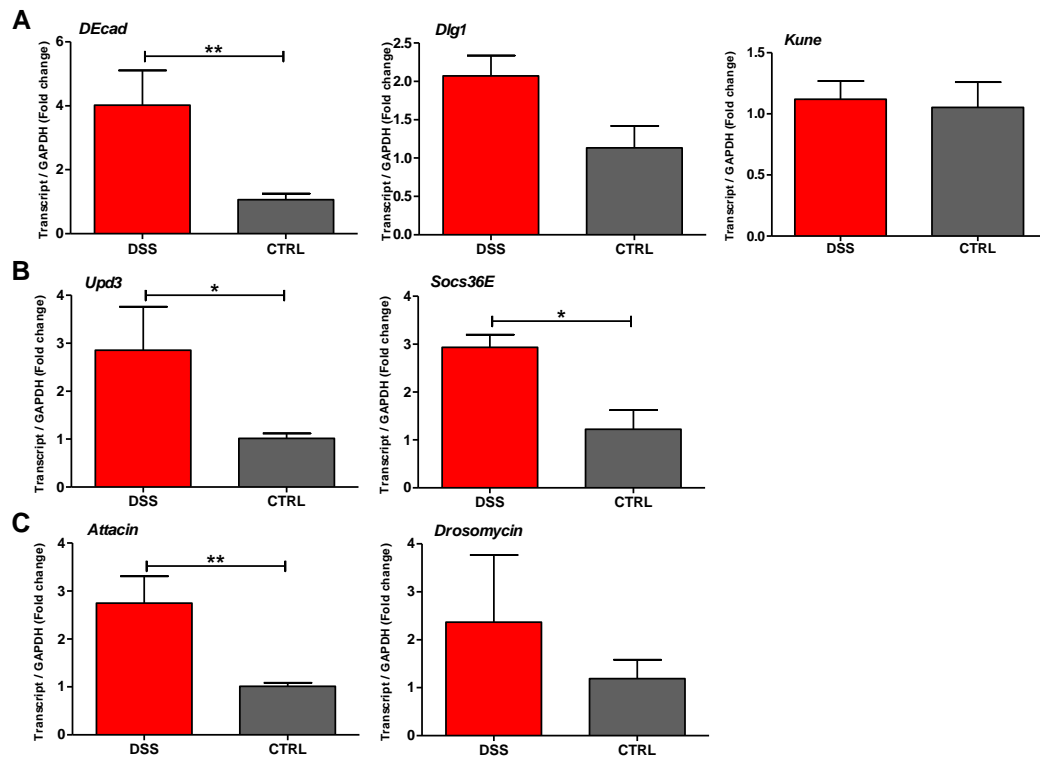


Fig.3.30: Effect of DSS treatment for 12 days on the transcriptional profile of candidate genes in the *Drosophila* hindgut. Each panel represents the mRNA levels of different gene categories: genes regulating the gut septate junction (Panel A); genes regulating the regenerative inflammatory signaling and ISCs proliferation (Panel B); and genes regulating antimicrobial defense and gut-microbiota interactions (Panel C). All transcripts are normalized by *Gapdh-1*. The differential expression is expressed as log fold change ($2^{-\Delta\Delta C_t}$) in transcript abundance in DSS-treated, and control groups. Values represent means \pm SEM for 5 biological replicates; * $p < 0.05$, ** $p < 0.01$, ns: non-significant.

3.2.7 Spatiotemporal gut-wide transcriptional dysregulation in the *Drosophila* DSS-induced colitis model

Basically, volcano plot is a scatter plots used to display omics data. However, it is used to graphically summarize the magnitude of transcript expression fold changes versus statistical significance (p-value). The log₂ of the fold change in the transcript expression of each candidate genes and the corresponding p-value (-log₁₀) are plotted on the x-axis and y-axis, respectively. The horizontal line (at value 1.3) indicates the p value threshold (-log₁₀ (0.05)) .The two dashed vertical lines are set to mark the threshold in transcript regulation. Genes represented by data points in the range of between +1 and -1 threshold represent genes that are unchanged after DSS treatment. On the other hand, data points distributed in the upper left [I.e. > +1 fold change & > 1,3 (-log 0.05)] represent genes that are up-regulated after DSS treatment.

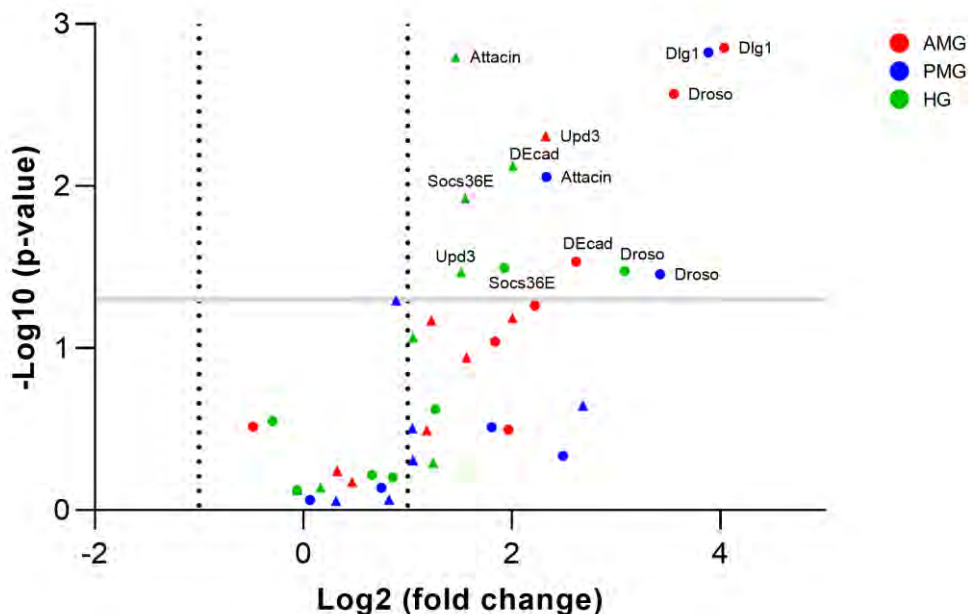


Fig.3.31: Volcano plot depicts the top 15 up-regulated genes in the *Drosophila* gut at day 6 and 12 post DSS treatment. Values represent means \pm SEM for 5 biological replicates; Regardless of statistical significance, data points presented in red=anterior midgut; in blue=posterior midgut; in green=hindgut. Data points presented in circle refer to day-6 post DSS treatment. Data points presented in triangle refer to day-12 post DSS treatment. The differential expression is expressed as log₂ fold change in transcript abundance in DSS-treated, and control groups. Values represent means \pm SEM for 5 biological replicates.

3.2.8 Gene-gene interactions in the *Drosophila* gut at day-6 post DSS treatment.

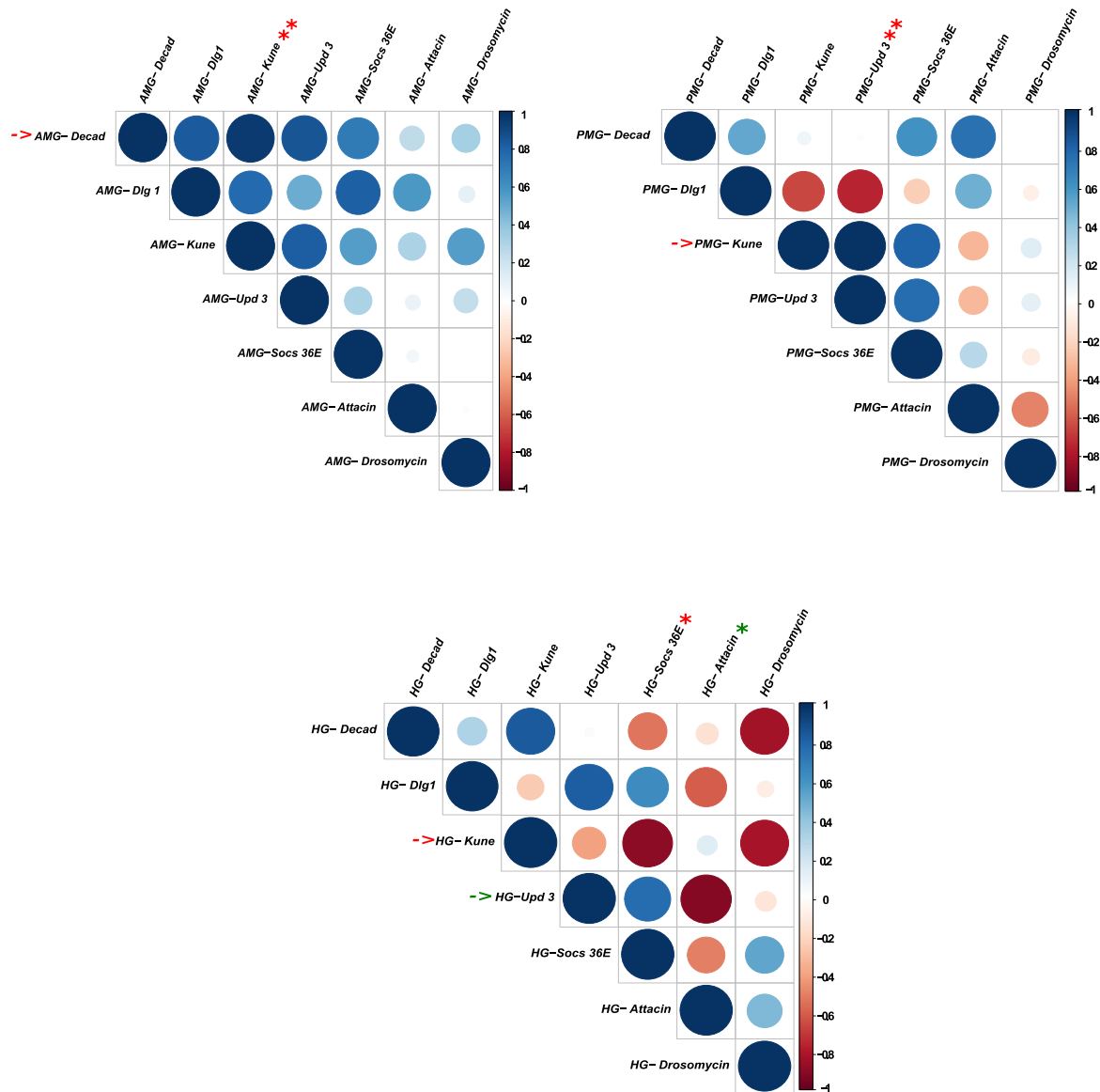


Fig.3.32: Corplot depicts the pairwise correlation between fold change of candidate transcript expression in different gut regions at day-6 post DSS treatment. Correlation graph depicts strength and direction of pairwise correlations between log fold change ($2^{-\Delta\Delta Ct}$) of all candidate genes. Pearson's r represented by the color gradient for blue (positively)- or red (negatively)- correlated pairs. The color of circles corresponds to the direction of correlations whilst color intensities and size are directly proportional to strength and significance of correlation, respectively. Regardless of statistical significance, colors of asterisks and arrows represent pairs. Values represent means \pm SEM for 5 biological replicates; * $p < 0.05$, ** $p < 0.01$.

3.2.9 Gene-gene interactions in the *Drosophila* gut at day-12 post DSS treatment.

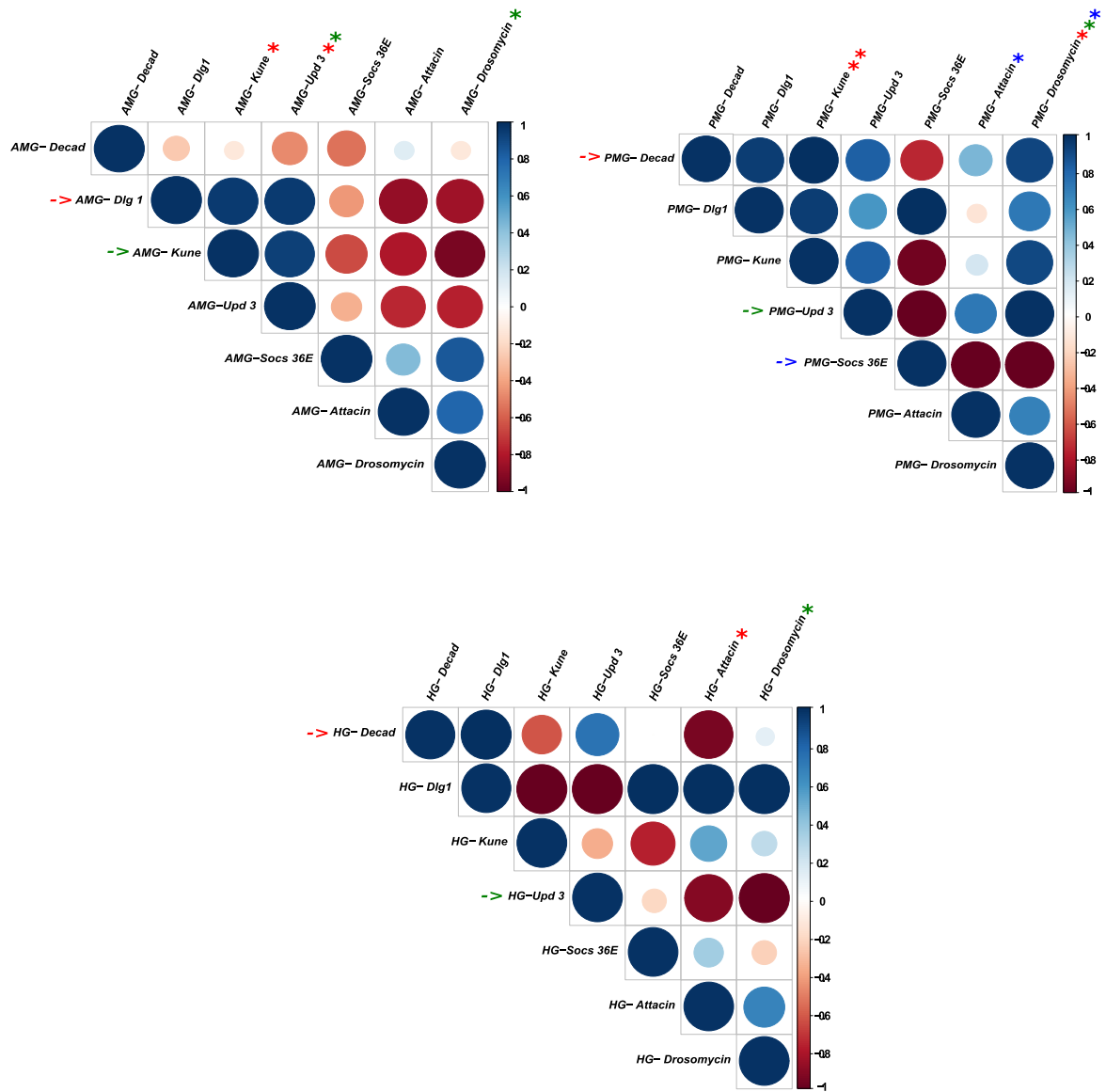


Fig.3.33: Corplot depicts the pairwise correlation between fold change of candidate transcript expression in different gut regions at day-12 post DSS treatment. Correlation graph depicts strength and direction of pairwise correlations between log fold change ($2^{-\Delta\Delta Ct}$) of all candidate genes. Pearson's r represented by the color gradient for blue (positively)- or red (negatively)- correlated pairs. The color of circles corresponds to the direction of correlations whilst color intensities and size are directly proportional to strength and significance of correlation, respectively. Regardless of statistical significance, colors of asterisks and arrows represent pairs. Values represent means \pm SEM for 5 biological replicates; * $p < 0.05$, ** $p < 0.01$.

3.2.10 Six-day recovery period impacts the restoration of transcriptional dysregulation in the *Drosophila* anterior midgut

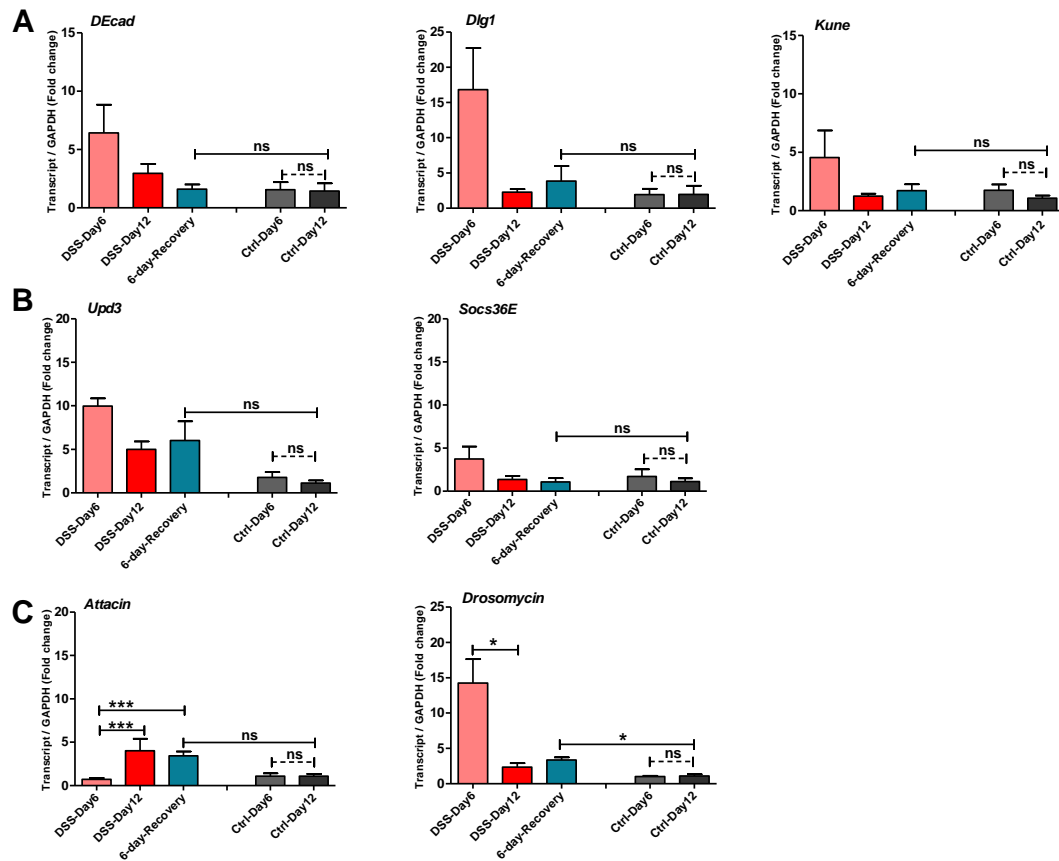


Fig.3.34: Effect of 6-day recovery period after 6-day DSS treatment on the transcriptional profile of candidate genes in the *Drosophila* anterior midgut. Each panel represents the mRNA levels of different gene categories: genes regulating the gut septate junction (Panel A); genes regulating the regenerative inflammatory signaling and ISCs proliferation (Panel B); and genes regulating antimicrobial defense and gut-microbiota interactions (Panel C). All transcripts are normalized by *Gapdh-1*. The differential expression is expressed as log fold change ($2^{-\Delta\Delta Ct}$) in transcript abundance in DSS-treated, and control groups. Regardless to the commonly used color code, dark red color=DSS treatment for 12 days; pale red=DSS treatment for 6 days; blue= recovery group; pale grey= non-treated controls at day 6; dark grey= non-treated controls at day 12. Values represent means \pm SEM for 5 biological replicates; * $p < 0.05$, ** $p < 0.01$, *** $p < 0.001$, ns: non-significant.

3.2.11 Six-day recovery period impacts the restoration of transcriptional dysregulation in the *Drosophila* posterior midgut

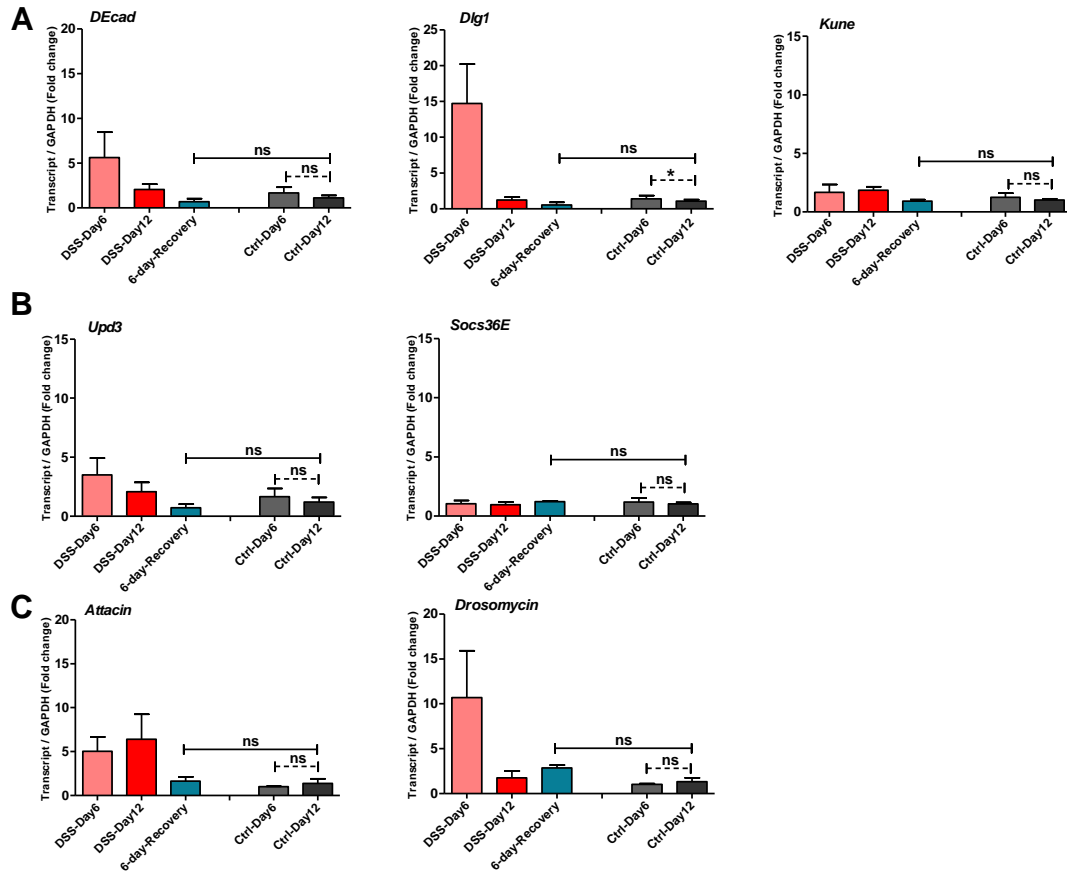


Fig.3.35: Effect of 6-day recovery period after 6-day DSS treatment on the transcriptional profile of candidate genes in the *Drosophila* posterior midgut. Each panel represents the mRNA levels of different gene categories: genes regulating the gut septate junction (Panel A); genes regulating the regenerative inflammatory signaling and ISCs proliferation (Panel B); and genes regulating antimicrobial defense and gut-microbiota interactions (Panel C). All transcripts are normalized by *Gapdh-1*. The differential expression is expressed as log fold change ($2^{-\Delta\Delta C_t}$) in transcript abundance in DSS-treated, and control groups. Regardless to the commonly used color code, dark red color=DSS treatment for 12 days; pale red=DSS treatment for 6 days; blue= recovery group; pale grey= non-treated controls at day 6; dark grey= non-treated controls at day 12. Values represent means \pm SEM for 5 biological replicates; * $p < 0.05$, ** $p < 0.01$, *** $p < 0.001$, ns: non-significant.

3.2.12 Six-day recovery period impacts the restoration of transcriptional dysregulation in the *Drosophila* hindgut

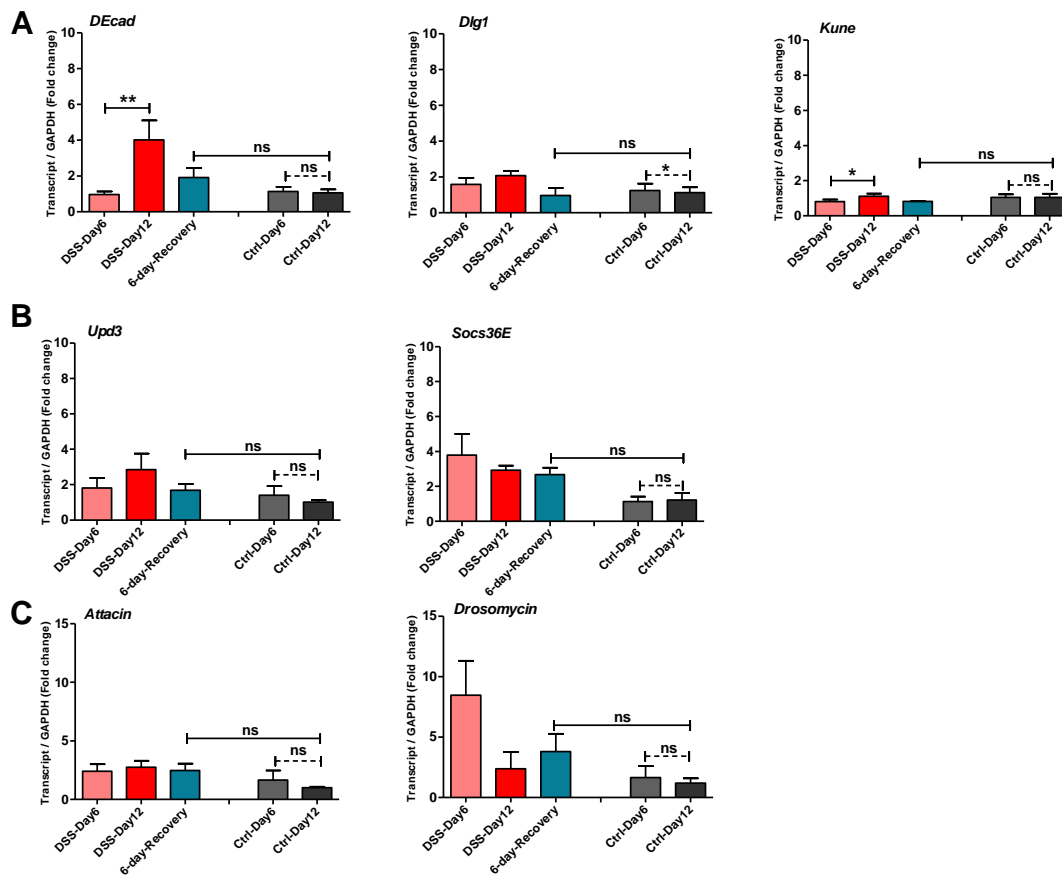


Fig.3.36: Effect of 6-day recovery period after 6-day DSS treatment on the transcriptional profile of candidate genes in the *Drosophila* hindgut. Each panel represents the mRNA levels of different gene categories: genes regulating the gut septate junction (Panel A); genes regulating the regenerative inflammatory signaling and ICS proliferation (Panel B); and genes regulating antimicrobial defense and gut-microbiota interactions (Panel C). All transcripts are normalized by *Gapdh-1*. The differential expression is expressed as log fold change ($2^{-\Delta\Delta C_t}$) in transcript abundance in DSS-treated, and control groups. Regardless to the commonly used color code, dark red color=DSS treatment for 12 days; pale red= DSS treatment for 6 days; blue= recovery group; pale grey= non-treated controls at day 6; dark grey= non-treated controls at day 12. Values represent means \pm SEM for 5 biological replicates; * $p < 0.05$, ** $p < 0.01$, *** $p < 0.001$, ns: non-significant.

3.2.13 Gene-gene interactions in the *Drosophila* gut after 6-day recovery period

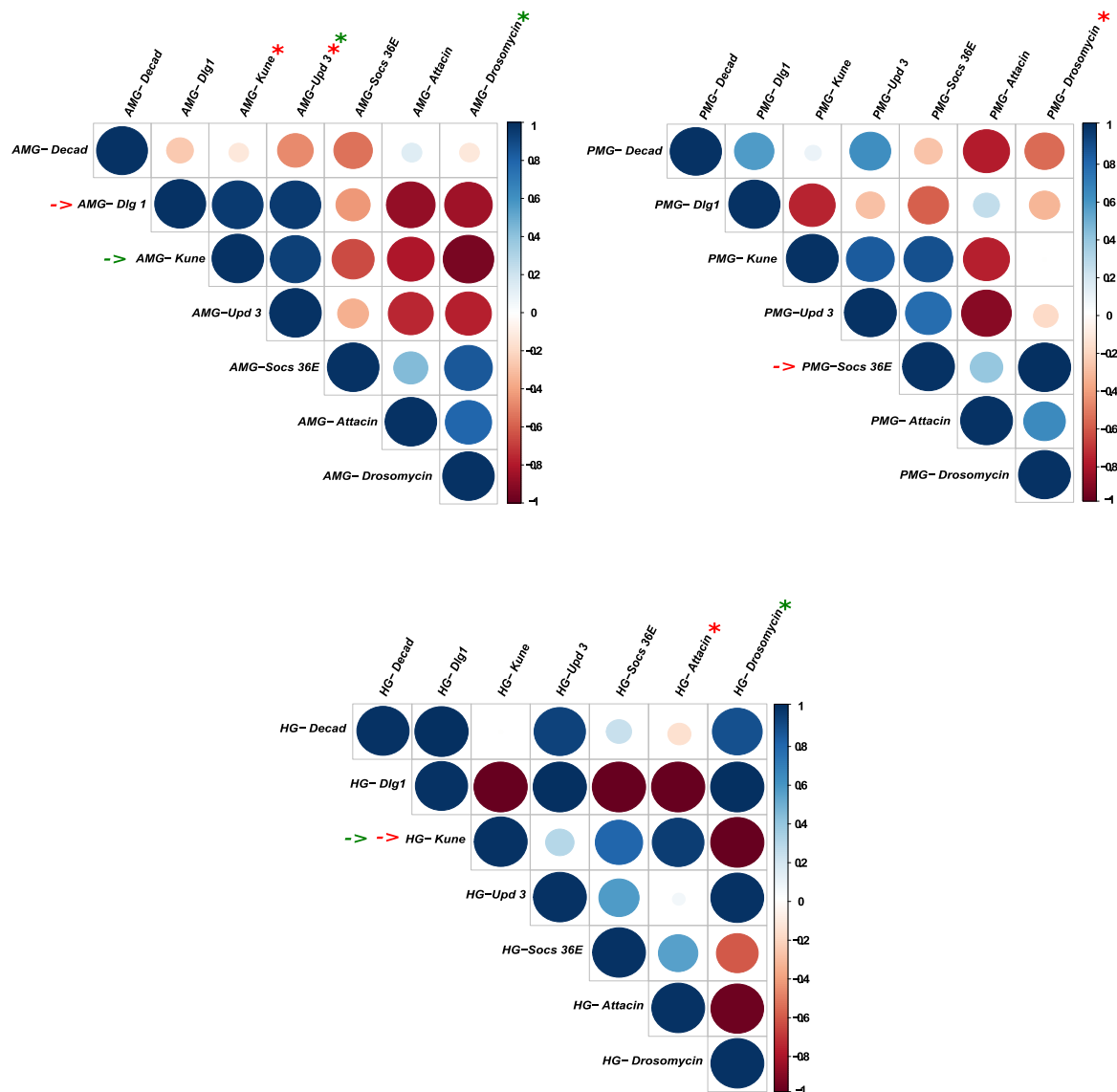


Fig.3.37: Corrplot depicts the pairwise correlation between fold change of candidate transcript expression in different gut regions after 6-day recovery period. Correlation graph depicts strength and direction of pairwise correlations between log fold change ($2^{-\Delta\Delta Ct}$) of all candidate genes. Pearson's r represented by the color gradient for blue (positively)- or red (negatively)- correlated pairs. The color of circles corresponds to the direction of correlations whilst color intensities and size are directly proportional to strength and significance of correlations, respectively. Regardless of statistical significance, colors of asterisks and arrows represent pairs. Values represent means \pm SEM for 5 biological replicates; * $p < 0.05$, ** $p < 0.01$.

3.3 Spatiotemporal gut-wide microbiota profiling in DSS-induced *Drosophila* colitis-like model

3.3.1 Effect of 6-day DSS treatment on the *Drosophila* fecal microbiota community structure

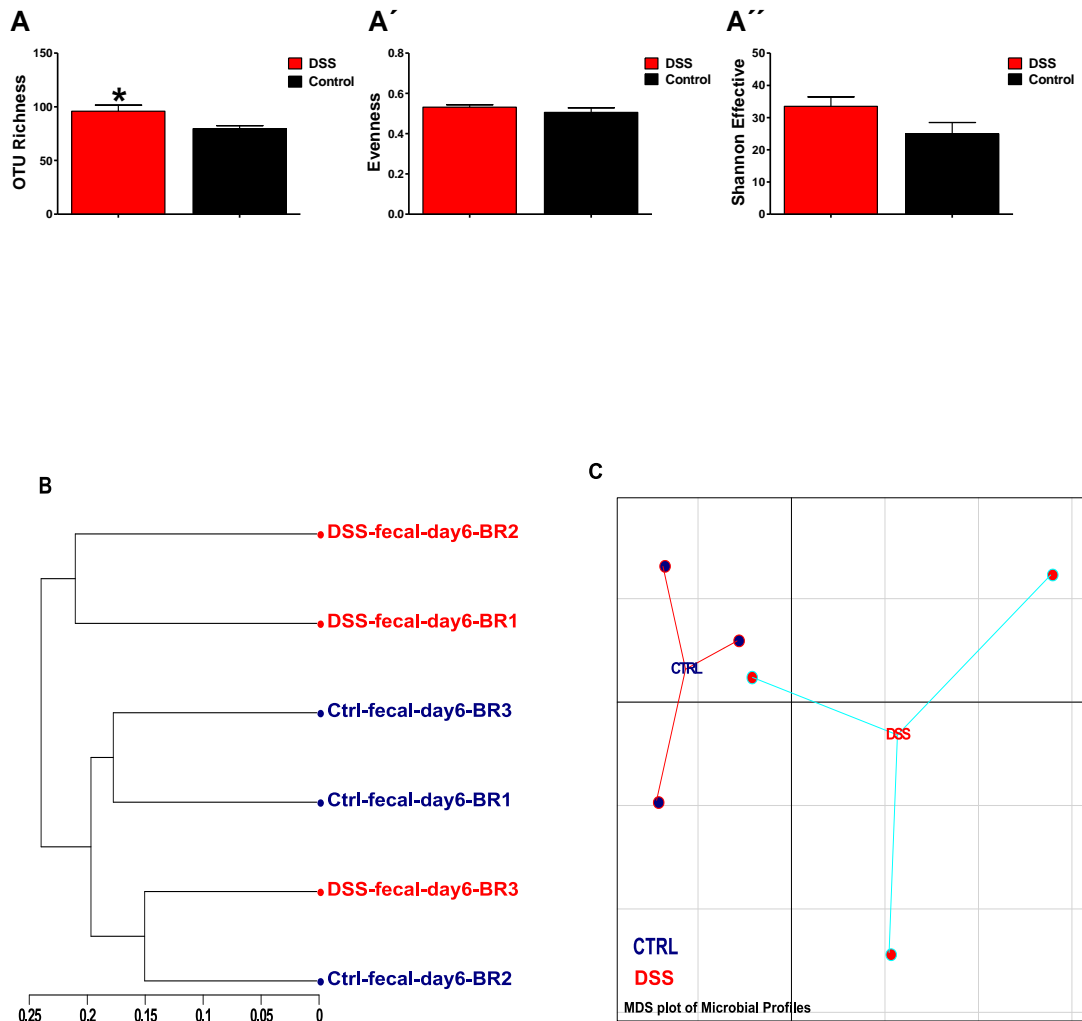


Fig.3.38: Graphs depict multiple aspects of fecal microbiota community structure after 6-day post DSS treatment. Phylogenetic diversity is presented as alpha-diversity and beta-diversity on normalized counts. Alpha-diversity (Panel A) is summarized as OTU richness (A), Evenness (A') and Shannon effective (A''). Beta-diversity is carried out using generalized UniFrac distance metric and presented by the dendrogram (Panel B) and MDS (Panel C) of all samples. Values represent means ± SEM for 3 biological replicates. CTRL: controls; BR: Biological replicates; MDS: multidimensional scaling. *p<0.05.

3.3.2 Effect of 6-day DSS treatment for on the *Drosophila* fecal microbiota abundance at higher taxonomic ranks

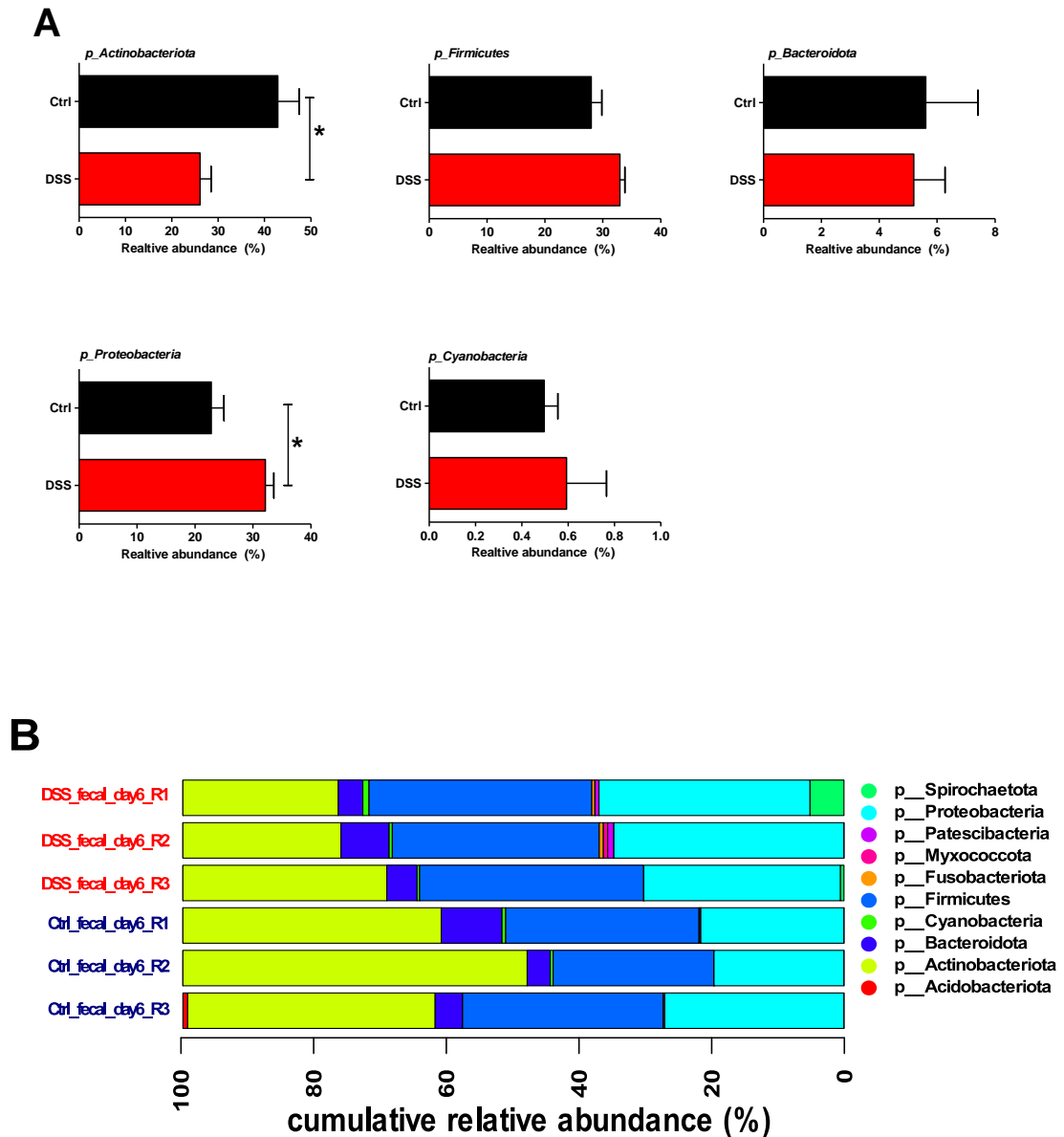
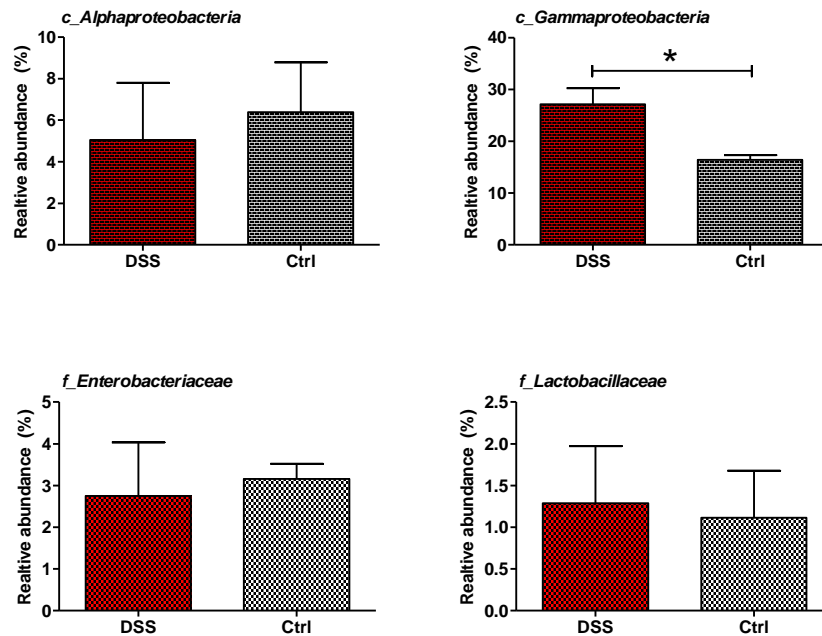


Fig.3.39: Graphs depict differentially abundant and discriminating taxa of fecal microbiota after 6-day post DSS treatment. Relative abundance of all zOTUs reveals major phyla with their informative ratio (Panel A). Taxonomic pinning at the phyla levels shows cumulative relative abundance (%) of major and minor phyla (Panel B). Values represent means \pm SEM for 3 biological replicates. Ctrl: controls; R=BR: Biological replicates; p_: phylum. * $p < 0.05$.

3.3.3 Effect of 6-day DSS treatment on the *Drosophila* fecal microbiota abundance at lower taxonomic ranks

A



B

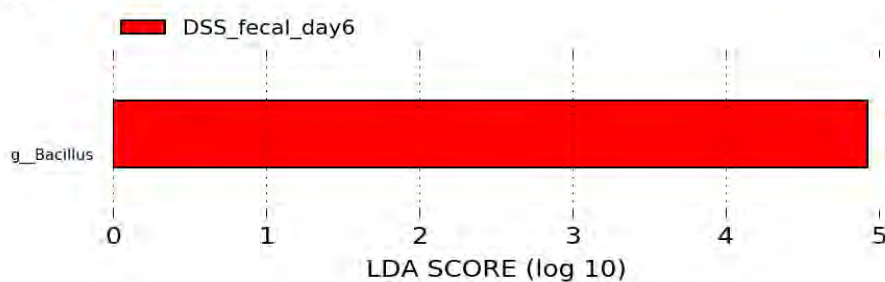


Fig.3.40: Graphs depict selected differentially abundant families, classes and microbial biomarker(s) of fecal microbiota after 6-day post DSS treatment. Relative abundance of all zOTUs reveals major classes of proteobacteria as well as other relevant families with their informative ratio (Panel A). Linear discriminant analysis (LDA>2.0) coupled with effect size measurements (Panel B). Values represent means± SEM for 3 biological replicates. Ctrl: controls; LDA: Linear discriminant analysis; c_: class; f_: family; g_: genus. *p<0.05.

3.3.4 Effect of DSS treatment for 6 days on the interaction of different parameters of fecal microbiota community and physiologic correlates

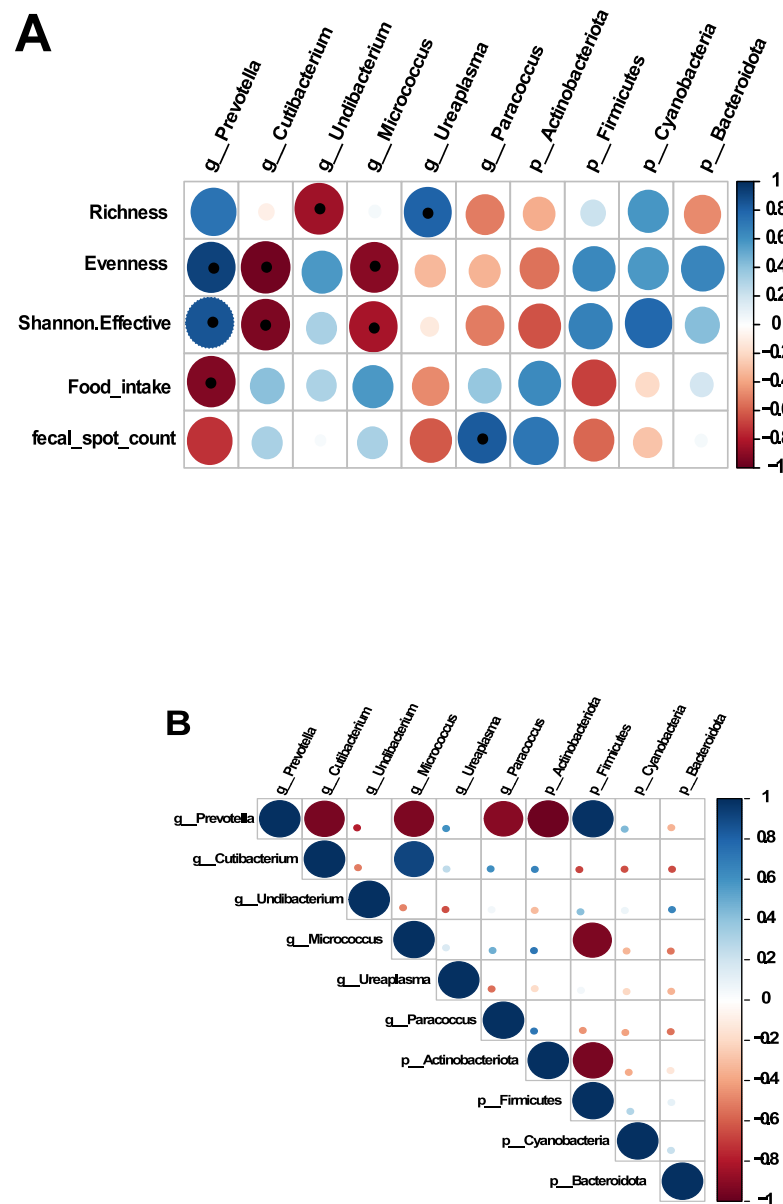


Fig.3.41: A graphical display of correlations arrays across differentially-abundant taxonomic ranks of fecal microbiota and physiologic parameters after 6-day post DSS treatment. Pearson's pairwise correlations between relative abundance of taxa (at phyla and genus levels) and quantitative gut phenotypes (panel A) and taxa-taxa interactions (panel B). Pearson's r represented by the color gradient for blue (positively)- or red (negatively)- correlated pairs. The color of circles corresponds to the direction of correlations whilst color intensities and size are directly proportional to strength and significance of correlation, respectively. Black dots mark data points that pass the threshold of the correlation coefficient r p-value. Values represent means \pm SEM for 3 biological replicates (in taxonomic variables) and 5 biological replicates (physiologic variables). p_:phylum; g_: genus.

3.3.5 Effect of 6-day DSS treatment on the *Drosophila* midgut microbiota community structure

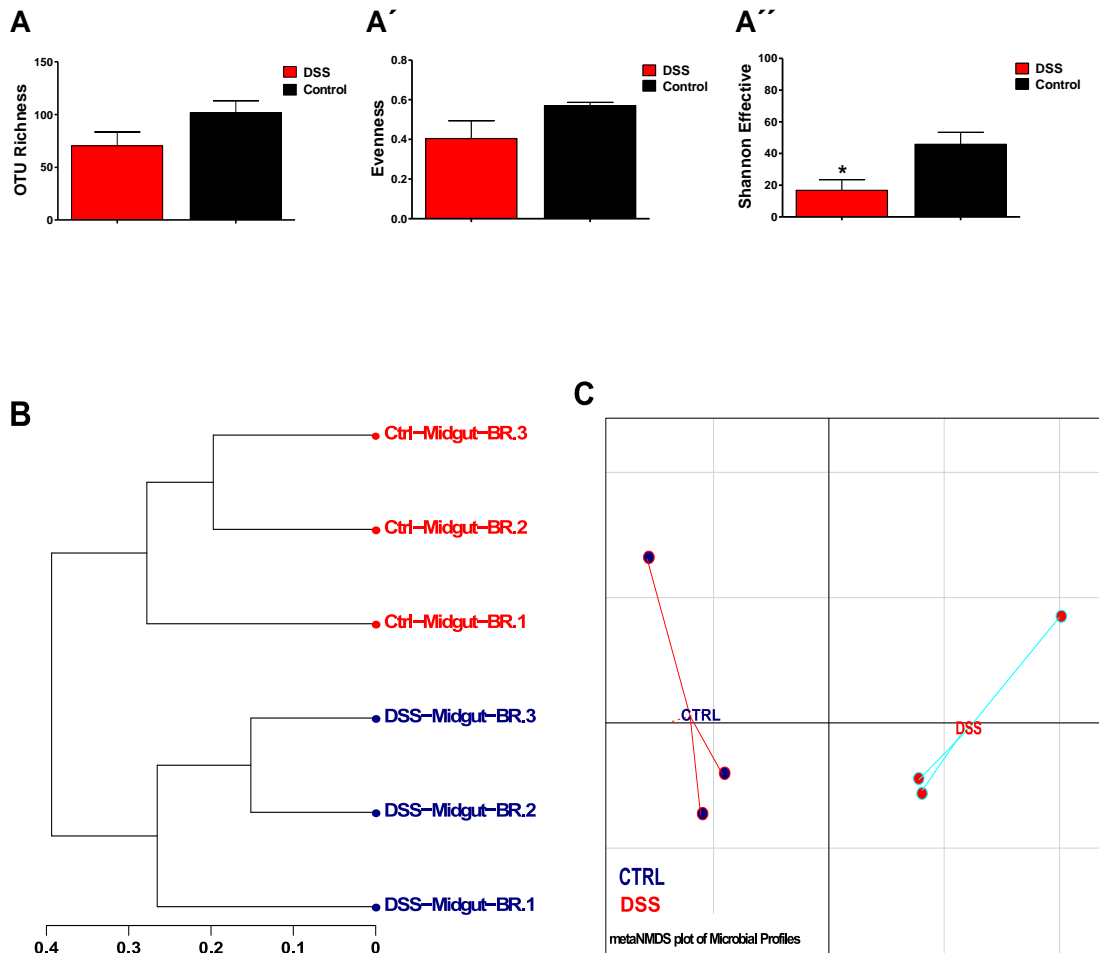


Fig.3.42: Graphs depict multiple aspects of midgut microbiota community structure after 6-day post DSS treatment. Phylogenetic diversity is presented as alpha-diversity and beta-diversity on normalized counts. Alpha-diversity (Panel A) is summarized as OTU richness (A), Evenness (A') and Shannon effective (A''). Beta-diversity is carried out using generalized UniFrac distance metric and presented by the dendrogram (Panel B) and metaMDS (Panel C) of all samples. Values represent means ± SEM for 3 biological replicates. CTRL: controls; BR: Biological replicates; metaMDS: non-metric multidimensional scaling. *p<0.05.

3.3.6 Effect of 6-day DSS treatment for on the *Drosophila* midgut microbiota abundance at higher taxonomic ranks

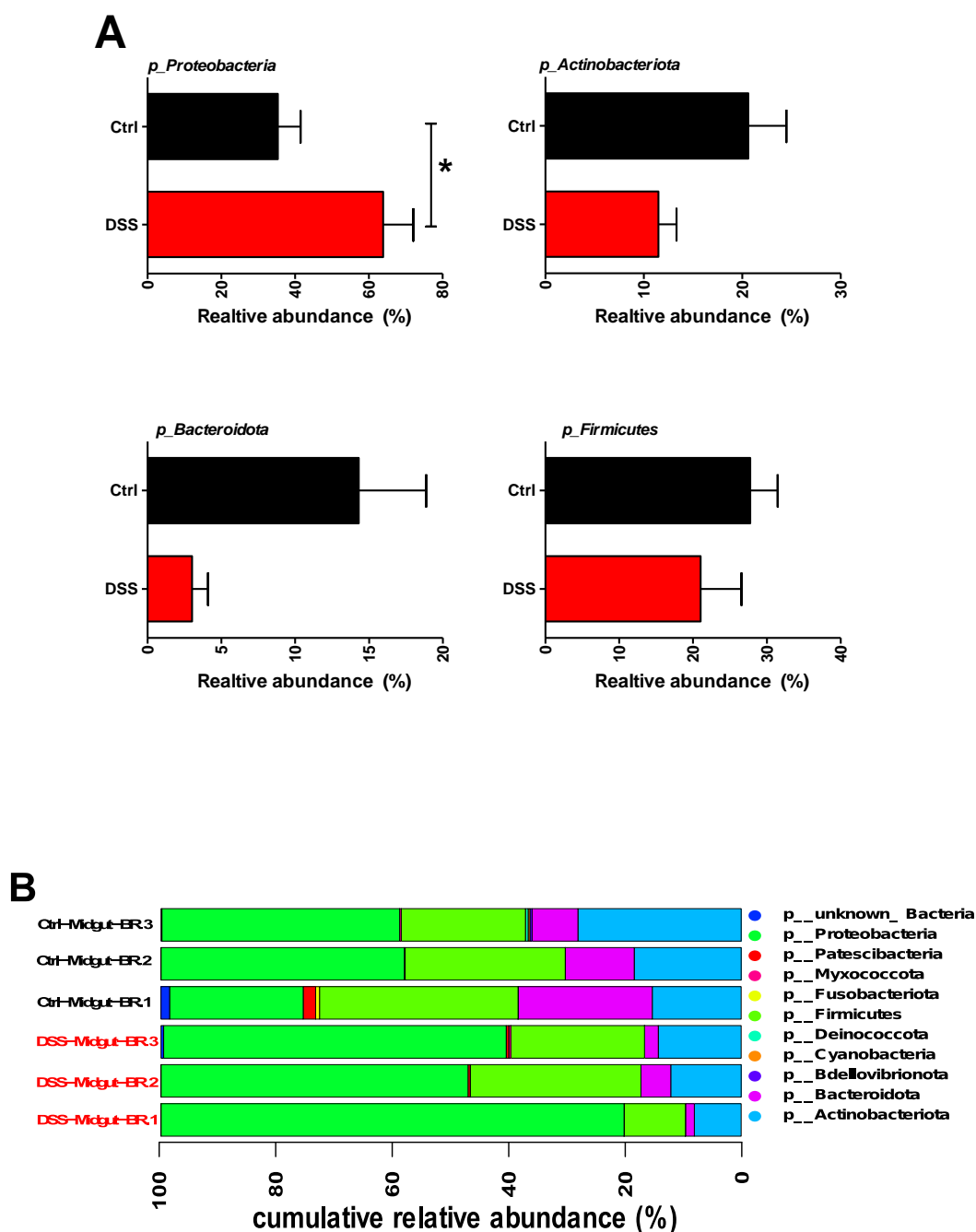


Fig.3.43: Graphs depict differentially abundant and discriminating taxa in the midgut microbiota after 6-day post DSS treatment. Relative abundance of all zOTUs reveals major phyla with their informative ratio (Panel A). Taxonomic pinning at the phyla levels shows cumulative relative abundance (%) of major and minor phyla (Panel B). Values represent means \pm SEM for 3 biological replicates. Ctrl: controls; BR: Biological replicates; p_: phylum. * $p < 0.05$.

3.3.7 Effect of 6-day DSS treatment on the *Drosophila* midgut microbiota abundance at lower taxonomic ranks

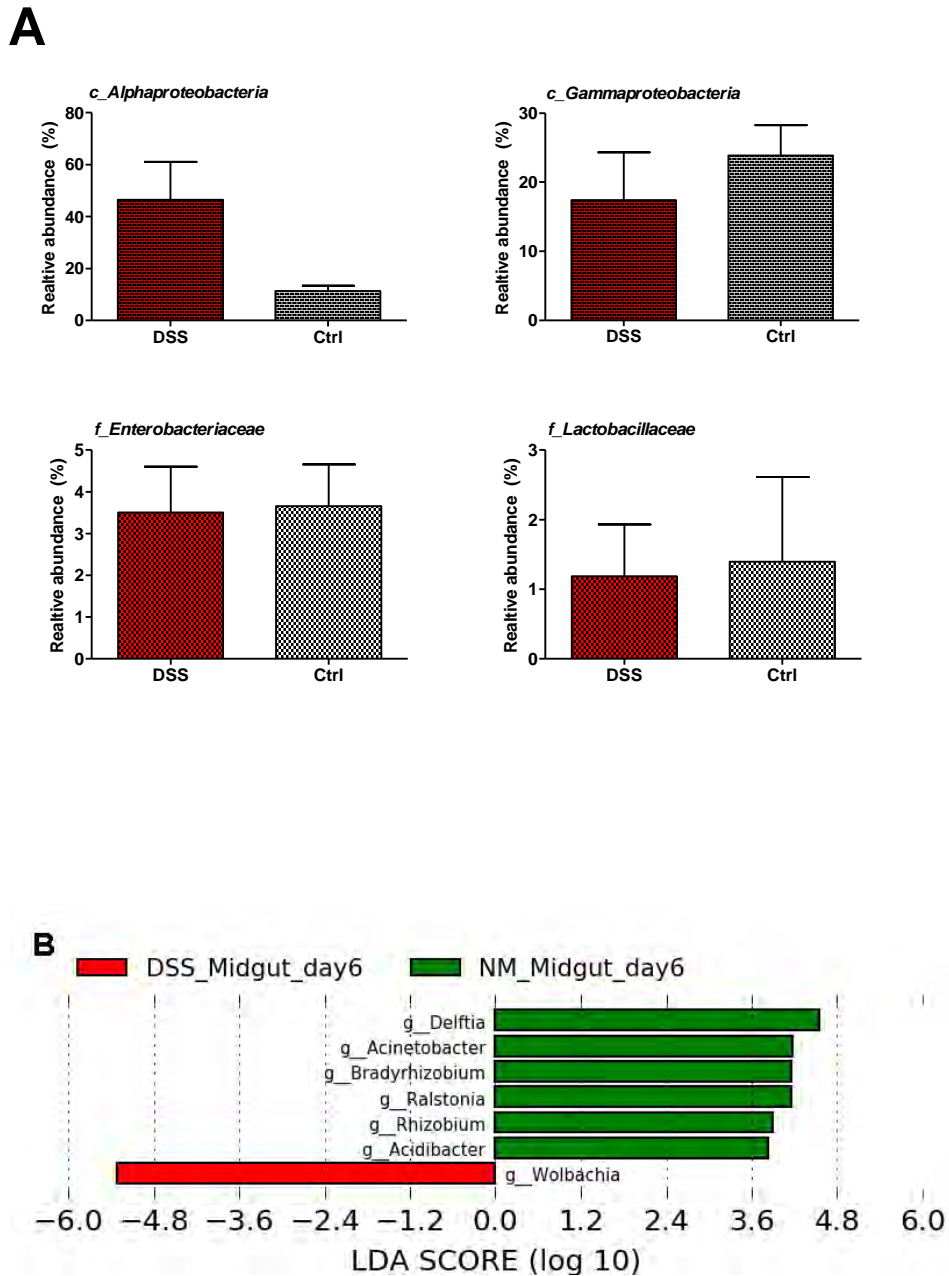


Fig.3.44: Graphs depict selected differentially abundant families, classes and microbial biomarker(s) midgut microbiota after 6-day post DSS treatment. Relative abundance of all zOTUs reveals major classes of proteobacteria as well as other relevant families with their informative ratio (Panel A). Linear discriminant analysis (LDA>2.0) coupled with effect size measurements (Panel B). Values represent means± SEM for 3 biological replicates. Ctrl: controls; LDA: Linear discriminant analysis; c_: class; f_: family; g_: genus.

3.3.8 Effect of 6-day DSS treatment on the *Drosophila* hindgut microbiota community structure

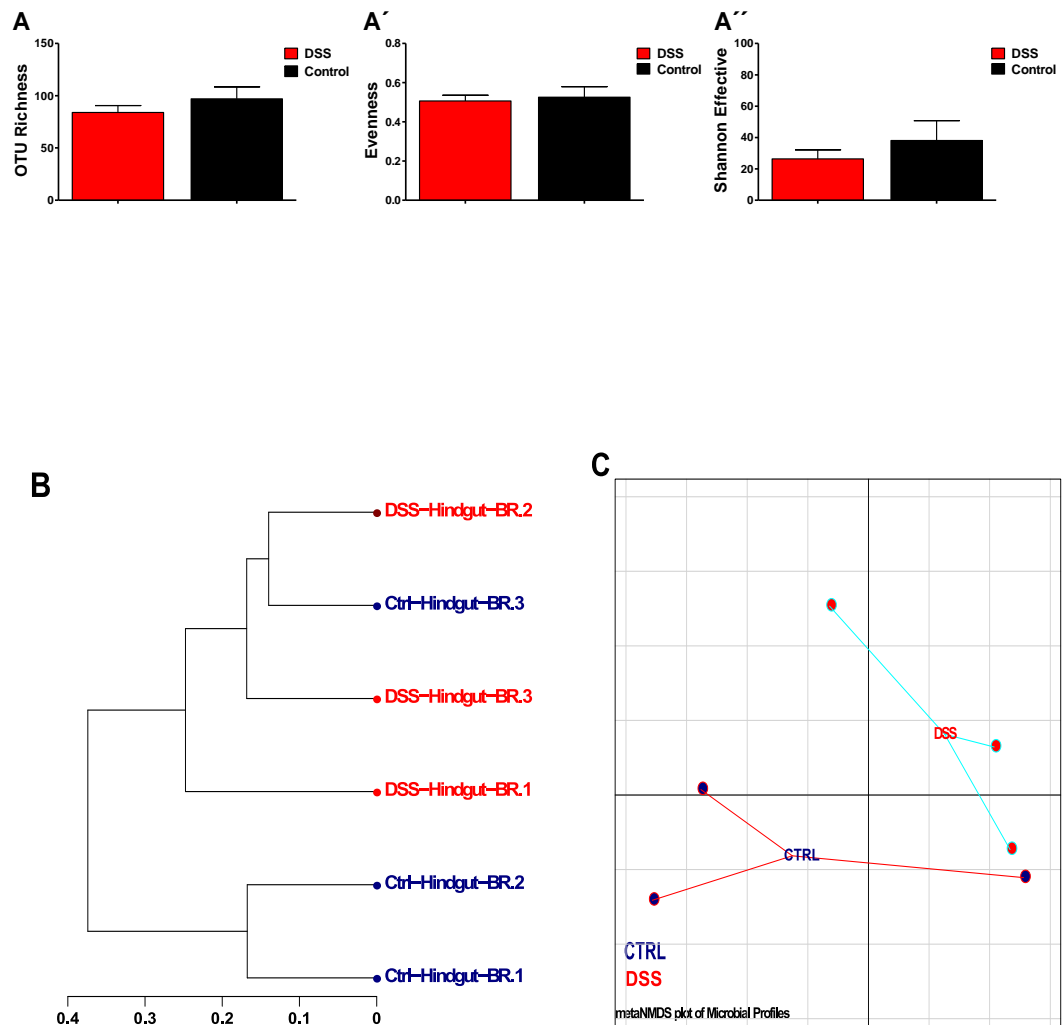


Fig.3.45: Graphs depict multiple aspects of hindgut microbiota community structure after 6-day post DSS treatment. Phylogenetic diversity is presented as alpha-diversity and beta-diversity on normalized counts. Alpha-diversity (Panel A) is summarized as OTU richness (A), Evenness (A') and Shannon effective (A''). Beta-diversity is carried out using generalized UniFrac distance metric and presented by the dendrogram (Panel B) and metaNMDS (Panel C) of all samples. Values represent means \pm SEM for 3 biological replicates. CTRL: controls; BR: Biological replicates; metaMDS: non-metric multidimensional scaling.

3.3.9 Effect of 6-day DSS treatment for on the *Drosophila* hindgut microbiota abundance at higher taxonomic ranks

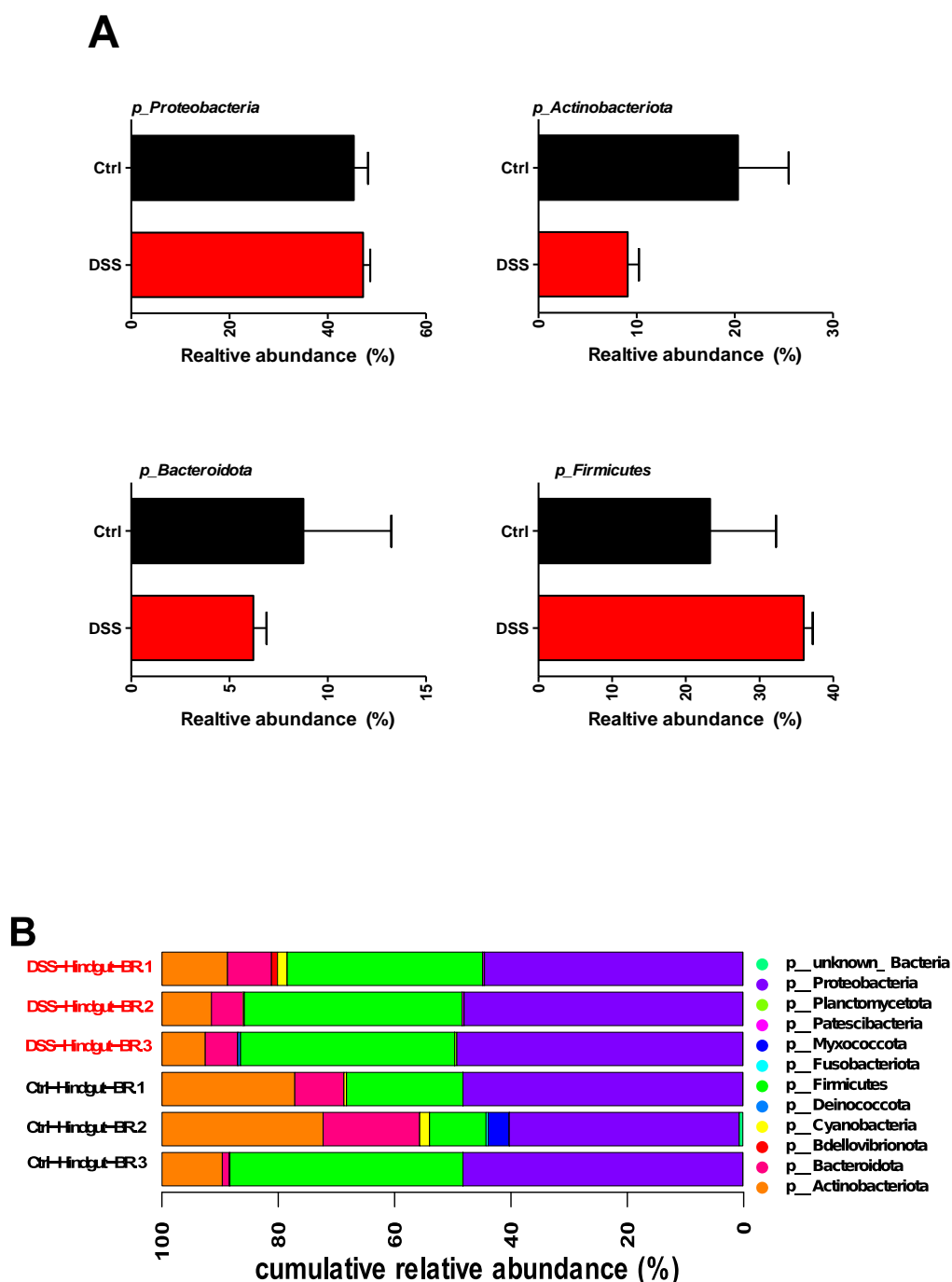


Fig.3.46: Graphs depict differentially abundant and discriminating taxa in the hindgut microbiota after 6-day post DSS treatment. Relative abundance of all zOTUs reveals major phyla with their informative ratio (Panel A). Taxonomic pinning at the phyla levels shows cumulative relative abundance (%) of major and minor phyla (Panel B). Values represent means \pm SEM for 3 biological replicates. Ctrl: controls; BR: Biological replicates; p_: phylum.

3.3.10 Effect of 6-day DSS treatment on the *Drosophila* hindgut microbiota abundance at lower taxonomic ranks

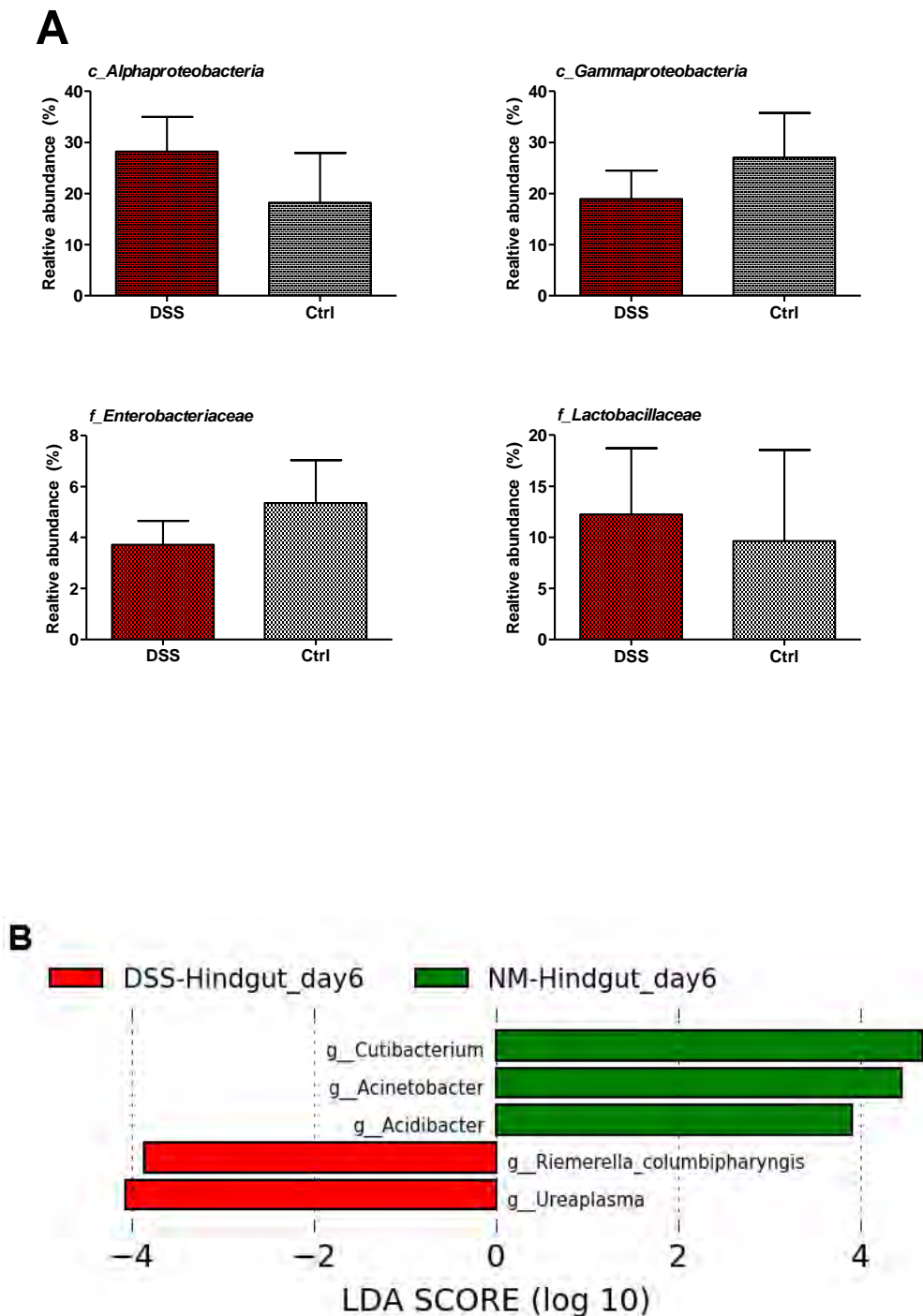


Fig.3.47: Graphs depict selected differentially abundant families, classes and microbial biomarker(s) of hindgut microbiota after 6-day post DSS treatment. Relative abundance of all zOTUs reveals major classes of proteobacteria as well as other relevant families with their informative ratio (Panel A). Linear discriminant analysis (LDA>2.0) coupled with effect size measurements (Panel B). Values represent means± SEM for 3 biological replicates. Ctrl: controls; LDA: Linear discriminant analysis; c_: class; f_: family; g_: genus.

3.3.11 Effect of 12-day DSS treatment on the *Drosophila* fecal microbiota community structure

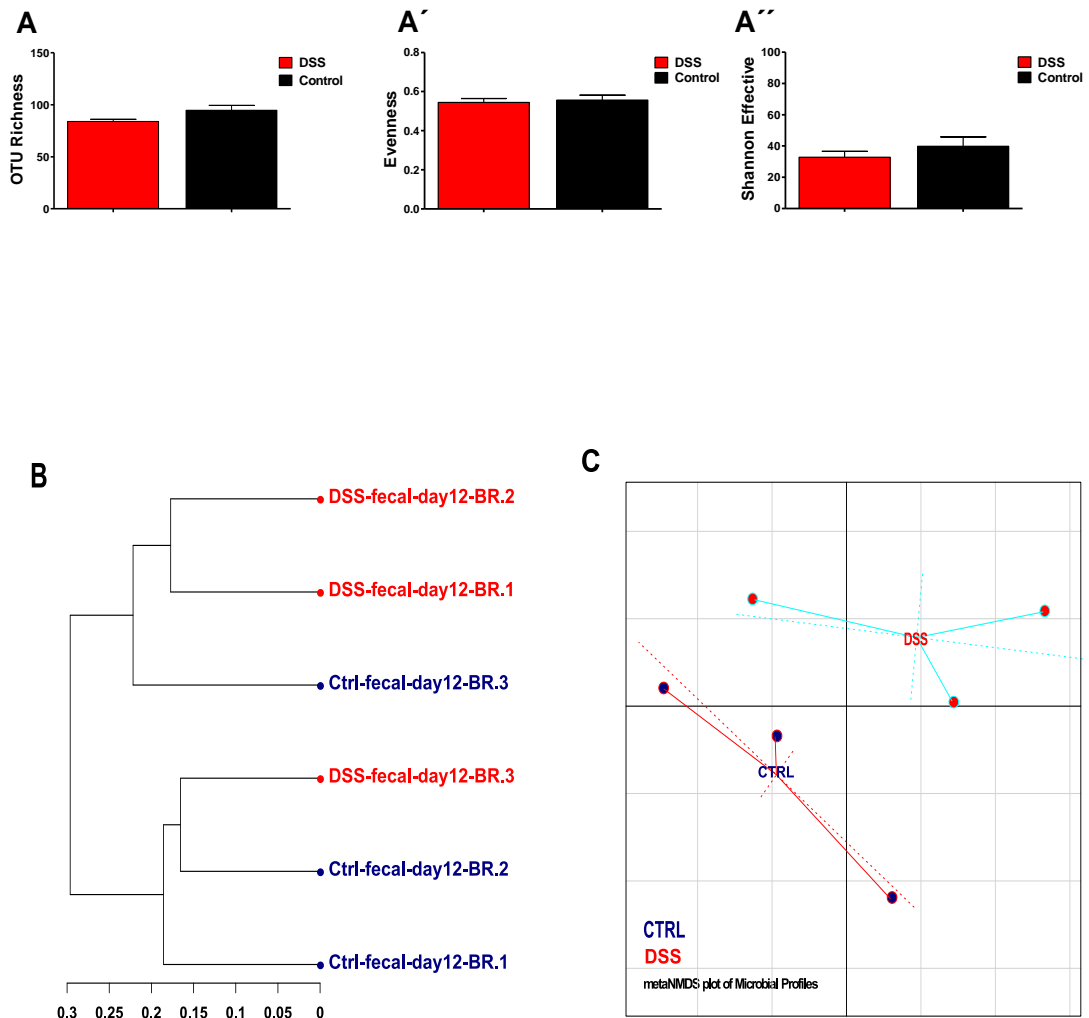


Fig.3.48: Graphs depict multiple aspects of fecal microbiota community structure after 12-day post DSS treatment. Phylogenetic diversity is presented as alpha-diversity and beta-diversity on normalized counts. Alpha-diversity (Panel A) is summarized as OTU richness (A), Evenness (A') and Shannon effective (A''). Beta-diversity is carried out using generalized UniFrac distance metric and presented by the dendrogram (Panel B) and MDS (Panel C) of all samples. Values represent means \pm SEM for 3 biological replicates. CTRL: controls; BR: Biological replicates; NMDS: non-metric multidimensional scaling.

3.3.12 Effect of 12-day DSS treatment for on the *Drosophila* fecal microbiota abundance at higher taxonomic ranks

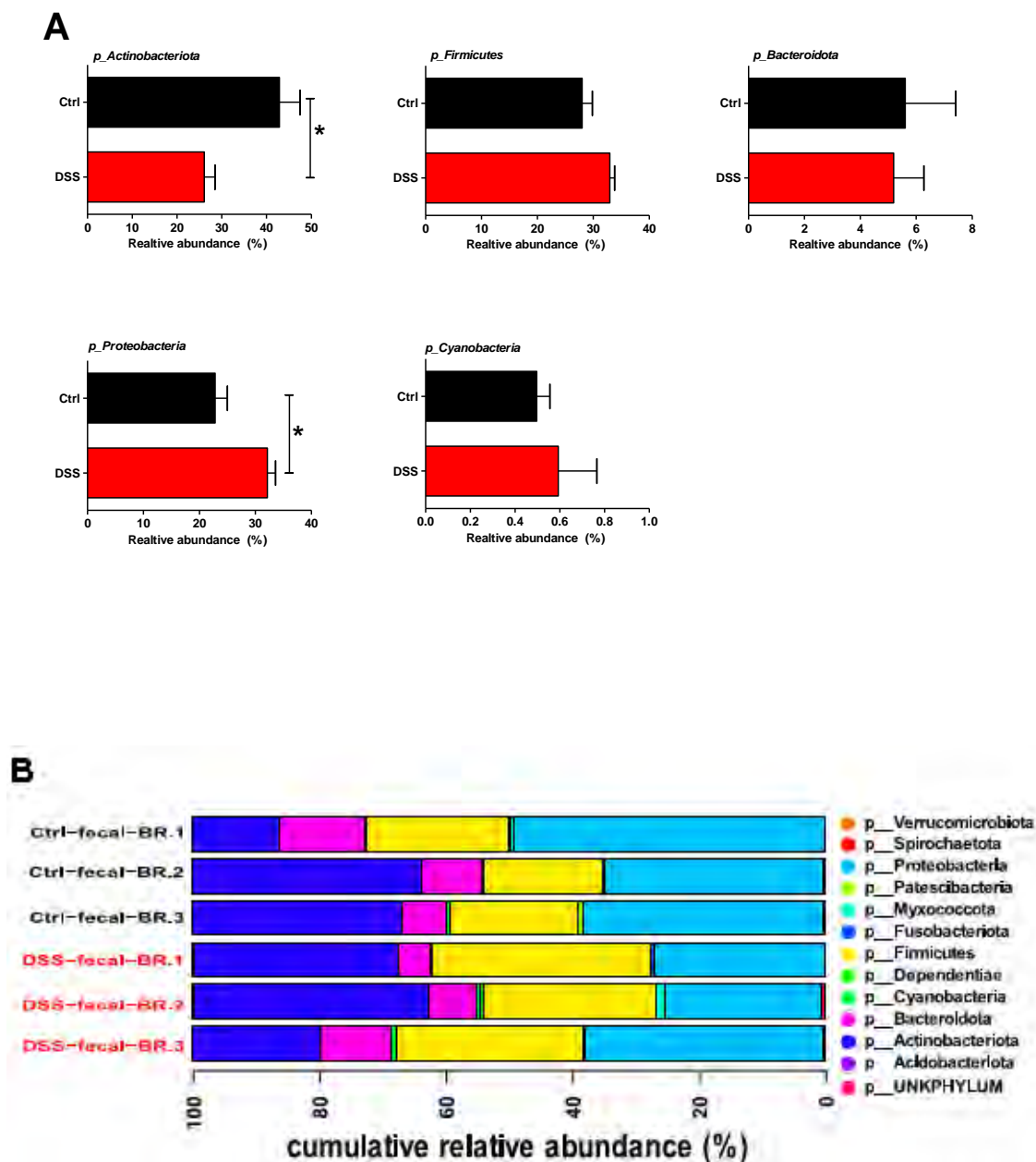


Fig.3.49: Graphs depict differentially abundant and discriminating taxa of fecal microbiota after 12-day post DSS treatment. Relative abundance of all zOTUs reveals major phyla with their informative ratio (Panel A). Taxonomic pinning at the phyla levels shows cumulative relative abundance (%) of major and minor phyla (Panel B). Values represent means \pm SEM for 3 biological replicates. Ctrl: controls; R=BR: Biological replicates; p_: phylum.

3.3.13 Effect of 12-day DSS treatment on the *Drosophila* fecal microbiota abundance at lower taxonomic ranks

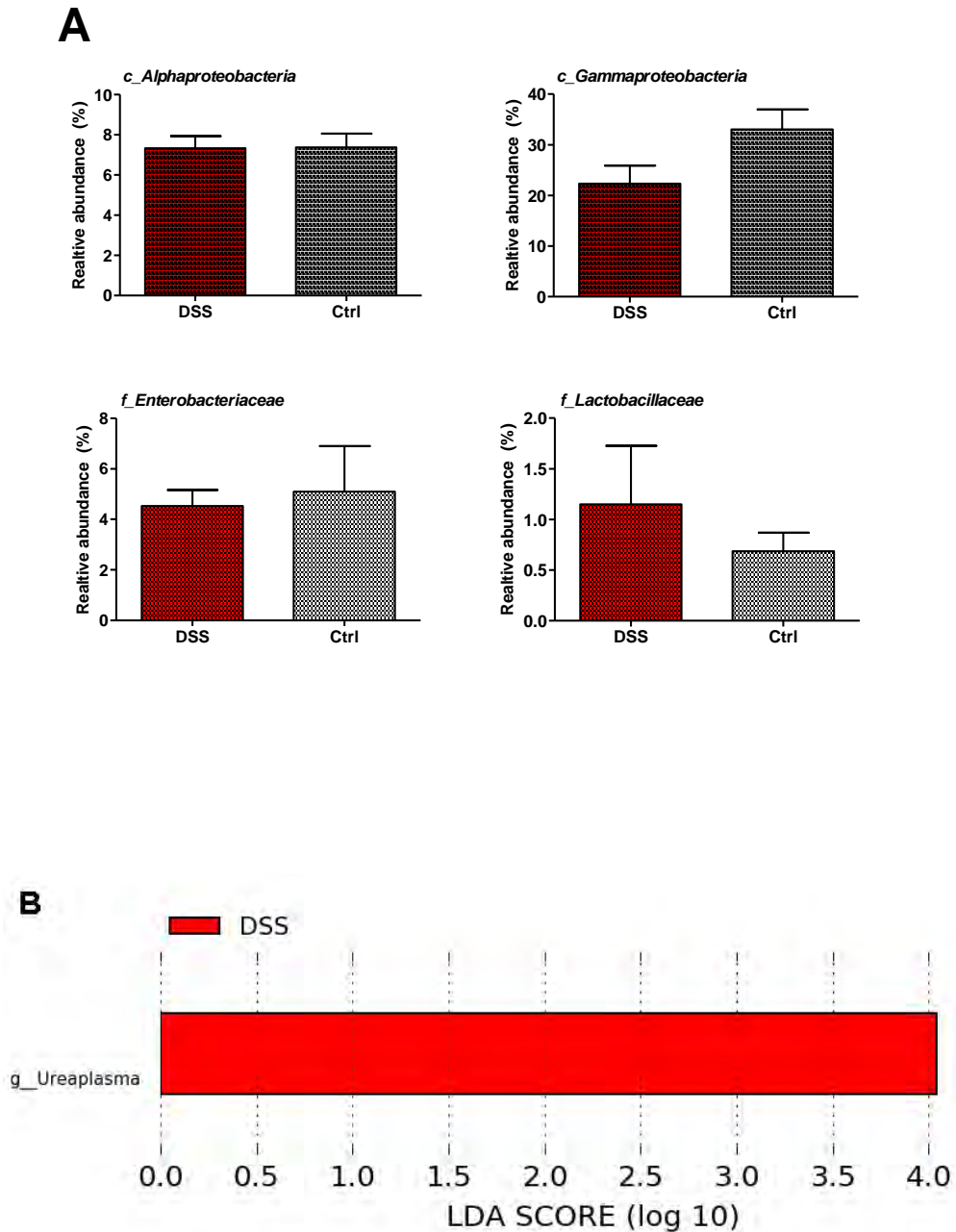


Fig.3.50: Graphs depict selected differentially abundant families, classes and microbial biomarker(s) of fecal microbiota after 12-day post DSS treatment. Relative abundance of all zOTUs reveals major classes of proteobacteria as well as other relevant families with their informative ratio (Panel A). Linear discriminant analysis (LDA>2.0) coupled with effect size measurements (Panel B). Values represent means± SEM for 3 biological replicates. Ctrl: controls; LDA: Linear discriminant analysis; c_: class; f_: family; g_: genus. *p<0.05.

3.3.14 Effect of 12-day DSS treatment on the *Drosophila* midgut microbiota community structure

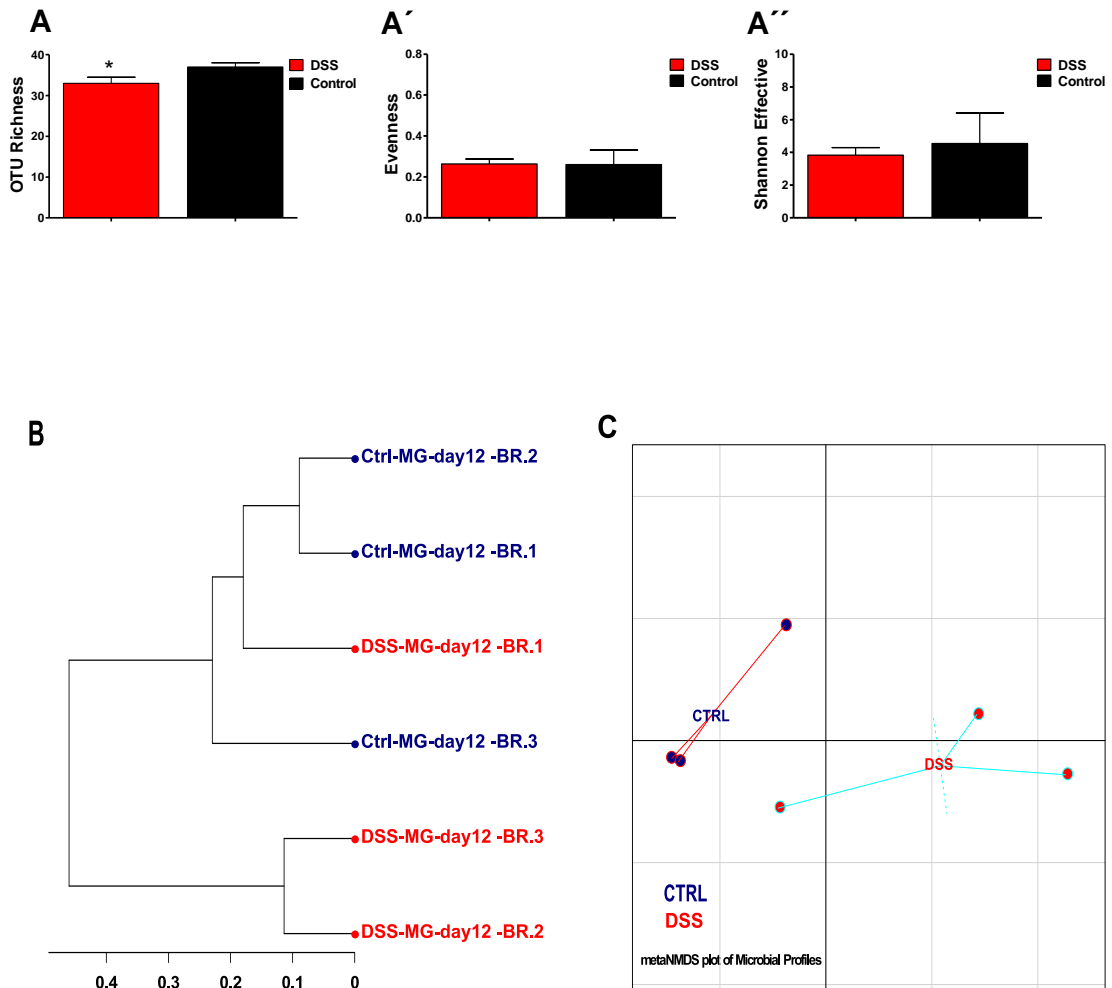


Fig.3.51: Graphs depict multiple aspects of midgut microbiota community structure after 12-day post DSS treatment. Phylogenetic diversity is presented as alpha-diversity and beta-diversity on normalized counts. Alpha-diversity (Panel A) is summarized as OTU richness (A), Evenness (A') and Shannon effective (A''). Beta-diversity is carried out using generalized UniFrac distance metric and presented by the dendrogram (Panel B) and metaNMDS (Panel C) of all samples. Values represent means ± SEM for 3 biological replicates. CTRL: controls; BR: Biological replicates; metaMDS: Non-metric multidimensional scaling. *p<0.05.

3.3.15 Effect of 12-day DSS treatment for on the *Drosophila* midgut microbiota abundance at higher taxonomic ranks

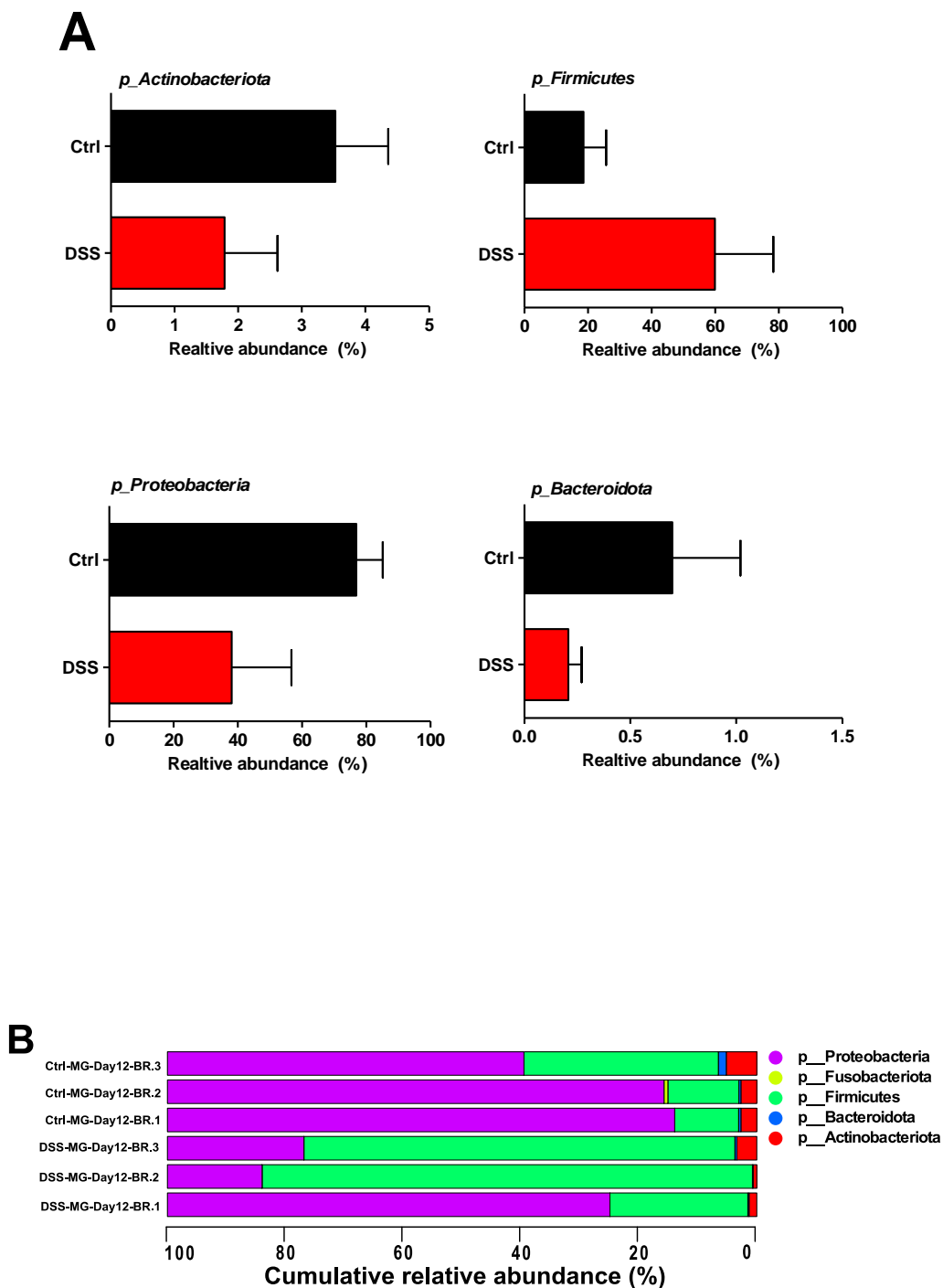


Fig.3.52: Graphs depict differentially abundant and discriminating taxa in the midgut microbiota after 12-day post DSS treatment. Relative abundance of all zOTUs reveals major phyla with their informative ratio (Panel A). Taxonomic pinning at the phyla levels shows cumulative relative abundance (%) of major and minor phyla (Panel B). Values represent means \pm SEM for 3 biological replicates. Ctrl: controls; MG: midgut; BR: Biological replicates; p_: phylum.

3.3.16 Effect of 12-day DSS treatment on the *Drosophila* midgut microbiota abundance at lower taxonomic ranks

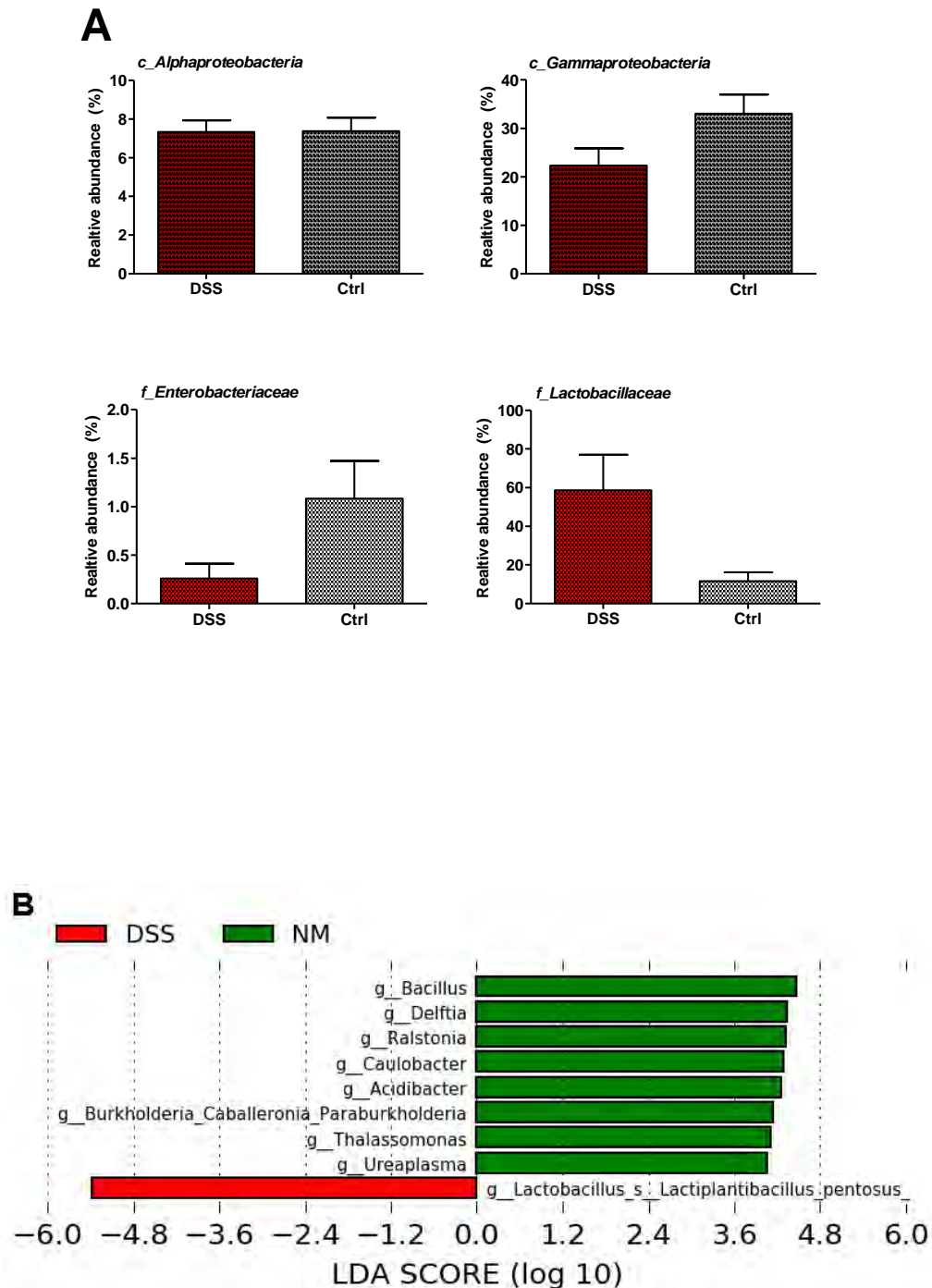


Fig.3.53: Graphs depict selected differentially abundant families, classes and microbial biomarker(s) midgut microbiota after 12-day post DSS treatment. Relative abundance of all zOTUs reveals major classes of proteobacteria as well as other relevant families with their informative ratio (Panel A). Linear discriminant analysis (LDA>2.0) coupled with effect size measurements (Panel B). Values represent means± SEM for 3 biological replicates. Ctrl: controls; LDA: Linear discriminant analysis; c_: class; f_: family; g_: genus; s_: species.

3.3.17 Effect of 12-day DSS treatment on the *Drosophila* hindgut microbiota community structure

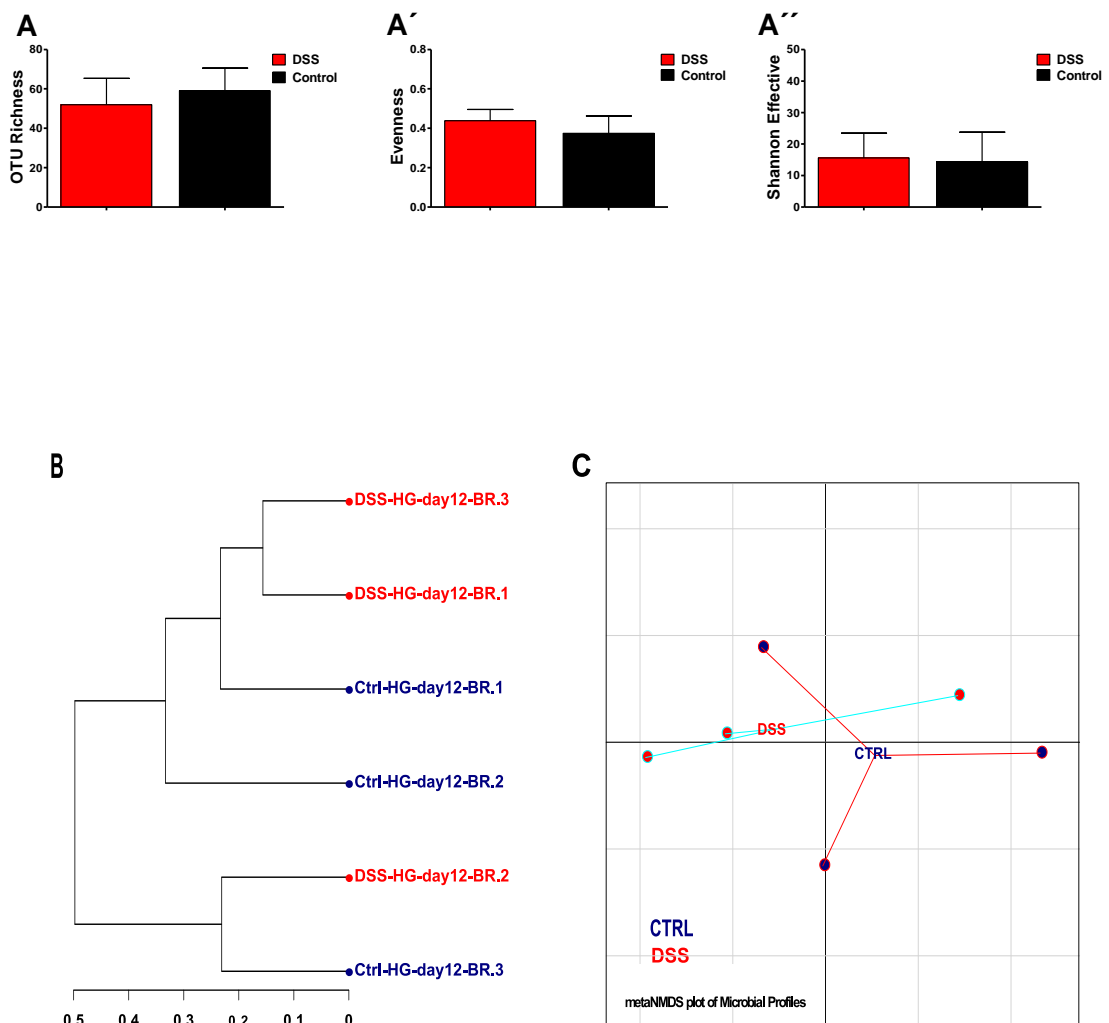


Fig.3.54: Graphs depict multiple aspects of hindgut microbiota community structure after 12-day post DSS treatment. Phylogenetic diversity is presented as alpha-diversity and beta-diversity on normalized counts. Alpha-diversity (Panel A) is summarized as OTU richness (A), Evenness (A') and Shannon effective (A''). Beta-diversity is carried out using generalized UniFrac distance metric and presented by the dendrogram (Panel B) and metaNMDS (Panel C) of all samples. Values represent means ± SEM for 3 biological replicates. CTRL: controls; BR: Biological replicates; HG: hindgut; metaMDS: Non-metric multidimensional scaling.

3.3.18 Effect of 12-day DSS treatment for on the *Drosophila* hindgut microbiota abundance at higher taxonomic ranks

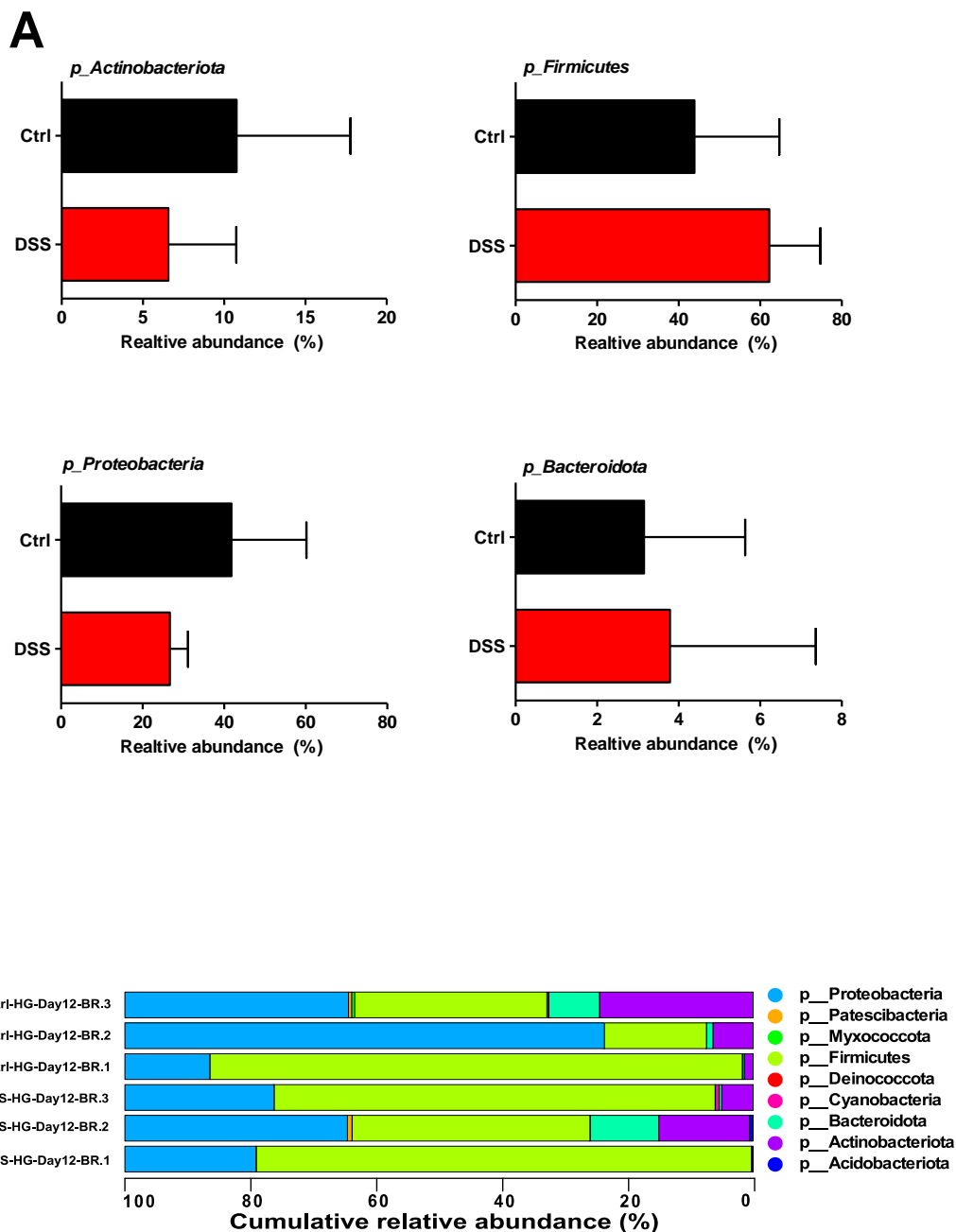


Fig.3.55: Graphs depict differentially abundant and discriminating taxa in the hindgut microbiota after 12-day post DSS treatment. Relative abundance of all zOTUs reveals major phyla with their informative ratio (Panel A). Taxonomic pinning at the phyla levels shows cumulative relative abundance (%) of major and minor phyla (Panel B). Values represent means \pm SEM for 3 biological replicates. Ctrl: controls; BR: Biological replicates; HG: hindgut; p_: phylum.

3.3.19 Effect of 12-day DSS treatment on the *Drosophila* hindgut microbiota abundance at lower taxonomic ranks

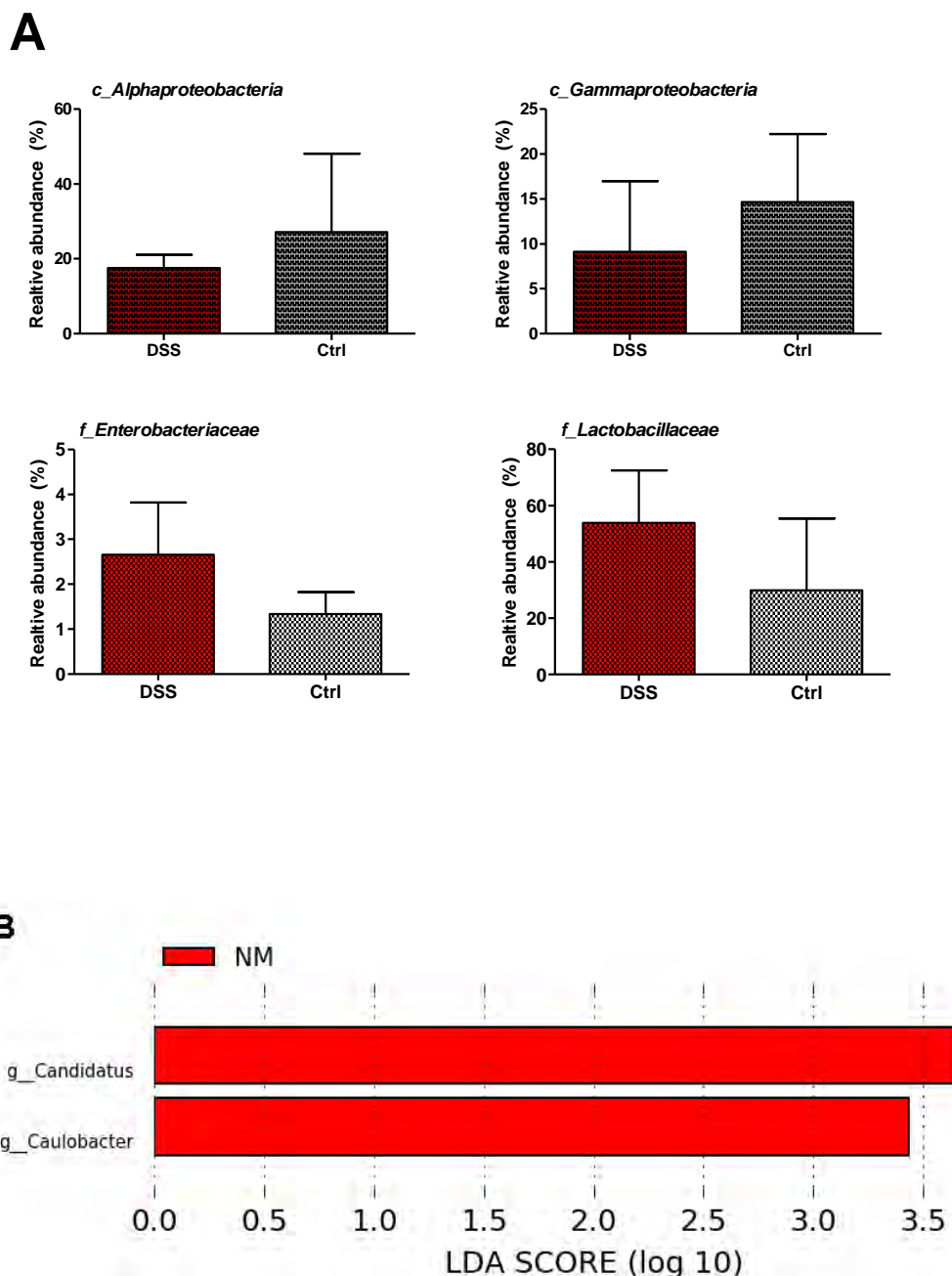


Fig.3.56: Graphs depict selected differentially abundant families, classes and microbial biomarker(s) of hindgut microbiota after 12-day post DSS treatment. Relative abundance of all zOTUs reveals major classes of proteobacteria as well as other relevant families with their informative ratio (Panel A). Linear discriminant analysis (LDA>2.0) coupled with effect size measurements (Panel B). Values represent means± SEM for 3 biological replicates. NM: controls fed on normal media; LDA: Linear discriminant analysis; c_: class; f_: family; g_: genus.

3.3.20 Effect of 6-day recovery period on the *Drosophila* fecal microbiota community structure

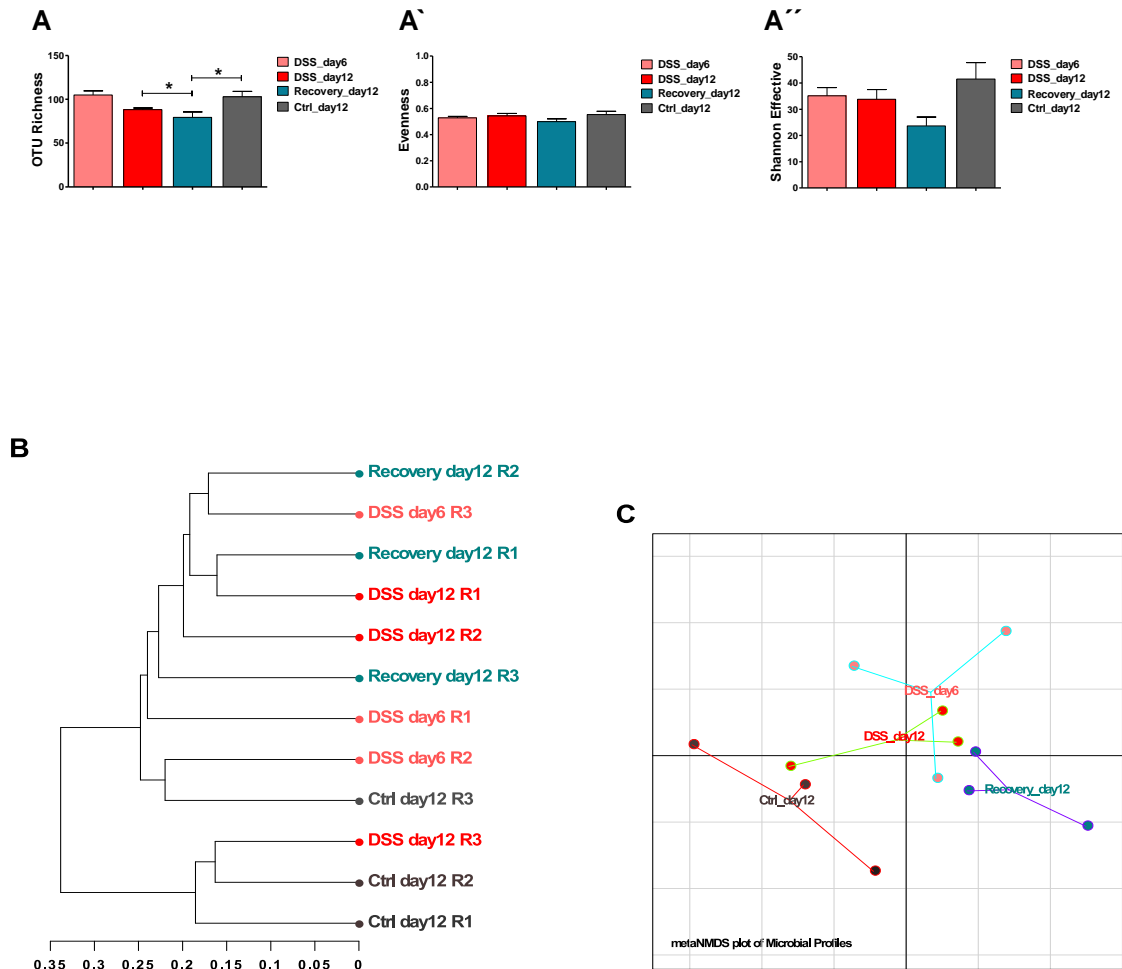


Fig.3.57: Graphs depict multiple aspects of fecal microbiota community structure after 6-day recovery period post 6-days DSS treatment. Phylogenetic diversity is presented as alpha-diversity and beta-diversity on normalized counts. Alpha-diversity (Panel A) is summarized as OTU richness (A), Evenness (A') and Shannon effective (A''). Beta-diversity is carried out using generalized UniFrac distance metric and presented by the dendrogram (Panel B) and metaNMDS (Panel C) of all samples. Values represent means \pm SEM for 3 biological replicates. Ctrl: controls; R: Biological replicate; Recovery_day12 refers to the experimental group that was recovered on normal media after 6-Day DSS treatment. NMDS: non-metric multidimensional scaling. * $p < 0.05$.

3.3.21 Effect of 6-day recovery period on the *Drosophila* fecal microbiota abundance at higher taxonomic ranks

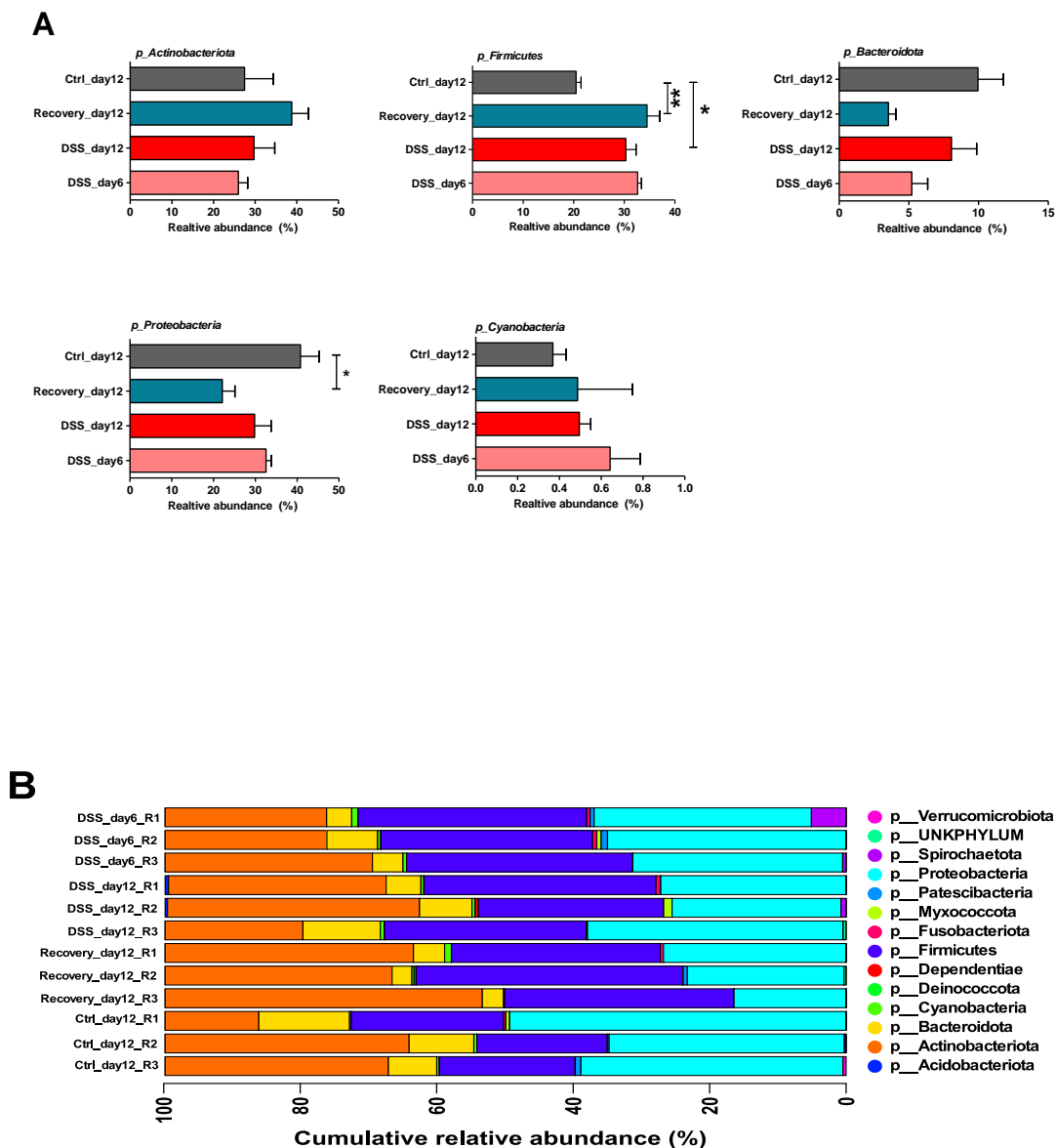


Fig.3.58: Graphs depict selected differentially abundant families, classes and microbial biomarker(s) of fecal microbiota after 6-day recovery period post 6-days DSS treatment. Relative abundance of all zOTUs reveals major classes of proteobacteria as well as other relevant families with their informative ratio (Panel A). Linear discriminant analysis (LDA>2.0) coupled with effect size measurements (Panel B). Values represent means± SEM for 3 biological replicates. Ctrl: controls; R: Biological replicate; Recovery_day12 refers to the experimental group that was recovered on normal media after 6-Day DSS treatment; LDA: Linear discriminant analysis. *p<0.05; **p<0.01.

3.3.22 Effect of 6-day recovery period on the *Drosophila* fecal microbiota abundance at lower taxonomic ranks

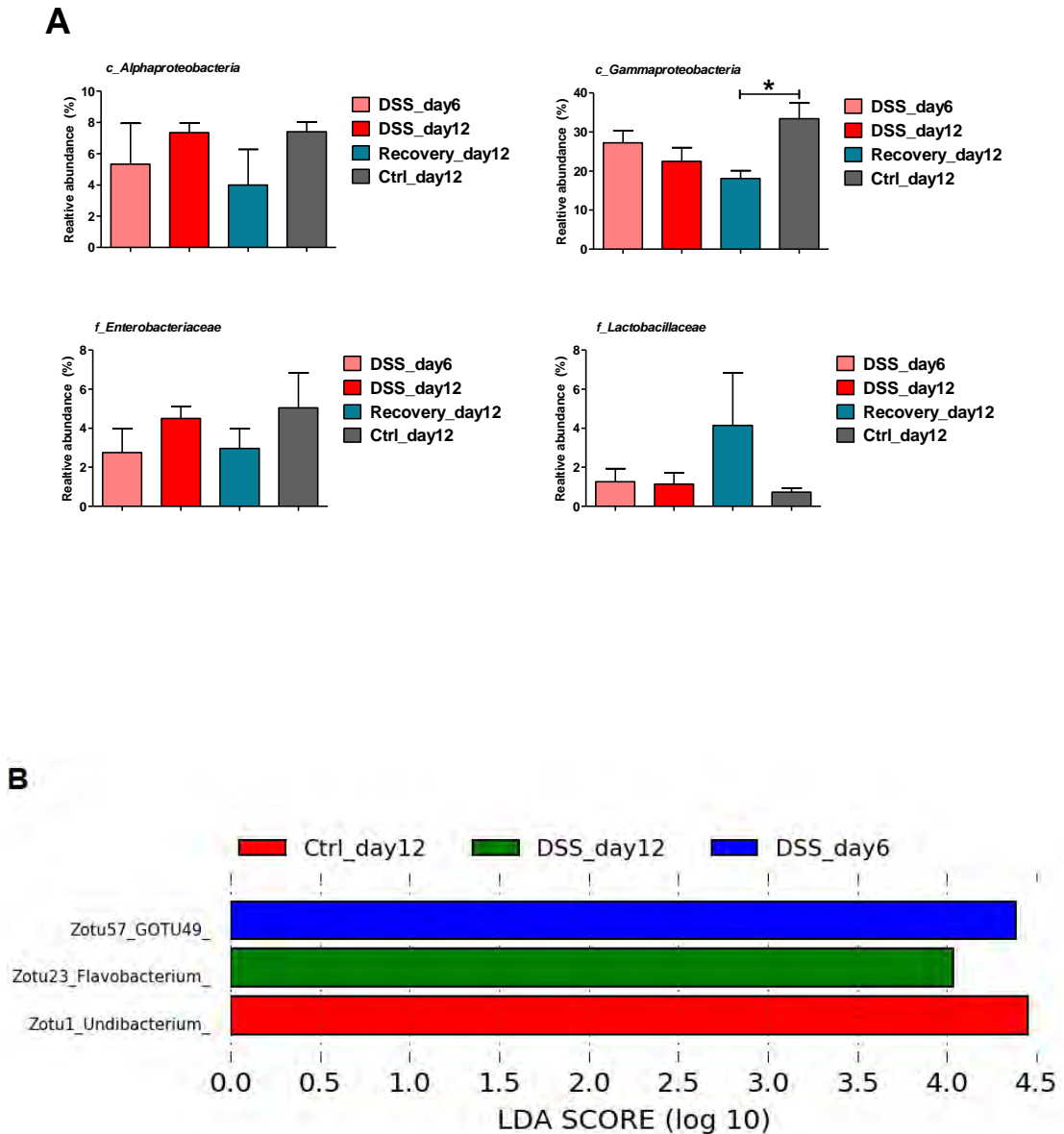


Fig.3.59: Graphs depict selected differentially abundant families, classes and microbial biomarker(s) of midgut microbiota after 6-day recovery period post DSS treatment. Relative abundance of all zOTUs reveals major classes of proteobacteria as well as other relevant families with their informative ratio (Panel A). Linear discriminant analysis (LDA>2.0) coupled with effect size measurements (Panel B). Values represent means± SEM for 3 biological replicates. Ctrl: controls; R: Biological replicate; Recovery_day12 refers to the experimental group that was recovered on normal media after 6-Day DSS treatment; LDA: Linear discriminant analysis; ZOTU: zero-radius Operational Taxonomic Unit; c_: class; f_: family. *p<0.05; **p<0.01.

3.3.23 Effect of 6-day recovery period on the *Drosophila* midgut microbiota community structure

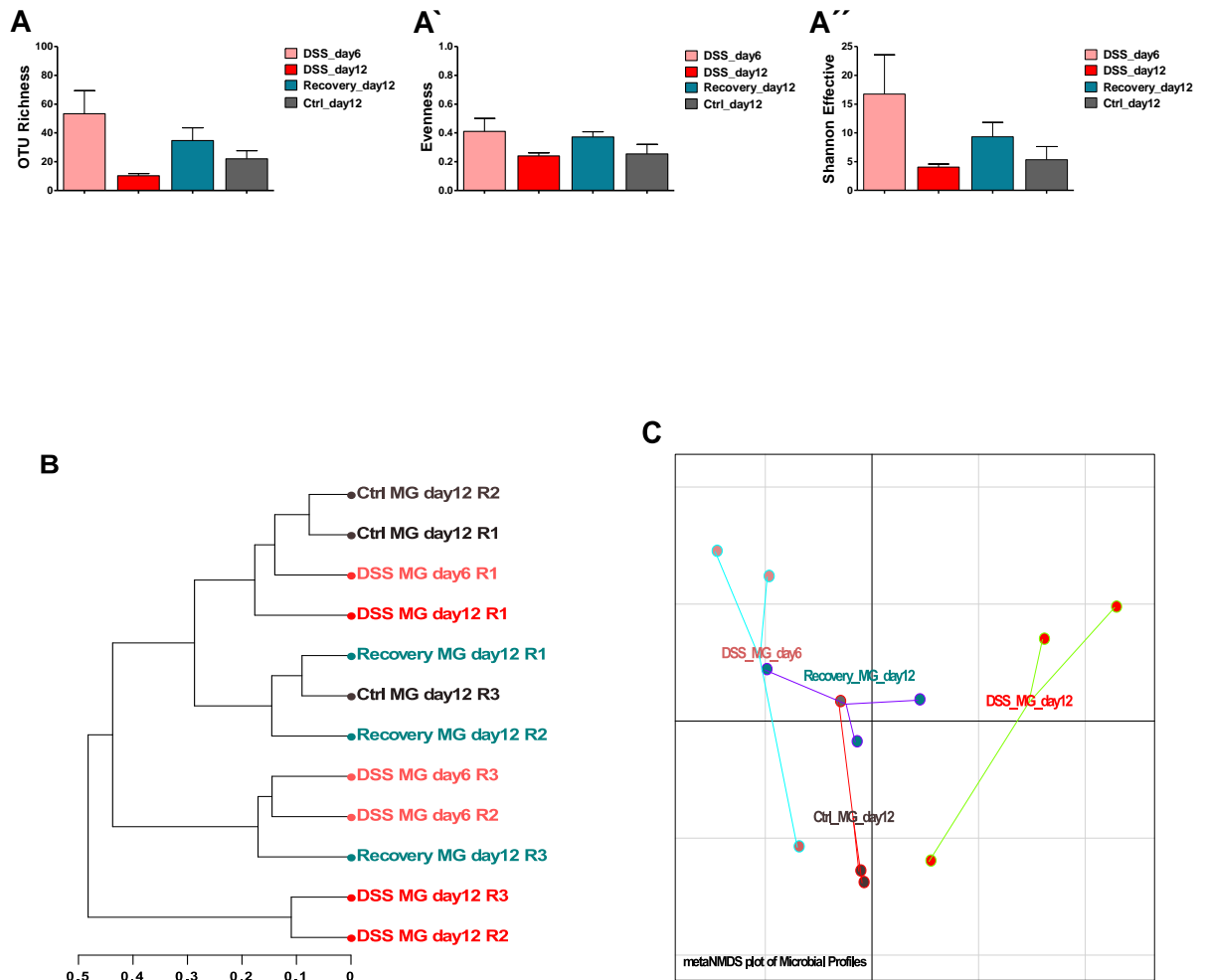


Fig.3.60: Graphs depict multiple aspects of midgut microbiota community structure after 6-day recovery period post 6-days DSS treatment. Phylogenetic diversity is presented as alpha-diversity and beta-diversity on normalized counts. Alpha-diversity (Panel A) is summarized as OTU richness (A), Evenness (A') and Shannon effective (A''). Beta-diversity is carried out using generalized UniFrac distance metric and presented by the dendrogram (Panel B) and metaNMDS (Panel C) of all samples. Values represent means \pm SEM for 3 biological replicates. Ctrl: controls; R: Biological replicate; Recovery_day12 refers to the experimental group that was recovered on normal media after 6-Day DSS treatment; MG: midgut; NMDS: non-metric multidimensional scaling.

3.3.24 Effect of 6-day recovery period on the *Drosophila* midgut microbiota abundance at higher taxonomic ranks

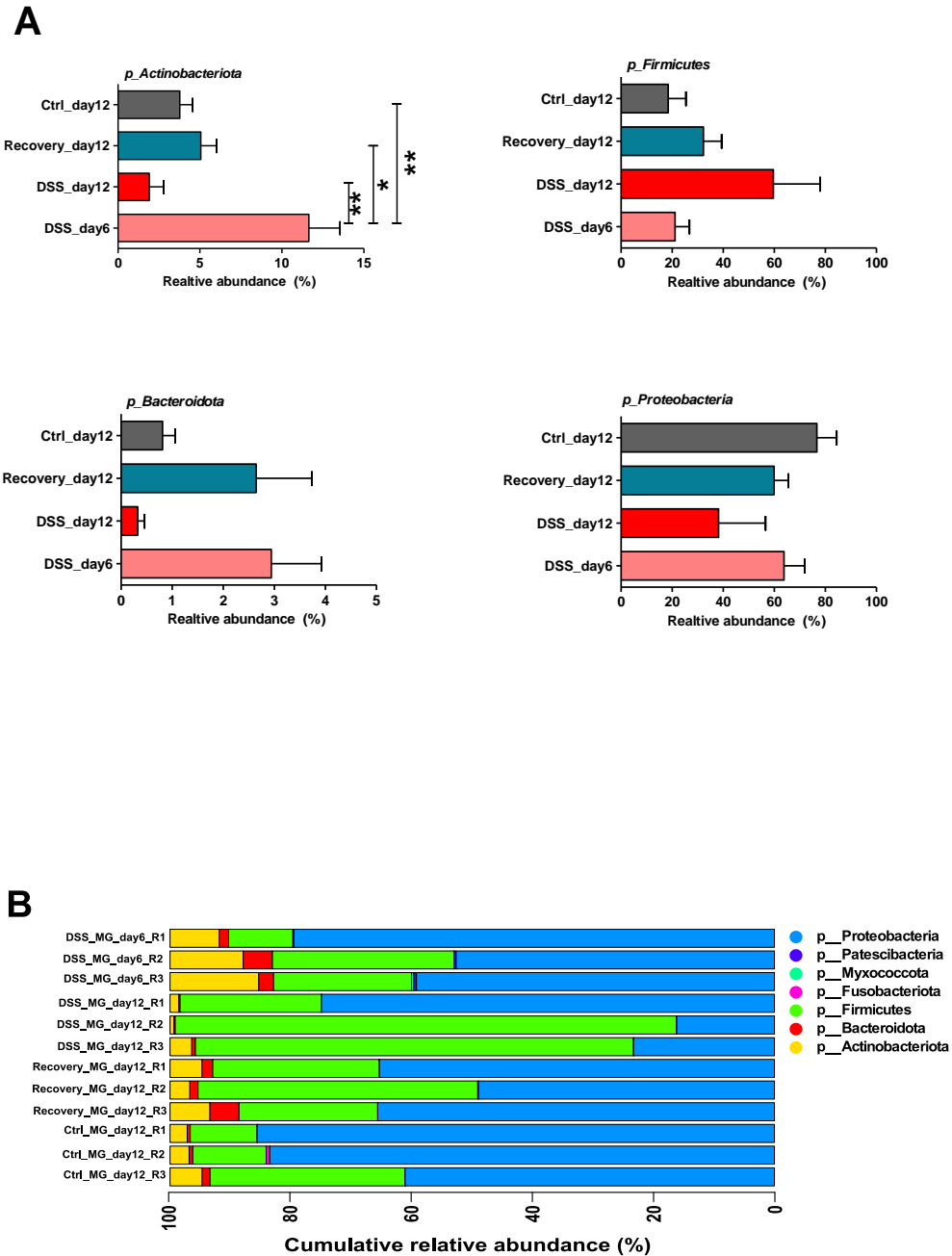


Fig.3.61: Graphs depict differentially abundant and discriminating taxa in the midgut microbiota after 6-day recovery period post 6-days DSS treatment. Relative abundance of all zOTUs reveals major phyla with their informative ratio (Panel A). Taxonomic pinning at the phyla levels shows cumulative relative abundance (%) of major and minor phyla (Panel B). Values represent means \pm SEM for 3 biological replicates. Ctrl: controls; R: Biological replicate; Recovery_day12 refers to the experimental group that was recovered on normal media after 6-Day DSS treatment; MG: midgut; p_: phylum. * $p < 0.05$; ** $p < 0.01$.

3.3.25 Effect of 6-day recovery period on the *Drosophila* midgut microbiota abundance at lower taxonomic ranks

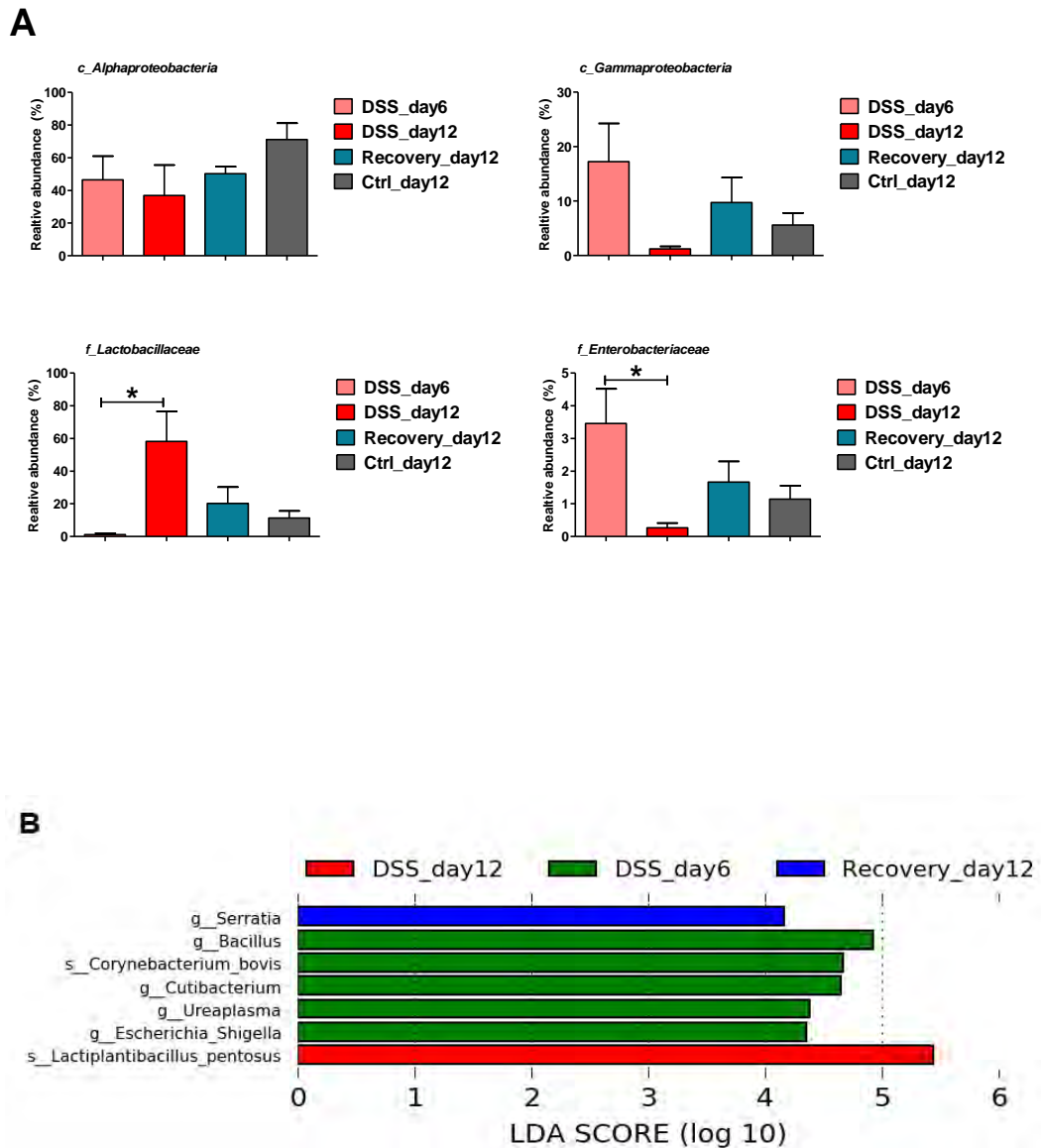


Fig.3.62: Graphs depict selected differentially abundant families, classes and microbial biomarker(s) of midgut microbiota after 6-day recovery period post 6-days DSS treatment. Relative abundance of all zOTUs reveals major classes of proteobacteria as well as other relevant families with their informative ratio (Panel A). Linear discriminant analysis (LDA>2.0) coupled with effect size measurements (Panel B). Values represent means± SEM for 3 biological replicates. Ctrl: controls; Recovery_day12 refers to the experimental group that was recovered on normal media after 6-Day DSS treatment. LDA: Linear discriminant analysis; c_: class; f_: family; g_: genus; s_: species (refined based on EzBioCloud microbiome taxonomic profiling). *p<0.05

3.3.26 Effect of 6-day recovery period on the *Drosophila* hindgut microbiota community structure

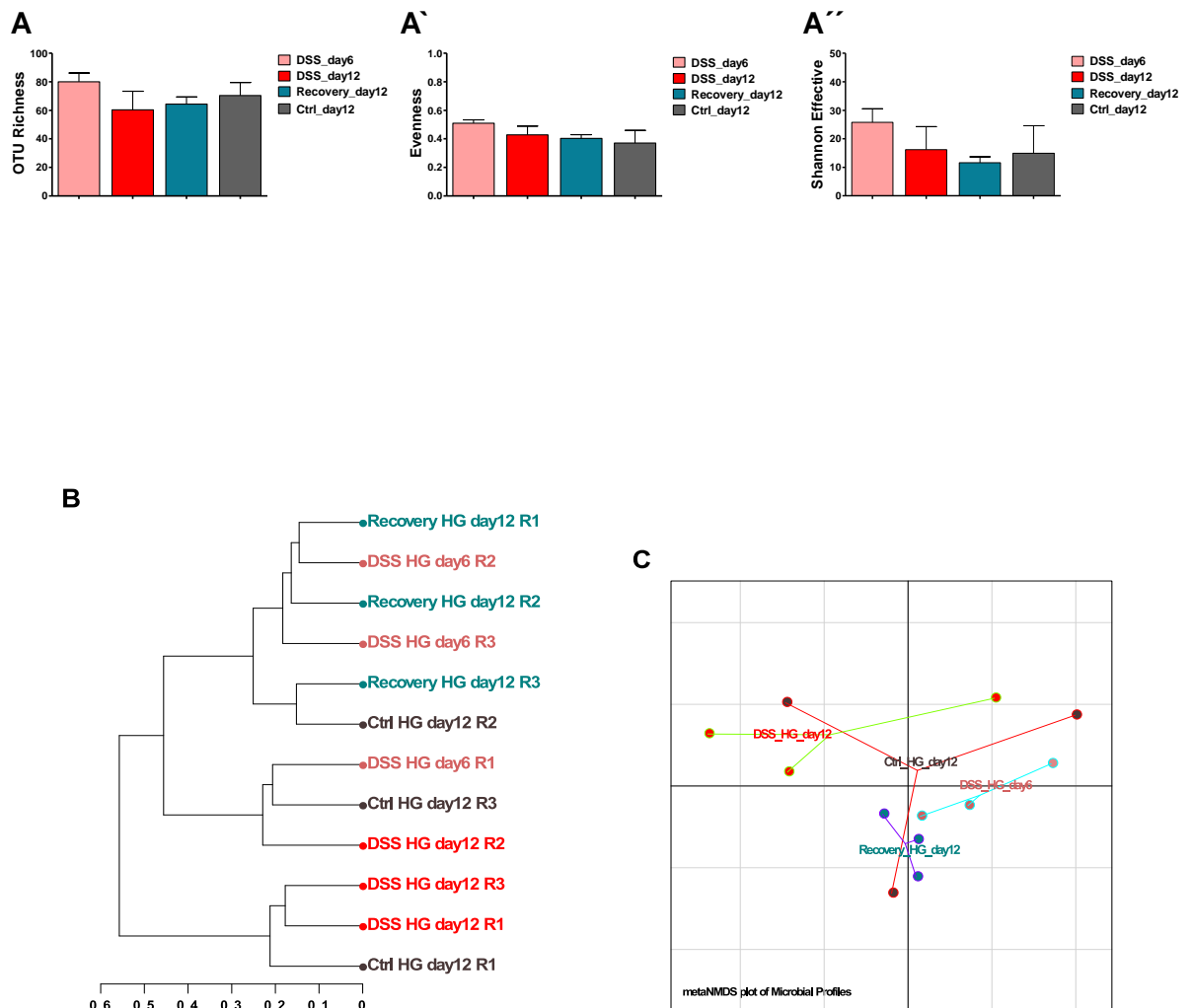


Fig.3.63: Graphs depict multiple aspects of hindgut microbiota community structure after 6-day recovery period post 6-days DSS treatment. Phylogenetic diversity is presented as alpha-diversity and beta-diversity on normalized counts. Alpha-diversity (Panel A) is summarized as OTU richness (A), Evenness (A') and Shannon effective (A''). Beta-diversity is carried out using generalized UniFrac distance metric and presented by the dendrogram (Panel B) and metaNMDS (Panel C) of all samples. Values represent means \pm SEM for 3 biological replicates. Ctrl: controls; Recovery_day12 refers to the experimental group that was recovered on normal media after 6-Day DSS treatment; HG: hindgut; NMDS: non-metric multidimensional scaling.

3.3.27 Effect of 6-day recovery period on the *Drosophila* hindgut microbiota abundance at higher taxonomic ranks

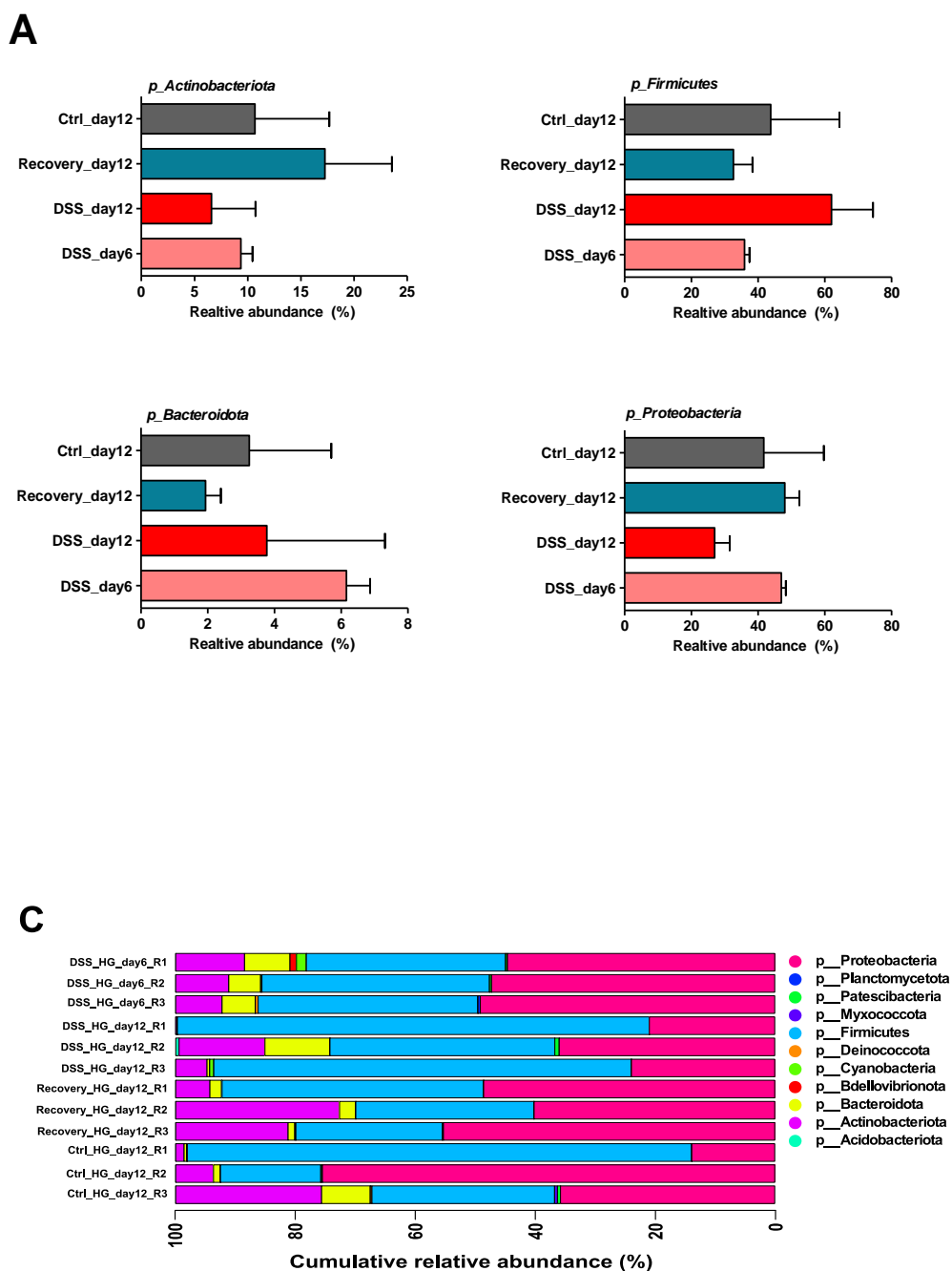


Fig.3.64: Graphs depict differentially abundant and discriminating taxa in the hindgut microbiota after 6-day recovery period post 6-days DSS treatment. Relative abundance of all zOTUs reveals major phyla with their informative ratio (Panel A). Taxonomic pinning at the phyla levels shows cumulative relative abundance (%) of major and minor phyla (Panel B). Values represent means \pm SEM for 3 biological replicates. Ctrl: controls; Recovery_day12 refers to the experimental group that was recovered on normal media after 6-Day DSS treatment; p_: phylum.

3.3.28 Effect of 6-day recovery period on the *Drosophila* hindgut microbiota abundance at lower taxonomic ranks

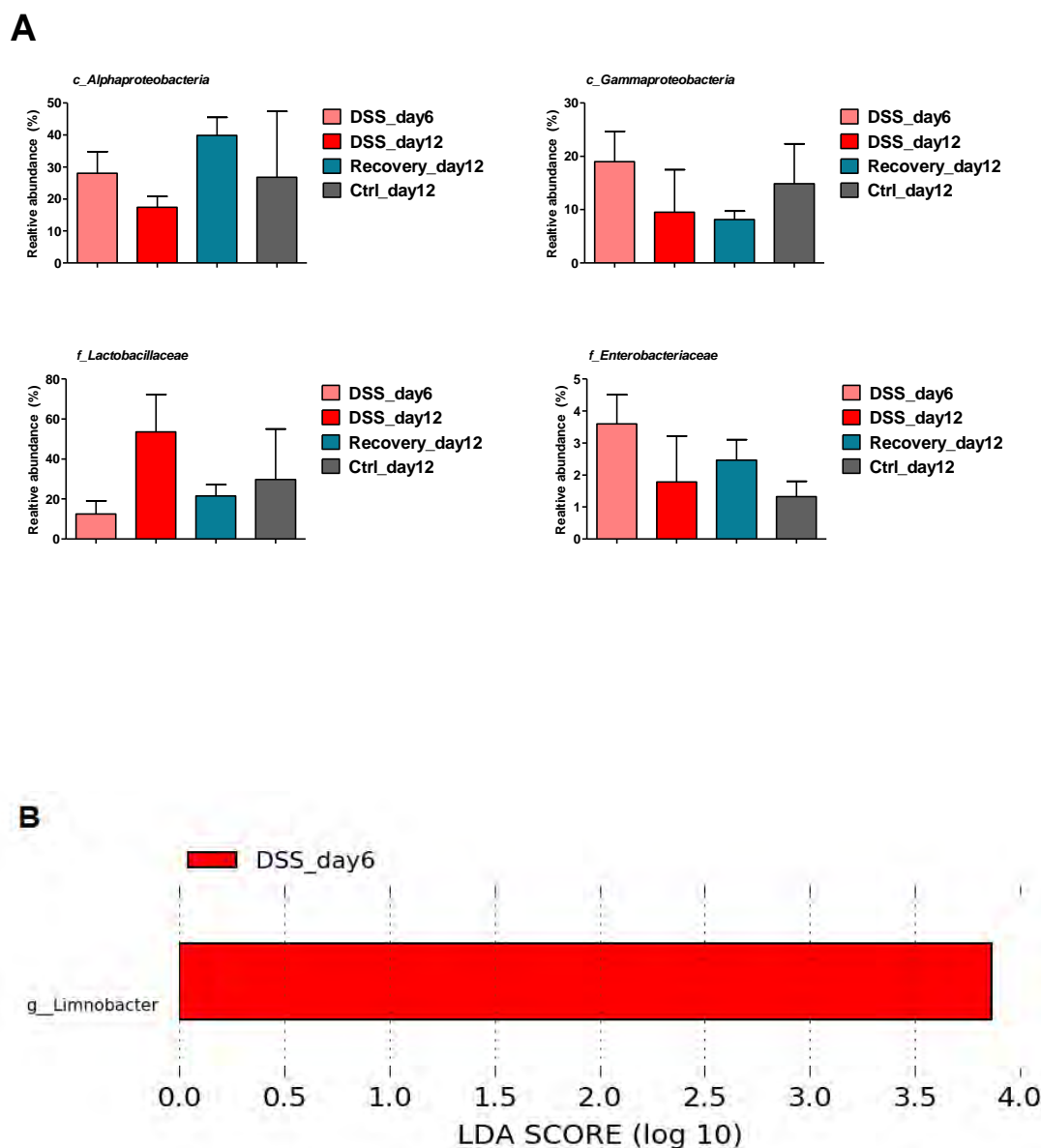


Fig.3.65: Graphs depict selected differentially abundant families, classes and microbial biomarker(s) of hindgut microbiota after 6-day recovery post 6-days DSS treatment. Relative abundance of all zOTUs reveals major classes of proteobacteria as well as other relevant families with their informative ratio (Panel A). Linear discriminant analysis (LDA>2.0) coupled with effect size measurements (Panel B). Values represent means± SEM for 3 biological replicates. Ctrl: controls; Recovery_day12 refers to the experimental group that was recovered on normal media after 6-Day DSS treatment LDA: Linear discriminant analysis; c_: class; f_: family; g_: genus.

3.3.29 Effect of 6-day DSS treatment on the male *Drosophila* fecal microbiota community structure

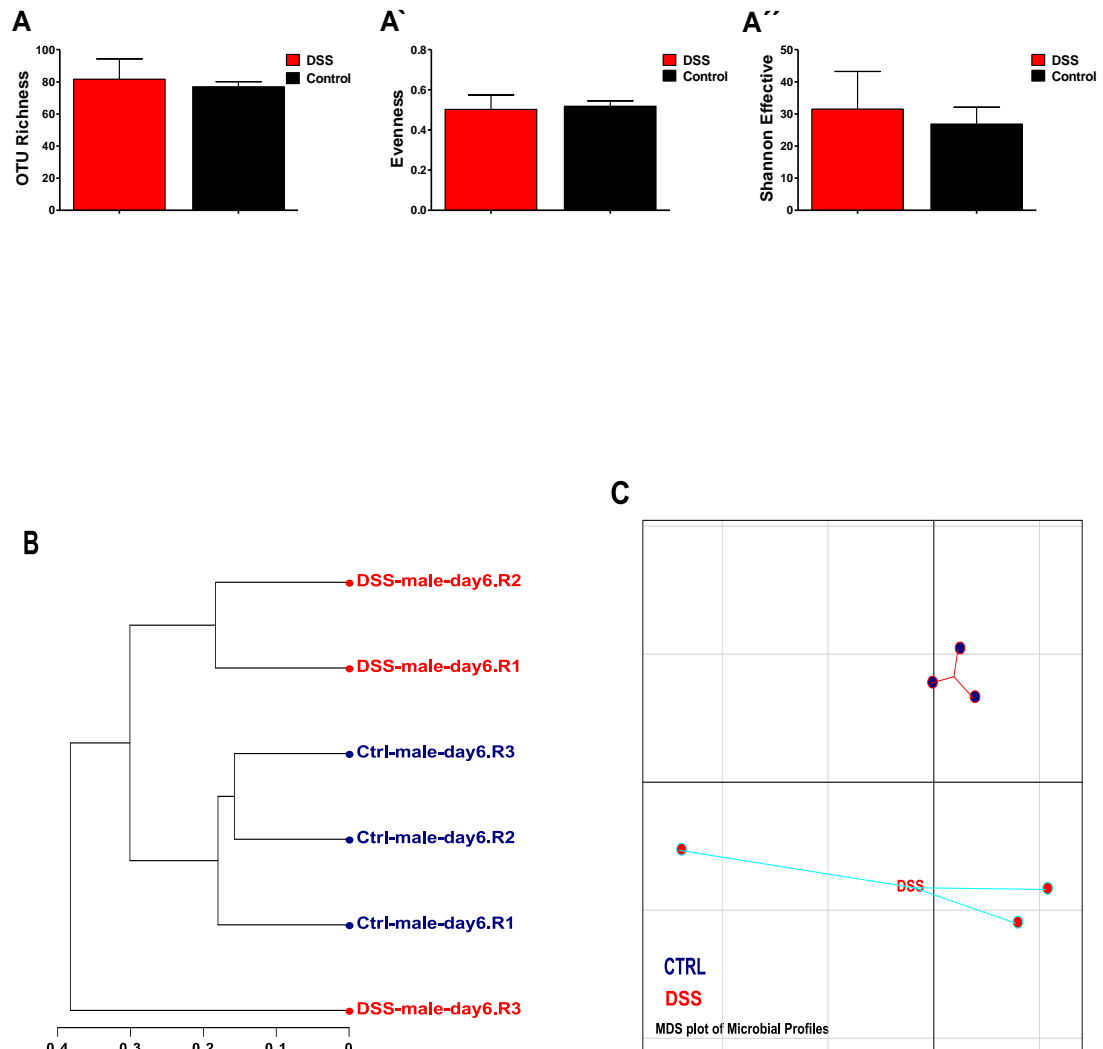
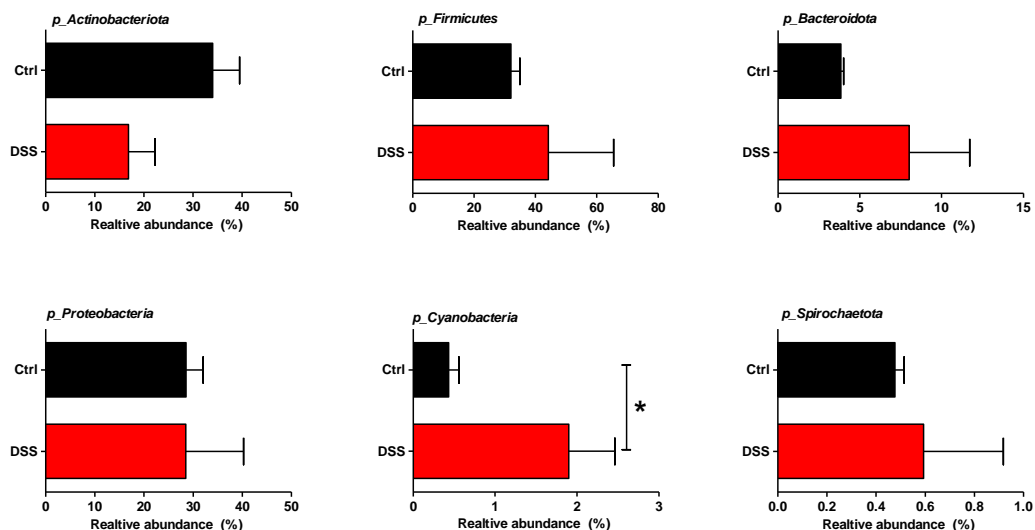


Fig.3.66: Graphs depict multiple aspects of male fecal microbiota community structure after 6-day DSS treatment. Phylogenetic diversity is presented as alpha-diversity and beta-diversity on normalized counts. Alpha-diversity (Panel A) is summarized as OTU richness (A), Evenness (A') and Shannon effective (A''). Beta-diversity is carried out using generalized UniFrac distance metric and presented by the dendrogram (Panel B) and MDS (Panel C) of all samples. Values represent means ± SEM for 3 biological replicates. Ctrl: controls; R: Biological replicates; MDS: multidimensional scaling.

3.3.30 Effect of 6-day DSS treatment for on the male *Drosophila* fecal microbiota abundance at higher taxonomic ranks

A



B

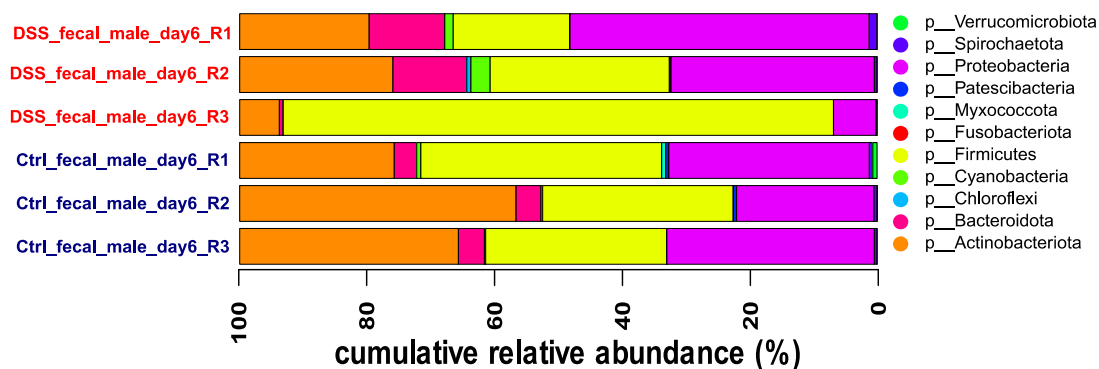
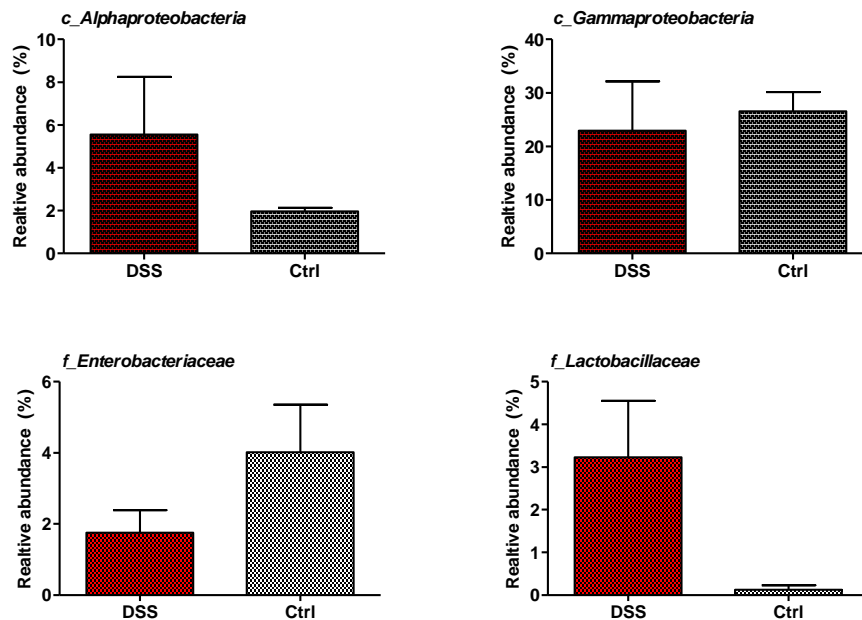


Fig.3.67: Graphs depict differentially abundant and discriminating taxa in the male fecal microbiota after 6-day DSS treatment. Relative abundance of all zOTUs reveals major phyla with their informative ratio (Panel A). Taxonomic pinning at the phyla levels shows cumulative relative abundance (%) of major and minor phyla (Panel B). Values represent means \pm SEM for 3 biological replicates. Ctrl: controls; R: Biological replicates; p_: phylum. *p<0.05.

3.3.31 Effect of 6-day DSS treatment on the male *Drosophila* fecal microbiota abundance at lower taxonomic ranks

A



B

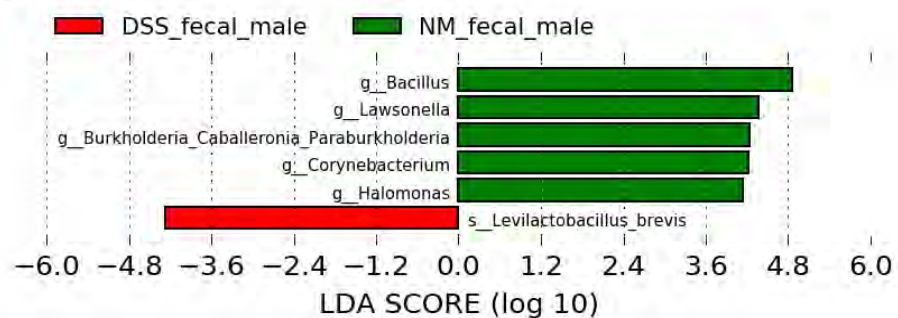


Fig.3.68: Graphs depict selected differentially abundant families, classes and microbial biomarker(s) of male fecal microbiota after 6-day DSS treatment. Relative abundance of all zOTUs reveals major classes of proteobacteria as well as other relevant families with their informative ratio (Panel A). Linear discriminant analysis (LDA>2.0) coupled with effect size measurements (Panel B). Values represent means± SEM for 3 biological replicates. NM: controls fed on normal media; LDA: Linear discriminant analysis; c_: class; f_: family; g_: genus; s__: species (refined based on EzBioCloud microbiome taxonomic profiling).

4. Discussion

4.1. DSS-induced *Drosophila* colitis-like model has a theoretical rationale

Inflammatory bowel disease with its subsets UC and CD is investigated experimentally in different vertebrate model organisms such as rats [156], mice [157] and zebrafish [158]. One of the widely implemented chemically-induced experimental models is the acute/chronic DSS-Induced Colitis model owing to its simplicity, rapidity and enhanced reproducibility. It also helps recapitulate most clinical and pathological features of the human IBD especially UC with emphasis on the innate immune response and the implication of intestinal microbiota [157], [159], [160], [164]. No single model reflects the complexity of the complex IBD pathology, but each model is informative for one or another major aspect of disease, and altogether with evolving new model systems can lead to an in-depth understanding of the reciprocal host-microbiota interactions involved in the disease onset, progression and remission [157], [168]. *Drosophila melanogaster* has been proven to be a reliable translational model of human diseases. In principle, cost-effectiveness, reduced turnaround experimentation time, conserved as well as the inherent nature of feasibly-manipulated intestinal stem cell lineage have been driving many *Drosophila* researchers to establish different effective genetic/physiologic frameworks that can be used to elucidate many aspects of human gut inflammation and related pathologies and host-microbiota interaction [90], [169], [171], [172], [173]. Dextran sodium sulfate (DSS) was used in many *Drosophila* studies as a DSS-injury model to investigate intestinal stem cell proliferation and tissue regeneration (Fig. 1.4) [161], [175]. Nevertheless, none of these studies have addressed either the phenotypic characteristics of the human IBD/ experimental DSS-induced colitis or the impact of host-gut microbiota interaction on inflammation. In this project, the *Drosophila* model of acute DSS-induced colitis-like phenotype was established following the '3Rs' principle—relatively replace, reduce and refine – a policy that provides a framework for implementation of non-mammalian systems [176]. The precise objectives are to establish clinically-relevant disease endpoints in *Drosophila*, to investigate the epithelial barrier function; to unravel the initiation and progression of innate aspects of intestinal inflammation at organismal, cellular and molecular levels in a temporal and spatial context, and to validate the potential interrelation between gut microecology and inflammation.

4.2. Developing reproducible and quantitative disease endpoints (DEs) of DSS-induced colitis-like phenotype in the *Drosophila*.

Typically, most of the human disease models in rodents have been proved to fulfill aspects of face validity (eg. signs and symptoms). However, in some cases this validity is partial because the model organism does not replicate the entire clinical picture of the human counterpart [177], [178]. Striking implementation of the *Drosophila* as a pre-clinical model has markedly emphasized on the superior advantage of cross-species comparison [72], [179], [180]. In murine model of DSS-induced colitis, histopathologic analysis and disease activity index (DAI) are the gold standard estimates of inflammation. Disease activity index (DAI) is determined by scoring multiple phenotypes of the living animals, such as weight loss, stool consistency and stool blood. Additional surrogate blood biomarkers are implemented as quantitative estimate of intestinal permeability (eg. serum concentration of orally-administered FITC-dextran tracer) and inflammatory status (serum TNF- α). On the other hand, other inflammatory markers are performed on colonic tissues to quantify infiltrating tissue neutrophils (e.g. Myeloperoxidase, MPO) as well as mRNA/protein levels of relevant tissue cytokines (e.g. IL-6) [49], [181].

In this project, most of the DSS-induced disease outcomes are mirrored in *Drosophila* in a systematic top-down manner in order to establish quantitative read-out proxy/ies for colitis. Importantly, all DSS-induced *Drosophila* colitis-like phenotypes are reported as disease endpoints (DEs) at both the organismal 'clinical-like' level as well as the histologic levels.

4.2.1. Disease endpoint 1 (DE01): Reduced survival and activity in DSS-induced colitis that mimics the rodent model, but with reversed sexual dimorphism

DSS was administered ad libitum at a 5% concentration for a period of 12 days. Total *Drosophila* activity is monitored daily as a proxy of disease onset and progression. DSS administration induces a significant reduction of mean *Drosophila* activity (45,1%) in female flies as soon as day1 post treatment (Fig. 3.4) as well as a significant gradual reduction in survivability (Fig. 3.1) which reflects the underlying morbidity triggered by DSS. The major finding is that median survival in female flies

is reproducibly monitored between day 6-7 (at day 6.5) that is partially consistent with other similar studies in flies [182] and mice [183]. Moreover; female flies showed a significant partial recovery following a 6-day period of DSS removal after day 6 post DSS treatment (Fig.3.3).

In principle, minor differences in DSS treatment outcomes among studies are attributed to multiple factors such as concentration, manufacturer, and batch [184].

Interestingly, male flies show a significant reduced susceptibility to DSS with a double median survival (12 days) compared to DSS-treated female (Fig.3.1). In comparison to DSS-induced colitis in mice, male mice are highly susceptible to colitis. Sex difference in susceptibility is attributed to behavioral or hormonal factors [185]. On the other hand, survival advantage in male flies is proved to be influenced by differential abundance of specific gut microbial taxa (Fig.3.63 – 3.65).

In this project, treatment protocol was applied mainly to female flies, unless stated otherwise, and designed to present different phases of survivorship: first phase represents a cohort of flies-at-risk post treatment that is sampled/tested at day 6; second phase represents a parallel cohort of flies-at-risk that is sampled/tested at day 12; and additional recovery phase that represents another parallel cohort of the first phase, however shifted from DSS treatment to normal media at day 6 and sampled/tested at day 12 (Fig. 3.3). Interestingly, this kind of experimental design is introduced for the first time in the Community of *Drosophila* model of human diseases. The importance of the second phase and recovery groups is to tackle dynamic changes in the gut physiology and ecology under treatment and DSS-withdrawal conditions at different time points.

4.2.2. Disease endpoint 2 (DE02): Appetite loss is a surrogate marker of DSS-induced colitis

Appetite loss is reported in active IBD with higher frequency in CD compared to UC [186], [187]. Nevertheless, it is less scored in animal models of DSS-colitis. Basically, DSS-induced colitis in murine models is established by the oral administration of DSS via drinking water. DSS consumption rate is roughly estimated to be 8 ml/day per animal [49], [181]. Unlike the licking behavior in rodents, flies accessed food by proboscis extension with a roughly estimated cumulative consumption of less than 8 μ L/fly/day (Fig. 2.1). In this project, non-

invasive read-out phenotypes of accumulative food consumption and excretion were combined to quantitatively measure appetite in DSS-treated animals. Since defecation rate in *Drosophila* is an indirect appetite marker, food intake was measured, in parallel, as a direct marker [128], [148]. The major findings are that DSS-treated flies manifested a 63,5% reduction in cumulative food consumption (Fig. 3.6) that is in line with the finding of DSS-induced colitis in mice [188]. Moreover, DSS treatment results in a 42,7 % reduction in defecation rate (Fig. 3.5). Importantly, hypophagic eating behavior during intestinal inflammation in human and DSS-induced colitis is reported to be attributed to increased pro-inflammatory cytokines and deregulated gut hormones/ neuropeptides [189], [190]. However, the causal relationship in the *Drosophila* DSS-induced colitis-like model needs further testing.

4.2.3. Disease endpoint 3 (DE03): Weight loss is an informative extra-intestinal marker of DSS-induced colitis

Undoubtedly, weight loss is reported in patients with IBD especially during flare-ups. It is largely attributed primarily to decreased food intake [186], [191]. It is also considered as a universal marker of active disease in murine models of DSS-induced colitis [49], [192]. Unlike the poikilothermic model organisms (eg. Zebrafish), *D. melanogaster* is a powerful model organism to study organismal weight loss and related wasting of skeletal muscle and adipose tissue mass (eg. in cachexia) [193], [194], [195]. The major findings are that DSS-treated flies manifested a significant reduction in body weight (7,3%) and 34,4% reduction in total body triglycerides (Fig.3.7). Interestingly, body-weight reduction of 1 to 10 % in mouse model of DSS-induced colitis is scored as 1 unit of disease activity index (DAI) [192]. Consistent with the appetite loss and decreased defecation rate in DSS-treated flies, weight loss and reduced body fat could be a formal validation of the aforementioned DE02. Moreover, the potential association of increased energy cost and weight loss phenotype needs further testing.

4.2.4. Disease endpoint 4 (DE04): Migration of *Drosophila* plasmatocytes (macrophage-like) to the injured gut is a quantitative surrogate marker of DSS-induced colitis.

In principle, intestinal macrophages are key players in intestinal innate immune response. They act by maintaining the microbiological and cellular homeostasis of the intestinal mucosa via multiple mechanisms such as phagocytosis and wound healing. Homeostatic perturbation also participates in the development of intestinal inflammation and pathogenesis of IBDs [196], [197]. Interestingly, the *Drosophila* gut plasmatocytes of the monocyte lineage share a striking functional homology with mammalian macrophages. They are involved in phagocytosis, wound healing and production of extracellular matrix (ECM) components [198], [199]. Unsurprisingly, recent independent transcriptome studies on intestinal macrophages isolated from IBD patients and the *Drosophila* plasmatocytes showed shared gene ontology between some human genes and their *Drosophila* orthologs (eg. *TIMP1* and *NF-κB*) [197], [200]. Pathological recruitment and accumulation of macrophages in the inflamed gut was implemented as a biomarker of active disease in IBD patients (eg. fecal calprotectin), mice (eg. tissue myeloperoxidase, MPO) and zebrafish model of IBD as well as in *Drosophila* model of gut inflammation [116], [147], [201], [202], [203], [204], [205]. The major finding in this part is that circulating Hemolectin-positive plasmatocytes showed a marked directional collective migration from the circulation to the dorsal part of the abdomen in the DSS-treated flies compared to controls. Interestingly, *Spiroplasma*-infected *Drosophila* showed a typical phenotype [127]. To test whether plasmatocytes adhere to a specific gut region, the whole gut was dissected, washed and immune-stained. Plasmatocytes showed an evident adherence to the visceral muscle of the distal posterior midgut (PMG) (Fig. 3.8 B). In order to establish a reliable read-out phenotype, plasmatocyte migration marker (PMM) was developed as a direct quantitative surrogate marker of inflammation. A significant reduction (41,4%) of circulating abdominal plasmatocytes in DSS-treated flies is quantified under visual inspection. Interestingly, the established PRI is superior to the corresponding MPO (in mice) and neutrophilic inflammation index (in Zebrafish) because of its feasibility, non-invasiveness, suitability for time-series (follow-up) analysis, and cost-effectiveness [203], [205], [206], [207]. The only limitation of the PRI measurement is the tendency for quantitative bias that is circumvented by inclusion of technical replicates (repeated counting).

4.2.5. Disease endpoint 5 (DE05): Smurfness combined with disrupted visceral muscle and tight junction is more frequent in the *Drosophila* DSS-induced colitis.

Intestinal barrier function plays a crucial role in preventing the influx of luminal antigens and translocation of commensal/ pathogenic microbes. Barrier integrity is regulated by many tight junction (TJ) proteins (eg. zonulins in humans or its *Drosophila* homolog, Pvd) in order to control gut hyper-permeability. Dys-regulated gut paracellular permeability results in gut leakiness, aka leaky gut syndrome (LGS), with further triggering of local (intestinal) and systemic (extra-intestinal) inflammatory responses in IBD as well as other chronic inflammatory and metabolic disorders [208], [209], [210], [211].

Several non-invasive biomarkers have been developed to investigate the disrupted barrier functions such as sugar probes (urinary lactulose/ Mannitol ratio) and serum/ fecal zonulin in humans [212], [213]. Furthermore, the FITC-dextran-based in vivo permeability assay is widely adopted in mouse model of colitis as indirect non-invasive quantitative marker of leaky gut [214].

Unsurprisingly, the power of transparent *Drosophila* 'ventral' body is harnessed to develop a direct, non-invasive, cost-effective intestinal permeability assay -so-called "Smurf assay"- for the in vivo assessment of barrier integrity [115]. In principle, smurf assessment in the *Drosophila* longevity testing is presented as a continuous age-dependent phenotype [216].

In this project, the DSS-induced smurfness/ gut leakiness (referred to as DIS) is; however, manifested as a binary, age- independent, intermediate phenotype with two subtypes, dead smurfs (in DSS treatment group) and live smurfs (in age-matched control group). Upon DSS treatment, the frequency of dead smurfs increases to reach a normalized proportion of 57,7% of total dead flies at day 6 post treatment (Fig.3.9; Table 7-1). This data is in line with the conception that considers IBD as an impaired barrier disease [218].

Further, the potential bacterial translocation as a sequel to DIS is investigated. Fly food supplemented with GFP- or mCherry-labeled *E. coli* shows a similar pattern of blue food translocation (Fig. 3.11). This result indicates that gut paracellular leakiness in the *Drosophila* model of DSS-induced colitis allows translocation of food macromolecules (eg. Blue dye, 792,8 Da) as well as larger luminal microbes

(eg. *E. coli* with TEM-based estimated size 1,5 μm [119]). This data is in line with the increased bacterial translocation (BT) in both CD and UC with subsequent induction of both local and systemic proinflammatory responses as well as antimicrobial peptide secretion [219], [220]. Interestingly, this unique finding of influx of live bacteria associated with the DIS phenotype in *Drosophila* highlights the utility of this phenotype as one-of-a-kind in vivo, direct, and non-invasive marker of BT in animal models of DSS-induced colitis.

Unlike the linear trend in the aging-associated smurfness [216], DIS phenotype presented with a non-linear trend (Table 7-1) that is consistent with data reported in DSS-colitis model in mice [217]. Furthermore, DIS is presented with different severity grades of leakiness. The severity of leakiness increases in caudal-to-cranial manner that is scored based on the blue hue difference (Fig.3.9). The leakiness grade is proportional to activity reduction that reflects active/ severe disease, however, calculating the frequency of each severity grade in DIS is misleading because of the accelerated progression to death in DAS compared with the aging-associated smurfs.

Taken together, an acceptable hypothesis appears to be that DIS phenotype in younger flies is better to be implemented as a binary phenotype of epithelial barrier dysfunction as well as an adjunct mortality indicator to the survivorship and activity, but not to be implemented as a quantitative continuous maker of leakiness.

In this project, the location of the barrier loss across the gut was further characterized at the gross morphologic and histologic levels. The morphology of dissected midgut is shown to be less stiff in DIS compared to the hindgut (Fig. 7.1). Providing that there is a great anatomical homology between the *Drosophila* hindgut and the human large intestine [90], [221], [222], this data is partly in line with the enhanced leakiness in the human small intestine compared to the large intestine [223].

Moreover, immunostaining of the *Drosophila* visceral muscles of posterior midgut indicates a clear disruption of sarcometric integrity of the peristalsis muscles (Fig. 3.12 &3.13). These findings are consistent with the reported phenotype of DSS-based basement membrane damage [224]. To test the hypothesis whether there is a potential damage to the components of paracellular diffusion barrier, immunostating of selected septate junction (SJ) proteins (coracle and discs-large-1)

was performed. A significant pattern of irregular staining of coracle and *dlg-1* indicates dysregulated cell-cell communication in terms of loss of cell polarity and adhesion (Fig.3.14& 3.15). This finding is consistent with similar trends in both human IBD and murine DSS-induced colitis [225], [226]. Taken together, histologic findings provide another layer of direct evidence that collateral disruption of basement membrane/ muscle function and septate junction localization in the midgut is the main characteristic/hallmark of DIS phenotype.

Despite protein quantification of immune-stained leaky gut has been reported [104], it is difficult to accurately calculate the densitometry-based expression. To this end, quantitative differential gene expression of candidate septate and adherens junction genes were analyzed. Differential gene expression analysis revealed that three of the tested candidate genes, *Dlg1*, *DEcad* and *kune-kune* are significantly up-regulated in DSS-induced smurfness (Fig. 7.5). Remarkably, antibody staining of Discs large protein clearly demonstrates showed a decreased abundance at the protein level (Fig. 3.15). Despite the increased abundance of transcripts, there is a histologically-confirmed loss of barrier integrity. These findings are not in line with previous findings that these genes are down-regulated in ageing-induced dysfunctional barrier, albeit shared common phenotypic and histologic characteristics of DSS-induced smurfness [104]. One possible explanation for these contradictory findings is that the duration of DSS-induced Smurfness is extremely shorter (i.e. acute) than aging-induced smurfness (i.e. chronic). Furthermore, the tested genes consist of AU-rich elements predicted by AREsite2 (Fig.7.8) [266]. Hence, post-transcriptional modification by ARE-mediated mRNA decay could be regulated differently in inflammaging-related smurfness. The other possible, and more likely explanation, is that other potential molecular players could disrupt the proper stability, assembly and localization of those proteins to the septate junctions in DSS-induced smurfness.

To translate these findings, spatiotemporal gene expression analysis is performed in different gut regions (AMG, PMG and HG) in three treatment groups: DSS-treated, untreated animals and recovered animals. Relative abundance data indicate that at day 6 post DSS treatment *DEcad*, *Dlg1*, and *Kune-kune* are expressed in gradients along the anterior-posterior axis of the midgut. *Dlg1* is extremely up-regulated in the midgut with a significant 16,3 fold increase and a significant 14,7 fold increase in the anterior midgut (AMG) and the posterior midgut

(PMG), respectively. *DEcad* is moderately up-regulated with a significant 6,1 fold increase in the AMG. However, *Kune-Kune* is slightly up-regulated in the AMG and PMG, but fails to survive the statistical significance. In contrast to the midgut, *Dlg1*, *DEcad* and *Kune-kune* show a trend of down-regulation in the hindgut (Table 7-3; Fig. 3.25 – 3.27, Fig. 3.31). As expected, these findings together with the morphology-based differential leakiness between midgut and hindgut (Fig. 7.1) confirm that hindgut is less affected by DSS. Further, at day 12 post DSS treatment, gene expression analysis reveals a pan-gut slight up-regulation of all genes compared to day 6 post treatment (Table 7-3). Upon 6-day-recovery period from DSS treatment, *DEcad*, *Dlg1* and *Kune-kune* show a trend of down-regulation in the PMG but not in the AMG (Table 7-3). In principle, interpreting spatiotemporal gene expression results in the way to draw functional cross-talks between genes is challenging due to stochasticity of gene expression [227]. However, these data strongly indicate that differential expression of *DEcad*, *Dlg1* and *Kune-kune* in the PMG provides a regionalized transcriptional signature that reflects physiological resilience to DSS-induced colitis.

In attempt to investigate whether the abundance of the candidate SJ-related genes have functional relationships with other molecular players, co-expression analysis of SJ-related genes with components of JAK/STAT-pathways (*Upd3* and *Socs36E*) is tested. These findings indicate a significant positive correlation between different SJ components and *Upd3* in the AMG and PMG but not in the HG (Fig. 3.32). These data are in line with the reported efficacy of anti-IL-6 (vertebrate homolog of *Upd3*) in reducing intestinal permeability and inflammation in DSS-induced colitis [228]. Together, providing that co-expressed genes are regulated by the same transcriptional machinery or functionally-related protein complex, it could be assumed that both *Upd3* and the studied SJ genes share common transcription factors.

Collectively, these results provide a conceptual and a translational framework of studying paracellular gut leakiness in the *Drosophila* model of DSS-induced colitis at the morphologic, histologic and molecular levels. Adopting this framework could be instrumental in screening candidate chemopreventive agents that potentially mitigate paracellular hyper-permeability leaky gut syndrome and associated disorders.

4.2.6. Disease endpoint 6 (DE06): Epithelial dysplasia of the *Drosophila* midgut progenitor cells is reliable marker of *Drosophila* DSS-induced colitis.

Basically, activity of intestinal stem cell (ISC) in terms of proliferation and differentiation is a major aspect of mucosal homeostasis. Dysplasia, dysregulation of ISC proliferation and differentiation, impairs tissue renewal and is associated with DSS-induced inflammation in *Drosophila*, mice as well as in human IBD [229], [230], [231]. Myriads of signaling pathways have been reported to stemness in the *Drosophila* gut include *escargot* (*esg*), *Notch*, JAK/Stat [232], [233], [234]. In this project, two *Drosophila* lines that express GFP under the control of the *escargot* (*esg*) and *upd3* drivers were utilized. Data reveal that female flies exhibit a DSS-induced hyper-proliferative response in the ISC microenvironment (Fig. 3.16). It is obvious that dysplastic gut phenotype is characterized by significant regenerative response in both AMG and PMG, but not in the HG (Fig. 7.2). Precisely, the PMG is shown to be highly dysplastic and hyperplastic than the AMG. It is widely reported that the adult *Drosophila* hindgut proliferates in response to tissue damage while lacks active ISCs [237], [238]. Quite interestingly, upon 6-day-recovery period from DSS treatment, an irreversibility of functional stemness is more obvious in the PMG than in the AMG that reflects differential functional loss of ISCs (Fig. 12).

Tellingly, gene expression data indicate that *upd3* is significantly up-regulated in the AMG with 4,6 fold increase compared to the PMG at day-6-post DSS treatment. These findings are in line with the increased level of IL-6 in both murine DSS-induced colitis and in IBD patients [228], [235], [236]. Further, prolonged DSS treatment for 12 days results in a highly significant and sustained up-regulation of *upd3* in the AMG (5 fold increase) compared to the PMG. Upon 6-day-recovery, *upd3* is sustainably up-regulated in the AMG (6 fold) whereas it tends to be down-regulated in the PMG (Table 7-3; fig. 3.34 – 3.36). These findings indicate that sustained over-expression of *upd3* is a critical determinant for ISC homeostasis in response to DSS-induced damage.

One of the most important highlights arisen from the abovementioned smurfness and dysplastic phenotypes is that PMG is severely affected by DSS-induced tissue damage with a much lesser tendency of resolution after recovery from DSS treatment. It also raises the possibility that *escargot*-reporter (*esg*-Gal4> GFP) provides a reliable, rescuable phenotype that reflects DSS-induced dysfunctional barrier and JAK-STAT pathway activation. To this end, multiple hypotheses based

on the escargot-reporter were tested. The first hypothesis to be tested is whether comparative reduction in the DSS-induced mortality of male *Drosophila* is affected by the degree of dysplasia. Interestingly, DSS-treated male escargot-reporter flies exhibit a less pronounced dysplasia (Fig. 3.17) that is in line with the reported sexually dimorphic ISC proliferation [239]. The second hypothesis is to test whether the dysplasia induction is caused by direct effect of DSS on ISCs or by indirect reciprocal effect of DSS and gut microbiota. For that reason, axenic (germ-free) escargot-reporter female flies were generated for further treatment with either DSS or fecal microbiota transferred from DSS-treated animals. Data indicate that tissue-damaging effect of the DSS can induce dysplasia independent of microbial cues (Fig. 3.20).

Since DSS treatment is reported to induce intestinal dysbiosis in mice [162], this notion led to further testing whether transfer of whole gut microbiota from donor wild-type female *W¹¹¹⁸* flies -treated with DSS for either 6 or 12 days- to the recipient escargot-reporter female flies could drive dysplasia. Interestingly, gut microbiota transferred after prolonged DSS treatment (12 days), but not after 6-day treatment, led to moderate ISCs hyper-proliferation in recipient animals (Fig. 3.21). These findings indicate that gut microbiota transfer can recapitulate the dysplastic phenotype independent of the DSS effect. An attempt to decode the DSS-induced spatio-temporal differences of the abundance and composition of fecal and tissue resident microbiota 'dark matter' is made by 16S rRNA amplicon sequencing.

4.3. *Drosophila* DSS-induced colitis is an informative model of host-microbiota interaction in the human IBD

The *Drosophila melanogaster* is being implemented as a very promising model in dissecting complex host-microbe and host- endosymbiont interactions in terms of the impact of microbe on various organismal phenotypes, including behavior, life span, and disease resistance [240], [241], [242], [243], [244]. Despite the fact that the *Drosophila* gut lacks some aspects of mammalian gut such as dense mucus layer and high fermentative capacity, many studies supported its potential as a valuable and cost-effective tool for fundamental discovery of microbiome function [245], [246], [247].

In IBD, most of the discovered risky genes are associated with the host-microbiota interactions in the gut microbial ecosystem. This notion emphasized that the key feature of IBD is the shift of an interspecies balance of microbiota community (known as eubiosis) towards imbalanced microbial community (known as dysbiosis). The dysbiotic state is generally characterized by decreased community diversity and a shift in bacterial taxa [248], [249], [250].

In the present study, best practices in designing microbiome studies are considered in order to generate meaningful results that reflect the corresponding microecological scenarios. Importantly, both cross-sectional and longitudinal designs were conducted and presented in three model groups (henceforth model-6, model-12 and model-6-recovery). In principle, cross-sectional design is informative in understanding the potential perturbing effect of DSS on the gut ecosystem. However, longitudinal design with intervention (i.e. 6-day-recovery period on normal media) is crucial to investigate how microbial community structure and composition change over time in relation to disease progression and remission. Furthermore, fundamental macroecological principles such as resistance and resilience are implemented to tackle biological processes governing microbial dynamics.

Since the dysbiotic gut microbiota in IBD is more pronounced in mucosal samples compared to the fecal counterparts [251], [252], the present study was designed to identify fecal-associated microbiota and tissue-associated microbiota in the pan midgut and hindgut. The only limitation in the study design is that midgut is technically difficult to be dissected as AMG and PMG because of potential cross-contamination with luminal microbes. Altogether, this meticulous design enables deciphering spatial and temporal events in the gut ecology, which in turn add another layer of understanding the microbiota residency in the context of gut physiology.

4.3.1. Characteristics of fecal-associated and tissue-associated microbiotas in-house reared *W¹¹⁸ Drosophila*

Miseq Illumina sequencing of the hypervariable V1 and V2 region of bacterial 16S rRNA gene produced > 40,000 paired reads per sample. The number of sequences were sufficient to be assigned into de-noised amplicon sequence variant (ASV) at 97% sequence identity based on the latest version of SILVA database.

Microbiota composition is presented in normalized relative abundance at different taxonomic levels. The fecal-associated microbiota community is classified into 4 major phyla [Actinobacteriota (~45,5 %), Firmicutes (~30,3 %), Proteobacteria (~17,7 %) and Bacteroidetes (~5,3 %)] and 2 minor phyla [Tenericutes (~0,7 %) and Cyanobacteria (~0,2 %)]. Alternatively, the midgut-associated microbiota community is classified into 4 major phyla [Actinobacteriota (~24,1 %), Firmicutes (~29,7 %), Proteobacteria (~27,5 %) and Bacteroidetes (~16,5 %)] and 3 minor phyla [Tenericutes (~1,2 %), Fusobacteria (~0,2 %) and Candidatus Saccharibacteria (~0.8 %)]. On the other hand, the hindgut-associated microbiota community is classified into 4 major phyla [Actinobacteriota (~25,5 %), Firmicutes (~31,8 %), Proteobacteria (~33,55 %) and Bacteroidetes (~8,1 %)] and 2 minor phyla [Tenericutes (~0.7 %) and Fusobacteria (~0,1 %) and Cyanobacteria (~0,75 %). Obviously, midgut-associated community is characterized by a community structure with a comparable co-occurrence of major phyla in addition to one extra unique minor phylum belongs to Candidatus Saccharibacteria, which in turn reflects specific inter-microbial interactions and niche specialization (Table 7-4& Fig. 7.6).

Despite the present study is the first attempt to investigate the DSS-gut-microbiota interplay, any future taxonomic discordance should be attributed to either the lab-brew experimental diet or the targeted region of the bacterial 16S rRNA.

The community structure of the midgut-associated microbiota is presented with the highest *alpha*-diversity estimates at the level of both species richness (number of taxonomic groups, which is used as a proxy for understanding diversity) and Shannon effective index (a measure of the actual diversity) followed by the hindgut-associated microbiota. However, the fecal-associated microbiota is the less diverse community (Shannon effective index = 33,4) in comparison to the midgut-associated microbiota (Shannon effective index = 45,8) and hindgut-associated microbiota (Shannon effective index = 38,1). Taken together, studying midgut-associated microbiota is superior in terms of community diversity and taxonomic resolution (Table 7-5, 7-6& 7-7).

To test the hypothesis that whether each community-associated microbiota from those groups has a distinct features, *beta*-diversity analysis was performed. Results indicate a highly significant separation of fecal-associated microbiota, midgut-

associated microbiota and hindgut-associated microbiota clusters (Fig 7.7). In turn, pairwise comparison across those groups (i.e. fecal-associated microbiota vs. midgut-associated microbiota vs. hindgut-associated microbiota) is misleading.

4.3.2. Community structure of the *Drosophila* DSS-induced colitis model

In principle, diversity estimates are determined based on the abundance of taxa and calculated to describe the complexity of the ecological community. A reduction in microbial diversity mirrors the instability of the ecosystem and its impaired function (i.e. dysbiosis) [253], [254].

In this section, the impact of DSS on the longitudinal stability of the gut microbiota in the previously mentioned model groups (model-6, model-12 and model-6-recovery) is discussed at the level of *alpha*- and *beta*-diversity.

Alpha-diversity describes the diversity within an ecosystem (i.e. within-sample) which is mostly represented by species richness and Shannon index. Alternatively, *beta*-diversity describes the difference between two ecosystems (i.e. inter-sample distances matrix) and represented by generalized UniFrac with a phylogenetic distance matrix visualized (as clusters in quadrant) by the non-metric Multi-Dimensional Scaling (NMDS), which is the most robust unconstrained ordination method recommended in ecological analysis, together with a dendrogram representing a hierarchical clustering of all samples under the study. Significance of clusters separation is calculated by a PERMANOVA test.

Studying *alpha*-diversity of model-6 reveals that DSS treatment causes 30,8% reduction in species richness and a significant sharp reduction (63,3%) in Shannon effective index of the midgut-associated microbiota. Similar trends were observed for the hindgut-associated microbiota (13,4% and 30,6% reduction in richness and Shannon index, respectively) and the fecal-associated microbiota (20,5% and 34,2% reduction in richness and Shannon index, respectively). Notably, no further extensive decline was observed in *alpha*-diversity indices in model-12. Further testing of the model-6-recovery indicates lack of restorative capacity of the gut ecosystem after 6 days of recovery post DSS treatment.

On projection of beta-diversity matrix of the model-6 on multidimensional scaling plot, samples from the DSS groups were clustered into cluster separated from the

corresponding samples of the control group. The midgut-associated microbiota group showed the best distinct clustering pattern compared to the hindgut-associated microbiota and fecal-associated microbiota. Most of the DSS-treated replicates were well-separated in both multidimensional scaling (MDS) plot and the dendrogram (Fig. 3.38, 3.42 & 3.45). Further, MDS plot of all subsets of model-12 and model-6-recovery fail to clearly separate sample clusters with distinct boundaries. The possible explanation is that lack of previously published benchmark datasets in the context of DSS and the *Drosophila* microbiota hampered *a priori* assignment of the proper sample size for adequate permutations and statistical power.

Through the above results, it becomes clear that midgut-associated microbiota is superior over hindgut-associated microbiota and fecal-associated microbiota in studying the effect of DSS on microbiota community structure.

It is also evident that 5% DSS treatment for 6 days causes a significant reduction of the midgut microbiota diversity. Interestingly, those three aspects of microbiota community structure in the *Drosophila* DSS-induced colitis model are typically consistent with published data on murine DSS-induced colitis and human active IBDs [60], [254], [255], [256], [257]. Together, this result highlights the successfulness of the established *Drosophila* DSS-induced colitis model in recapitulating major aspects of microbial ecology. It also encourages proper implementation of the *Drosophila* midgut-associated microbiota in studying the interplay of any candidate stressor with microbiota together with an in-depth downstream analysis of relative abundance at higher (Phylum) and lower (genus) taxonomy levels.

4.3.3. Microbial imbalance of the *Drosophila* DSS-induced colitis at different taxonomic levels

In principle, decreased alpha-diversity is a proxy for DSS-driven microbial diversity shifts and reflects a dysbiotic state of over-abundance of superior bacterial species that won the competition for nutrients and niche occupation. However, it does not provide sufficient granularity about taxonomic variation (i.e. microbial signature of the disease). In this section, the impact of DSS on the relative abundance of different taxonomic ranks of the gut microbiota is discussed. These ranks include

the 4 major phyla (Actinobacteriota, Firmicutes, Bacteroidota and Proteobacteria); 2 classes belonging to Proteobacteria (Alphaproteobacteria and Gammaproteobacteria), as well as 2 families belonging to Proteobacteria (Enterobacteriaceae) and Firmicutes (Lactobacillaceae). These lower taxonomic ranks are reported to be associated with DSS-induced colitis and human IBDs [258], [259], [260].

In model-6, DSS-treated animals showed a significant increase in the relative abundance of Proteobacteria (80,9 % in midgut-associated microbiota, 41% in fecal-associated microbiota). In contrast, other major phyla belongs to the midgut-associated microbiota community shows a marked reduction in abundance (-78,9% of Bacteroidota; - 44,2% of Actinobacteriota; -24,2% of Firmicutes) in the DSS-treated animal compared with controls. These results are consistent with most of the published reports on murine DSS-colitis and human IBDs as well as other inflammatory and autoimmune diseases [258], [259], [260], [261], [262], [263]. Further, Proteobacteria phyla is blooming only in the midgut-associated microbiota community of model-6 but not in the corresponding hindgut-associated microbiota community. This data add another layer of understanding the transcriptional dysregulation of *Upd3*, *Drosomycin* and *Attacin* in the gut (Table 7-3); in turn highlight the potential inflammation-driven selection of Proteobacteria over other taxonomic phyla. Together, these results are concordant with published data on the interplay between microbiota and antimicrobial peptides in the context of intestinal inflammation [264], [265].

5 Conclusion& outlook

In general, the established *Drosophila* model of DSS-induced colitis was shown to be successful in recapitulating major aspects of experimental colitis. Also, it provides a framework for experimentation considering a longitudinal design with inclusion of recovery groups. The recovery group is important in addressing the potential resilience on the level of gut physiology and ecology.

Since most of the phenotypic, gene expression and the microbiota analyses were mainly conducted on *W¹¹¹⁸* *Drosophila* line, generalizability of the current findings is expected to be limited if replicated in other genotypes. Furthermore, correlation of gene co-expression and taxa-taxa interaction analyses provided insights into the

underlying cross-talks. However, these results warrant future studies with precise experimental design for proper inferring of causality.

6 References

1. Silverberg, M. S., Satsangi, J., Ahmad, T., Arnott, I. D., Bernstein, C. N., Brant, S. R., Caprilli, R., Colombel, J. F., Gasche, C., Geboes, K., Jewell, D. P., Karban, A., Loftus, E. V., Jr, Peña, A. S., Riddell, R. H., Sachar, D. B., Schreiber, S., Steinhart, A. H., Targan, S. R., Vermeire, S., ... Warren, B. F. (2005). Toward an integrated clinical, molecular and serological classification of inflammatory bowel disease: report of a Working Party of the 2005 Montreal World Congress of Gastroenterology. *Canadian journal of gastroenterology = Journal canadien de gastroenterologie*, 19 Suppl A, 5A–36A. <https://doi.org/10.1155/2005/269076>
2. Delmondes, L. M., Nunes, M. O., Azevedo, A. R., Oliveira, M. M., Coelho, L. E., & Torres-Neto, J. D. (2015). Clinical and Sociodemographic Aspects of Inflammatory Bowel Disease Patients. *Gastroenterology research*, 8(3-4), 207–215. <https://doi.org/10.14740/gr649w>
3. Ananthakrishnan A. N. (2015). Epidemiology and risk factors for IBD. *Nature reviews. Gastroenterology & hepatology*, 12(4), 205–217. <https://doi.org/10.1038/nrgastro.2015.34>
4. Pimentel, M., Chang, M., Chow, E. J., Tabibzadeh, S., Kirit-Kiriak, V., Targan, S. R., & Lin, H. C. (2000). Identification of a prodromal period in Crohn's disease but not ulcerative colitis. *The American journal of gastroenterology*, 95(12), 3458–3462. <https://doi.org/10.1111/j.1572-0241.2000.03361.x>
5. Cosnes, J., Gower-Rousseau, C., Seksik, P., & Cortot, A. (2011). Epidemiology and natural history of inflammatory bowel diseases. *Gastroenterology*, 140(6), 1785–1794. <https://doi.org/10.1053/j.gastro.2011.01.055>
6. Gramlich, T., & Petras, R. E. (2007). Pathology of inflammatory bowel disease. *Seminars in pediatric surgery*, 16(3), 154–163. <https://doi.org/10.1053/j.sempedsurg.2007.04.005>
7. Vavricka, S. R., Schoepfer, A., Scharl, M., Lakatos, P. L., Navarini, A., & Rogler, G. (2015). Extraintestinal Manifestations of Inflammatory Bowel Disease. *Inflammatory bowel diseases*, 21(8), 1982–1992. <https://doi.org/10.1097/MIB.0000000000000392>
8. Molodecky, N. A., Soon, I. S., Rabi, D. M., Ghali, W. A., Ferris, M., Chernoff, G., Benchimol, E. I., Panaccione, R., Ghosh, S., Barkema, H. W., & Kaplan, G. G. (2012). Increasing incidence and prevalence of the inflammatory bowel diseases with time, based on systematic review. *Gastroenterology*, 142(1), 46–e30. <https://doi.org/10.1053/j.gastro.2011.10.001>
9. Kaplan, G. G., & Windsor, J. W. (2021). The four epidemiological stages in the global evolution of inflammatory bowel disease. *Nature reviews. Gastroenterology & hepatology*, 18(1), 56–66. <https://doi.org/10.1038/s41575-020-00360-x>
10. Esmat, S., El Nady, M., Elfekki, M., Elsherif, Y., & Naga, M. (2014). Epidemiological and clinical characteristics of inflammatory bowel diseases in Cairo, Egypt. *World journal of gastroenterology*, 20(3), 814–821. <https://doi.org/10.3748/wjg.v20.i3.814>
11. Baumgart, D. C., & Sandborn, W. J. (2007). Inflammatory bowel disease: clinical aspects and established and evolving therapies. *Lancet (London, England)*, 369(9573), 1641–1657. [https://doi.org/10.1016/S0140-6736\(07\)60751-X](https://doi.org/10.1016/S0140-6736(07)60751-X)
12. Ananthakrishnan A. N. (2014). The exposome in inflammatory bowel disease. *Tropical gastroenterology : official journal of the Digestive Diseases Foundation*, 35(3), 135–140. <https://doi.org/10.7869/tg.200>
13. Brajdić, A., & Mijandrušić-Sinčić, B. (2012). Insights to the Ethiopathogenesis of the Inflammatory Bowel Disease. *INFLAMMATORY BOWEL*, 1.
14. Loddo, I., & Romano, C. (2015). Inflammatory Bowel Disease: Genetics, Epigenetics, and Pathogenesis. *Frontiers in immunology*, 6, 551. <https://doi.org/10.3389/fimmu.2015.00551>
15. Cho, J. H., & Brant, S. R. (2011). Recent insights into the genetics of inflammatory bowel disease. *Gastroenterology*, 140(6), 1704–1712. <https://doi.org/10.1053/j.gastro.2011.02.046>
16. Uhlig, H. H., Schwerd, T., Koletzko, S., Shah, N., Kammermeier, J., Elkadri, A., Ouahed, J., Wilson, D. C., Travis, S. P., Turner, D., Klein, C., Snapper, S. B., Muise, A. M., & COLORS in IBD Study Group and NEOPICS (2014). The diagnostic approach to monogenic very early onset inflammatory bowel disease. *Gastroenterology*, 147(5), 990–1007.e3. <https://doi.org/10.1053/j.gastro.2014.07.023>

17. Liu, J. Z., van Sommeren, S., Huang, H., Ng, S. C., Alberts, R., Takahashi, A., Ripke, S., Lee, J. C., Jostins, L., Shah, T., Abedian, S., Cheon, J. H., Cho, J., Dayani, N. E., Franke, L., Fuyuno, Y., Hart, A., Juyal, R. C., Juyal, G., Kim, W. H., ... Weersma, R. K. (2015). Association analyses identify 38 susceptibility loci for inflammatory bowel disease and highlight shared genetic risk across populations. *Nature genetics*, 47(9), 979–986. <https://doi.org/10.1038/ng.3359>
18. Cooney, R., Baker, J., Brain, O., Danis, B., Pichulik, T., Allan, P., Ferguson, D. J., Campbell, B. J., Jewell, D., & Simmons, A. (2010). NOD2 stimulation induces autophagy in dendritic cells influencing bacterial handling and antigen presentation. *Nature medicine*, 16(1), 90–97. <https://doi.org/10.1038/nm.2069>
19. McGovern, D. P., Kugathasan, S., & Cho, J. H. (2015). Genetics of Inflammatory Bowel Diseases. *Gastroenterology*, 149(5), 1163–1176.e2. <https://doi.org/10.1053/j.gastro.2015.08.001>
20. Sartor, R. B., & Mazmanian, S. K. (2012). Intestinal microbes in inflammatory bowel diseases. *The American journal of gastroenterology supplements*, 1(1), 15.
21. Amaral, F. A., Sachs, D., Costa, V. V., Fagundes, C. T., Cisalpino, D., Cunha, T. M., Ferreira, S. H., Cunha, F. Q., Silva, T. A., Nicoli, J. R., Vieira, L. Q., Souza, D. G., & Teixeira, M. M. (2008). Commensal microbiota is fundamental for the development of inflammatory pain. *Proceedings of the National Academy of Sciences of the United States of America*, 105(6), 2193–2197. <https://doi.org/10.1073/pnas.0711891105>
22. Nagalingam, N. A., & Lynch, S. V. (2012). Role of the microbiota in inflammatory bowel diseases. *Inflammatory bowel diseases*, 18(5), 968–984. <https://doi.org/10.1002/ibd.21866>
23. Frank, D. N., St Amand, A. L., Feldman, R. A., Boedeker, E. C., Harpaz, N., & Pace, N. R. (2007). Molecular-phylogenetic characterization of microbial community imbalances in human inflammatory bowel diseases. *Proceedings of the National Academy of Sciences of the United States of America*, 104(34), 13780–13785. <https://doi.org/10.1073/pnas.0706625104>
24. Sepehri, S., Kotlowski, R., Bernstein, C. N., & Krause, D. O. (2007). Microbial diversity of inflamed and noninflamed gut biopsy tissues in inflammatory bowel disease. *Inflammatory bowel diseases*, 13(6), 675–683. <https://doi.org/10.1002/ibd.20101>
25. Lepage, P., Häsler, R., Spehlmann, M. E., Rehman, A., Zvirbliene, A., Begun, A., Ott, S., Kupcinkas, L., Doré, J., Raedler, A., & Schreiber, S. (2011). Twin study indicates loss of interaction between microbiota and mucosa of patients with ulcerative colitis. *Gastroenterology*, 141(1), 227–236. <https://doi.org/10.1053/j.gastro.2011.04.011>
26. Manichanh, C., Borruel, N., Casellas, F., & Guarner, F. (2012). The gut microbiota in IBD. *Nature reviews. Gastroenterology & hepatology*, 9(10), 599–608. <https://doi.org/10.1038/nrgastro.2012.152>
27. Nishino, K., Nishida, A., Inoue, R., Kawada, Y., Ohno, M., Sakai, S., Inatomi, O., Bamba, S., Sugimoto, M., Kawahara, M., Naito, Y., & Andoh, A. (2018). Analysis of endoscopic brush samples identified mucosa-associated dysbiosis in inflammatory bowel disease. *Journal of gastroenterology*, 53(1), 95–106. <https://doi.org/10.1007/s00535-017-1384-4>
28. Presley, L. L., Ye, J., Li, X., Leblanc, J., Zhang, Z., Ruegger, P. M., Allard, J., McGovern, D., Ippoliti, A., Roth, B., Cui, X., Jeske, D. R., Elashoff, D., Goodglick, L., Braun, J., & Borneman, J. (2012). Host-microbe relationships in inflammatory bowel disease detected by bacterial and metaproteomic analysis of the mucosal-luminal interface. *Inflammatory bowel diseases*, 18(3), 409–417. <https://doi.org/10.1002/ibd.21793>
29. Morgan, X. C., Tickle, T. L., Sokol, H., Gevers, D., Devaney, K. L., Ward, D. V., Reyes, J. A., Shah, S. A., LeLeiko, N., Snapper, S. B., Bousvaros, A., Korzenik, J., Sands, B. E., Xavier, R. J., & Huttenhower, C. (2012). Dysfunction of the intestinal microbiome in inflammatory bowel disease and treatment. *Genome biology*, 13(9), R79. <https://doi.org/10.1186/gb-2012-13-9-r79>
30. Persky, S. E., & Brandt, L. J. (2000). Treatment of recurrent *Clostridium difficile*-associated diarrhea by administration of donated stool directly through a colonoscope. *The American journal of gastroenterology*, 95(11), 3283–3285. <https://doi.org/10.1111/j.1572-0241.2000.03302.x>
31. Kahn, S. A., Gorawara-Bhat, R., & Rubin, D. T. (2012). Fecal bacteriotherapy for ulcerative colitis: patients are ready, are we?. *Inflammatory bowel diseases*, 18(4), 676–684. <https://doi.org/10.1002/ibd.21775>
32. Tighe, M. P., Cummings, J. R., & Afzal, N. A. (2011). Nutrition and inflammatory bowel disease: primary or adjuvant therapy. *Current opinion in clinical nutrition and metabolic care*, 14(5), 491–496. <https://doi.org/10.1097/MCO.0b013e328349eb4d>

33. Calabrese, E., Yanai, H., Shuster, D., Rubin, D. T., & Hanauer, S. B. (2012). Low-dose smoking resumption in ex-smokers with refractory ulcerative colitis. *Journal of Crohn's & colitis*, 6(7), 756–762. <https://doi.org/10.1016/j.crohns.2011.12.010>
34. Harries, A. D., Baird, A., & Rhodes, J. (1982). Non-smoking: a feature of ulcerative colitis. *British medical journal (Clinical research ed.)*, 284(6317), 706. <https://doi.org/10.1136/bmj.284.6317.706>
35. Cosnes J. (2004). Tobacco and IBD: relevance in the understanding of disease mechanisms and clinical practice. *Best practice & research. Clinical gastroenterology*, 18(3), 481–496. <https://doi.org/10.1016/j.bpg.2003.12.003>
36. Lakatos, P. L., Szamosi, T., & Lakatos, L. (2007). Smoking in inflammatory bowel diseases: good, bad or ugly?. *World journal of gastroenterology*, 13(46), 6134–6139. <https://doi.org/10.3748/wjg.v13.i46.6134>
37. Lo Sasso, G., Phillips, B. W., Sewer, A., Battey, J., Kondylis, A., Talikka, M., Titz, B., Guedj, E., Peric, D., Bornand, D., Dulize, R., Merg, C., Corciulo, M., Ouadi, S., Yanuar, R., Tung, C. K., Ivanov, N. V., Peitsch, M. C., & Hoeng, J. (2020). The reduction of DSS-induced colitis severity in mice exposed to cigarette smoke is linked to immune modulation and microbial shifts. *Scientific reports*, 10(1), 3829. <https://doi.org/10.1038/s41598-020-60175-3>
38. Galvez, J., Rodríguez-Cabezas, M. E., & Zarzuelo, A. (2005). Effects of dietary fiber on inflammatory bowel disease. *Molecular nutrition & food research*, 49(6), 601–608. <https://doi.org/10.1002/mnfr.200500013>
39. Amre, D. K., D'Souza, S., Morgan, K., Seidman, G., Lambrette, P., Grimard, G., Israel, D., Mack, D., Ghadirian, P., Deslandres, C., Chotard, V., Budai, B., Law, L., Levy, E., & Seidman, E. G. (2007). Imbalances in dietary consumption of fatty acids, vegetables, and fruits are associated with risk for Crohn's disease in children. *The American journal of gastroenterology*, 102(9), 2016–2025. <https://doi.org/10.1111/j.1572-0241.2007.01411.x>
40. Ananthakrishnan, A. N., Khalili, H., Konijeti, G. G., Higuchi, L. M., de Silva, P., Korzenik, J. R., Fuchs, C. S., Willett, W. C., Richter, J. M., & Chan, A. T. (2013). A prospective study of long-term intake of dietary fiber and risk of Crohn's disease and ulcerative colitis. *Gastroenterology*, 145(5), 970–977. <https://doi.org/10.1053/j.gastro.2013.07.050>
41. Witkowski, M., Witkowski, M., Gagliani, N., & Huber, S. (2018). Recipe for IBD: can we use food to control inflammatory bowel disease?. *Seminars in immunopathology*, 40(2), 145–156. <https://doi.org/10.1007/s00281-017-0658-5>
42. John, S., Luben, R., Shrestha, S. S., Welch, A., Khaw, K. T., & Hart, A. R. (2010). Dietary n-3 polyunsaturated fatty acids and the aetiology of ulcerative colitis: a UK prospective cohort study. *European journal of gastroenterology & hepatology*, 22(5), 602–606. <https://doi.org/10.1097/MEG.0b013e3283352d05>
43. Devkota, S., Wang, Y., Musch, M. W., Leone, V., Fehlner-Peach, H., Nadimpalli, A., Antonopoulos, D. A., Jabri, B., & Chang, E. B. (2012). Dietary-fat-induced taurocholic acid promotes pathobiont expansion and colitis in Il10^{-/-} mice. *Nature*, 487(7405), 104–108. <https://doi.org/10.1038/nature11225>
44. Shin, J. T., & Fishman, M. C. (2002). From Zebrafish to human: modular medical models. *Annual review of genomics and human genetics*, 3, 311–340. <https://doi.org/10.1146/annurev.genom.3.031402.131506>
45. Schartl M. (2014). Beyond the zebrafish: diverse fish species for modeling human disease. *Disease models & mechanisms*, 7(2), 181–192. <https://doi.org/10.1242/dmm.012245>
46. Marjoram, L., & Bagnat, M. (2015). Infection, Inflammation and Healing in Zebrafish: Intestinal Inflammation. *Current pathobiology reports*, 3(2), 147–153. <https://doi.org/10.1007/s40139-015-0079-x>
47. Waldner, M. J., & Neurath, M. F. (2009). Chemically induced mouse models of colitis. *Current protocols in pharmacology*, Chapter 5, . <https://doi.org/10.1002/0471141755.ph0555s46>
48. Uhlig, H. H., & Powrie, F. (2009). Mouse models of intestinal inflammation as tools to understand the pathogenesis of inflammatory bowel disease. *European journal of immunology*, 39(8), 2021–2026. <https://doi.org/10.1002/eji.200939602>
49. Chassaing, B., Aitken, J. D., Malleshappa, M., & Vijay-Kumar, M. (2014). Dextran sulfate sodium (DSS)-induced colitis in mice. *Current protocols in immunology*, 104, 15.25.1–15.25.14. <https://doi.org/10.1002/0471142735.im1525s104>

50. Vijay-Kumar, M., Wu, H., Aitken, J., Kolachala, V. L., Neish, A. S., Sitaraman, S. V., & Gewirtz, A. T. (2007). Activation of toll-like receptor 3 protects against DSS-induced acute colitis. *Inflammatory bowel diseases*, 13(7), 856–864. <https://doi.org/10.1002/ibd.20142>
51. Rose, W. A., 2nd, Sakamoto, K., & Leifer, C. A. (2012). Multifunctional role of dextran sulfate sodium for in vivo modeling of intestinal diseases. *BMC immunology*, 13, 41. <https://doi.org/10.1186/1471-2172-13-41>
52. Tanaka, T., Kohno, H., Suzuki, R., Yamada, Y., Sugie, S., & Mori, H. (2003). A novel inflammation-related mouse colon carcinogenesis model induced by azoxymethane and dextran sodium sulfate. *Cancer science*, 94(11), 965–973. <https://doi.org/10.1111/j.1349-7006.2003.tb01386.x>
53. Wirtz, S., Neufert, C., Weigmann, B., & Neurath, M. F. (2007). Chemically induced mouse models of intestinal inflammation. *Nature protocols*, 2(3), 541–546. <https://doi.org/10.1038/nprot.2007.41>
54. Whittam, C. G., Williams, A. D., & Williams, C. S. (2010). Murine Colitis modeling using Dextran Sulfate Sodium (DSS). *Journal of visualized experiments : JoVE*, (35), 1652. <https://doi.org/10.3791/1652>
55. Dieleman, L. A., Ridwan, B. U., Tennyson, G. S., Beagley, K. W., Bucy, R. P., & Elson, C. O. (1994). Dextran sulfate sodium-induced colitis occurs in severe combined immunodeficient mice. *Gastroenterology*, 107(6), 1643–1652. [https://doi.org/10.1016/0016-5085\(94\)90803-6](https://doi.org/10.1016/0016-5085(94)90803-6)
56. Strober, W., Fuss, I. J., & Blumberg, R. S. (2002). The immunology of mucosal models of inflammation. *Annual review of immunology*, 20, 495–549. <https://doi.org/10.1146/annurev.immunol.20.100301.064816>
57. Perše, M., & Cerar, A. (2012). Dextran sodium sulphate colitis mouse model: traps and tricks. *Journal of biomedicine & biotechnology*, 2012, 718617. <https://doi.org/10.1155/2012/718617>
58. Laroui, H., Ingersoll, S. A., Liu, H. C., Baker, M. T., Ayyadurai, S., Charania, M. A., Laroui, F., Yan, Y., Sitaraman, S. V., & Merlin, D. (2012). Dextran sodium sulfate (DSS) induces colitis in mice by forming nano-lipocomplexes with medium-chain-length fatty acids in the colon. *PLoS one*, 7(3), e32084. <https://doi.org/10.1371/journal.pone.0032084>
59. Okayasu, I., Hatakeyama, S., Yamada, M., Ohkusa, T., Inagaki, Y., & Nakaya, R. (1990). A novel method in the induction of reliable experimental acute and chronic ulcerative colitis in mice. *Gastroenterology*, 98(3), 694–702. [https://doi.org/10.1016/0016-5085\(90\)90290-h](https://doi.org/10.1016/0016-5085(90)90290-h)
60. Munyaka, P. M., Rabbi, M. F., Khafipour, E., & Ghia, J. E. (2016). Acute dextran sulfate sodium (DSS)-induced colitis promotes gut microbial dysbiosis in mice. *Journal of basic microbiology*, 56(9), 986–998. <https://doi.org/10.1002/jobm.201500726>
61. Perrimon, N., Bonini, N. M., & Dhillon, P. (2016). Fruit flies on the front line: the translational impact of *Drosophila*. *Disease models & mechanisms*, 9(3), 229–231. <https://doi.org/10.1242/dmm.024810>
62. Perrimon, N., Pitsouli, C., & Shilo, B. Z. (2012). Signaling mechanisms controlling cell fate and embryonic patterning. *Cold Spring Harbor perspectives in biology*, 4(8), a005975. <https://doi.org/10.1101/cshperspect.a005975>
63. Ugur, B., Chen, K., & Bellen, H. J. (2016). *Drosophila* tools and assays for the study of human diseases. *Disease models & mechanisms*, 9(3), 235–244. <https://doi.org/10.1242/dmm.023762>
64. Chien, S., Reiter, L. T., Bier, E., & Gribskov, M. (2002). Homophila: human disease gene cognates in *Drosophila*. *Nucleic acids research*, 30(1), 149–151. <https://doi.org/10.1093/nar/30.1.149>
65. Yamamoto, S., Jaiswal, M., Charng, W. L., Gambin, T., Karaca, E., Mirzaa, G., Wiszniewski, W., Sandoval, H., Haelterman, N. A., Xiong, B., Zhang, K., Bayat, V., David, G., Li, T., Chen, K., Gala, U., Harel, T., Pehlivan, D., Penney, S., Vissers, L., ... Bellen, H. J. (2014). A *Drosophila* genetic resource of mutants to study mechanisms underlying human genetic diseases. *Cell*, 159(1), 200–214. <https://doi.org/10.1016/j.cell.2014.09.002>
66. Chintapalli, V. R., Wang, J., & Dow, J. A. (2007). Using FlyAtlas to identify better *Drosophila melanogaster* models of human disease. *Nature genetics*, 39(6), 715–720. <https://doi.org/10.1038/ng2049>
67. Ma, D., Storelli, G., Mitchell, M., & Leulier, F. (2015). Studying host-microbiota mutualism in *Drosophila*: Harnessing the power of gnotobiotic flies. *Biomedical journal*, 38(4), 285–293. <https://doi.org/10.4103/2319-4170.158620>

68. Willoughby, L. F., Schlosser, T., Manning, S. A., Parisot, J. P., Street, I. P., Richardson, H. E., Humbert, P. O., & Brumby, A. M. (2013). An in vivo large-scale chemical screening platform using *Drosophila* for anti-cancer drug discovery. *Disease models & mechanisms*, 6(2), 521–529. <https://doi.org/10.1242/dmm.009985>
69. Alfa, R. W., & Kim, S. K. (2016). Using *Drosophila* to discover mechanisms underlying type 2 diabetes. *Disease models & mechanisms*, 9(4), 365–376. <https://doi.org/10.1242/dmm.023887>
70. Roeder, T., Isermann, K., Kallsen, K., Uliczka, K., & Wagner, C. (2012). A *Drosophila* asthma model - what the fly tells us about inflammatory diseases of the lung. *Advances in experimental medicine and biology*, 710, 37–47. https://doi.org/10.1007/978-1-4419-5638-5_5
71. Millburn, G. H., Crosby, M. A., Gramates, L. S., Tweedie, S., & FlyBase Consortium (2016). FlyBase portals to human disease research using *Drosophila* models. *Disease models & mechanisms*, 9(3), 245–252. <https://doi.org/10.1242/dmm.023317>
72. Kasai, Y., & Cagan, R. (2010). *Drosophila* as a tool for personalized medicine: a primer. *Personalized medicine*, 7(6), 621–632. <https://doi.org/10.2217/pme.10.65>
73. Das, T., & Cagan, R. (2010). *Drosophila* as a novel therapeutic discovery tool for thyroid cancer. *Thyroid : official journal of the American Thyroid Association*, 20(7), 689–695. <https://doi.org/10.1089/thy.2010.1637>
74. Baranski, T. J., Kraja, A. T., Fink, J. L., Feitosa, M., Lenzini, P. A., Borecki, I. B., Liu, C. T., Cupples, L. A., North, K. E., & Province, M. A. (2018). A high throughput, functional screen of human Body Mass Index GWAS loci using tissue-specific RNAi *Drosophila melanogaster* crosses. *PLoS genetics*, 14(4), e1007222. <https://doi.org/10.1371/journal.pgen.1007222>
75. Pendse, J., Ramachandran, P. V., Na, J., Narisu, N., Fink, J. L., Cagan, R. L., Collins, F. S., & Baranski, T. J. (2013). A *Drosophila* functional evaluation of candidates from human genome-wide association studies of type 2 diabetes and related metabolic traits identifies tissue-specific roles for dHHEX. *BMC genomics*, 14, 136. <https://doi.org/10.1186/1471-2164-14-136>
76. Guven-Maiorov, E., Tsai, C. J., & Nussinov, R. (2017). Structural host-microbiota interaction networks. *PLoS computational biology*, 13(10), e1005579. <https://doi.org/10.1371/journal.pcbi.1005579>
77. Kostic, A. D., Howitt, M. R., & Garrett, W. S. (2013). Exploring host-microbiota interactions in animal models and humans. *Genes & development*, 27(7), 701–718. <https://doi.org/10.1101/gad.212522.112>
78. Deng, H., Yang, S., Zhang, Y., Qian, K., Zhang, Z., Liu, Y., Wang, Y., Bai, Y., Fan, H., Zhao, X., & Zhi, F. (2018). *Bacteroides fragilis* Prevents *Clostridium difficile* Infection in a Mouse Model by Restoring Gut Barrier and Microbiome Regulation. *Frontiers in microbiology*, 9, 2976. <https://doi.org/10.3389/fmicb.2018.02976>
79. Murillo-Rincon, A. P., Klimovich, A., Pemöller, E., Taubenheim, J., Mortzfeld, B., Augustin, R., & Bosch, T. (2017). Spontaneous body contractions are modulated by the microbiome of *Hydra*. *Scientific reports*, 7(1), 15937. <https://doi.org/10.1038/s41598-017-16191-x>
80. Hill, J. H., Franzosa, E. A., Huttenhower, C., & Guillemin, K. (2016). A conserved bacterial protein induces pancreatic beta cell expansion during zebrafish development. *eLife*, 5, e20145. <https://doi.org/10.7554/eLife.20145>
81. Trinder, M., Daisley, B. A., Dube, J. S., & Reid, G. (2017). *Drosophila melanogaster* as a High-Throughput Model for Host-Microbiota Interactions. *Frontiers in microbiology*, 8, 751. <https://doi.org/10.3389/fmicb.2017.00751>
82. Koyle, M. L., Veloz, M., Judd, A. M., Wong, A. C., Newell, P. D., Douglas, A. E., & Chaston, J. M. (2016). Rearing the Fruit Fly *Drosophila melanogaster* Under Axenic and Gnotobiotic Conditions. *Journal of visualized experiments : JoVE*, (113), 54219. <https://doi.org/10.3791/54219>
83. Kietz, C., Pollari, V., & Meinander, A. (2018). Generating Germ-Free *Drosophila* to Study Gut-Microbe Interactions: Protocol to Rear *Drosophila* Under Axenic Conditions. *Current protocols in toxicology*, 77(1), e52. <https://doi.org/10.1002/cptx.52>
84. Gómez, E., Martín, F., Nogacka, A. M., Salazar, N., Aláez, L., Alcorta, E., Gueimonde, M., & De Los Reyes-Gavilán, C. G. (2019). Impact of probiotics on development and behaviour in *Drosophila melanogaster* - a potential in vivo model to assess probiotics. *Beneficial microbes*, 10(2), 179–188. <https://doi.org/10.3920/BM2018.0012>

85. Brand, A. H., & Perrimon, N. (1993). Targeted gene expression as a means of altering cell fates and generating dominant phenotypes. *Development (Cambridge, England)*, 118(2), 401–415. <https://doi.org/10.1242/dev.118.2.401>
86. Phelps, C. B., & Brand, A. H. (1998). Ectopic gene expression in *Drosophila* using GAL4 system. *Methods (San Diego, Calif.)*, 14(4), 367–379. <https://doi.org/10.1006/meth.1998.0592>
87. Kelly, S. M., Elchert, A., & Kahl, M. (2017). Dissection and Immunofluorescent Staining of Mushroom Body and Photoreceptor Neurons in Adult *Drosophila melanogaster* Brains. *Journal of visualized experiments : JoVE*, (129), 56174. <https://doi.org/10.3791/56174>
88. Buchon, N., Osman, D., David, F. P., Fang, H. Y., Boquete, J. P., Deplancke, B., & Lemaitre, B. (2013). Morphological and molecular characterization of adult midgut compartmentalization in *Drosophila*. *Cell reports*, 3(5), 1725–1738. <https://doi.org/10.1016/j.celrep.2013.04.001>
89. Dutta, D., Dobson, A. J., Houtz, P. L., Gläßner, C., Revah, J., Korzelius, J., Patel, P. H., Edgar, B. A., & Buchon, N. (2015). Regional Cell-Specific Transcriptome Mapping Reveals Regulatory Complexity in the Adult *Drosophila* Midgut. *Cell reports*, 12(2), 346–358. <https://doi.org/10.1016/j.celrep.2015.06.009>
90. Apidianakis, Y., & Rahme, L. G. (2011). *Drosophila melanogaster* as a model for human intestinal infection and pathology. *Disease models & mechanisms*, 4(1), 21–30. <https://doi.org/10.1242/dmm.003970>
91. Li, H., & Jasper, H. (2016). Gastrointestinal stem cells in health and disease: from flies to humans. *Disease models & mechanisms*, 9(5), 487–499. <https://doi.org/10.1242/dmm.024232>
92. Buchon, N., Osman, D., David, F. P., Fang, H. Y., Boquete, J. P., Deplancke, B., & Lemaitre, B. (2013). Morphological and molecular characterization of adult midgut compartmentalization in *Drosophila*. *Cell reports*, 3(5), 1725–1738. <https://doi.org/10.1016/j.celrep.2013.04.001>
93. Buchon, N., & Osman, D. (2015). All for one and one for all: Regionalization of the *Drosophila* intestine. *Insect biochemistry and molecular biology*, 67, 2–8. <https://doi.org/10.1016/j.ibmb.2015.05.015>
94. Dutta, D., Buchon, N., Xiang, J., & Edgar, B. A. (2015). Regional Cell Specific RNA Expression Profiling of FACS Isolated *Drosophila* Intestinal Cell Populations. *Current protocols in stem cell biology*, 34, 2F.2.1–2F.2.14. <https://doi.org/10.1002/9780470151808.sc02f02s34>
95. Marianes, A., & Spradling, A. C. (2013). Physiological and stem cell compartmentalization within the *Drosophila* midgut. *eLife*, 2, e00886. <https://doi.org/10.7554/eLife.00886>
96. Miguel-Aliaga, I., Jasper, H., & Lemaitre, B. (2018). Anatomy and Physiology of the Digestive Tract of *Drosophila melanogaster*. *Genetics*, 210(2), 357–396. <https://doi.org/10.1534/genetics.118.300224>
97. Lea, T. (2015). Epithelial cell models; general introduction. *The Impact of Food Bioactives on Health*, 95–102.
98. Zihni, C., Mills, C., Matter, K., & Balda, M. S. (2016). Tight junctions: from simple barriers to multifunctional molecular gates. *Nature reviews. Molecular cell biology*, 17(9), 564–580. <https://doi.org/10.1038/nrm.2016.80>
99. Balda, M. S., & Matter, K. (2016). Tight junctions as regulators of tissue remodelling. *Current opinion in cell biology*, 42, 94–101. <https://doi.org/10.1016/j.ceb.2016.05.006>
100. Lynch, A. M., & Hardin, J. (2009). The assembly and maintenance of epithelial junctions in *C. elegans*. *Frontiers in bioscience (Landmark edition)*, 14(4), 1414–1432. <https://doi.org/10.2741/3316>
101. Cox, E. A., & Hardin, J. (2004). Sticky worms: adhesion complexes in *C. elegans*. *Journal of cell science*, 117(Pt 10), 1885–1897. <https://doi.org/10.1242/jcs.01176>
102. Tepass, U., Tanentzapf, G., Ward, R., & Fehon, R. (2001). Epithelial cell polarity and cell junctions in *Drosophila*. *Annual review of genetics*, 35, 747–784. <https://doi.org/10.1146/annurev.genet.35.102401.091415>
103. Rera, M., Clark, R. I., & Walker, D. W. (2012). Intestinal barrier dysfunction links metabolic and inflammatory markers of aging to death in *Drosophila*. *Proceedings of the National Academy of Sciences of the United States of America*, 109(52), 21528–21533. <https://doi.org/10.1073/pnas.1215849110>

104. Clark, R. I., Salazar, A., Yamada, R., Fitz-Gibbon, S., Morselli, M., Alcaraz, J., Rana, A., Rera, M., Pellegrini, M., Ja, W. W., & Walker, D. W. (2015). Distinct Shifts in Microbiota Composition during *Drosophila* Aging Impair Intestinal Function and Drive Mortality. *Cell reports*, 12(10), 1656–1667. <https://doi.org/10.1016/j.celrep.2015.08.004>
105. Zwick, R. K., Ohlstein, B., & Klein, O. D. (2019). Intestinal renewal across the animal kingdom: comparing stem cell activity in mouse and *Drosophila*. *American journal of physiology. Gastrointestinal and liver physiology*, 316(3), G313–G322. <https://doi.org/10.1152/ajpgi.00353.2018>
106. Amoyel, M., & Bach, E. A. (2012). Functions of the *Drosophila* JAK-STAT pathway: Lessons from stem cells. *JAK-STAT*, 1(3), 176–183. <https://doi.org/10.4161/jkst.21621>
107. Myllymäki, H., & Rämet, M. (2014). JAK/STAT pathway in *Drosophila* immunity. *Scandinavian journal of immunology*, 79(6), 377–385. <https://doi.org/10.1111/sji.12170>
108. Kuraishi, T., Hori, A., & Kurata, S. (2013). Host-microbe interactions in the gut of *Drosophila melanogaster*. *Frontiers in physiology*, 4, 375. <https://doi.org/10.3389/fphys.2013.00375>
109. Panayidou, S., & Apidianakis, Y. (2013). Regenerative inflammation: lessons from *Drosophila* intestinal epithelium in health and disease. *Pathogens (Basel, Switzerland)*, 2(2), 209–231. <https://doi.org/10.3390/pathogens2020209>
110. Gold, K. S., & Brückner, K. (2014). *Drosophila* as a model for the two myeloid blood cell systems in vertebrates. *Experimental hematology*, 42(8), 717–727. <https://doi.org/10.1016/j.exphem.2014.06.002>
111. Gold, K. S., & Brückner, K. (2015). Macrophages and cellular immunity in *Drosophila melanogaster*. *Seminars in immunology*, 27(6), 357–368. <https://doi.org/10.1016/j.smim.2016.03.010>
112. Banerjee, U., Girard, J. R., Goins, L. M., & Spratford, C. M. (2019). *Drosophila* as a Genetic Model for Hematopoiesis. *Genetics*, 211(2), 367–417. <https://doi.org/10.1534/genetics.118.300223>
113. Tirouvanziam, R., Davidson, C. J., Lipsick, J. S., & Herzenberg, L. A. (2004). Fluorescence-activated cell sorting (FACS) of *Drosophila* hemocytes reveals important functional similarities to mammalian leukocytes. *Proceedings of the National Academy of Sciences of the United States of America*, 101(9), 2912–2917. <https://doi.org/10.1073/pnas.0308734101>
114. Mase, A., Augsburg, J., & Brückner, K. (2021). Macrophages and Their Organ Locations Shape Each Other in Development and Homeostasis - A *Drosophila* Perspective. *Frontiers in cell and developmental biology*, 9, 630272. <https://doi.org/10.3389/fcell.2021.630272>
115. Buchon, N., Silverman, N., & Cherry, S. (2014). Immunity in *Drosophila melanogaster*--from microbial recognition to whole-organism physiology. *Nature reviews. Immunology*, 14(12), 796–810. <https://doi.org/10.1038/nri3763>
116. Woodcock, K. J., Kierdorf, K., Pouchelon, C. A., Vivancos, V., Dionne, M. S., & Geissmann, F. (2015). Macrophage-derived upd3 cytokine causes impaired glucose homeostasis and reduced lifespan in *Drosophila* fed a lipid-rich diet. *Immunity*, 42(1), 133–144. <https://doi.org/10.1016/j.immuni.2014.12.023>
117. Leitão, A. C. B. (2014). *Hematopoiesis in the Drosophila larva: beyond the lymph gland*. NOVA University Lisbon, Portugal.
118. Hartenstein V. (2020). One too many: the surprising heterogeneity of *Drosophila* macrophages. *The EMBO journal*, 39(12), e105199. <https://doi.org/10.15252/emboj.2020105199>
119. Lee, E., Shon, H. K., & Cho, J. (2010). Biofouling characteristics using flow field-flow fractionation: effect of bacteria and membrane properties. *Bioresource technology*, 101(5), 1487–1493. <https://doi.org/10.1016/j.biortech.2009.08.041>
120. Ridley, E. V., Wong, A. C., & Douglas, A. E. (2013). Microbe-dependent and nonspecific effects of procedures to eliminate the resident microbiota from *Drosophila melanogaster*. *Applied and environmental microbiology*, 79(10), 3209–3214. <https://doi.org/10.1128/AEM.00206-13>
121. Flores, R., Shi, J., Gail, M. H., Gajer, P., Ravel, J., & Goedert, J. J. (2012). Assessment of the human faecal microbiota: II. Reproducibility and associations of 16S rRNA pyrosequences. *European journal of clinical investigation*, 42(8), 855–863. <https://doi.org/10.1111/j.1365-2362.2012.02659.x>

122. Agaisse, H., Petersen, U. M., Boutros, M., Mathey-Prevot, B., & Perrimon, N. (2003). Signaling role of hemocytes in *Drosophila* JAK/STAT-dependent response to septic injury. *Developmental cell*, 5(3), 441–450. [https://doi.org/10.1016/s1534-5807\(03\)00244-2](https://doi.org/10.1016/s1534-5807(03)00244-2)
123. Micchelli, C. A., & Perrimon, N. (2006). Evidence that stem cells reside in the adult *Drosophila* midgut epithelium. *Nature*, 439(7075), 475–479. <https://doi.org/10.1038/nature04371>
124. Zeng, X., Chauhan, C., & Hou, S. X. (2010). Characterization of midgut stem cell- and enteroblast-specific Gal4 lines in *Drosophila*. *Genesis (New York, N.Y. : 2000)*, 48(10), 607–611. <https://doi.org/10.1002/dvg.20661>
125. Rhea, J. M., Wegener, C., & Bender, M. (2010). The proprotein convertase encoded by *amontillado* (*amon*) is required in *Drosophila* corpora cardiaca endocrine cells producing the glucose regulatory hormone AKH. *PLoS genetics*, 6(5), e1000967. <https://doi.org/10.1371/journal.pgen.1000967>
126. Guo, Z., Driver, I., & Ohlstein, B. (2013). Injury-induced BMP signaling negatively regulates *Drosophila* midgut homeostasis. *The Journal of cell biology*, 201(6), 945–961. <https://doi.org/10.1083/jcb.201302049>
127. Garcia-Arreaez, M. G., Masson, F., Escobar, J., & Lemaitre, B. (2019). Functional analysis of RIP toxins from the *Drosophila* endosymbiont *Spiroplasma poulsonii*. *BMC microbiology*, 19(1), 46. <https://doi.org/10.1186/s12866-019-1410-1>
128. Ja, W. W., Carvalho, G. B., Mak, E. M., de la Rosa, N. N., Fang, A. Y., Liong, J. C., Brummel, T., & Benzer, S. (2007). Prandiology of *Drosophila* and the CAFE assay. *Proceedings of the National Academy of Sciences of the United States of America*, 104(20), 8253–8256. <https://doi.org/10.1073/pnas.0702726104>
129. Hildebrandt, A., Bickmeyer, I., & Kühnlein, R. P. (2011). Reliable *Drosophila* body fat quantification by a coupled colorimetric assay. *PloS one*, 6(9), e23796. <https://doi.org/10.1371/journal.pone.0023796>
130. Micchelli C. A. (2014). Whole-mount immunostaining of the adult *Drosophila* gastrointestinal tract. *Methods (San Diego, Calif.)*, 68(1), 273–279. <https://doi.org/10.1016/j.ymeth.2014.03.022>
131. Rueden, C. T., Schindelin, J., Hiner, M. C., DeZonia, B. E., Walter, A. E., Arena, E. T., & Eliceiri, K. W. (2017). ImageJ2: ImageJ for the next generation of scientific image data. *BMC bioinformatics*, 18(1), 529. <https://doi.org/10.1186/s12859-017-1934-z>
132. Alexandre C. (2008). Cuticle preparation of *Drosophila* embryos and larvae. *Methods in molecular biology (Clifton, N.J.)*, 420, 197–205. https://doi.org/10.1007/978-1-59745-583-1_11
133. Blanco, M. J., Learte, A., Marchena, M. A., Muñoz-Sáez, E., Cid, M. A., Rodríguez-Martín, I., & Sánchez-Camacho, C. (2018). Tracing Gene Expression Through Detection of β -galactosidase Activity in Whole Mouse Embryos. *Journal of visualized experiments : JoVE*, (136), 57785. <https://doi.org/10.3791/57785>
134. Pfaffl M. W. (2001). A new mathematical model for relative quantification in real-time RT-PCR. *Nucleic acids research*, 29(9), e45. <https://doi.org/10.1093/nar/29.9.e45>
135. Andersen, C. L., Jensen, J. L., & Ørntoft, T. F. (2004). Normalization of real-time quantitative reverse transcription-PCR data: a model-based variance estimation approach to identify genes suited for normalization, applied to bladder and colon cancer data sets. *Cancer research*, 64(15), 5245–5250. <https://doi.org/10.1158/0008-5472.CAN-04-0496>
136. Lagkouvardos, I., Joseph, D., Kapfhammer, M., Giritli, S., Horn, M., Haller, D., & Clavel, T. (2016). IMNGS: A comprehensive open resource of processed 16S rRNA microbial profiles for ecology and diversity studies. *Scientific reports*, 6, 33721. <https://doi.org/10.1038/srep33721>
137. Edgar R. C. (2013). UPARSE: highly accurate OTU sequences from microbial amplicon reads. *Nature methods*, 10(10), 996–998. <https://doi.org/10.1038/nmeth.2604>
138. Edgar, R. C., Haas, B. J., Clemente, J. C., Quince, C., & Knight, R. (2011). UCHIME improves sensitivity and speed of chimera detection. *Bioinformatics (Oxford, England)*, 27(16), 2194–2200. <https://doi.org/10.1093/bioinformatics/btr381>
139. Quast, C., Pruesse, E., Yilmaz, P., Gerken, J., Schweer, T., Yarza, P., Peplies, J., & Glöckner, F. O. (2013). The SILVA ribosomal RNA gene database project: improved data processing and web-based tools. *Nucleic acids research*, 41(Database issue), D590–D596. <https://doi.org/10.1093/nar/gks1219>

140. Yoon, S. H., Ha, S. M., Kwon, S., Lim, J., Kim, Y., Seo, H., & Chun, J. (2017). Introducing EzBioCloud: a taxonomically united database of 16S rRNA gene sequences and whole-genome assemblies. *International journal of systematic and evolutionary microbiology*, 67(5), 1613–1617. <https://doi.org/10.1099/ijsem.0.001755>
141. Lagkouvardos, I., Fischer, S., Kumar, N., & Clavel, T. (2017). Rhea: a transparent and modular R pipeline for microbial profiling based on 16S rRNA gene amplicons. *PeerJ*, 5, e2836. <https://doi.org/10.7717/peerj.2836>
142. Michael Friendly (2002) Corrgrams, *The American Statistician*, 56:4, 316-324, DOI: 10.1198/000313002533 <https://kwstat.github.io/corrgram>
143. Di Pierro F. (2021). Gut Microbiota Parameters Potentially Useful in Clinical Perspective. *Microorganisms*, 9(11), 2402. <https://doi.org/10.3390/microorganisms9112402>
144. Segata, N., Izard, J., Waldron, L., Gevers, D., Miropolsky, L., Garrett, W. S., & Huttenhower, C. (2011). Metagenomic biomarker discovery and explanation. *Genome biology*, 12(6), R60. <https://doi.org/10.1186/gb-2011-12-6-r60>
145. Sekiya, S., Murata, M., Arai, S., Murayama, H., Kawasaki, A., Ashida, N., Okada, K., & Ikemoto, M. (2016). Enzyme-linked immunosorbent assay for S100A9 in the stool of rats with dextran sulfate sodium-induced colitis. *Journal of immunological methods*, 439, 44–49. <https://doi.org/10.1016/j.jim.2016.09.009>
146. Araki, Y., Bamba, T., Mukaisho, K., Kanauchi, O., Ban, H., Bamba, S., Andoh, A., Fujiyama, Y., Hattori, T., & Sugihara, H. (2012). Dextran sulfate sodium administered orally is depolymerized in the stomach and induces cell cycle arrest plus apoptosis in the colon in early mouse colitis. *Oncology reports*, 28(5), 1597–1605. <https://doi.org/10.3892/or.2012.1969>
147. Oehlers, S. H., Flores, M. V., Hall, C. J., Wang, L., Ko, D. C., Crosier, K. E., & Crosier, P. S. (2017). A whole animal chemical screen approach to identify modifiers of intestinal neutrophilic inflammation. *The FEBS journal*, 284(3), 402–413. <https://doi.org/10.1111/febs.13976>
148. Cognigni, P., Bailey, A. P., & Miguel-Aliaga, I. (2011). Enteric neurons and systemic signals couple nutritional and reproductive status with intestinal homeostasis. *Cell metabolism*, 13(1), 92–104. <https://doi.org/10.1016/j.cmet.2010.12.010>
149. Wu, Q., Yu, G., Park, S. J., Gao, Y., Ja, W. W., & Yang, M. (2020). Excreta Quantification (EX-Q) for Longitudinal Measurements of Food Intake in Drosophila. *iScience*, 23(1), 100776. <https://doi.org/10.1016/j.isci.2019.100776>
150. Perše, M., & Cerar, A. (2012). Dextran sodium sulphate colitis mouse model: traps and tricks. *Journal of biomedicine & biotechnology*, 2012, 718617. <https://doi.org/10.1155/2012/718617>
151. Elsherif, Y., Alexakis, C., & Mendall, M. (2014). Determinants of Weight Loss prior to Diagnosis in Inflammatory Bowel Disease: A Retrospective Observational Study. *Gastroenterology research and practice*, 2014, 762191. <https://doi.org/10.1155/2014/762191>
152. Lo Sasso, G., Phillips, B. W., Sewer, A., Battey, J., Kondylis, A., Talikka, M., Titz, B., Guedj, E., Peric, D., Bornand, D., Dulize, R., Merg, C., Corciulo, M., Ouadi, S., Yanuar, R., Tung, C. K., Ivanov, N. V., Peitsch, M. C., & Hoeng, J. (2020). The reduction of DSS-induced colitis severity in mice exposed to cigarette smoke is linked to immune modulation and microbial shifts. *Scientific reports*, 10(1), 3829. <https://doi.org/10.1038/s41598-020-60175-3>
153. Telonis-Scott, M., Guthridge, K. M., & Hoffmann, A. A. (2006). A new set of laboratory-selected *Drosophila melanogaster* lines for the analysis of desiccation resistance: response to selection, physiology and correlated responses. *The Journal of experimental biology*, 209(Pt 10), 1837–1847. <https://doi.org/10.1242/jeb.02201>
154. Morris, S. N., Coogan, C., Chamseddin, K., Fernandez-Kim, S. O., Kolli, S., Keller, J. N., & Bauer, J. H. (2012). Development of diet-induced insulin resistance in adult *Drosophila melanogaster*. *Biochimica et biophysica acta*, 1822(8), 1230–1237. <https://doi.org/10.1016/j.bbadis.2012.04.012>
155. Ukena, S. N., Singh, A., Dringenberg, U., Engelhardt, R., Seidler, U., Hansen, W., Bleich, A., Bruder, D., Franzke, A., Rogler, G., Suerbaum, S., Buer, J., Gunzer, F., & Westendorf, A. M. (2007). Probiotic *Escherichia coli* Nissle 1917 inhibits leaky gut by enhancing mucosal integrity. *PLoS one*, 2(12), e1308. <https://doi.org/10.1371/journal.pone.0001308>

156. Martin, J. C., Bériou, G., & Josien, R. (2016). Dextran Sulfate Sodium (DSS)-Induced Acute Colitis in the Rat. *Methods in molecular biology (Clifton, N.J.)*, 1371, 197–203. https://doi.org/10.1007/978-1-4939-3139-2_12
157. Kiesler, P., Fuss, I. J., & Strober, W. (2015). Experimental Models of Inflammatory Bowel Diseases. *Cellular and molecular gastroenterology and hepatology*, 1(2), 154–170. <https://doi.org/10.1016/j.jcmgh.2015.01.006>
158. Chuang, L. S., Morrison, J., Hsu, N. Y., Labrias, P. R., Nayar, S., Chen, E., Villaverde, N., Facey, J. A., Boschetti, G., Giri, M., Castillo-Martin, M., Thin, T. H., Sharma, Y., Chu, J., & Cho, J. H. (2019). Zebrafish modeling of intestinal injury, bacterial exposures and medications defines epithelial *in vivo* responses relevant to human inflammatory bowel disease. *Disease models & mechanisms*, 12(8), dmm037432. <https://doi.org/10.1242/dmm.037432>
159. Wirtz, S., Popp, V., Kindermann, M., Gerlach, K., Weigmann, B., Fichtner-Feigl, S., & Neurath, M. F. (2017). Chemically induced mouse models of acute and chronic intestinal inflammation. *Nature protocols*, 12(7), 1295–1309. <https://doi.org/10.1038/nprot.2017.044>
160. Solomon, L., Mansor, S., Mallon, P., Donnelly, E., Hoper, M., Loughrey, M., ... & Gardiner, K. (2010). The dextran sulphate sodium (DSS) model of colitis: an overview. *Comparative clinical pathology*, 19(3), 235-239.
161. Amcheslavsky, A., Jiang, J., & Ip, Y. T. (2009). Tissue damage-induced intestinal stem cell division in *Drosophila*. *Cell stem cell*, 4(1), 49–61. <https://doi.org/10.1016/j.stem.2008.10.016>
162. Jialing, L., Yangyang, G., Jing, Z., Xiaoyi, T., Ping, W., Liwei, S., & Simin, C. (2020). Changes in serum inflammatory cytokine levels and intestinal flora in a self-healing dextran sodium sulfate-induced ulcerative colitis murine model. *Life sciences*, 263, 118587. <https://doi.org/10.1016/j.lfs.2020.118587>
163. Chang, C. S., Liao, Y. C., Huang, C. T., Lin, C. M., Cheung, C., Ruan, J. W., Yu, W. H., Tsai, Y. T., Lin, I. J., Huang, C. H., Liou, J. S., Chou, Y. H., Chien, H. J., Chuang, H. L., Juan, H. F., Huang, H. C., Chan, H. L., Liao, Y. C., Tang, S. C., Su, Y. W., ... Kao, C. Y. (2021). Identification of a gut microbiota member that ameliorates DSS-induced colitis in intestinal barrier enhanced *Dusp6*-deficient mice. *Cell reports*, 37(8), 110016. <https://doi.org/10.1016/j.celrep.2021.110016>
164. Park, H., Yeo, S., Kang, S., & Huh, C. S. (2021). Longitudinal Microbiome Analysis in a Dextran Sulfate Sodium-Induced Colitis Mouse Model. *Microorganisms*, 9(2), 370. <https://doi.org/10.3390/microorganisms9020370>
165. von Frieling, J., Faisal, M. N., Sporn, F., Pfefferkorn, R., Nolte, S. S., Sommer, F., Rosenstiel, P., & Roeder, T. (2020). A high-fat diet induces a microbiota-dependent increase in stem cell activity in the *Drosophila* intestine. *PLoS genetics*, 16(5), e1008789. <https://doi.org/10.1371/journal.pgen.1008789>
166. Bonfini, A., Liu, X., & Buchon, N. (2016). From pathogens to microbiota: How *Drosophila* intestinal stem cells react to gut microbes. *Developmental and comparative immunology*, 64, 22–38. <https://doi.org/10.1016/j.dci.2016.02.008>
167. Zhou, F., Rasmussen, A., Lee, S., & Agaisse, H. (2013). The UPD3 cytokine couples environmental challenge and intestinal stem cell division through modulation of JAK/STAT signaling in the stem cell microenvironment. *Developmental biology*, 373(2), 383–393. <https://doi.org/10.1016/j.ydbio.2012.10.023>
168. Caruso, R., Lo, B. C., & Núñez, G. (2020). Host-microbiota interactions in inflammatory bowel disease. *Nature reviews. Immunology*, 20(7), 411–426. <https://doi.org/10.1038/s41577-019-0268-7>
169. Pandey, U. B., & Nichols, C. D. (2011). Human disease models in *Drosophila melanogaster* and the role of the fly in therapeutic drug discovery. *Pharmacological reviews*, 63(2), 411–436. <https://doi.org/10.1124/pr.110.003293>
170. Ji, D., Sun, H., Yang, W., Gao, M., & Xu, H. (2022). Transfer of Human Microbiome to *Drosophila* Gut Model. *Microorganisms*, 10(3), 553. <https://doi.org/10.3390/microorganisms10030553>
171. Zaidman-Rémy, A., Regan, J. C., Brandão, A. S., & Jacinto, A. (2012). The *Drosophila* larva as a tool to study gut-associated macrophages: PI3K regulates a discrete hemocyte population at the proventriculus. *Developmental and comparative immunology*, 36(4), 638–647. <https://doi.org/10.1016/j.dci.2011.10.013>
172. Kuraishi, T., Hori, A., & Kurata, S. (2013). Host-microbe interactions in the gut of *Drosophila melanogaster*. *Frontiers in physiology*, 4, 375. <https://doi.org/10.3389/fphys.2013.00375>

173. Ludington, W. B., & Ja, W. W. (2020). *Drosophila* as a model for the gut microbiome. *PLoS pathogens*, 16(4), e1008398. <https://doi.org/10.1371/journal.ppat.1008398>
174. Zhou, Y., Liu, Z., Chen, Y., & Jin, L. H. (2016). Identification of the protective effects of traditional medicinal plants against SDS-induced *Drosophila* gut damage. *Experimental and therapeutic medicine*, 12(4), 2671–2680. <https://doi.org/10.3892/etm.2016.3641>
175. Howard, A. M., LaFever, K. S., Fenix, A. M., Scurrah, C. R., Lau, K. S., Burnette, D. T., Bhave, G., Ferrell, N., & Page-McCaw, A. (2019). DSS-induced damage to basement membranes is repaired by matrix replacement and crosslinking. *Journal of cell science*, 132(7), jcs226860. <https://doi.org/10.1242/jcs.226860>
176. Fenwick, N., Griffin, G., & Gauthier, C. (2009). The welfare of animals used in science: how the "Three Rs" ethic guides improvements. *The Canadian veterinary journal = La revue veterinaire canadienne*, 50(5), 523–530.
177. Varga, O. E., Hansen, A. K., Sandøe, P., & Olsson, I. A. (2010). Validating animal models for preclinical research: a scientific and ethical discussion. *Alternatives to laboratory animals : ATLA*, 38(3), 245–248. <https://doi.org/10.1177/026119291003800309>
178. Potashkin, J. A., Blume, S. R., & Runkle, N. K. (2010). Limitations of animal models of Parkinson's disease. *Parkinson's disease*, 2011, 658083. <https://doi.org/10.4061/2011/658083>
179. Wang, Y., Moussian, B., Schaeffeler, E., Schwab, M., & Nies, A. T. (2018). The fruit fly *Drosophila melanogaster* as an innovative preclinical ADME model for solute carrier membrane transporters, with consequences for pharmacology and drug therapy. *Drug discovery today*, 23(10), 1746–1760. <https://doi.org/10.1016/j.drudis.2018.06.002>
180. Nainu, F., Bahar, M. A., Sartini, S., Rosa, R. A., Rahmah, N., Kamri, R. A., ... & Wahyudin, E. (2022). Proof-of-Concept Preclinical Use of *Drosophila melanogaster* in the Initial Screening of Immunomodulators. *Scientia Pharmaceutica*, 90(1), 11
181. Oliveira, L. G., Cunha, A. L., Duarte, A. C., Castañón, M. C., Chebli, J. M., & Aguiar, J. A. (2014). Positive correlation between disease activity index and matrix metalloproteinases activity in a rat model of colitis. *Arquivos de gastroenterologia*, 51(2), 107–112. <https://doi.org/10.1590/s0004-28032014000200007>
182. Liu, W. S., Chen, M. C., Chiu, K. H., Wen, Z. H., & Lee, C. H. (2012). Amelioration of dextran sodium sulfate-induced colitis in mice by *Rhodobacter sphaeroides* extract. *Molecules (Basel, Switzerland)*, 17(11), 13622–13630. <https://doi.org/10.3390/molecules171113622>
183. Liu, Z., Chen, Y., Zhang, H., & Jin, L. H. (2016). *Crocus sativus* L. protects against SDS-induced intestinal damage and extends lifespan in *Drosophila melanogaster*. *Molecular medicine reports*, 14(6), 5601–5606. <https://doi.org/10.3892/mmr.2016.5944>
184. Perše, M., & Cerar, A. (2012). Dextran sodium sulphate colitis mouse model: traps and tricks. *Journal of biomedicine & biotechnology*, 2012, 718617. <https://doi.org/10.1155/2012/718617>
185. Bábíčková, J., Tóthová, L., Lengyelová, E., Bartoňová, A., Hodosy, J., Gardlík, R., & Celec, P. (2015). Sex Differences in Experimentally Induced Colitis in Mice: a Role for Estrogens. *Inflammation*, 38(5), 1996–2006. <https://doi.org/10.1007/s10753-015-0180-7>
186. Hartman, C., Eliakim, R., & Shamir, R. (2009). Nutritional status and nutritional therapy in inflammatory bowel diseases. *World journal of gastroenterology*, 15(21), 2570–2578. <https://doi.org/10.3748/wjg.15.2570>
187. Moran, G. W., Leslie, F. C., & McLaughlin, J. T. (2013). Crohn's disease affecting the small bowel is associated with reduced appetite and elevated levels of circulating gut peptides. *Clinical nutrition (Edinburgh, Scotland)*, 32(3), 404–411. <https://doi.org/10.1016/j.clnu.2012.08.024>
188. Gerges, S. (2017). EFFECT OF DSS ADMINISTRATION AND SULFASALAZINE TREATMENT ON BODY WEIGHT AND OXIDATIVE STRESS IN EXPERIMENTAL ULCERATIVE COLITIS IN MICE. *Al-Azhar Journal of Pharmaceutical Sciences*, 55(1), 97-108.
189. Moran, G. W., & Thapaliya, G. (2021). The Gut-Brain Axis and Its Role in Controlling Eating Behavior in Intestinal Inflammation. *Nutrients*, 13(3), 981. <https://doi.org/10.3390/nu13030981>

190. Ghomraoui, F. A., Alotaibi, S. T., Alharthi, M. A., Asiri, S. S., Almadi, M. A., Alharbi, O. R., Azzam, N. A., Aljebreen, A. M., Saeed, M., Hajkder, B., Saeed, W., & Alzoghaibi, M. A. (2017). Plasma ghrelin and leptin in patients with inflammatory bowel disease and its association with nutritional status. *Saudi journal of gastroenterology : official journal of the Saudi Gastroenterology Association*, 23(3), 199–205. https://doi.org/10.4103/sjg.SJG_575_16
191. Rigaud, D., Angel, L. A., Cerf, M., Carduner, M. J., Melchior, J. C., Sautier, C., René, E., Apfelbaum, M., & Mignon, M. (1994). Mechanisms of decreased food intake during weight loss in adult Crohn's disease patients without obvious malabsorption. *The American journal of clinical nutrition*, 60(5), 775–781. <https://doi.org/10.1093/ajcn/60.5.775>
192. Park, Y. H., Kim, N., Shim, Y. K., Choi, Y. J., Nam, R. H., Choi, Y. J., Ham, M. H., Suh, J. H., Lee, S. M., Lee, C. M., Yoon, H., Lee, H. S., & Lee, D. H. (2015). Adequate Dextran Sodium Sulfate-induced Colitis Model in Mice and Effective Outcome Measurement Method. *Journal of cancer prevention*, 20(4), 260–267. <https://doi.org/10.15430/JCP.2015.20.4.260>
193. Testa, N. D., Ghosh, S. M., & Shingleton, A. W. (2013). Sex-specific weight loss mediates sexual size dimorphism in *Drosophila melanogaster*. *PloS one*, 8(3), e58936. <https://doi.org/10.1371/journal.pone.0058936>
194. Musselman, L. P., & Kühnlein, R. P. (2018). *Drosophila* as a model to study obesity and metabolic disease. *The Journal of experimental biology*, 221(Pt Suppl 1), jeb163881. <https://doi.org/10.1242/jeb.163881>
195. Saavedra, P., & Perrimon, N. (2019). *Drosophila* as a Model for Tumor-Induced Organ Wasting. *Advances in experimental medicine and biology*, 1167, 191–205. https://doi.org/10.1007/978-3-030-23629-8_11
196. Han, X., Ding, S., Jiang, H., & Liu, G. (2021). Roles of Macrophages in the Development and Treatment of Gut Inflammation. *Frontiers in cell and developmental biology*, 9, 625423. <https://doi.org/10.3389/fcell.2021.625423>
197. Dharmasiri, S., Garrido-Martin, E. M., Harris, R. J., Bateman, A. C., Collins, J. E., Cummings, J., & Sanchez-Elsner, T. (2021). Human Intestinal Macrophages Are Involved in the Pathology of Both Ulcerative Colitis and Crohn Disease. *Inflammatory bowel diseases*, 27(10), 1641–1652. <https://doi.org/10.1093/ibd/izab029>
198. Meister M. (2004). Blood cells of *Drosophila*: cell lineages and role in host defence. *Current opinion in immunology*, 16(1), 10–15. <https://doi.org/10.1016/j.coi.2003.11.002>
199. Gold, K. S., & Brückner, K. (2015). Macrophages and cellular immunity in *Drosophila melanogaster*. *Seminars in immunology*, 27(6), 357–368. <https://doi.org/10.1016/j.smim.2016.03.010>
200. Ramond, E., Dudzic, J. P., & Lemaitre, B. (2020). Comparative RNA-Seq analyses of *Drosophila* plasmatocytes reveal gene specific signatures in response to clean injury and septic injury. *PloS one*, 15(6), e0235294. <https://doi.org/10.1371/journal.pone.0235294>
201. Foell, D., Wittkowski, H., Ren, Z., Turton, J., Pang, G., Daebritz, J., Ehrchen, J., Heidemann, J., Borody, T., Roth, J., & Clancy, R. (2008). Phagocyte-specific S100 proteins are released from affected mucosa and promote immune responses during inflammatory bowel disease. *The Journal of pathology*, 216(2), 183–192. <https://doi.org/10.1002/path.2394>
202. Sipponen T. (2013). Diagnostics and prognostics of inflammatory bowel disease with fecal neutrophil-derived biomarkers calprotectin and lactoferrin. *Digestive diseases (Basel, Switzerland)*, 31(3-4), 336–344. <https://doi.org/10.1159/000354689>
203. Kim, J. J., Shajib, M. S., Manocha, M. M., & Khan, W. I. (2012). Investigating intestinal inflammation in DSS-induced model of IBD. *Journal of visualized experiments : JoVE*, (60), 3678. <https://doi.org/10.3791/3678>
204. Hall, C., Flores, M. V., Storm, T., Crosier, K., & Crosier, P. (2007). The zebrafish lysozyme C promoter drives myeloid-specific expression in transgenic fish. *BMC developmental biology*, 7, 42. <https://doi.org/10.1186/1471-213X-7-42>
205. Madi, J. R., Outa, A. A., Ghannam, M., Hussein, H. M., Shehab, M., Hasan, Z., Fayad, A. A., Shirinian, M., & Rahal, E. A. (2021). *Drosophila melanogaster* as a Model System to Assess the Effect of Epstein-Barr Virus DNA on Inflammatory Gut Diseases. *Frontiers in immunology*, 12, 586930. <https://doi.org/10.3389/fimmu.2021.586930>

206. Yu, Y., Chen, J., Zhang, X., Wang, Y., Wang, S., Zhao, L., & Wang, Y. (2021). Identification of anti-inflammatory compounds from Zhongjing formulae by knowledge mining and high-content screening in a zebrafish model of inflammatory bowel diseases. *Chinese medicine*, 16(1), 42. <https://doi.org/10.1186/s13020-021-00452-z>
207. Silva, N. V., Carregosa, D., Gonçalves, C., Vieira, O. V., Nunes Dos Santos, C., Jacinto, A., & Crespo, C. L. (2021). A Dietary Cholesterol-Based Intestinal Inflammation Assay for Improving Drug-Discovery on Inflammatory Bowel Diseases. *Frontiers in cell and developmental biology*, 9, 674749. <https://doi.org/10.3389/fcell.2021.674749>
208. Michielan, A., & D'Inca, R. (2015). Intestinal Permeability in Inflammatory Bowel Disease: Pathogenesis, Clinical Evaluation, and Therapy of Leaky Gut. *Mediators of inflammation*, 2015, 628157. <https://doi.org/10.1155/2015/628157>
209. Kinashi, Y., & Hase, K. (2021). Partners in Leaky Gut Syndrome: Intestinal Dysbiosis and Autoimmunity. *Frontiers in immunology*, 12, 673708. <https://doi.org/10.3389/fimmu.2021.673708>
210. Turner J. R. (2009). Intestinal mucosal barrier function in health and disease. *Nature reviews. Immunology*, 9(11), 799–809. <https://doi.org/10.1038/nri2653>
211. Tajik, N., Frech, M., Schulz, O., Schälter, F., Lucas, S., Azizov, V., Dürholz, K., Steffen, F., Omata, Y., Rings, A., Bertog, M., Rizzo, A., Iljazovic, A., Basic, M., Kleyer, A., Culemann, S., Krönke, G., Luo, Y., Überla, K., Gaip, U. S., ... Zaiss, M. M. (2020). Targeting zonulin and intestinal epithelial barrier function to prevent onset of arthritis. *Nature communications*, 11(1), 1995. <https://doi.org/10.1038/s41467-020-15831-7>
212. Linsalata, M., Riezzo, G., Clemente, C., D'Attoma, B., & Russo, F. (2020). Noninvasive Biomarkers of Gut Barrier Function in Patients Suffering from Diarrhea Predominant-IBS: An Update. *Disease markers*, 2020, 2886268. <https://doi.org/10.1155/2020/2886268>
213. Hoshiko, H., Feskens, E., Oosterink, E., Ariens, R., Mes, J. J., & de Wit, N. (2021). Identification of leaky gut-related markers as indicators of metabolic health in Dutch adults: The Nutrition Questionnaires plus (NQplus) study. *PloS one*, 16(6), e0252936. <https://doi.org/10.1371/journal.pone.0252936>
214. Yan, Y., Kolachala, V., Dalmasso, G., Nguyen, H., Laroui, H., Sitaraman, S. V., & Merlin, D. (2009). Temporal and spatial analysis of clinical and molecular parameters in dextran sodium sulfate induced colitis. *PloS one*, 4(6), e6073. <https://doi.org/10.1371/journal.pone.0006073>
215. Rera, M., Clark, R. I., & Walker, D. W. (2012). Intestinal barrier dysfunction links metabolic and inflammatory markers of aging to death in *Drosophila*. *Proceedings of the National Academy of Sciences of the United States of America*, 109(52), 21528–21533. <https://doi.org/10.1073/pnas.1215849110>
216. Dambrose, E., Monnier, L., Ruisheng, L., Aguilaniu, H., Joly, J. S., Tricoire, H., & Rera, M. (2016). Two phases of aging separated by the Smurf transition as a public path to death. *Scientific reports*, 6, 23523. <https://doi.org/10.1038/srep23523>
217. Yan, Y., Kolachala, V., Dalmasso, G., Nguyen, H., Laroui, H., Sitaraman, S. V., & Merlin, D. (2009). Temporal and spatial analysis of clinical and molecular parameters in dextran sodium sulfate induced colitis. *PloS one*, 4(6), e6073. <https://doi.org/10.1371/journal.pone.0006073>
218. Jäger, S., Stange, E. F., & Wehkamp, J. (2013). Inflammatory bowel disease: an impaired barrier disease. *Langenbeck's archives of surgery*, 398(1), 1–12. <https://doi.org/10.1007/s00423-012-1030-9>
219. Vrakas, S., Mountzouris, K. C., Michalopoulos, G., Karamanolis, G., Papatheodoridis, G., Tzathas, C., & Gazouli, M. (2017). Intestinal Bacteria Composition and Translocation of Bacteria in Inflammatory Bowel Disease. *PloS one*, 12(1), e0170034. <https://doi.org/10.1371/journal.pone.0170034>
220. Linares, R., Francés, R., Gutiérrez, A., & Juanola, O. (2021). Bacterial Translocation as Inflammatory Driver in Crohn's Disease. *Frontiers in cell and developmental biology*, 9, 703310. <https://doi.org/10.3389/fcell.2021.703310>
221. Capo, F., Wilson, A., & Di Cara, F. (2019). The Intestine of *Drosophila melanogaster*: An Emerging Versatile Model System to Study Intestinal Epithelial Homeostasis and Host-Microbial Interactions in Humans. *Microorganisms*, 7(9), 336. <https://doi.org/10.3390/microorganisms7090336>
222. Mistry, R., Kounatidis, I., & Ligoxygakis, P. (2016). Exploring interactions between pathogens and the *Drosophila* gut. *Developmental and comparative immunology*, 64, 3–10. <https://doi.org/10.1016/j.dci.2016.01.016>

223. Camilleri M. (2019). Leaky gut: mechanisms, measurement and clinical implications in humans. *Gut*, 68(8), 1516–1526. <https://doi.org/10.1136/gutjnl-2019-318427>
224. Howard, A. M., LaFever, K. S., Fenix, A. M., Scurrah, C. R., Lau, K. S., Burnette, D. T., Bhave, G., Ferrell, N., & Page-McCaw, A. (2019). DSS-induced damage to basement membranes is repaired by matrix replacement and crosslinking. *Journal of cell science*, 132(7), jcs226860. <https://doi.org/10.1242/jcs.226860>
225. Poritz, L. S., Garver, K. I., Green, C., Fitzpatrick, L., Ruggiero, F., & Koltun, W. A. (2007). Loss of the tight junction protein ZO-1 in dextran sulfate sodium induced colitis. *The Journal of surgical research*, 140(1), 12–19. <https://doi.org/10.1016/j.jss.2006.07.050>
226. Shen, L., Su, L., & Turner, J. R. (2009). Mechanisms and functional implications of intestinal barrier defects. *Digestive diseases (Basel, Switzerland)*, 27(4), 443–449. <https://doi.org/10.1159/000233282>
227. Raj, A., & van Oudenaarden, A. (2008). Nature, nurture, or chance: stochastic gene expression and its consequences. *Cell*, 135(2), 216–226. <https://doi.org/10.1016/j.cell.2008.09.050>
228. Xiao, Y. T., Yan, W. H., Cao, Y., Yan, J. K., & Cai, W. (2016). Neutralization of IL-6 and TNF- α ameliorates intestinal permeability in DSS-induced colitis. *Cytokine*, 83, 189–192. <https://doi.org/10.1016/j.cyto.2016.04.012>
229. Liu, Q., & Jin, L. H. (2017). Tissue-resident stem cell activity: a view from the adult *Drosophila* gastrointestinal tract. *Cell communication and signaling : CCS*, 15(1), 33. <https://doi.org/10.1186/s12964-017-0184-z>
230. Clapper, M. L., Cooper, H. S., & Chang, W. C. (2007). Dextran sulfate sodium-induced colitis-associated neoplasia: a promising model for the development of chemopreventive interventions. *Acta pharmacologica Sinica*, 28(9), 1450–1459. <https://doi.org/10.1111/j.1745-7254.2007.00695.x>
231. Shah, S. C., & Itzkowitz, S. H. (2019). Management of Inflammatory Bowel Disease-Associated Dysplasia in the Modern Era. *Gastrointestinal endoscopy clinics of North America*, 29(3), 531–548. <https://doi.org/10.1016/j.giec.2019.02.008>
232. Korzelius, J., Naumann, S. K., Loza-Coll, M. A., Chan, J. S., Dutta, D., Oberheim, J., Gläßer, C., Southall, T. D., Brand, A. H., Jones, D. L., & Edgar, B. A. (2014). Escargot maintains stemness and suppresses differentiation in *Drosophila* intestinal stem cells. *The EMBO journal*, 33(24), 2967–2982. <https://doi.org/10.15252/embj.201489072>
233. Ohlstein, B., & Spradling, A. (2006). The adult *Drosophila* posterior midgut is maintained by pluripotent stem cells. *Nature*, 439(7075), 470–474. <https://doi.org/10.1038/nature04333>
234. Beebe, K., Lee, W. C., & Micchelli, C. A. (2010). JAK/STAT signaling coordinates stem cell proliferation and multilineage differentiation in the *Drosophila* intestinal stem cell lineage. *Developmental biology*, 338(1), 28–37. <https://doi.org/10.1016/j.ydbio.2009.10.045>
235. Nagy, P., Kovács, L., Sándor, G. O., & Juhász, G. (2016). Stem-cell-specific endocytic degradation defects lead to intestinal dysplasia in *Drosophila*. *Disease models & mechanisms*, 9(5), 501–512. <https://doi.org/10.1242/dmm.023416>
236. Li, Y., de Haar, C., Chen, M., Deuring, J., Gerrits, M. M., Smits, R., Xia, B., Kuipers, E. J., & van der Woude, C. J. (2010). Disease-related expression of the IL6/STAT3/SOCS3 signalling pathway in ulcerative colitis and ulcerative colitis-related carcinogenesis. *Gut*, 59(2), 227–235. <https://doi.org/10.1136/gut.2009.184176>
237. Takashima, S., Mkrtychyan, M., Younossi-Hartenstein, A., Merriam, J. R., & Hartenstein, V. (2008). The behaviour of *Drosophila* adult hindgut stem cells is controlled by Wnt and Hh signalling. *Nature*, 454(7204), 651–655. <https://doi.org/10.1038/nature07156>
238. Fox, D. T., & Spradling, A. C. (2009). The *Drosophila* hindgut lacks constitutively active adult stem cells but proliferates in response to tissue damage. *Cell stem cell*, 5(3), 290–297. <https://doi.org/10.1016/j.stem.2009.06.003>
239. Hudry, B., Khadayate, S., & Miguel-Aliaga, I. (2016). The sexual identity of adult intestinal stem cells controls organ size and plasticity. *Nature*, 530(7590), 344–348. <https://doi.org/10.1038/nature16953>
240. Ludington, W. B., & Ja, W. W. (2020). *Drosophila* as a model for the gut microbiome. *PLoS pathogens*, 16(4), e1008398. <https://doi.org/10.1371/journal.ppat.1008398>

241. Fischer, C. N., Trautman, E. P., Crawford, J. M., Stabb, E. V., Handelsman, J., & Broderick, N. A. (2017). Metabolite exchange between microbiome members produces compounds that influence *Drosophila* behavior. *eLife*, 6, e18855. <https://doi.org/10.7554/eLife.18855>
242. Lee, H. Y., Lee, S. H., Lee, J. H., Lee, W. J., & Min, K. J. (2019). The role of commensal microbes in the lifespan of *Drosophila melanogaster*. *Aging*, 11(13), 4611–4640. <https://doi.org/10.18632/aging.102073>
243. Sansone, C. L., Cohen, J., Yasunaga, A., Xu, J., Osborn, G., Subramanian, H., Gold, B., Buchon, N., & Cherry, S. (2015). Microbiota-Dependent Priming of Antiviral Intestinal Immunity in *Drosophila*. *Cell host & microbe*, 18(5), 571–581. <https://doi.org/10.1016/j.chom.2015.10.010>
244. Henry, L. P., Fernandez, M., Wolf, S., & Ayroles, J. (2022). Wolbachia interacts with the microbiome to shape fitness-associated traits during seasonal adaptation in *Drosophila melanogaster*. *bioRxiv*. <https://doi.org/10.1101/2022.05.31.494239>
245. Douglas A. E. (2018). The *Drosophila* model for microbiome research. *Lab animal*, 47(6), 157–164. <https://doi.org/10.1038/s41684-018-0065-0>
246. Neophytou, C., & Pitsouli, C. (2022). How Gut Microbes Nurture Intestinal Stem Cells: A *Drosophila* Perspective. *Metabolites*, 12(2), 169. <https://doi.org/10.3390/metabo12020169>
247. Liu, X., Nagy, P., Bonfini, A., Houtz, P., Bing, X. L., Yang, X., & Buchon, N. (2022). Microbes affect gut epithelial cell composition through immune-dependent regulation of intestinal stem cell differentiation. *Cell reports*, 38(13), 110572. <https://doi.org/10.1016/j.celrep.2022.110572>
248. Caruso, R., Lo, B. C., & Núñez, G. (2020). Host-microbiota interactions in inflammatory bowel disease. *Nature reviews. Immunology*, 20(7), 411–426. <https://doi.org/10.1038/s41577-019-0268-7>
249. Pickard, J. M., Zeng, M. Y., Caruso, R., & Núñez, G. (2017). Gut microbiota: Role in pathogen colonization, immune responses, and inflammatory disease. *Immunological reviews*, 279(1), 70–89. <https://doi.org/10.1111/imr.12567>
250. Round, J. L., & Mazmanian, S. K. (2009). The gut microbiota shapes intestinal immune responses during health and disease. *Nature reviews. Immunology*, 9(5), 313–323. <https://doi.org/10.1038/nri2515>
251. Eckburg, P. B., Bik, E. M., Bernstein, C. N., Purdom, E., Dethlefsen, L., Sargent, M., Gill, S. R., Nelson, K. E., & Relman, D. A. (2005). Diversity of the human intestinal microbial flora. *Science (New York, N.Y.)*, 308(5728), 1635–1638. <https://doi.org/10.1126/science.1110591>
252. Yilmaz, B., Juillerat, P., Øyås, O., Ramon, C., Bravo, F. D., Franc, Y., Fournier, N., Michetti, P., Mueller, C., Geuking, M., Pittet, V., Maillard, M. H., Rogler, G., Swiss IBD Cohort Investigators, Wiest, R., Stelling, J., & Macpherson, A. J. (2019). Microbial network disturbances in relapsing refractory Crohn's disease. *Nature medicine*, 25(2), 323–336. <https://doi.org/10.1038/s41591-018-0308-z>
253. Finotello, F., Mastrorilli, E., & Di Camillo, B. (2018). Measuring the diversity of the human microbiota with targeted next-generation sequencing. *Briefings in bioinformatics*, 19(4), 679–692. <https://doi.org/10.1093/bib/bbw119>
254. Gong, D., Gong, X., Wang, L., Yu, X., & Dong, Q. (2016). Involvement of Reduced Microbial Diversity in Inflammatory Bowel Disease. *Gastroenterology research and practice*, 2016, 6951091. <https://doi.org/10.1155/2016/6951091>
255. Ding, S., Ma, Y., Liu, G., Yan, W., Jiang, H., & Fang, J. (2019). *Lactobacillus brevis* Alleviates DSS-Induced Colitis by Reprogramming Intestinal Microbiota and Influencing Serum Metabolome in Murine Model. *Frontiers in physiology*, 10, 1152. <https://doi.org/10.3389/fphys.2019.01152>
256. Clooney, A. G., Eckenberger, J., Laserna-Mendieta, E., Sexton, K. A., Bernstein, M. T., Vagianos, K., Sargent, M., Ryan, F. J., Moran, C., Sheehan, D., Sleator, R. D., Targownik, L. E., Bernstein, C. N., Shanahan, F., & Claesson, M. J. (2021). Ranking microbiome variance in inflammatory bowel disease: a large longitudinal intercontinental study. *Gut*, 70(3), 499–510. <https://doi.org/10.1136/gutjnl-2020-321106>
257. Forster, S. C., Clare, S., Beresford-Jones, B. S., Harcourt, K., Notley, G., Stares, M. D., Kumar, N., Soderholm, A. T., Adoum, A., Wong, H., Morón, B., Brandt, C., Dougan, G., Adams, D. J., Maloy, K. J., Pedicord, V. A., & Lawley, T. D. (2022). Identification of gut microbial species linked with disease variability in a widely used mouse model of colitis. *Nature microbiology*, 7(4), 590–599. <https://doi.org/10.1038/s41564-022-01094-z>

258. Berry, D., Kuzyk, O., Rauch, I., Heider, S., Schwab, C., Hainzl, E., Decker, T., Müller, M., Strobl, B., Schleper, C., Urich, T., Wagner, M., Kenner, L., & Loy, A. (2015). Intestinal Microbiota Signatures Associated with Inflammation History in Mice Experiencing Recurring Colitis. *Frontiers in microbiology*, 6, 1408. <https://doi.org/10.3389/fmicb.2015.01408>
259. Chang, C. S., Liao, Y. C., Huang, C. T., Lin, C. M., Cheung, C., Ruan, J. W., Yu, W. H., Tsai, Y. T., Lin, I. J., Huang, C. H., Liou, J. S., Chou, Y. H., Chien, H. J., Chuang, H. L., Juan, H. F., Huang, H. C., Chan, H. L., Liao, Y. C., Tang, S. C., Su, Y. W., ... Kao, C. Y. (2021). Identification of a gut microbiota member that ameliorates DSS-induced colitis in intestinal barrier enhanced Dusp6-deficient mice. *Cell reports*, 37(8), 110016. <https://doi.org/10.1016/j.celrep.2021.110016>
260. Zakerska-Banaszak, O., Tomczak, H., Gabryel, M., Baturo, A., Wolko, L., Michalak, M., Malinska, N., Mankowska-Wierzbicka, D., Eder, P., Dobrowolska, A., Slomski, R., & Skrzypczak-Zielinska, M. (2021). Dysbiosis of gut microbiota in Polish patients with ulcerative colitis: a pilot study. *Scientific reports*, 11(1), 2166. <https://doi.org/10.1038/s41598-021-81628-3>
261. Rizzatti, G., Lopetuso, L. R., Gibiino, G., Binda, C., & Gasbarrini, A. (2017). Proteobacteria: A Common Factor in Human Diseases. *BioMed research international*, 2017, 9351507. <https://doi.org/10.1155/2017/9351507>
262. Mohammed, J. P., & Mattner, J. (2009). Autoimmune disease triggered by infection with alphaproteobacteria. *Expert review of clinical immunology*, 5(4), 369–379. <https://doi.org/10.1586/ECI.09.23>
263. Shang, Y., Zhai, Z., Huang, J., Li, L., & Zuo, X. (2022). Specific alterations in mucosa-associated bacterial composition in ulcerative colitis (UC) patients with different degrees of inflammation. *Biotechnology & Biotechnological Equipment*, 36(1), 200-208.
264. Zong, X., Fu, J., Xu, B., Wang, Y., & Jin, M. (2020). Interplay between gut microbiota and antimicrobial peptides. *Animal nutrition (Zhongguo xu mu shou yi xue hui)*, 6(4), 389–396. <https://doi.org/10.1016/j.aninu.2020.09.002>
265. Gubatan, J., Holman, D. R., Puntasecca, C. J., Polevoi, D., Rubin, S. J., & Rogalla, S. (2021). Antimicrobial peptides and the gut microbiome in inflammatory bowel disease. *World journal of gastroenterology*, 27(43), 7402–7422. <https://doi.org/10.3748/wjg.v27.i43.7402>
266. Fallmann, J., Sedlyarov, V., Tanzer, A., Kovarik, P., & Hofacker, I. L. (2016). AREsite2: an enhanced database for the comprehensive investigation of AU/GU/U-rich elements. *Nucleic acids research*, 44(D1), D90–D95. <https://doi.org/10.1093/nar/gkv1238>

7. Appendix

Table 7-1: Cumulative death events induced by LG

DSS-treated groups (3 biological replicates, n=100)			
Days post treatment	Average cumulative total No. of all dead flies	Average cumulative total No. of dead flies with LG	% LG-driven mortality
Day_0	0.00	0.00	0.00
Day_1	7.00	4.00	57.14
Day_2	15.00	6.00	40.00
Day_3	20.00	12.00	60.00
Day_4	25.00	17.00	68.00
Day_5	36.00	23.00	63.89
Day_6	41.00	25.00	60.98
Control groups (3 biological replicates n=100)			
Days post treatment	Average cumulative total No. of all dead flies	Average cumulative total No. of dead flies with LG	
Day_0	0.00	0.00	
Day_1	1.00	1.00	
Day_2	1.00	2.00	
Day_3	2.00	2.00	
Day_4	4.00	3.00	
Day_5	6.00	3.00	

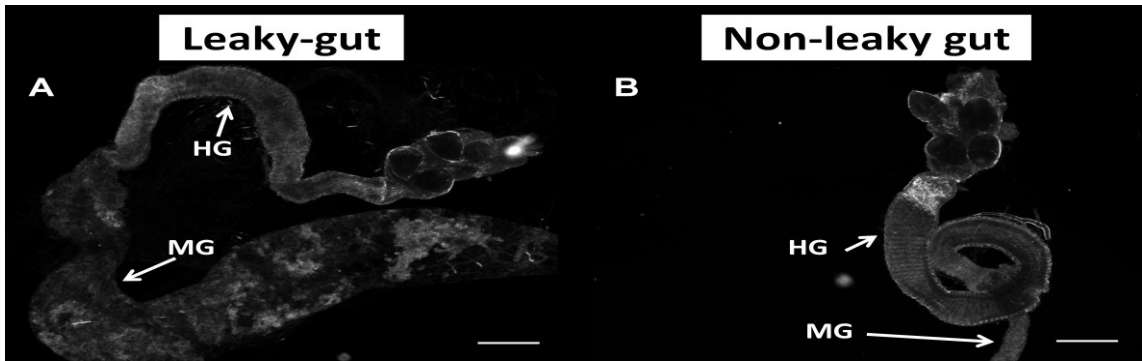


Fig.7.1: Representative images of dissected gut of w^{118} female *Drosophila*.
 MG: midgut; HG: hindgut. Scale bar = 50 μm .

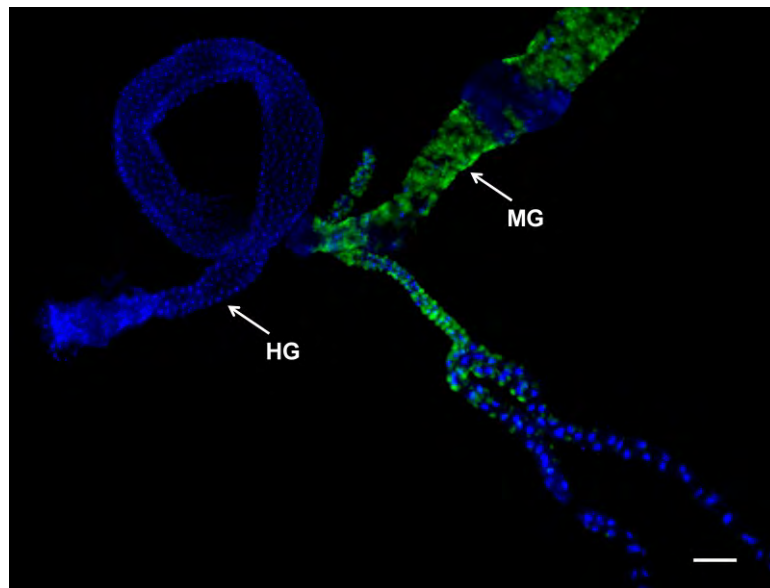


Fig.7.2: Representative images of dissected gut of DSS-treated *esg-Gal4>GFP Drosophila*.
 MG: midgut; HG: hindgut. GFP: green fluorescent protein. Cell nuclei are visualized by DAPI - (blue)
 Scale bar = 100 μm .

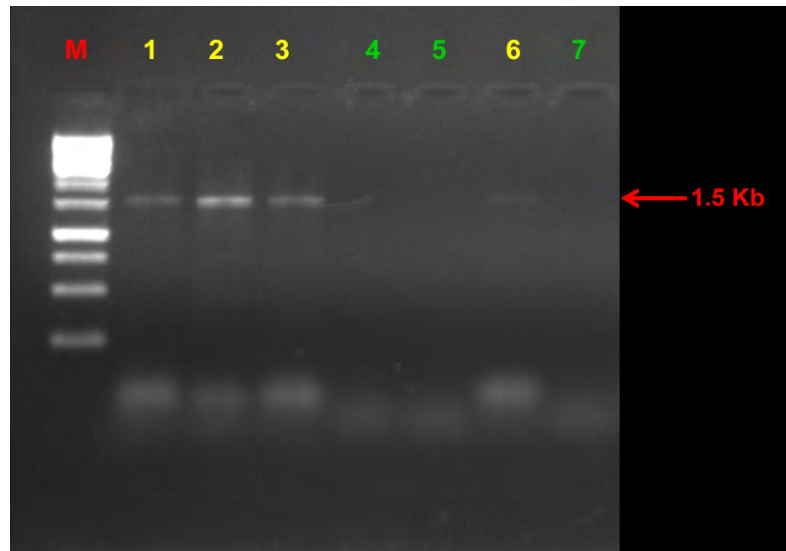


Fig.7.3: Representative image of 2% agarose gel electrophoresis of 16s rRNA diagnostic PCR using 16SA1 and 16SB1 primers targeting 16s rRNA gene. M: Molecular weight marker (1Kb); red arrow indicates the targeted amplicon size. Yellow-labeled lanes denote to samples with incomplete removal of bacterial community in preparation of the axenic animals; green-labeled lanes denotes bacterial-free samples (i.e. germ-free animal cohort).

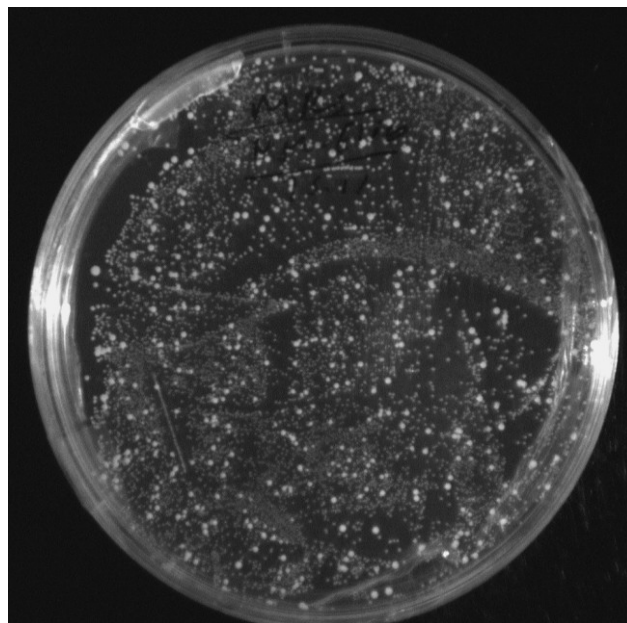


Fig.7.4: Representative MRS agar plate showing a growth of *Lactobacillus sp* as a viability indicator of microbial community preparations.

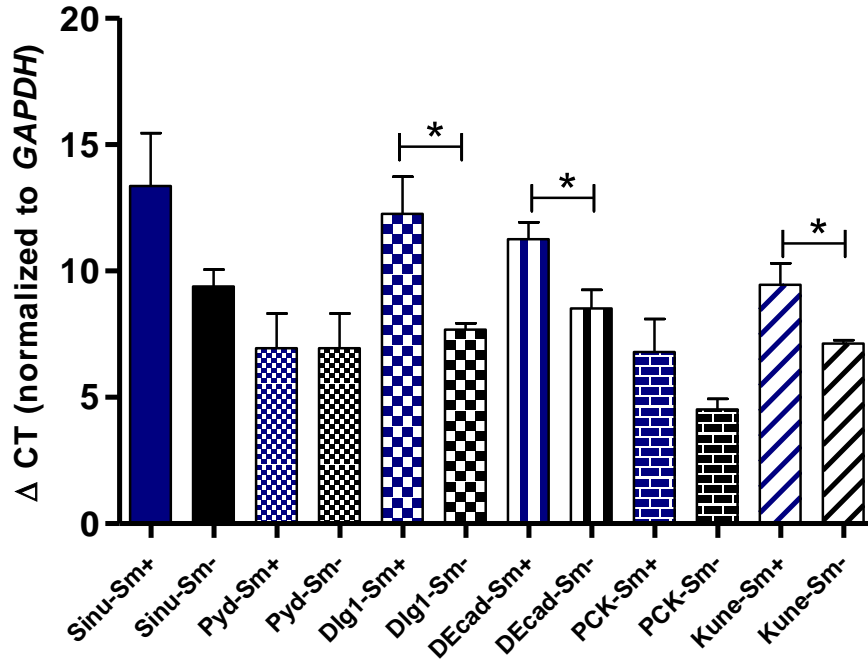


Fig.7.5: Prioritization of candidate septate junction genes, differentially expressed in the *Drosophila* gut. sm+: smurf flies with leaky gut; sm-: non-smurf flies. Sinu: Sinuous, Pyd: polychaetoid; Decad: *Drosophila* Cadherin, Pck: Pickel; kune: kune-kune. Values represent means \pm SEM for 3 biological replicates; *p<0.05.

Table 7-2: A Summary of average fold change in transcript levels and corresponding significance

Sample_ID	Mean_Fold_change	2-tail p value	Log2 fold change	-log10 p-value
Day6_AMG_DEcad	6.12	0.0292	2.61	1.53
Day6_AMG_Dlg1	16.36	0.0014	4.03	2.85
Day6_AMG_Kune	3.91	0.3187	1.97	0.50
Day6_AMG_Upd3	4.65	0.0015	2.22	2.82
Day6_AMG_Socs36E	3.57	0.0210	1.84	1.68
Day6_AMG_Attacin	0.72	0.3043	-0.48	0.52
Day6_AMG_Droso	11.72	0.0027	3.55	2.57
Day12_AMG_DEcad	2.96	0.1141	1.56	0.94
Day12_AMG_Dlg1	2.27	0.3212	1.18	0.49
Day12_AMG_Kune	1.25	0.5717	0.32	0.24
Day12_AMG_Upd3	5.00	0.0049	2.32	2.31

Day12_AMG_Socs36E	1.38	0.6665	0.47	0.18
Day12_AMG_Attacin	4.01	0.0652	2.00	1.19
Day12_AMG_Droso	2.34	0.0673	1.22	1.17
Day6_PMG_DEcad	5.62	0.4604	2.49	0.34
Day6_PMG_Dlg1	14.73	0.0015	3.88	2.82
Day6_PMG_Kune	1.68	0.7265	0.75	0.14
Day6_PMG_Upd3	3.50	0.3066	1.81	0.51
Day6_PMG_Socs36E	1.05	0.8652	0.06	0.06
Day6_PMG_Attacin	5.03	0.0088	2.33	2.06
Day6_PMG_Droso	10.70	0.0349	3.42	1.46
Day12_PMG_DEcad	2.06	0.3109	1.04	0.51
Day12_PMG_Dlg1	1.24	0.8717	0.31	0.06
Day12_PMG_Kune	1.85	0.0507	0.89	1.29
Day12_PMG_Upd3	2.07	0.4926	1.05	0.31
Day12_PMG_Socs36E	0.96	0.7439	-0.06	0.13
Day12_PMG_Attacin	6.41	0.2258	2.68	0.65
Day12_PMG_Droso	1.77	0.8587	0.82	0.07
Day6_HG_DEcad	0.96	0.7522	-0.06	0.12
Day6_HG_Dlg1	1.58	0.6045	0.66	0.22
Day6_HG_Kune	0.81	0.2807	-0.30	0.55
Day6_HG_Upd3	1.81	0.6263	0.86	0.20
Day6_HG_Socs36E	3.80	0.0320	1.93	1.49
Day6_HG_Attacin	2.40	0.2383	1.26	0.62
Day6_HG_Droso	8.46	0.0334	3.08	1.48
Day12_HG_DEcad	4.02	0.0075	2.01	2.12
Day12_HG_Dlg1	2.07	0.0859	1.05	1.07
Day12_HG_Kune	1.12	0.7225	0.16	0.14
Day12_HG_Upd3	2.86	0.0340	1.51	1.47
Day12_HG_Socs36E	2.93	0.0119	1.55	1.92
Day12_HG_Attacin	2.75	0.0016	1.46	2.80
Day12_HG_Droso	2.37	0.5077	1.24	0.29

Table 7-3: A Summary of average fold change in transcript levels in DSS-treated and recovery groups

	Day6	Day12	Recovery
AMG-DEcad	6.123948714	2.957645894	1.609739819
PMG-DEcad	5.620381446	2.061655234	0.68814063
HG-DEcad	0.959359536	4.020028064	1.912757325

AMG-Dlg1	16.36269496	2.273398471	3.86930219
PMG-Dlg1	14.72865548	1.242861404	0.52175872
HG-Dlg1	1.579949388	2.072053777	0.960888398

AMG-Kune	3.906440321	1.25226716	1.727003577
PMG-Kune	1.679701139	1.850493208	0.928879968
HG-Kune	0.814767358	1.119851506	0.819307576

AMG-Upd3	4.646918167	4.999071421	6.019383193
PMG-Upd3	3.496364192	2.07261518	0.704654135
HG-Upd3	1.809435157	2.856515759	1.684612411

AMG-Socs	3.574172713	1.382476356	1.097950228
PMG-Socs	1.045403454	0.962175417	1.213713423
HG-Socs	3.79867882	2.933230752	2.673558847

AMG-Attacin	0.716906283	4.00898446	3.421503967
PMG-Attacin	5.031408803	6.409622526	1.649982439
HG-Attacin	2.400719931	2.748340024	2.467283086

AMG-Droso	11.71872605	2.336999016	3.374184178
PMG-Droso	10.6964044	1.765380617	2.850208503
HG-Droso	8.460517269	2.369281233	3.808078538

Table 7-4: A Summary of % relative abundance of the major phyla in *Drosophila* fecal droppings, midgut tissue and hindgut tissue.

	Fecal droppings	Midgut	Hindgut
p__Actinobacteria	45.78	24.10	25.47
p__Bacteroidetes	5.27	16.46	8.10
p__Firmicutes	30.30	29.70	31.78
p__Proteobacteria	17.70	27.45	33.46
p__Tenericutes	0.68	1.18	0.69
p__Fusobacteria		0.69	0.40
p__Cyanobacteria	2.07		0.75
p__Candidatus Saccharibacteria		2.29	

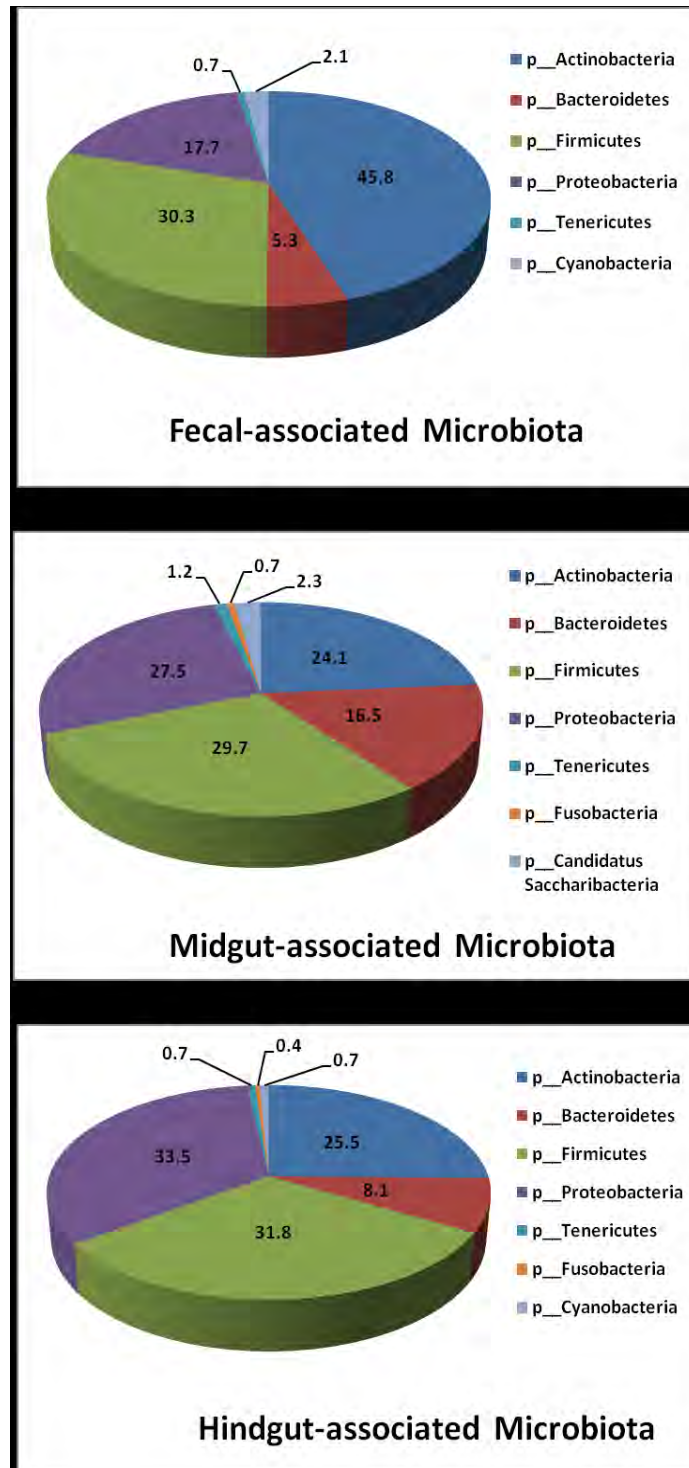


Fig.7.6: Ecological distribution of major phyla in the *Drosophila* fecal, midgut tissue and hindgut tissue samples based on Illumina Miseq sequencing of the V1-V2 region the bacterial 16S rRNA gene. Values represent means \pm SEM for 3 biological replicates

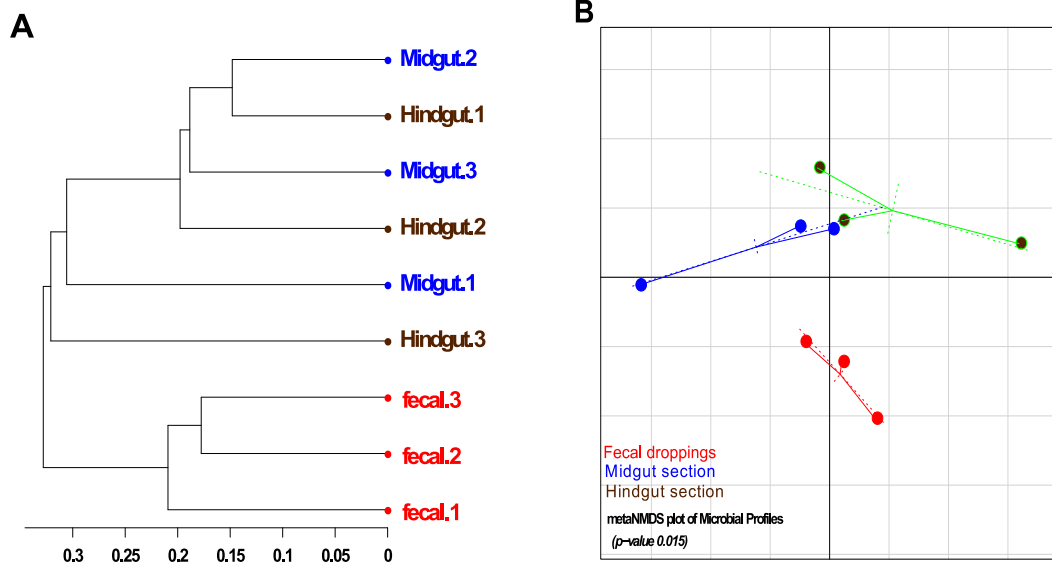


Fig.7.7: Graphs depict a significant difference in community structure between fecal, midgut and hindgut tissue samples. Beta-diversity is carried out using generalized UniFrac distance metric and presented by the dendrogram (Panel A) and metaNMDS (Panel B) of all samples. Values represent means \pm SEM for 3 biological replicates. Numbers in the denrogram refers to independent biological replicates; metaMDS: non-metric multidimensional scaling.

Table 7-5: Correlation coefficient r and significance of the fecal microbiota correlation matrix (Corrplot)

variable1	variable2	correlation	pValue
Richness	g__Undibacterium	-0.8431	0.00431
Richness	g__Ureaplasma	0.8005	0.01699
Evenness	g__Prevotella	0.9241	0.00292
Evenness	g__Cutibacterium	-0.9676	0.00000
Evenness	g__Micrococcus	-0.9090	0.00027
Evenness	p__Firmicutes	0.6426	0.04509
Evenness	p__Bacteroidota	0.6571	0.03898
Shannon.Effective	g__Prevotella	0.8577	0.01357
Shannon.Effective	g__Cutibacterium	-0.9364	0.00007
Shannon.Effective	g__Micrococcus	-0.8202	0.00365
Shannon.Effective	p__Actinobacteriota	-0.6366	0.04781
Shannon.Effective	p__Firmicutes	0.6724	0.03318
Shannon.Effective	p__Cyanobacteria	0.7885	0.00672
Food_intake	g__Prevotella	-0.9263	0.00272
Food_intake	p__Actinobacteriota	0.6341	0.04898
Food_intake	p__Firmicutes	-0.6881	0.02784
fecal_spot_count	g__Paracoccus	0.8334	0.01017
fecal_spot_count	p__Actinobacteriota	0.7269	0.01722
g__Prevotella	g__Cutibacterium	-0.9460	0.00126
g__Prevotella	g__Micrococcus	-0.9360	0.00192
g__Prevotella	g__Paracoccus	-0.9030	0.01365
g__Prevotella	p__Actinobacteriota	-0.9750	0.00019
g__Prevotella	p__Firmicutes	0.9863	0.00004
g__Cutibacterium	g__Micrococcus	0.9178	0.00018
g__Cutibacterium	p__Actinobacteriota	0.6608	0.03751
g__Cutibacterium	p__Firmicutes	-0.6794	0.03070
g__Cutibacterium	p__Cyanobacteria	-0.6458	0.04367
g__Cutibacterium	p__Bacteroidota	-0.6507	0.04162
g__Micrococcus	p__Actinobacteriota	0.7257	0.01752
g__Micrococcus	p__Firmicutes	-0.8087	0.00462
g__Paracoccus	p__Actinobacteriota	0.7208	0.04365
p__Actinobacteriota	p__Firmicutes	-0.9415	0.00005

Red color denotes values \geq the preset threshold for r (-0.8 & +0.8) and p-value (<0.05)

Table 7-6: A Summary of relative change in the *Drosophila* fecal microbiota abundance after 6-day and 12-day DSS treatment

Fecal_Day6	DSS	Ctrl	relative change
Richness	96.000	79.667	20.502
Shannon.Effective	33.470	24.940	34.202
p__Actinobacteriota	26.091	42.868	-39.136
p__Bacteroidota	5.199	5.607	-7.263
p__Cyanobacteria	0.593	0.332	78.823
p__Firmicutes	32.969	27.982	17.823
p__Proteobacteria	32.168	22.809	41.035
c__Alphaproteobacteria	5.045	6.394	-21.090
c__Gammaproteobacteria	27.122	16.415	65.234
f__Enterobacteriaceae	2.750	3.159	-12.923
f__Lactobacillaceae	1.289	1.114	15.670

Fecal_Day12	DSS	Ctrl	relative change
Richness	84.000	94.667	-11.268
Shannon.Effective	32.863	39.730	-17.283
p__Actinobacteriota	29.732	27.779	7.031
p__Bacteroidota	8.114	10.034	-19.137
p__Cyanobacteria	0.445	0.334	33.202
p__Firmicutes	30.454	20.480	48.702
p__Proteobacteria	29.697	40.443	-26.571
c__Alphaproteobacteria	7.342	7.379	-0.505
c__Gammaproteobacteria	22.356	33.064	-32.388
f__Enterobacteriaceae	4.529	5.099	-11.187
f__Lactobacillaceae	1.151	0.685	67.866

First column denotes alpha-diversity indices, major phyla, and lower taxonomic ranks. Second and third columns denote average values/ relative abundance. Third column denotes the relative change calculated by the equation $[(\text{DSS value} - \text{Control value}) / \text{Control value}] \times 100$

Table 7-7: A Summary of relative change in the *Drosophila* midgut microbiota abundance after 6-day and 12-day DSS treatment

Midgut_Day6			
	DSS	Ctrl	relative chang
Richness	70.333	101.667	-30.820
Shannon.Effective	16.803	45.807	-63.317
p__Actinobacteriota	11.499	20.630	-44.262
p__Bacteroidota	3.013	14.305	-78.941
p__Firmicutes	21.023	27.744	-24.224
p__Proteobacteria	63.925	35.319	80.993
c__Alphaproteobacteria	46.512	11.434	306.801
c__Gammaproteobacteria	17.414	23.886	-27.096
f__Enterobacteriaceae	3.510	3.659	-4.057
f__Lactobacillaceae	1.187	1.397	-15.036

Midgut_Day12			
	DSS	Ctrl	relative chang
Richness	33.000	37.000	-10.811
Shannon.Effective	3.833	4.543	-15.627
p__Actinobacteriota	1.788	3.529	-49.331
p__Bacteroidota	0.208	0.699	-70.225
p__Firmicutes	59.910	18.616	221.813
p__Proteobacteria	38.094	76.938	-50.488
c__Alphaproteobacteria	37.054	72.351	-48.786
c__Gammaproteobacteria	1.040	4.588	-77.333
f__Enterobacteriaceae	0.261	1.084	-75.940
f__Lactobacillaceae	58.631	11.656	403.017

First column denotes alpha-diversity indices, major phyla, and lower taxonomic ranks. Second and third columns denote average values/ relative abundance. Third column denotes the relative change calculated by the equation $[(DSS \text{ value} - \text{Control value}) / \text{Control value}] \times 100$

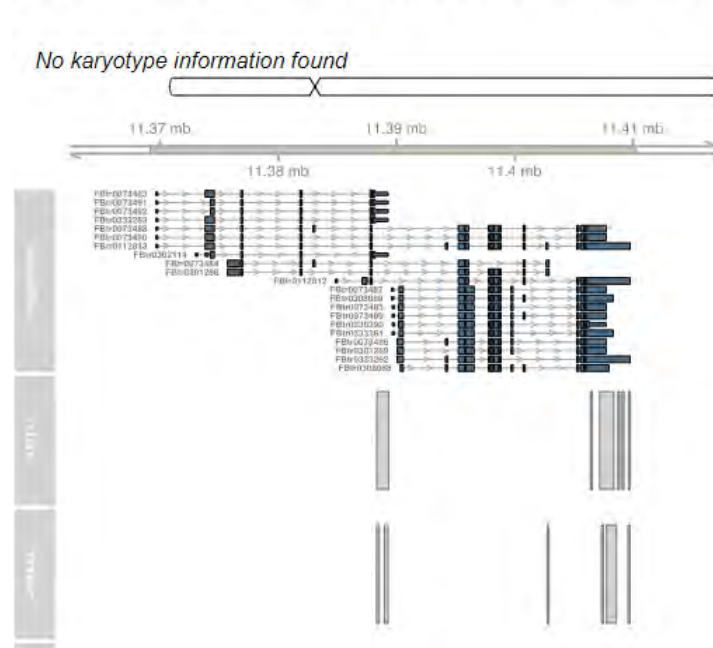
Table 7-8: A Summary of relative change in the *Drosophila* hindgut microbiota abundance after 6-day and 12-day DSS treatment

Hingut_Day6			
	DSS	Ctrl	relative change
Richness	84.000	97.000	-13.402
Shannon.Effective	26.430	38.107	-30.642
p__Actinobacteriota	9.084	20.328	-55.311
p__Bacteroidota	6.213	8.774	-29.196
p__Firmicutes	36.017	23.303	54.555
p__Proteobacteria	47.230	45.309	4.240
c__Alphaproteobacteria	28.232	18.212	55.023
c__Gammaproteobacteria	18.998	27.097	-29.890
<i>f__Enterobacteriaceae</i>	3.715	5.359	-30.692
<i>f__Lactobacillaceae</i>	12.257	9.657	26.926

Hingut_Day12			
	DSS	Ctrl	relative change
Richness	52.000	59.000	-11.864
Shannon.Effective	15.597	14.353	8.662
p__Actinobacteriota	6.578	10.769	-38.921
p__Bacteroidota	3.789	3.147	20.395
p__Firmicutes	62.308	43.863	42.053
p__Proteobacteria	26.669	41.797	-36.193
c__Alphaproteobacteria	17.552	27.154	-35.363
c__Gammaproteobacteria	9.117	14.642	-37.733
<i>f__Enterobacteriaceae</i>	1.771	1.336	32.516
<i>f__Lactobacillaceae</i>	53.855	29.993	79.556

First column denotes alpha-diversity indices, major phyla, and lower taxonomic ranks. Second and third columns denote average values/ relative abundance. Third column denotes the relative change calculated by the equation $[(\text{DSS value} - \text{Control value}) / \text{Control value}] \times 100$

**Search results for "dlg1" identified as "FBgn0001624"
in species "Drosophila_melanogaster"
genomic coordinates "chrX:11369665-11409776:+"**



Genomic coordinates, annotation and linkout to experimental evidence for queried motifs

Chromosome	Start	End	Motif	Motif-family	Strand	Gene	Transcript
chrX	11408033	11408038	ATTTA	ATTTA	+	FBgn0001624	FBtr0112812
chrX	11408317	11408322	ATTTA	ATTTA	+	FBgn0001624	FBtr0112812
chrX	11408815	11408820	ATTTA	ATTTA	+	FBgn0001624	FBtr0112812
chrX	11409172	11409177	ATTTA	ATTTA	+	FBgn0001624	FBtr0112812
chrX	11409713	11409718	ATTTA	ATTTA	+	FBgn0001624	FBtr0112812

Fig.7.8: Image denotes AREsite2 graphical output of testing potential AU-rich elements in Dlg1 gene. FBgn0001624 is the flybase gene ID for *Dlg1*. ATTTA is one of the core adenylate uridylate (AU) rich elements. <http://rna.tbi.univie.ac.at/>